POLITECNICO DI TORINO

Master's degree in Civil Engineering – Structures and Infrastructures

Academic year 2021-2022
Graduation session March-April 2022

Structural Pavement Design According to the Russian Method: the Effects of Climate Change in Continental and Subarctic Zones

Supervisor:
Lucia Tsantilis

Co-supervisor:
Vladimir Sergeevich Churilin

Candidate:
Paolo Vaira

“Облетев Землю в корабле-спутнике, я увидел, как прекрасна наша планета.
Люди, будем хранить и преумножать эту красоту, а не разрушать её!”

Юрий Алексеевич Гагарин

“Orbiting Earth in the spaceship, I saw how beautiful our planet is.
People, let us preserve and increase this beauty, not destroy it!”

Yuri Alekseyevich Gagarin

Before starting, I would like to spend a few words for the people that accompanied me through this long academic career and the creation of this paper.

First of all, I would like to express my sincere gratitude to professor Lucia Tsantilis for the continuous guidance and support in completing my project and to professor Vladimir Churilin for his patience and constructive help and advice.

A particular mention goes to my parents: mom and dad, thank you for your precious teachings and for having me always supported in all my decisions, no matter what.

Thank you to all my family, to uncle Bubu, aunt Vivian and my beloved grandma Pina.

Thank you to my special friends Clarissa, Emma and Ilaria, for always being by my side and for adding so much sympathy and fun to all these years.

Thank you to my university colleague Francesca, for being such a great, supporting, loyal and comprehensive friend: I will never forget these years spent together and I know I can always count on you.

Thank you to all the guys I met during this amazing Siberian experience, particularly Sofia, Alexandra and Alessandro: the moments spent together will always have a special place in my heart and I will treasure them with much jealousy.

I would also like to give thanks to all the staff of Tomsk State University of Architecture and Building, in particular Natalia, Ekaterina, Nadya and Nika: thank you for all your invaluable help, for making me feel at home from the very first day and for introducing me to the wonderful Russian and Siberian culture.

Thank you to all the people I have met so far, for making me the guy I am today.

ABSTRACT

The following master's thesis project has been developed within the Erasmus+ program in the Russian Federation and outlines the results of a series of experimental activities carried out at Tomsk State University of Architecture and Building.

The objective of this study is to investigate climate change effects on road pavement design in areas characterized by continental and subarctic climates.

The impact of different phenomena such as temperature and precipitations increase, as well as frost depth reduction, has been widely discussed by many climatologists and plays a key role in cold regions pavement assessment.

The experimental activities, performed in the laboratories of the Road Construction Faculty, were focused on two reference sites, Tomsk and Salekhard, both located in the Siberia region. A series of test sections equipped with special sensors allowed the determination of temperature and volumetric water content of the subgrade soil, which eventually enabled the validation of the measured data with models available in the literature.

The project has been developed with the purpose of studying how road pavement design will be influenced fifty years hence in terms of layers thickness and leading failure criteria; to accomplish this, the following steps have been carried out:

- materials characterization and sensors calibration;
- modeling of the climatic data (temperature and frost depth);
- analysis of projections of climate models;
- pavement design according to the Russian standards.

Overall, results are coherent to what was stated in other climate change-related studies and showed non-negligible effects in terms of pavement design, especially when taking into account precipitations increase.

Since, to date, no official English version of the abovementioned Russian regulations is available, a personally realized translation has also been included in this paper.

SOMMARIO

La seguente tesi magistrale è stata sviluppata nell'ambito del programma Erasmus+ nella Federazione Russa e delinea i risultati di una serie di attività sperimentali svolte presso la Tomsk State University of Architecture and Building.

L'obiettivo dello studio è di indagare gli effetti dei cambiamenti climatici sulla progettazione delle pavimentazioni stradali in aree caratterizzate da climi continentali e subartici.

L'impatto di diversi fenomeni come l'aumento della temperatura e delle precipitazioni e la riduzione della profondità del gelo è stato ampiamente discusso da molti climatologi e ricopre un ruolo chiave nell'analisi delle pavimentazioni in zone fredde.

Le attività sperimentali, svolte nei laboratori della Facoltà di Costruzioni Stradali, si sono concentrate su due siti di riferimento, Tomsk e Salekhard, entrambi situati in Siberia. Una serie di sezioni di prova dotate di appositi sensori ha consentito la determinazione della temperatura e del contenuto d'acqua volumetrico del sottofondo, il che ha poi permesso di validare i dati misurati con i modelli disponibili nella letteratura.

Il progetto è stato sviluppato con lo scopo di studiare come la progettazione delle pavimentazioni stradali sarà influenzata tra cinquant'anni in termini di spessore degli strati e principali criteri di rottura; a tal fine sono stati effettuati i seguenti passaggi:

- caratterizzazione dei materiali e calibrazione dei sensori;
- modellazione dei dati climatici (temperatura e profondità del gelo);
- analisi delle proiezioni dei modelli climatici;
- progettazione della pavimentazione secondo gli standard russi.

Nel complesso, i risultati sono coerenti con quanto affermato in altri studi sui cambiamenti climatici e hanno mostrato effetti non trascurabili in termini di progettazione delle pavimentazioni, soprattutto in relazione all'aumento delle precipitazioni.

Poiché ad oggi non è disponibile alcuna versione inglese ufficiale delle suddette normative russe, in questo documento è stata inclusa anche una traduzione realizzata personalmente.

АННОТАЦИЯ

Магистерская диссертация подготовлена в рамках программы Erasmus+ на территории Российской Федерации и представляет собой результаты полевых и лабораторных работ, выполненных в Томском государственном архитектурно-строительном университете.

Цель исследования заключается в изучении влияния изменений климата на проектирование дорожных одежд для районов с континентальным и субарктическим климатом.

Влияние изменяющихся метеорологических явлений, таких как температуры воздуха и осадков, а также изменения глубины промерзания, широко обсуждается климатологами и играет ключевую роль при проектировании дорожных покрытий в холодных регионах.

В лаборатории Дорожно-строительного факультета Томского государственного архитектурно-строительного университета выполнены калибровочные испытания датчиков объёмной влажности и температуры. Серии тестовых участков, расположенных в Сибири – Томск и Салехард, оборудованы датчиками объёмной влажности и температуры. Контролируемые параметры при мониторинге - температура и объёмная влажность земляного полотна. Полученные результаты по температуре грунта земляного полотна сопоставлены с классическими моделями промерзания.

Проект включает исследование влияния изменения климата на проектирование толщины слоёв дорожного покрытия и ключевых критериев прочности и устойчивости дорожных конструкций за период в 50 лет. В ходе исследования выполнены следующие шаги:

- определение характеристик материалов и калибровка датчиков;
- прогнозирование температуры и глубины промерзания грунтов земляного полотна;
- анализ прогнозов климатических моделей;

- проектирование дорожных одежд в соответствии с российскими нормами.

Результаты выполненной работы соотносятся с данными других исследований, посвящённых климатическим изменениям.

В настоящую работу также включён лично выполненный перевод российских норм проектирования дорожных одежд, поскольку на сегодняшний день не существует их официальной английской версии.

INDEX

PART 3: MODELING

PART 4: STRUCTURAL ANALYSIS

FIGURES AND TABLES LIST

INTRODUCTION

"This year, the wildfires in Siberia were twice as big as before, reaching the size of Belgium. People started noticing that something was wrong and started linking wildfires with climate. In Irkutsk region floods began and people started thinking that something wrong is happening with the climate."

Arshak Makichyan – climate activist

"The wildfires burning in Russia now are bigger than all the fires raging across the globe combined, bigger than those in the US, Canada, Turkey and Greece put together. […] Smoke from them has reached Alaska and, for the first time in history, the North Pole."

Patrick Reevell – ABC News

"We don't go out in the afternoons. We sit at home, basically. It's hard to breathe. There was a lot of rain before. And now there isn't any rain at all. This summer, there hasn't been any."

Anna Rumyantseva – villager of Yakutia

"Before, it was possible to catch a seal on the ice through the end of June, but today it's already dangerous to walk the ice in May. Even in January, there are thaws with rain. I can't recall that happening before. Everywhere ice cover is melting, which before would have held up year-round. Sometimes the berries overripen and become soft and bad tasting. There are few cloudberries because the summer is hot."

Viktor Tkachenko – villager of Chukotka

"Nature has seriously deteriorated, taken offense at mankind. Spring arrives 2-3 weeks earlier than usual. Spring is harsh, always alternating between rain and frost. The first rain comes in May, but this was not the case before. The first thaw is at the end of April. The rivers break up much earlier than usual, around the 25th of May, when before, it was June 10-15. Summer has become intolerably hot. On the ocean, good ice doesn't form. Before, the ocean ice broke up in the middle of May, but the ice didn't recede very far. We hunted all summer on the ice."

Grigoriy Rykhtyn - villager of Chukotka

Climate change effects are now evident to everyone. Every day, news reports extreme events such as droughts, floods, wildfires, unexpected snowfalls, etc. and in recent years countries worldwide have been struggling to find a solution to the catastrophic consequences mankind is forced to face.
The following master's thesis aims to investigate only one of the many areas in which climate change is showing its effects, namely, cold regions pavement design.

The project has been developed within the Erasmus+ program in the Russian Federation between September 2021 and February 2022, at Tomsk State University of Architecture and Building (henceforth referred to as TSUAB) in Tomsk, West Siberia; all the experimental activities have been carried out in the laboratories of the Road Construction Faculty.
The paper objectives are to perform an assessment in terms of climate change of the available data (temperature and precipitations) in the Siberia region and to study how these effects will influence flexible pavement design in fifty years.
Descriptions, theoretical overviews, calculations and overall conclusions have been organized in the following framework:

- *chapter 2* lists the main conclusions that have been drawn in Russia and Siberia regarding climate change, such as temperature and precipitations increase, retiring permafrost, snowmelt, fire danger, etc.; different papers available in the literature have been taken as reference documents. An overview of the central bodies and organizations involved in this field is also presented;
- *chapter 3* contains a detailed characterization of the two sites under analysis, Tomsk and Salekhard, regarding geographic location, territory subdivision, landscape and climate, as well as a description of the instrumented test sections in terms of layers thickness and material and sensors placement, installed with the purpose of collecting temperature and volumetric water content information of the subgrade soil.

  An overview of the road-climatic zoning classification system used in the Russian Federation is also presented;

- *chapter 4* depicts the features of the TEROS 11/12 sensors installed in the test sections and outlines the laboratory procedure (according to the Russian standards) used to calibrate the volumetric water content data;
- *chapter 5* describes the temperature analysis carried out to model the available information; precisely, a combination of different methodologies from the literature has been applied. Measured and calculated data were finally validated;
- *chapter 6* contains an overview of the theoretical basis regarding frost penetration, such as the heat transfer problem; different freezing depth models (Neumann's, Stefan's and Berggren's) are presented.

  Subsequently, temperature data have been used to retrieve frost depth values in the different test sections and finally validated by means of the modified Berggren's formula;
- *chapter 7* is devoted to the trend analysis of past weather data in Tomsk and Salekhard for the last 100 and 50 years. Average, minimum and maximum temperatures, as well as daily precipitations, have been submitted to different statistical tests to find some significant conclusions in terms of climate change. A linear analysis of the frost depth and freezing index values was also performed for the two reference sites;
- *chapter 8* contains the calculations regarding the design of two simple pavement cross-sections in Tomsk and Salekhard following the Russian regulations. The same analysis has then been again performed by taking into account the conclusions outlined in *chapter 2* and *chapter 7* to study how pavement design will be influenced fifty years hence;
- *annex 1* contains the temperature trend plots for different test sections and days of the analyzed period considering the temperature model outlined in *chapter 5*;
- *annex 2* is a personally realized translation of the Russian standards ODN 218.046-01: *Design of Flexible Road Pavements* since no official English version is yet available in the literature.

Part 1:

Climate Change

CLIMATE CHANGE IN RUSSIA: A LOOK AT SIBERIA

The following chapter is aimed to summarize the main findings of the papers available in the literature in terms of climate change in Russia and Siberia.
This step is fundamental to understand which are the main effects of climatic variations and will help the reader understand the importance and the impact of these phenomena on today and future's society.
The following paragraphs will also be helpful to acquire a general overview regarding temperature rise and precipitations increase, which constitute the key parameters that will be taken into account for the pavement design analysis proposed in *chapter 8* and that represents the goal of this master's thesis.

2.1 AN OVERVIEW

Starting from the last decades of the 20th century, following the acquisition and elaboration of new climatic and palaeoclimatological data, a shared awareness of the presence of climate change began to spread in the scientific community. At the same time, in the political sphere, the need to review the socio-economic development model aimed to guarantee the long-term well-being of the population and the safeguarding of the planet's natural resources was brought to the attention of the UN member states.
In this context, the study of climate becomes an essential tool for understanding climate change and acts as a support for strategic decisions aimed at the mitigation and adaptation to its effects.
Today scholars are trying to stress the importance of this issue, explaining how the radical changes in the last 150 years are essentially to be attributed to the reckless action of man, who has changed his lifestyle by pursuing a continuous, increasingly rapid progress, regardless of its effects on the environment, both in the short and in the long term.

Since 1950 the changes are, in fact, unprecedented and it is certainly no coincidence that the decline began and continued in conjunction with the phases of strong economic growth and industrial development.

At the international level, the reference for climate change is the Intergovernmental Panel on Climate Change (IPCC), set up by the UN bodies, the World Meteorological Organization (WMO) and the United Nations Environment Programme (UNEP) in 1988.

In this context, the IPCC plays the role of the international reference institution for assessing the climate and climate-altering gas emissions. This organization has the purpose of evaluating, based on scientific, technical and socio-economic data and evidence, the risk of climate change induced by humanity and its possible consequences and has the ability to suggest solutions for reducing these variations.

To date, 195 countries take part in this body, which is configured as a neutral information tool on which governments and political decision-makers can base their choices and actions. It is mainly based on the need for these to have a scientific, reliable, transparent and objective support in order to understand the risk deriving from climate change.

The scientific activity of the IPCC is based in Geneva and its main operation consists of the publication of periodic reports on the state and stage of climatic variations.

The IPCC is part of the United Nations; hence, it publishes its documents exclusively in its six official languages (Spanish, English, Chinese, Russian, French and Arabic). Special reports are periodically issued, which are developed by the three IPCC working groups, who publish thematic volumes that are then summarized in the evaluation reports:

- working group I: *The Physical Science Basis*;
- working group II: *Impacts, Adaptation and Vulnerability*;
- working group III: *Mitigation of Climate Change*.

Following the first IPCC report in 1992, the UN member states started to adopt the United Nations Framework Convention on Climate Change (UNFCCC), which, after the Kyoto protocol in 1997, became the shared basis on the matter.

The other reports were issued in 1995, 2001, 2007 and 2014, which have confirmed and made more and more evident the links between the accumulation of greenhouse gases in the atmosphere and the temperature rise and have also underlined the growing probability of extreme weather events, with the clarification that at the moment in where preventive measures are not taken to protect the environment, future climate changes could be much more significant than those observed so far and in the past.
The last report is set to be issued in 2022, although the group I paper has already been published.
Another important contribution of the IPCC is the 2011 special report on *Renewable Energy Sources and Climate Change Mitigation*. The main objective of this document is to scientifically evaluate the potential of using renewable energy in the mitigation of phenomena of climate change.
The conclusions of the paper suggest the implementation of intervention policies aimed at fully exploiting the technological potential given by renewable sources to reach the coverage of about 80% of the world's energy needs by 2050.

In order to understand the mechanisms that are causing global warming, the contribution of paleoclimatology has been fundamental in the research on climate-altering gasses, in particular the analysis of polar fossil ice cores, which allowed to reconstruct the CO_2 concentrations in the last tens of thousands of years.
Atmospheric concentrations of CO_2 are the result of different processes that either produce or remove CO_2 in the carbon cycle; during the last 10 000 years up to about 150 years ago, these levels had remained virtually unchanged. However, due to the burning of fossil fuels and forests, mainly caused by anthropogenic causes, concentrations started to rise, with the subsequent increase of the greenhouse effect.
The rise in greenhouse gas emissions into the atmosphere could cause further warming and induce changes in the global climate system during the 21st century, likely to be more important than those already observed in the previous century.
In 2019, atmospheric CO_2 concentrations were higher than in at any time in at least 2 million years and concentrations of CH_4 and N_2O were higher than in at least 800 000

years. Since 1750, increases in CO_2 (47%), CH_4 (156%) and N_2O (23%) far exceeded the multi-thousand-year natural changes between glacial and interglacial periods.

The determinants of climate change include the emissions of greenhouse gases (GHG), their concentrations in the atmosphere, the radiation balance and feedback from the climate system. The causes of anthropogenic origin are linked to the progress of socio-economic development. In fact, it is probable to find a net reduction of the same polluting emissions in periods of economic crisis.

2.2 CLIMATE CHANGE IN RUSSIA: A BRIEF SUMMARY

Russia is the largest country in the world, with a total surface of 17 864 345 km^2 spanning between Europe and Asia.

Its topography includes the world's deepest lake and Europe's highest mountain and its landscape is constituted by all the major vegetation zones, except for tropical rain forests. The terrain ranges from grassy steppes in the south to the tundra in the Polar North, covering almost 10% of the country. Russia's largest forested region, called taiga, covers an area of about the size of the United States and is mainly characterized by coniferous trees such as spruce, cedar, larch and fir.

Russia is also the coldest country in the world, with a mean annual temperature of -4,1 °C (1961-1990 measurement period). On the other hand, average values are not precise enough to describe the diversity of the territory, whose three climatic zones are further divided into eighteen climatic regions. For instance, average winter temperatures are above zero in the Black Sea coast (the warmest region), while in Eastern Siberia (the coldest region) these values can reach -40 °C. Average summer temperatures vary from 4-5 °C in the Far North to 20-22 °C in the southern areas.

The country is characterized by an abundance of solid precipitations (snow, hail and sleet) and an uneven distribution of rainfall throughout its territories due to its great extension: the mean annual precipitation is as low as 150 mm on the Arctic Islands and arid valleys of South-East Altai, up to 3200 mm on the Black Sea coast.

Russia is already experiencing the impacts of climate change in the form of milder winters, melting permafrost, changes in the precipitation patterns, the spread of diseases and increased incidence of extreme events such as droughts and flooding. It is believed that by 2030 the country will start to feel the impacts of climatic variations concerning both water and food supply.

Scientists agree that human behavior, especially the burning of coal, oil and gas and the destruction of forests, is the leading cause of the greenhouse effect.

Recent scientifically documented changes in climate have impacts on all climatic features, including temperature, precipitations, wind and cloudiness.

The average annual temperature anomaly in the whole country has reached about 1,6 °C, which is much higher than the global anomaly of 0,9 °C compared to pre-industrial time. The slope of the linear trend of annual temperature in 1976-2018 in the Russian Federation was 0,47 °C per decade, equal to 2,5 times more than the global rise for the same period (0,18 °C per decade) (**Figure 2.1** and **Figure 2.2** give a schematic representation of the temperature anomalies in the country).

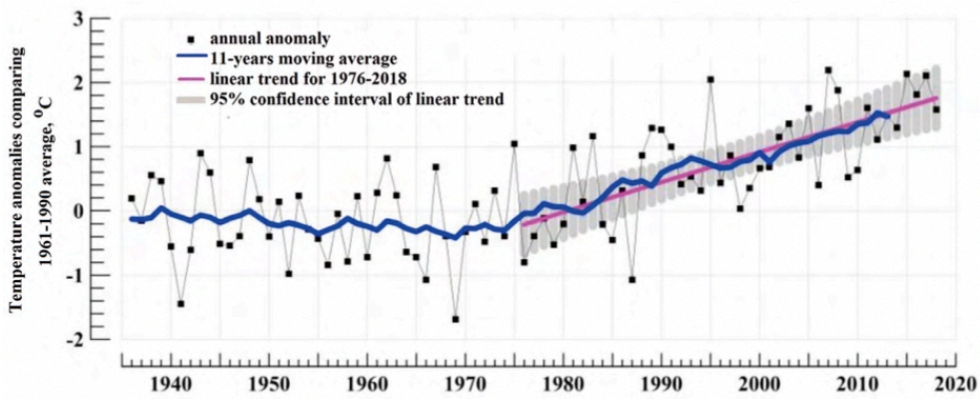

Figure 2.1: Mean annual temperature anomalies in Russia, calculated as deviations from the 1961-1990 average

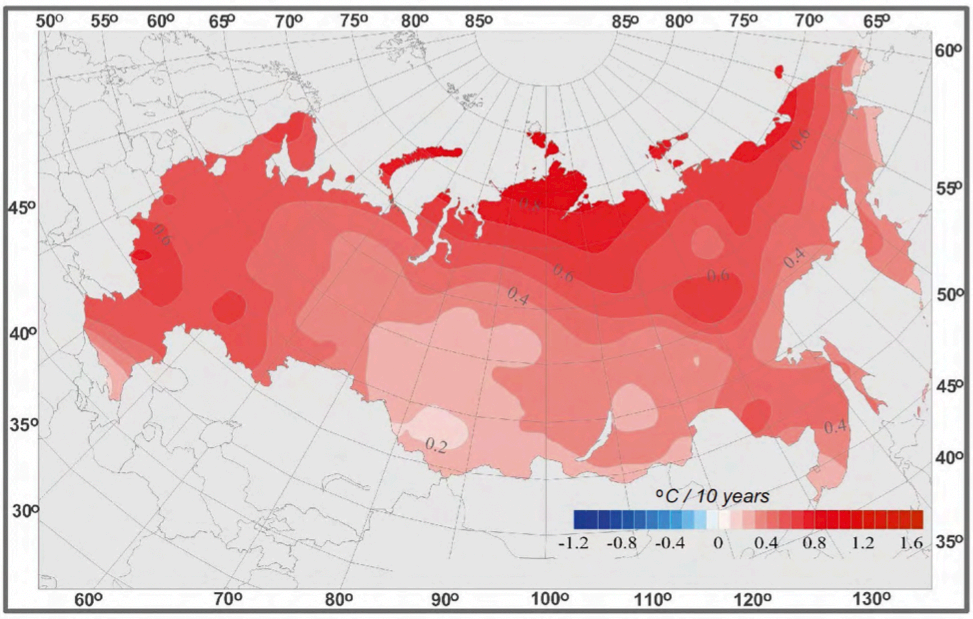

Figure 2.2: Trends of annual temperatures for 1976-2013 in Russia (expressed as degrees/10 years)

Annual precipitations have been increasing since 1980; the linear trend in the period 1976-2018 was +2,2 mm/month per decade (**Figure 2.3**). The spatial distribution of changes in mean annual precipitations per decade between 1976 and 2013 shows an increase in almost all regions of Russia, with a maximum in some central parts of the Far East (up to 15-20% per 10 years) (**Figure 2.4**).

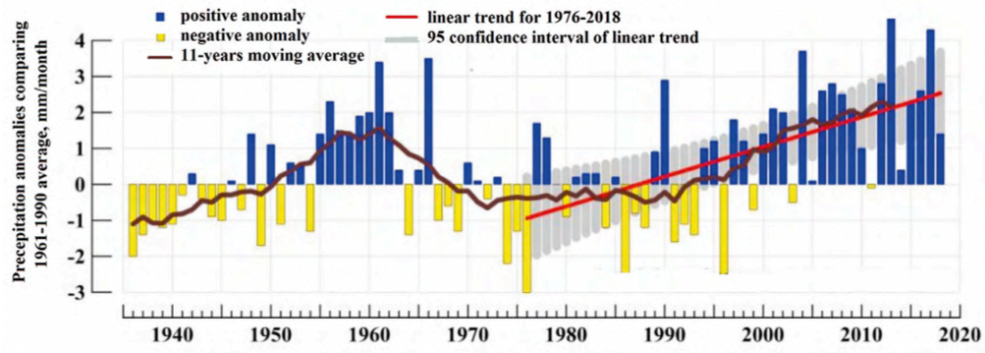

Figure 2.3: Precipitation anomalies between 1937 and 2018 related to the mean annual precipitations of 1961-1990 in Russia

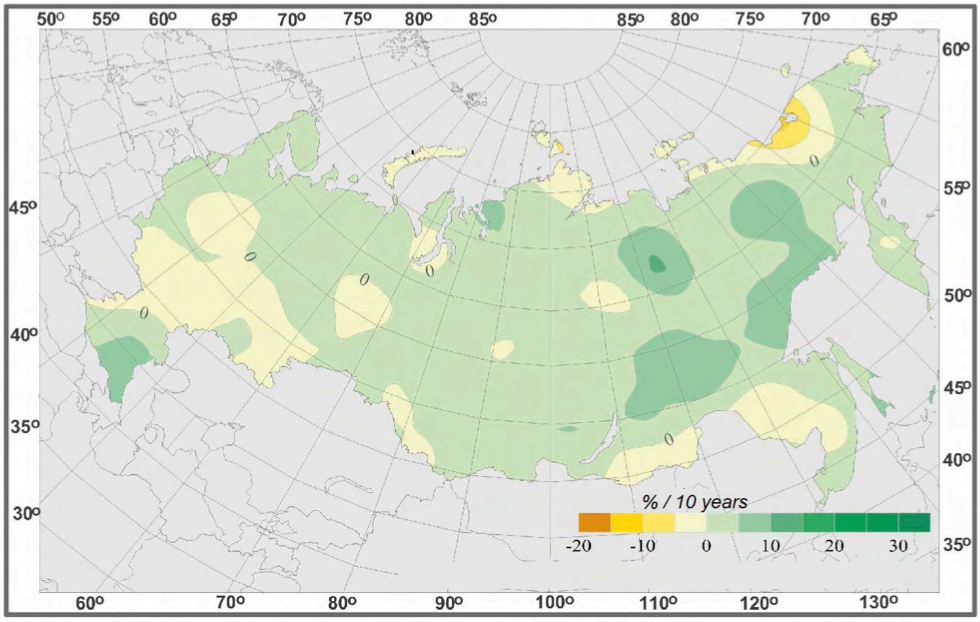

Figure 2.4: Changes in annual precipitations per decade in Russia in terms of percentage in 1976-2013

Moreover, Russia is the major emitter of greenhouse gases and, being a leading global supplier of fossil fuels, remains an influential force in international politics. Its extension occupies more than a tenth of the global land area, with nearly two-thirds underlain by methane-rich permafrost; hence, the impacts of temperature increases are likely to have global repercussions.

More than 60% of the Russian territory is covered by permafrost. The process of global warming has accelerated its destruction and it has been posited that changes in its depth may, in turn, accelerate the rate of temperature increase due to the release of large amounts of methane, which is approximately twenty-two times as potent a greenhouse gas as CO_2.

Thawing permafrost causes considerable damage to the infrastructures (**Figure 2.5**), such as the Far North roads, oil and gas pipelines, reservoirs, facilities, oil and gas industries and buildings.

The most affected regions include Chukotka, Upper Indigirka and Kolyma river basins, South-East Yakutia, a great part of the West Siberian valley, the Karskoe sea coast, Novaya Zemlya and some northern regions of European Russia. Well-developed infrastructures are present in these areas, such as gas and oil mining complexes, the

Nadym-Pur-Taz pipeline system located in North-West Siberia and Bibilinskaya atomic power station.

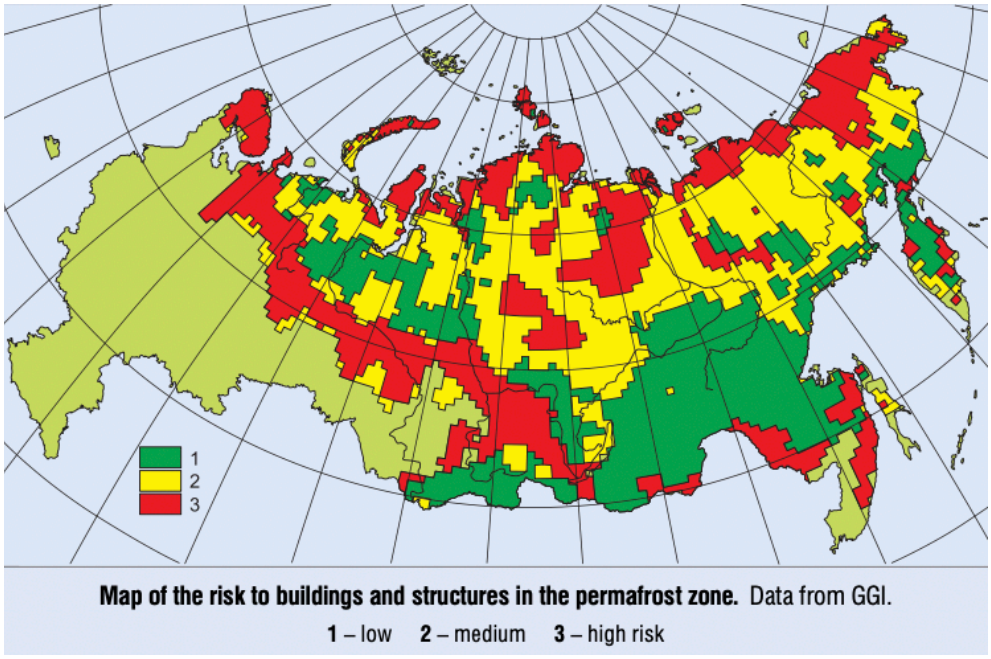

Figure 2.5: Severity level of the risk of buildings and structures located in the permafrost zone

2.2.1 CLIMATE CHANGE IN SIBERIA: CURRENT SITUATION AND FUTURE PROJECTIONS

Siberia is a vast natural region in the Asian part of Russia, bounded to the west by the Ural Mountains, to the east by watershed ranges running along the Pacific Ocean, to the north by the Arctic Ocean and to the south by the state border of the Russian Federation.

It is subdivided into Western and Eastern, although it is also possible to distinguish between Southern, North-Eastern and Central Siberia.

It has a total area of about 10 million km^2; the length from west to east is 7500 km, while from north to south is 3500 km.

Siberia is populated by about 38 000 000 inhabitants, which is 25,6% of the total population of the Russian Federation.

At present, warming has accelerated in high-latitude regions, with the mean annual temperature rising twice as fast as the global average.

On June 17, 2020, *The Guardian* reported that Russia experienced the highest temperatures in 2020, with the average from January to May being 5,3 °C above the 1951-1980 mean. On June 23, 2020, the WMO announced a new record temperature north of the Arctic Circle of 38 °C on June 20 in the Russian town of Verkhoyansk.

Compared to other zones in the Northern Hemisphere, Siberia is the region with the most significant temperature changes (1,39 °C/100 years) (**Figure 2.6**); these variations are higher than over Northern Asia (1,29 °C/100 years), the Arctic (1,28 °C/100 years) and over the entire hemisphere (0,77 °C/100 years) and it is expected that the Siberian trends will remain among the largest over the globe.

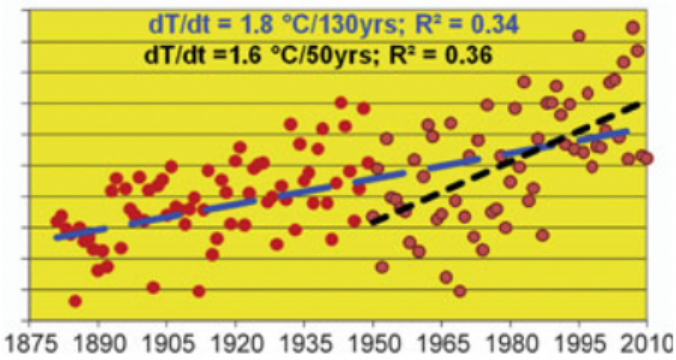

Figure 2.6: Annual surface air temperature anomalies for Siberia

Analyses of precipitations in the cold season revealed an increase over most of the region and assessments of available data showed that the maximum snow depth and the number of days with a snow cover greater than 20 cm are rising over most Siberia (**Figure 2.7**).

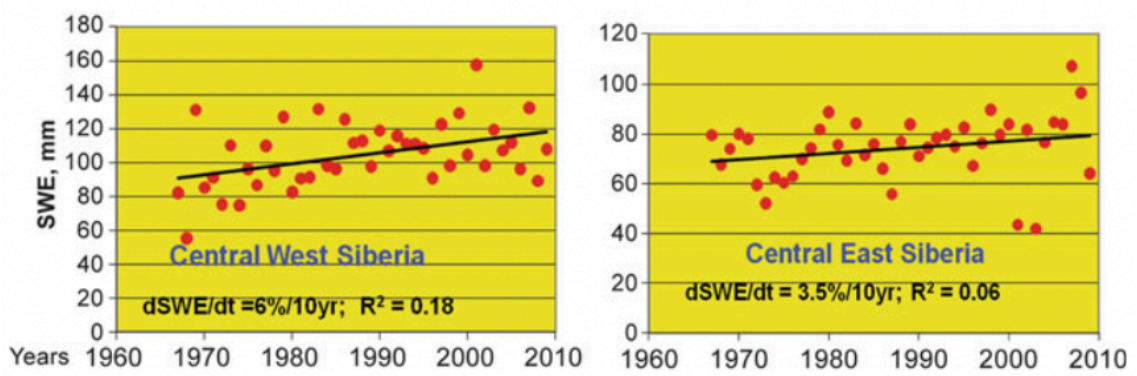

Figure 2.7: Changes in snow water equivalent over Northern Siberia

Moreover, important reductions in the heating degree days, defined as the sum of positive mean daily temperature anomalies from the base value, have been observed (between 8% and 12% over 44 years), as well as increases in the length of the frost-free period, described in **Table 2.1**.

Table 2.1: Average duration of the no-frost period (NFP) in Siberia south of the Arctic Circle and changes of its rates over the 1966-2009 period

Region	No-frost period, days	NFP change, days (10 year)$^{-1}$	NFP change, % (10 year)$^{-1}$
West Siberia, north of 55°N	110	2.3	2.1
West Siberia, south of 55°N	128	3.4	2.6
Central Siberia, north of 55°N	90	2.0	2.2
Central Siberia, south of 55°N	107	2.8	2.6

All trend estimates are statistically significant at the 0.01 level or above (except West Siberia north of 55°N where the trend estimate is statistically significant at the 0.05 level)

Figure 2.8 shows the variation of the number of days with thaw in West Siberia: it is possible to note that this value almost tripled, leading to earlier gradual snowmelt and higher following runoffs.

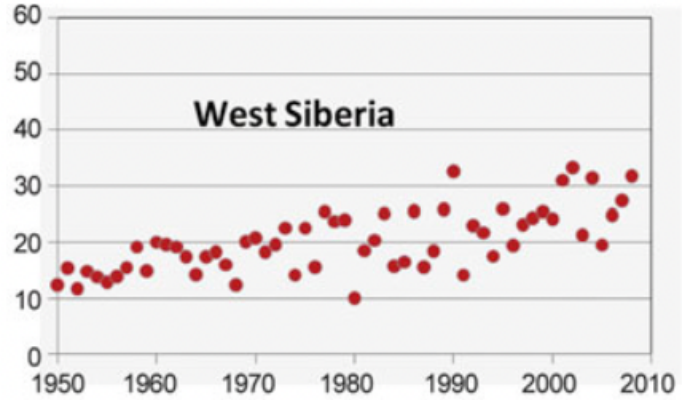

Figure 2.8: Annual number of days with thaw in West Siberia

Additionally, it has been observed that heavy and very heavy precipitations in Siberia have remarkably increased in the past five decades.

On the other hand, climate warming is expected to further increase in the 21st century: according to estimations, the surface air temperature may rise to 3 °C (even though, for some scenarios, this value may reach up to 6 °C), as shown in **Figure 2.9**.

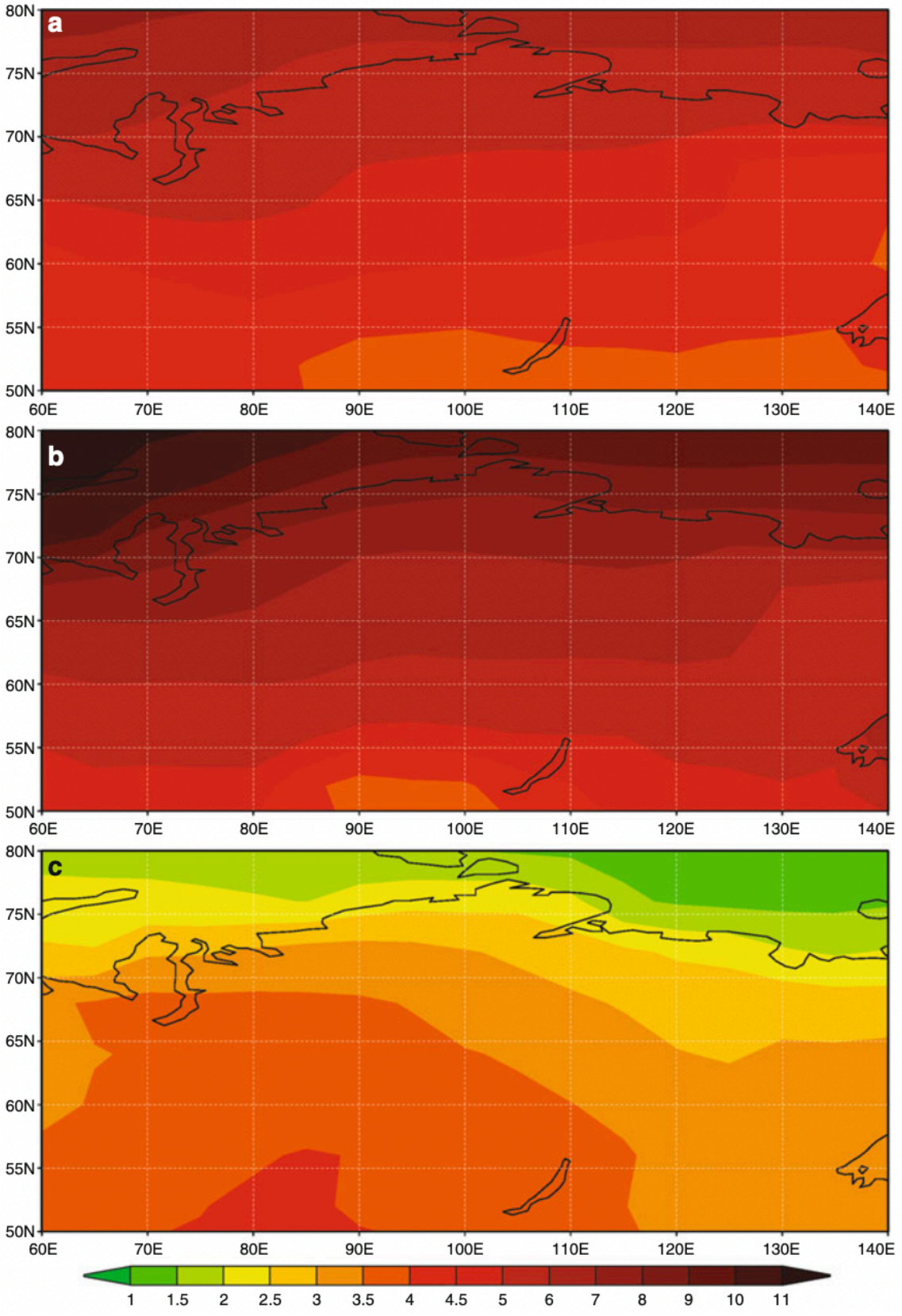

Figure 2.9: Model-derived surface air temperature changes between 2081-2100 compared with the period 1980-2000 for annual mean (a), winter mean (b) and summer mean (c)

Future projections of global climate models show that:

- T_{MAX} and T_{min} in winter will increase by 1-2 °C to the end of the 21st century in Southern Siberia and by 2-3 °C in Northern Siberia;
- T_{MAX} and T_{min} in summer will increase by 1-1,5 °C in Southern Siberia and by less than 0,5 °C in Northern Siberia;
- the frequency of precipitations will increase in winter and decrease in summer: in winter, precipitations are becoming more frequent and heavier; in summer, the overall will slightly change, but precipitation events will become less frequent and more intense;
- there is an expected increase of the permafrost table depth by 2-3 m in West Siberia, with a 0,5-1,5 m lowering in the middle of the 21st century (**Figure 2.10**);

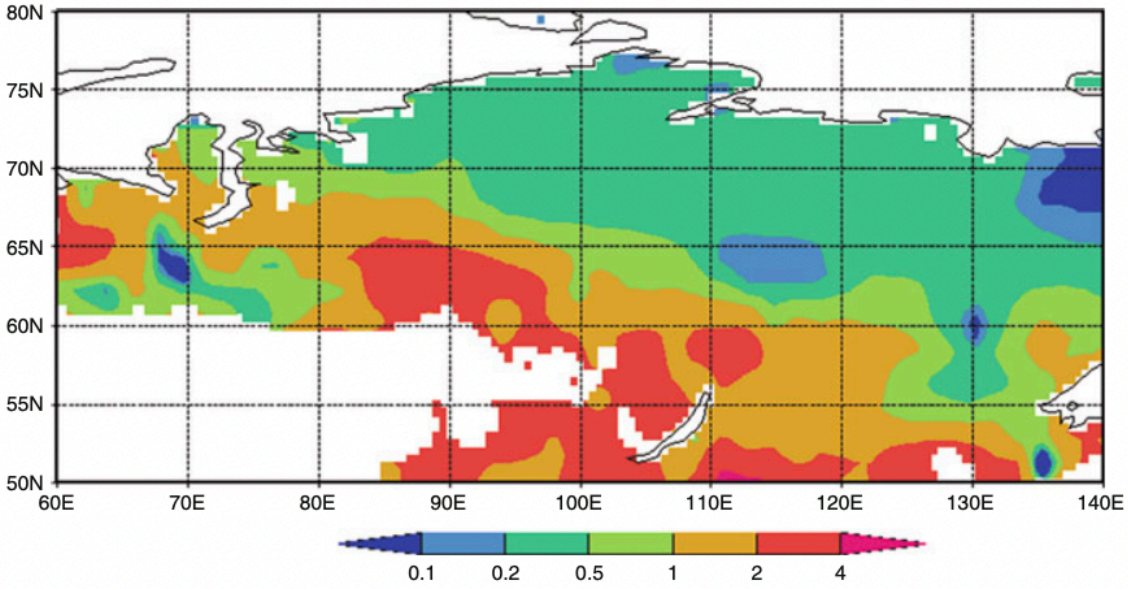

Figure 2.10: Model-derived changes of permafrost table depth for the period 2081-2100 compared with 1980-2000

- the number of days with extremely low temperatures in Northern Siberia is expected to decrease by 6-8 days by the middle of the 21st century;
- the number of days with extremely high temperatures is expected to increase up to 10-20 over Northern Siberia. In addition, the duration of periods with record hot weather is expected to rise;

- there is a strong likelihood that mutual changes of temperature and precipitation regimes over Siberia will lead to increases in probability and intensity of extreme climate and weather events such as droughts and fires: an increase of temperature by 1 °C could lead to an increase of drought areas up to 10%;
- because of early snowmelt, it is expected that the duration of fire danger weather could be prolonged by 1-1,5 months in Southern Siberia.

REFERENCES

BIBLIOGRAPHY

- Chestin I. E., Colloff N. A. – *Russia and Neighbouring Countries: Environmental, Economic and Social Impacts of Climate Change*, WWF Russia, Oxfam GB, Russian Federation, 2008;
- Ciavarella A., Cotterill D., Stott P., Kew S., Philip S., Van Oldenborgh G. J., Skålevåg A., Lorenz P., Robin Y., Otto F., Hauser Z. M., Seneviratne S. I., Lehner F., Zolina O. – *Prolonged Siberian Heat of 2020*, World Weather Attribution, United Kingdom, 2020;
- Di Gangi D., Onorati G. – *Cambiamenti climatici*, ARPAC-Relazione sullo stato dell'ambiente in Campania 2009, Italy, 2009 (in Italian);
- Furlan G. – *Cambiamento climatico: riconoscerlo e affrontarlo-Qualità della vita, rifugiati ambientali e conflitti* (master's thesis), Ca' Foscari University of Venice, Italy, 2019 (in Italian);
- Groisman P. Ya., Gutman G. – *Regional Environmental Changes in Siberia and Their Global Consequences*, Springer Environmental Science and Engineering, United States, 2013;
- Intergovernmental Panel on Climate Change – *Climate Change 2021: The Physical Science Basis-Summary for Policymakers*, Cambridge University Press, United Kingdom, 2021;
- Joint Global Change Research Institute, Battelle Memorial Institute – *Russia: the Impact of Climate Change to 2030*, National Intelligence Council, United States, 2009;
- Karlsson J., Serikova S., Vorobyev S. N., Rocher-Ros G., Denfeld B., Pokrovsky O. S. – *Carbon Emissions from Western Siberian Inland Waters*, Nature Communications, Sweden, 2021;

- Leskinen O., Lindner M., Verkerk P. J., Nabuurs G. J., Van Brusselen J., Kulikova E., Hassegawa M., Lerink B. – *Russian Forests and Climate Change*, What Science Can Tell Us 11, European Forest Institute, Germany, 2020;
- Sharmina M., Anderson K., Bows-Larkin A. – *Climate Change Regional Review: Russia*, Wiley Interdisciplinary Reviews Climate Change, John Wiley & Sons, United Kingdom, 2013.

SITOGRAPHY

- https://it.wikipedia.org/wiki/Russia (in Italian);
- https://ru.wikipedia.org/wiki/Сибирь (in Russian).

Part 2:

Experimentation

DESCRIPTION OF THE AREAS UNDER INVESTIGATION

The following chapter contains a detailed description of the areas and the test sections to which available data are referred; deep knowledge of the geographic location, the climatic zone, soils and materials properties (both in terms of pavement strata and subgrade), thicknesses, etc. of the investigated sites are fundamental to perform an accurate climate change assessment and carry out a valid pavement design, which is the goal of this master's thesis.

As already mentioned, two sites have been chosen for the analyses: Tomsk, located in the southwest of the Siberian Federal District, and Salekhard, based in the Arctic Circle, in the Yamalo-Nenets Autonomous Okrug, West Siberia (**Figure 3.1**).

Figure 3.1: Location of the analyzed sites

3.1 TOMSK

Tomsk is a small city of about 600 000 inhabitants with an extension of 294,6 km^2 located in the east of Western Siberia, on the banks of river Tom; it is the administrative center of the Tomsky District.

It has a latitude of 56°29′51′′N and a longitude of 84°58′27′′E and it is 117 m above sea level.

The city is located on the border of the West Siberian Plain and the Kuznetsk Alatau on the right bank of river Tom, 50 km from its confluence with river Ob.

The offset of the applicable time from UTC is +7:00; in accordance with the applied time and geographic longitude, the mean solar noon occurs at 1:20 pm.

Within the framework of the administrative divisions, Tomsk is a city of regional subordination, the districts of which are subordinate to seven rural localities. It forms the municipal formation of the Tomsk City under oblast jurisdiction, with the status of urban district, which includes eight settlements (one city and seven rural zones); districts in the city are not municipalities and are non-independent administrative-territorial units.

As a municipal division, Tomsk City under oblast jurisdiction is incorporated as Tomsk Urban Okrug.

Tomsk is administratively divided into four city districts: Kirovsky, Leninsky, Oktyabrsky and Sovetsky (**Figure 3.2**).

Figure 3.2: Tomsk districts subdivision

Tomsk is located on the edge of the natural taiga zone: impenetrable forests and swamps stretch to the north, while broad-leaved and mixed forests and forest-steppes alternate to the south.

The city's terrain is uneven and characterized by a height difference reaching 70 m; the following elements of the river valley are distinguished: floodplain, terraces and the interfluves of the Tom-Malaya Kirgizka and Tom-Ushayka watersheds.

Tomsk is characterized by a continental-cyclonic climate (transitional from European temperate continental to Siberian sharply continental), with long severe winters and short, sometimes hot, moderately humid summers; the cold period of the year begins in

November, with the formation of a permanent snow cover that lasts about 170 days. A more detailed description of average, minimum and maximum temperatures, as well as total precipitations, is reported in *chapter 7*.

The location of the city in the zone of sharply continental climate, rugged terrain, high standing of groundwater and loose rocks easily amenable to erosion contribute to the development of ravines and landslides, which are very common in different parts of the city.

3.1.1 ROAD-CLIMATIC CLASSIFICATION

According to Russian regulations, pavements design and analysis depends on the so-called road-climatic zoning (for more details, please refer to *annex 2*, **Figure P.2.2** and **Table P.2.7**).

The basis for the detailed zoning of the Tomsk region is the taxonomic system, which makes a distinction among zone, sub-zone and district.

In this classification, the "road area" taxon corresponds to a homogeneous territory characterized by typical and similar conditions, such as climate, geology and topography. Moreover, on the territory of the road area, the same types of road structures are characterized by approximately comparable strength and stability.

According to the results of previous studies, three road-climatic zones (RCZ I, II and III), two sub-zones (flat and hilly) and six areas are recommended for the territory of the Tomsk region (**Figure 3.3**).

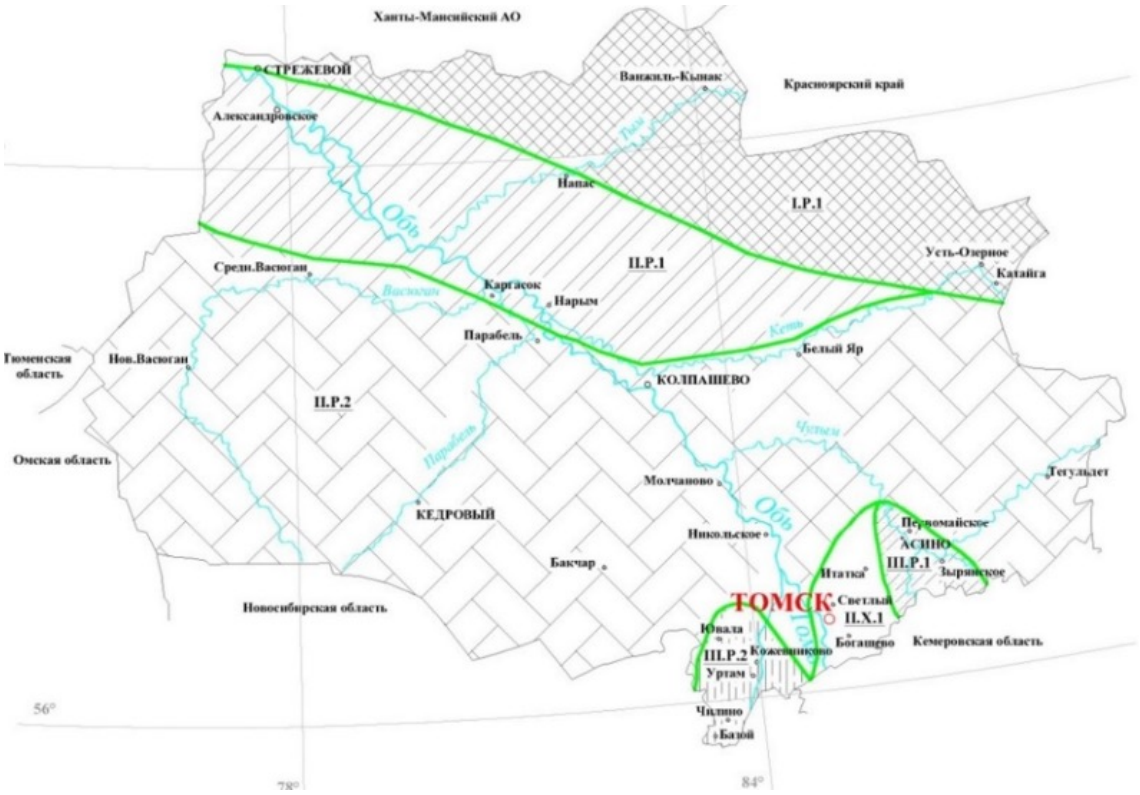

Figure 3.3: Schematic map of the road-climatic zoning of the territory of the Tomsk region

To characterize the moisture content of individual road areas on the territory of Tomsk, Selyaninov's hydrothermal coefficient was adopted, which is calculated according to the following formula:

$$K_s = \frac{P}{\sum \frac{T_{>10}}{10}}$$

where P is the sum of precipitation amounts and $T_{>10}$ is the sum of the temperatures for the months with mean temperature >10 °C.

This index has been applied in different studies related to the determination of moist and dry periods, the favorability of climate for agriculture or natural vegetation development and economic investigations, according to **Table 3.1**.

Table 3.1: Climate classification according to Selvaninov's coefficient

K_s	**Climate classification**
0,3	Very dry or arid

0,31-0,6	Dry
0,61-0,8	Moderately dry
0,81-1	Slightly dry
1,01-1,2	Slightly humid
1,21-1,4	Moderately humid
1,41-1,6	Humid
>1,61	Very humid

For RCZ III, a value of K_s=1÷1,4 is suggested, for zone II, K_s>1,4, whereas moisture content is not a characteristic indicator for zone I.

According to the road-climatic zoning, the study area belongs to zone II, hilly sub-zone and road area 1; **Table 3.2** shows the characteristics of the study area in the Tomsk region.

Table 3.2: Characteristics of Tomsk region soil

Characteristics of the road-climatic zone	**Characteristics of the road area**		
	Type of landscape	**Ground conditions**	**Moisture content (according to Selvanivov)**
Geographic zone of forests with excessive soil moisture	Hilly	Eluvial, deluvial, aeolian and lacustrine-alluvial deposits: loess-like loam, sandy loam and loess, sandy, gravelly soil	1,5-1,8

3.1.2 DESCRIPTION OF THE TEST SECTIONS

For both sites, several test sections have been equipped with a series of sensors TEROS 11 at different depths to collect data regarding subgrade temperature and volumetric water content; a detailed description of the principles on which these devices work is contained in *chapter 3*.

There are eight available test sections in Tomsk, all located in the Bogashevo-Luchanovo-Steklozavod road, connecting the city to Tomsk Bogashevo Airport.
Sensors are placed at a distance of 75 cm from the asphalt shoulder, at a depth of 40 cm, 70 cm and 140 cm from the pavement subgrade; a schematic representation of their position is reported in **Figure 3.4**.

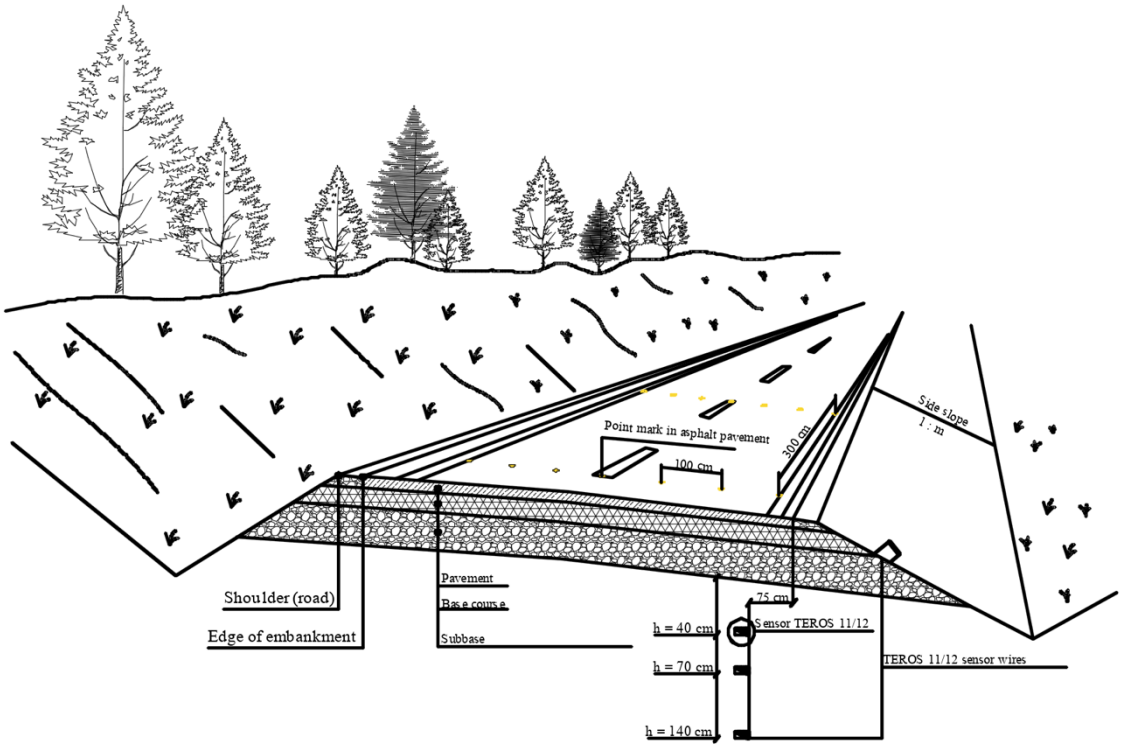

Figure 3.4: Sensors position for Tomsk test sections

Every section is also equipped with six rows of point marks at a relative longitudinal distance of 3 m; each line is constituted by seven markers with a transversal interspacing of 1 m, for a total width of 7 m. These elements constitute the reference location for the evaluation of the road vertical displacements (due to thaw heave) with respect to a landmark located outside the pavement system; this procedure is realized by means of a tacheometer and is generally carried out during the spring season: vertical displacements analysis will not be covered in this master's thesis.
Table 3.3 contains a detailed description of the position, materials and thicknesses of each section; the longitudinal slope of the carriageway ranges between 16‰ and 25‰.

Table 3.3: Tomsk test sections

Test section location*	**Pavement structure**		**Pavement subgrade material**
	Material	**Thickness [cm]**	
PK 11+23-PK 11+38	New asphalt concrete	8	Clayey soil
	RAP+cement+bitumen	15	
	Old asphalt concrete	35	
	Gravel-sand mix	19	
PK 12+91-PK 16+06	New asphalt concrete	10	
	Old asphalt concrete	25	
	Gravel-sand mix	27	
PK 23+54-PK 23+609	New asphalt concrete	9	
	RAP+cement+bitumen	17	
	Old asphalt concrete	18	
	Crushed stone	10	
	Gravel-sand mix	30	
	Geosynthetic non-woven fabric	/	
PK 24+56-PK 24+71	New asphalt concrete	10	
	Old asphalt concrete	5	
	Crushed stone	25	
	Geosynthetic non-woven fabric	/	
PK 28+80-PK 28+95	New asphalt concrete	10	
	RAP+cement+bitumen	15	
	Old asphalt concrete	12	
	Crushed stone	23	
	Geosynthetic non-woven fabric	/	
PK 30+08-PK 30+24	RAP+cement+bitumen	18	

	RCC	20	
	Gravel-sand mix	20	
PK 37+13-PK 37+28	RAP+cement+bitumen	15	
	Gravel-sand mix	20	
PK 37+97-PK 38+12	RAP	16	
	RCC	20	
	Gravel-sand mix	30	

**PK (picket) indicates a road section with a length of 100 m.*

Some images of Tomsk test sections are shown in **Figure 3.5** to **Figure 3.9**.

Figure 3.5: Test section 1 in Tomsk

Figure 3.6: Test section 4 in Tomsk

Figure 3.7: Test section 5 in Tomsk

Figure 3.8: Test section 6 in Tomsk

Figure 3.9: Test section 6 in Tomsk

As regards the subgrade, results from laboratory tests conducted in the Road Construction Faculty of TSUAB are reported in **Table 3.4** (materials from different test sections have been analyzed); soil classification has been performed following the standard ASTM D2487-17e1: *Standard Practice for Classification of Soils for Engineering Purposes (Unified Soil Classification System)*.

Table 3.4: Subgrade soil properties in Tomsk

Section number	Depth from the pavement bottom [m]	Particle density [g/cm³]	Water content [%]	Plastic limit	Liquid limit	Plasticity index	Liquidity index
1	0,7	2,62	26,19	25,6	34,67	9,06	0,06
2	0,7	2,75	28,94	18,57	31,36	12,79	0,03
3	1	2,66	15,23	10,03	25,4	15,37	0,33
4	0,4	2,7	25,1	26,1	42,9	16,8	<0
4	1	2,63	30,31	27,75	44,68	18,39	0,151
5	1	2,59	30,28	29,44	46,62	17	0,05
6	1	2,68	21,35	18,33	28,34	10,01	0,3
7	1	2,69	23,75	20,4	30,75	10,35	0,324
8	0,4	2,61	13,25	22,61	32,89	10,61	<0
8	1	2,66	22,31	23,11	36,33	13,22	<0

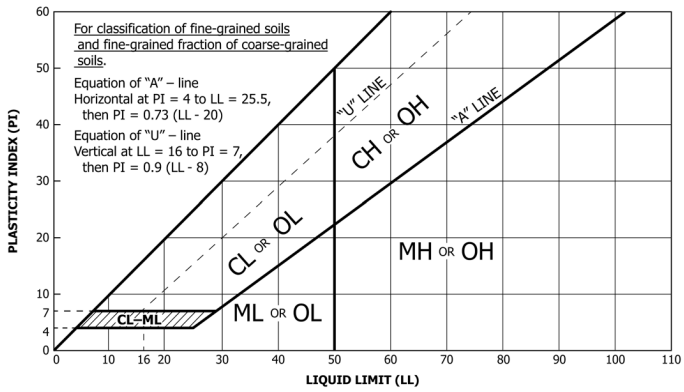

Figure 3.10: Plasticity chart

The soil can be classified as lean clay from the plasticity chart (**Figure 3.10**).

3.2 SALEKHARD

Salekhard is a town of about 50 000 inhabitants with an extension of 84,5 km^2 located in West Siberia; it is the administrative center of the Yamalo-Nenets Autonomous Okrug, which is part of the Tyumen region.
It has a latitude of 66°31'48''N and a longitude of 66°36'06''E and it is located 26 m above sea level; it is the only city in the world directly on the Arctic Circle.
Salekhard is located on the Poluy upland of the West Siberian Plain at the confluence of river Poluy with river Ob.
The offset of the applicable time from UTC is +5:00; in accordance with the applied time and geographic longitude, the mean solar noon in Salekhard occurs at 12:33 pm.

Within the framework of administrative divisions, it is, together with one rural locality, incorporated as the town of okrug significance of Salekhard, an administrative unit with a status equal to that of the districts.
As a municipal division, the town of okrug significance of Salekhard is incorporated as Salekhard Urban Okrug.
The city is located on the border of the subarctic and temperate climatic zones; summers are short and mild, while winters are severely cold (there are up to 200 days with stable frost and snow cover per year). Precipitations are moderate and significantly greater in summer than in winter; a more detailed description of average, minimum and maximum temperatures, as well as mean precipitations, is reported in *chapter 7*.

3.2.1 ROAD-CLIMATIC CLASSIFICATION

According to the road-climatic zoning, the study area belongs to zone I, flat sub-zone and road area 1-2 (**Figure 3.11**); **Table 3.5** shows the characteristics of the analyzed

sites in the Salekhard region (note that in this case, Selvaninov's hydrothermal coefficient is not a characteristic indicator).

Figure 3.11: Schematic map of the road-climatic zoning of the territory of the Yamalo-Nenets Autonomous Okrug

Table 3.5: Characteristics of the main elements of the geocomplexity of road areas on the territory of the Yamalo-Nenets Autonomous Okrug

Road-climatic zone	Characteristics of the road-climatic zone	Road area	Administrative center of the district	Characteristics of the road area	
				Type of landscape	Soil/permafrost conditions
I	Geographical zone characterized by vegetation typical of the tundra, forest-tundra and the northeastern part of the forest zone, which is typified by the distribution of permafrost soils	I.R.1	Novy Urengoy, Nadym, Shchuchye, Nyda	Flat	*
		I.H.1	Mount Kosvinsky Kamen	Hilly	
		I.G.1	Oche-Nyrd ridge, Khanmei ridge	Mountainous	
		I.R.2	Noyabrsk, Tarko-Sale, Muzhi, Pitlyar, Tolka	Flat	**
		I.H.2	Kharp	Hilly	
		I.G.2	Pik Polyarnii, Mount Payer, Mount Skalnaya	Mountainous	

**Ubiquitous distribution of permafrost soils, the thickness of which ranges from 200 m to 900 m (in some cases, even more than 900 m); the average annual temperature is -3/-5 °C to -12 °C and lower. Seasonal thaw depth ranges from 0,2 m to 2 m (predominant depth <1 m). Soils are characterized by a high content of various types of ice. Clayey, dusty, silty, tundra and marsh soils are widespread.*

***Almost ubiquitous distribution of permafrost soils, the thickness of which is 50 m to 400 m, and the average annual temperature is in the range of -1 °C to -5 °C. The depth of seasonal thawing is from 0,8 m to 3 m. Rocky, crushed stone, gravel-pebble and clayey soils are the most widespread. The intensive development of cryogenic processes characterizes the territory.*

3.2.2 DESCRIPTION OF THE TEST SECTIONS

For the case of Salekhard, sensors have been installed in eleven different test sections, as shown in **Figure 3.12**, characterized by both flexible and semi-rigid pavements; **Table 3.6** contains a description of the names and the locations in terms of latitude and longitude of the investigated points.

In this case, sensors are positioned at a depth of 50 cm, 100 cm and 150 cm from the pavement subgrade, as shown in **Figure 3.13**.

However, it should be noted that only five points are able to provide continuous information (hence, without the help of a data logger, which means no need for in-situ collection), three of which are semi-rigid pavements: for the purpose of the analysis, only values coming from flexible sections, i.e., 1 and 11, will be taken into account.

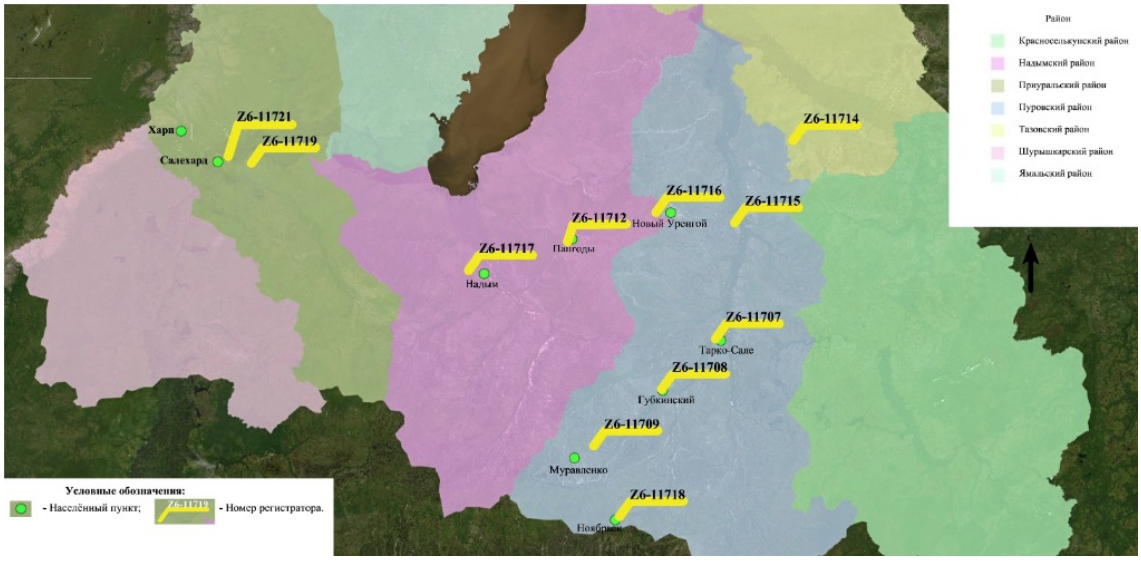

Figure 3.12: Distribution of Salekhard test sections

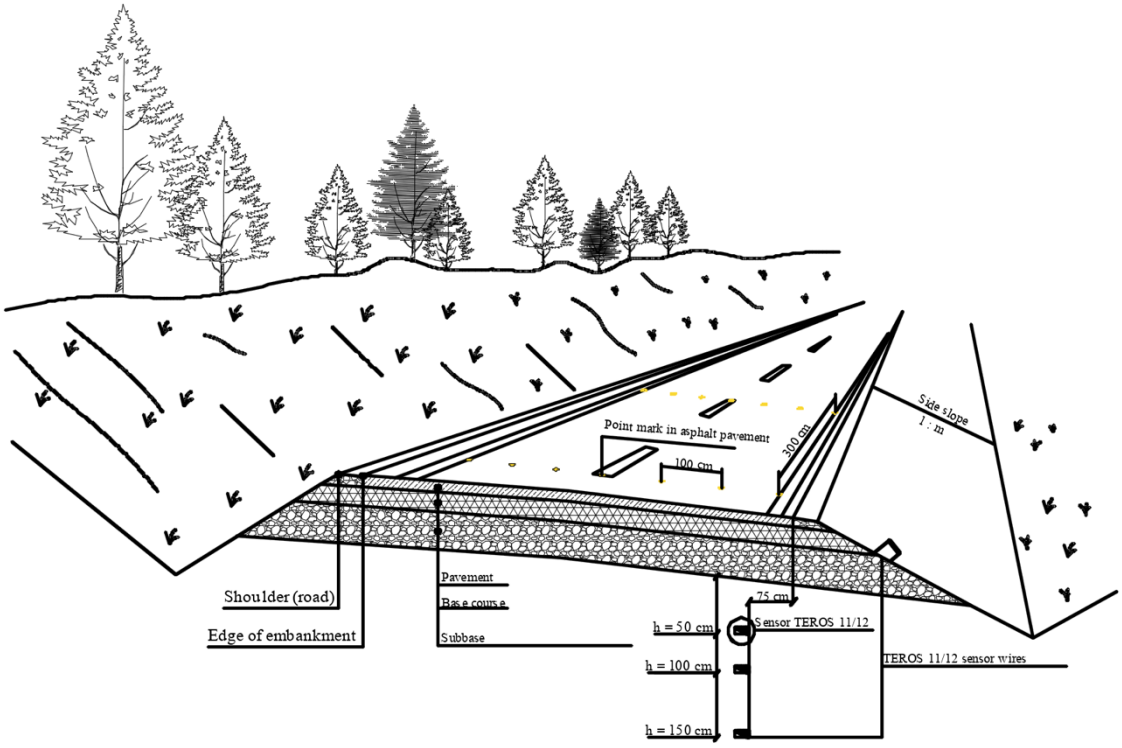

Figure 3.13: Sensors position for Salekhard test sections

Table 3.6: Geographical location of Salekhard test sections

Test section number	Sensor identification number	Geographical coordinates	
		Latitude	Longitude
1	Z6-11721	66°34'56,04''	66°51'26,17''
2	Z6-11719	66°31'41,54''	67°22'2,26''
3	Z6-11717	65°33'30,03''	72°11'40,22''
4	Z6-11712	65°49'3,9''	74°23'1,16''
5	Z6-11716	66°5'13,84''	76°20'57,61''
6	Z6-11714	66°43'28,01''	79°24'19,74''
7	Z6-11715	65°59'28,68''	78°5'37,36''
8	Z6-11707	64°55'19,37''	77°40'32,73''
9	Z6-11708	64°26'44,09''	76°28'14,4''
10	Z6-11709	63°53'35,69''	74°58'20,72''
11	Z6-11718	63°12'8,88''	75°33'10,93''

Note: loggers that provide continuous data are highlighted in green.

Table 2.7 contains a detailed description of the pavements stratigraphy and materials.

Table 3.7: Salekhard test sections

Test section location	**Pavement structure**		**Pavement subgrade material**
	Material	**Thickness [cm]**	
Access to village Gornoknyazevsk, km 1+695	Asphalt concrete	15	Sand
	Crushed stone	19	
	Sand	16	
	Gravel-sand mix	62	
Access to village Kharsaim, km 3+000	Gravel-sand mix	22	
Surgut-Salekhard, Nadym-Salekhard district, km 1000+000-km 1060+000	Asphalt concrete	13,5	
	Crushed stone	35,5	
Surgut-Salekhard, Pangody-Pravokhettinsky district, km 874+000	Asphalt concrete	17	
	Crushed stone	28	
Surgut-Salekhard, Novy Urengoy-Nyda railway station district, km 772+000	Asphalt concrete	16	
	Crushed stone	37	
Korotchaevo-Novozapolyarny, km 125+000	Asphalt concrete	16	
	Crushed stone	8	
	Concrete slab	16	
	Geosynthetic non-woven fabric	/	
Access to village Limbyayakha, km 2+000	Asphalt concrete	6	
	Concrete slab	18	

	Sand+cement	26	
Access to Tarko-Sale town, km 5+000	Asphalt concrete	11	
	Concrete slab	12	
Surgut-Salekhard, bypass Gubkinsky town, km 465+000	Asphalt concrete	11	
	Crushed stone	26	
Access to village Khanymey, km 5+000	Asphalt concrete	8,5	
	Concrete slab	14	
	Sand	10	
Noyabrsk-Vyngapurovsky, km 8+000	New asphalt concrete	6	
	Gravel-sand mix	7	
	Old asphalt concrete	7	
	Crushed stone	10	

Finally, regarding the subgrade soil, previous tests conducted in the TSUAB Road Construction Faculty laboratory allowed to perform classification and derive the main material properties, summarized in **Table 3.8** (results available only for a few loggers).

Table 3.8: Subgrade soil properties in Salekhard

Test number	Logger	Soil description	Density [g/cm³]			Natural humidity [%]	Porosity [%]	Porosity coefficient	Degree of humidity	Full moisture capacity [%]
			Particle	Wet	Dry					
			ρ_S	ρ	ρ_d	W_e	n	e	S_r	W_{sat}
1	*Z6-11715*	Medium sand	2,66	1,53	1,478	3,5	44,426	0,7944	0,1165	30,053
2	*Z6-11721*	Dusty sand	2,67	1,5	1,423	5,4	46,699	0,8761	0,1646	32,813
3	*Z6-11714*	Fine sand	2,64	1,47	1,373	7,1	48,01	0,9234	0,203	34,978
4	*Z6-11707*	Fine sand	2,65	1,44	1,381	4,3	47,901	0,9194	0,1239	34,695
5	*Z6-11718*	Dusty sand	2,61	1,71	1,542	10,9	40,922	0,6927	0,4107	26,54

REFERENCES

BIBLIOGRAPHY

- ASTM D2487-17e1: *Standard Practice for Classification of Soils for Engineering Purposes (Unified Soil Classification System)*, American Society for Testing Materials International, United States, 2017;
- Efimenko S. V., Badina M. V. – *Road Zoning of the Territory of Western Siberia*, Publishing House of Tomsk State University of Architecture and Building, Russian Federation, 2014 (in Russian);
- Efimenko S. V., Efimenko V. N., Badina M. V., Sukhorukov A. V., Churilin V. S., Afinogenov A. O. – *Standardization of Estimated Values of Clayey Soil Properties for the Quality Assurance in Road Design in Kuzbass*, Publishing House of Tomsk State University of Architecture and Building, Russian Federation, 2015 (in Russian);
- Evarte-Bundere G., Evarts-Bunders P. – *Using of the Hydrothermal Coefficient (HTC) for Interpretation of Distribution on Non-Native Tree Species in Latvia on Example of Cultivated Species of Genius Tilia*, Acta Biologica Universitatis Daugavpiliensis, Latvia, 2013;
- Vlădut A., Nikolova N., Licurici M. – *Aridity Assessment within Southern Romania and Northern Bulgaria*, Hrcatski Geografski Glasnic, Croatia, 2017.

SITOGRAPHY

- http://ecology-of.ru/priroda/klimat-goroda-tomsk/ (in Russian);
- http://www.worldclimateguide.co.uk/guides/russia-central-asia/;
- https://dateandtime.info/citycoordinates.php?id=1493197;
- https://dateandtime.info/it/citycoordinates.php?id=1489425;
- https://en.wikipedia.org/wiki/Tomsk;
- https://ru.wikipedia.org/wiki/Салеха́рд (in Russian);

- https://ru.wikipedia.org/wiki/Томск (in Russian);
- https://rutraveller.ru/resort/2631 (in Russian).

SENSORS THEORY AND CALIBRATION

The following chapter provides a summarized description of the main features that characterize the sensors installed in the investigated test sections in order to provide the readers with general knowledge on how these devices work; if more information is required, please refer to the official manuals.
In particular, TEROS 11 sensors produced by the American corporation METER Group have been used.

4.1 SENSORS PRINCIPLES

TEROS 11/12 are designed to measure the volumetric water content, the temperature and the electrical conductivity (TEROS 12 only) in soils and soilless substrata; a schematization is shown in **Figure 4.1**.
These devices determine the water content using capacitance/frequency domain technology and have an operating frequency of 70 MHz, which minimizes the effects of soil heterogeneity and salinity on the readings.
In particular, the volumetric water content (VWC) is measured between the needle 1 and 2, while the electrical conductivity (EC) between needle 2 and 3 by means of a thermistor installed in the center of the pointer using a stainless-steel electrode array.
A ferrite bar located 7,6 cm from the sensor isolates it from any interference (noise) in the signal.
When determining the volumetric moisture, the device range corresponds to 1010 ml (**Figure 4.2**).

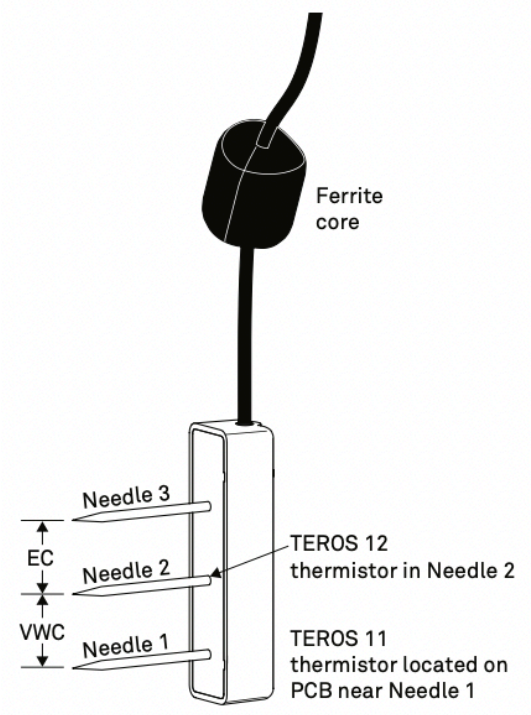

Figure 4.1: TEROS 11/12 scheme

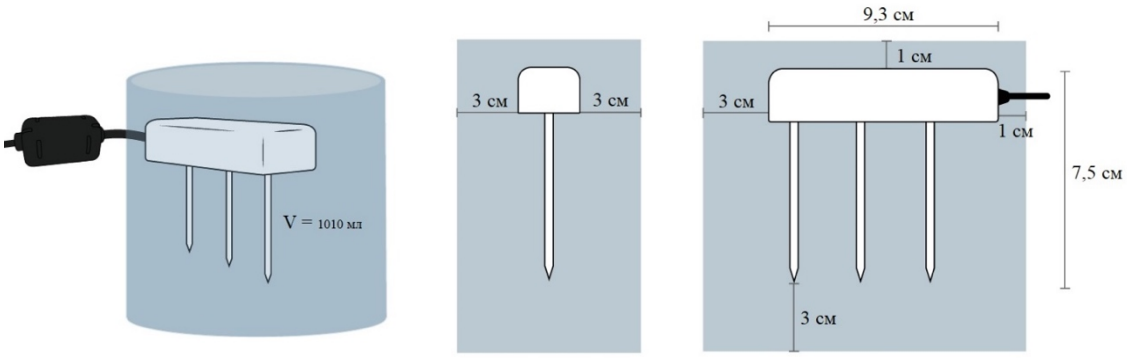

Figure 4.2: TEROS 11/12 volume of influence

These sensors have a low power requirement, making them ideal for permanent burial in the soil and continuous reading with a data logger or periodic reading with a handheld reader.

TEROS 11/12 sensors use an electromagnetic field to measure the dielectric permittivity of the surrounding medium. The device supplies a 70 MHz oscillating wave to the needles, which charge according to the material dielectric: the charge time is proportional to the substrate dielectric and volumetric water content.

TEROS 11/12 microprocessor measures the charge time and outputs a raw value based on the substrate dielectric permittivity; this number is then converted to VWC by a calibration equation specific to the substrate.
A generic formula is provided in the manual of the sensors:

$$VWC = 3{,}879 \cdot 10^{-4} \cdot RAW - 0{,}6956$$

where VWC [m^3/m^3] is the volumetric water content and RAW is the raw sensor output when read through the data logger.
However, it should be noted that the TEROS 11/12 are not sensitive to soil texture and electrical conductivity variations due to the fact that they run at a high measurement frequency; therefore, the generic calibration formula should result in reasonable absolute accuracy.

4.2 SENSORS CALIBRATION

The Road Construction Faculty of TSUAB adopted the following laboratory procedure to check and calibrate the basic equation. It should be noted that at the moment, researchers are still working on a calibration formula to be implemented in Salekhard data; hence, all the considerations below are only referred to Tomsk soil.

A box containing a soil volume greater than the sensors coverage area was assembled (**Figure 3.3**); the surface was covered with waterproof adhesive tape to prevent moisture seepage into the wooden structure.

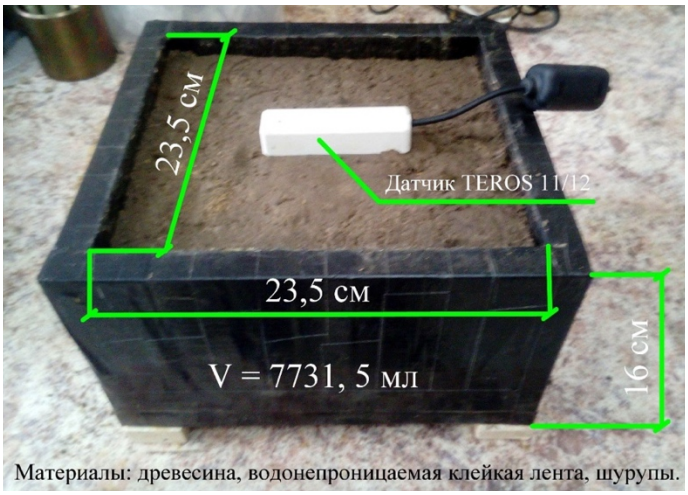

Figure 4.3: Generic view of the test box

Before taking the measurements, the sensor was covered with compacted soil for at least 1 cm.

After fixing the readings by the ProCheck recorder, the soil was carefully removed from the sensor and the device pulled out.

The next stage is to determine the density of the dry soil by the cutting ring method, following the Russian specification GOST 5180-2015: *Soils. Laboratory Methods for the Determination of Physical Characteristics*: three steel rings with a volume of 50 cm^3 were pressed in at different depths (**Figure 4.4**).

Figure 4.4: A pressed ring from the ground surface

Each cutting ring has been numbered and pre-weighted before testing.

The depressed device was then carefully trimmed and the protruding soil cut off the edges; the surface was then leveled and weighed on a balance with a sensitivity of 0,01 g.

Water was removed from the soil sample by putting it in an oven: drying was carried out at a temperature of 70 °C for two days.

The weight moisture content of the soil w is determined by the formula:

$$w = 100 \cdot \frac{m_1 - m_0}{m_0 - m}$$

where m_1 is the mass of the wet soil with the ring, m_0 is the mass of the dry soil with the ring and m is the mass of the ring.

The density of the dry soil ρ_{dry} is determined according to the equation:

$$\rho_{dry} = \frac{m_{dry}}{V}$$

in which m_{dry} is the mass of the dry sample without the ring and V is the volume.

The transition from the volumetric to the weight water content is carried out according to the following formula:

$$w = \frac{VWC}{\rho_{dry}}$$

Two experimental relationships between the RAW values from TEROS 11/12 and VWC have been developed from preliminary laboratory tests (**Figure 3.5**):

$$VWC = 3{,}952 \cdot 10^{-4} \cdot RAW - 0{,}6956$$

$$VWC = 0{,}3143 \cdot lnRAW - 2{,}1367$$

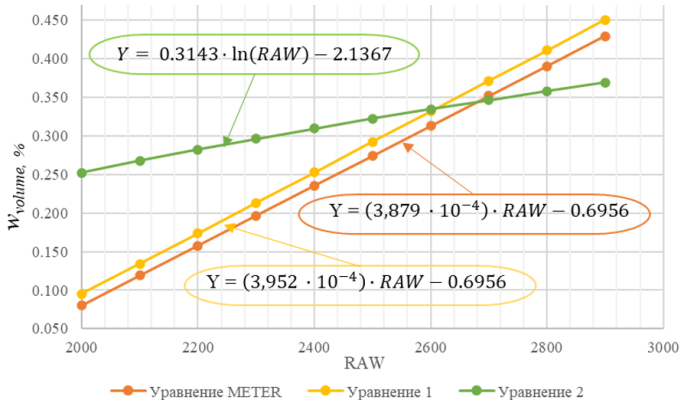

Figure 4.5: Theoretical relationships between RAW and VWC

The figure shows a significant difference between the second equation and the standard formula. To evaluate their adequacy, a comparison between the calculated moisture content and the one obtained in the laboratory through the cutting ring method was performed; the results are listed in **Table 4.1** (all measurements are related to the Bogashevo-Luchanovo-Steklozavod road, except for the first three rows, which are referred to the village of Loskutovo, in the Tomsk region)

Table 4.1: Results of calibration tests for TEROS 11/12 sensors

ρ_{dry} [g/cm³]	RAW	w [%] (from the cutting ring method)	w [%] (from equations)		
			Standard equation	Equation 1	Equation 2
1,6430	2806	0,2144	0,2391	0,2516	0,2183
1,6873	2611	0,1991	0,1880	0,1994	0,1992
1,6053	2611	0,2022	0,1976	0,2095	0,2093
1,6298	2582	0,1986	0,1877	0,1994	0,2040
1,5879	2570	0,1919	0,1897	0,2016	0,2085
1,4350	2310	0,1377	0,1397	0,1515	0,2074
1,4519	2249	0,1156	0,1218	0,1331	0,1992
1,6143	2531	0,1761	0,1774	0,1888	0,2021
1,4159	2423	0,1718	0,1725	0,1851	0,2208
1,5692	2566	0,1776	0,1910	0,2030	0,2107

In this case, the weight water content calculated through the cutting ring method was determined as the mean between the three measurements.

The comparison diagrams are reported in **Figure 4.6**, **Figure 4.7** and **Figure 4.8**.

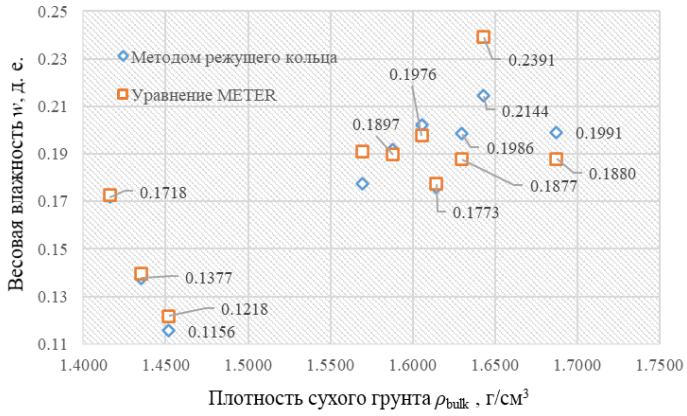

Figure 4.6: Soil moisture comparison between the cutting ring method and the standard equation

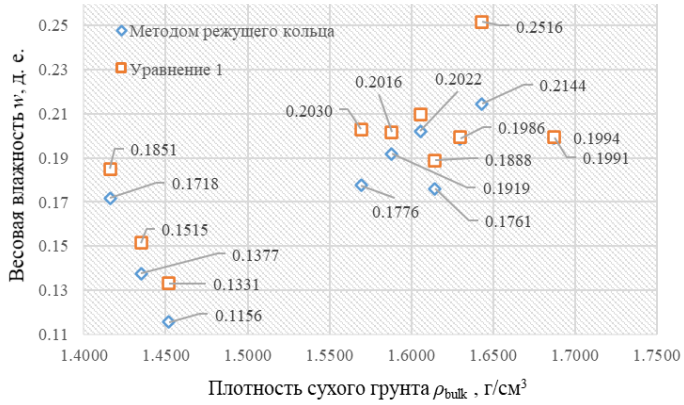

Figure 4.7: Soil moisture comparison between the cutting ring method and equation 1

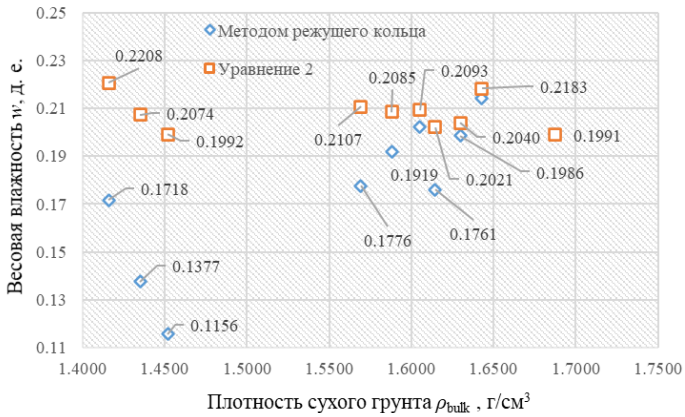

Figure 4.8: Soil moisture comparison between the cutting ring method and equation 2

It can be concluded that the equation proposed by METER Group shows good convergence (error≈2%) with the results obtained through the cutting ring method. On the other hand, the logarithmic equation is unsuitable for the data, except for a specific range of RAW values between 2600 and 2800.

REFERENCES

BIBLIOGRAPHY

- Efimenko S. V., Efimenko V. N., Badina M. V., Sukhorukov A. V., Churilin V. S., Afinogenov A. O. – *Standardization of Estimated Values of Clayey Soil Properties for the Quality Assurance in Road Design in Kuzbass*, Publishing House of Tomsk State University of Architecture and Building, Russian Federation, 2015 (in Russian);
- GOST 5180-2015: *Soils. Laboratory Methods for the Determination of Physical Characteristics*, Interstate Council for Standardization, Metrology and Certification (ISC), Moscow Standartinform, Russian Federation, 2019 (in Russian);
- *TEROS 11/12 user's manual*, METER Group, United States, 2018-2019.

Part 3:

Modeling

TEMPERATURE ASSESSMENT

This analysis aims to find a heat transfer model that can be representative of the test sections; in particular, an approach able to link the air and pavement temperature values with the subgrade data available from the sensors is needed.
After an in-depth literature review and a comparison among several methodologies, the best solution was found to be a combination of different temperature models.
It is hoped that the following outcomes will provide a valuable and straightforward tool for researchers to be used for past and future climate-related pavement analyses.

5.1 AVAILABLE DATA

As already mentioned, there are eight available test sections in Tomsk and eleven in Salekhard. Among the latter, only five of them do not require on-site data collection, three of which are semi-rigid pavements. Accordingly, for the purpose of this master's thesis, only two sections will be considered.
Sensors in Tomsk have been installed during the summer season in 2020; temperature and VWC data are available for the dates reported in **Table 5.1**.

Table 5.1: Available dates in Tomsk

Year	Available dates
2020	14/10-07/11-05/12-26/12
2021	15/01-23/01-06/02-11/02-27/02-13/03-20/03-27/03-03/04-10/04-16/04-24/04-30/04-12/05-18/05-03/06-04/09-18/09-25/09-12/10

Sensors in Salekhard have been installed during the summer season in 2021; in this case, daily temperature and VWC information are available between November 1 and December 5, 2021.
However, it should be noted that VWC data have not yet been calibrated; hence, they are still unusable.

5.2 DEVELOPMENT OF A TEMPERATURE MODEL

In order to calculate the temperature in the asphalt layers at different depths, the equation proposed by Park et al. can be used; this model was developed considering data collected from different in-service tests in Michigan, USA, and further validated using information from seven seasonal monitoring program sites in the United States, i.e., Colorado, Connecticut, Georgia, Nebraska, Minnesota, South Dakota and Texas. The validation results suggested that the model could be adapted to all seasons and other climatic and geographic regions; furthermore, Asefzadeh et al. adopted this approach for temperature values in Alberta, Canada, finding a significantly high correlation coefficient between measured and calculated data.
Park's equation can be written in the following form:

$$T_z = T_s + (-0{,}3451 \cdot z - 0{,}0432 \cdot z^2 + 0{,}00196 \cdot z^3) \cdot \sin(-6{,}3252 \cdot t + 5{,}0967)$$

where:

- T_z [°C] is the temperature at depth z;
- T_s [°C] is the temperature at the pavement surface;
- z [cm] is the depth from the surface;
- t is the time of temperature measurement in fractions of a day (this value has been derived from the hour of the day the sensors data have been acquired); values for Tomsk are reported in **Table 5.2**, while in Salekhard, all information was retrieved at 5 pm.

Table 5.2: Time of acquisition of Tomsk sensors data

Day	**Time of acquisition**
14/10/2020	1 pm
07/11/2020	4 pm
05/12/2020	8 am
26/12/2020	1 am
15/01/2021	11 am
23/01/2021	11 am
06/02/2021	8 am
11/02/2021	9 am
27/02/2021	8 am
13/03/2021	1 pm
20/03/2021	10 am
27/03/2021	11 am
03/04/2021	5 pm
10/04/2021	8 am
16/04/2021	5 pm
24/04/2021	8 am
30/04/2021	9 am
12/05/2021	9 am
18/05/2021	10 am
03/06/2021	9 pm
04/09/2021	7 pm
18/09/2021	4 pm
25/09/2021	1 pm
12/10/2021	12 pm

Regarding the surface temperature, the 24-h model proposed by Khan et al. can be adopted; the equation has been developed and validated using temperature data in New Mexico, USA, and the authors expect the approach to be used in cold regions pavement design.

The suggested formula is in the form of:

$$T_s = 26{,}081 - 0{,}844 \cdot w + 0{,}479 \cdot T_a - 0{,}187 \cdot RH - 0{,}0173 \cdot S + 0{,}0042254 \cdot w \cdot T_a + 0{,}00565 \cdot w \cdot RH + 0{,}0016 \cdot w \cdot S + 0{,}00342 \cdot T_a \cdot RH + 0{,}000117 \cdot T_a \cdot S + 5{,}7029 \cdot 10^{-5} \cdot RH \cdot S + 0{,}00425 \cdot T_a^2 + 1{,}9125 \cdot 10^{-5} \cdot S^2$$

where:

- T_s [°F] is the surface temperature;
- w [m/s] is the wind speed;
- T_a [°F] is the air temperature (derived from the National Centers for Environmental Information archive and the Russian database);
- RH [%] is the relative humidity;
- S [W/m^2] is the solar radiation.

Average monthly wind speed and relative humidity information for Tomsk and Salekhard are reported in **Table 5.3** and **Table 5.4**, respectively.

Table 5.3: Mean monthly values of relative humidity and wind speed for Tomsk

Month	*1*	*2*	*3*	*4*	*5*	*6*	*7*	*8*	*9*	*10*	*11*	*12*
***w* [m/s]**	1,7	1,7	1,7	2	1,9	1,4	1,2	1,2	1,3	1,6	1,8	1,6
***RH* [%]**	81	78	72	65	61	70	76	79	79	80	83	82

Table 5.4: Mean monthly values of relative humidity and wind speed for Salekhard

Month	*1*	*2*	*3*	*4*	*5*	*6*	*7*	*8*	*9*	*10*	*11*	*12*
***w* [m/s]**	2,5	2,5	2,9	3,3	3,4	3,5	3,2	2,8	2,7	3	2,4	2,5
***RH* [%]**	83	82	81	78	77	70	72	79	82	86	85	83

Solar radiation values can be determined following the indications suggested by Diefenderfer et al.

The daily solar radiation on a horizontal surface is given as:

$$H_0 = \frac{24}{\pi} \cdot I_{sc} \cdot E_0 \cdot sin\phi \cdot sin\delta \cdot \left(\frac{w_s \cdot \pi}{180} - tanw_s\right)$$

where H_0 is expressed in kJ/(m²·day) and I_{sc}=4871 kJ/(m²·day) is the solar constant.
The eccentricity factor E_0 can be calculated as:

$$E_0 = 1{,}00011 + 0{,}034221 \cdot cos\Gamma + 0{,}00128 \cdot sin\Gamma + 0{,}000719 \cdot cos(2 \cdot \Gamma) + 0{,}000077 \cdot sin(2 \cdot \Gamma)$$

where Γ [rad] is the day angle and is expressed as the following:

$$\Gamma = \frac{2 \cdot \pi \cdot (d - 1)}{365}$$

being d the day number of the year ranging from 1 to 365.
H_0 is also dependent on the latitude ϕ [°] and the solar declination δ [°]:

$$\delta = [0{,}006918 - 0{,}399912 \cdot cos\Gamma + 0{,}070257 \cdot sin\Gamma - 0{,}006758 \cdot cos(2 \cdot \Gamma) + 0{,}000907 \cdot sin(2 \cdot \Gamma) - 0{,}002697 \cdot cos(3 \cdot \Gamma) + 0{,}00148 \cdot sin(3 \cdot \Gamma)] \cdot \frac{180}{\pi}$$

Finally, w_s [°] is the sunrise hour angle, namely, the angle between the sun highest point each day (w_s=0°) and the location of the sun at sunrise or sunset:

$$w_s = [cos(-tan\phi \cdot tan\delta)]^{-1}$$

The solar radiation values have been converted knowing that 1 kJ/(m²·day)=0,0115740741 W/m².

Regarding the subgrade and non-asphaltic layers temperature, the equation suggested by Kasuda et al. can be used; the formula was developed considering ground temperature data located in several stations in the United States and successfully applied by Williams and Gold in Canada.
The equation is written as follows:

$$T = T_{mean} - T_{amp} \cdot e^{-z \cdot \sqrt{\frac{\pi}{365 \cdot \alpha}}} \cdot cos\left[\frac{2 \cdot \pi}{365} \cdot \left(t_{year} - t_{shift} - \frac{z}{2} \cdot \sqrt{\frac{365}{\pi \cdot \alpha}}\right)\right]$$

where:

- T [°C] is the soil temperature;
- T_{mean} [°C] is the average air temperature along a temperature cycle;
- T_{amp} [°C] is the amplitude of the air temperature along a temperature cycle;
- z [cm] is the depth below the surface;
- α [cm²/day] is the thermal diffusivity of the soil;
- t_{year} [days] is the current day;
- t_{shift} [days] is the day of the year in which the minimum air temperature occurs.

A temperature assessment for the period under consideration must be performed to determine these quantities.

Figure 5.1 shows the air temperature data between 14/10/2020 and 14/10/2021 for Tomsk; it is possible to see that a complete cycle lasts for about one year.

The average air temperature is equal to 0,796 °C; from the trend line plot, we can assume an amplitude of 20 °C and January 7 as the day in which the minimum air temperature is reached, hence, t_{shift}=7.

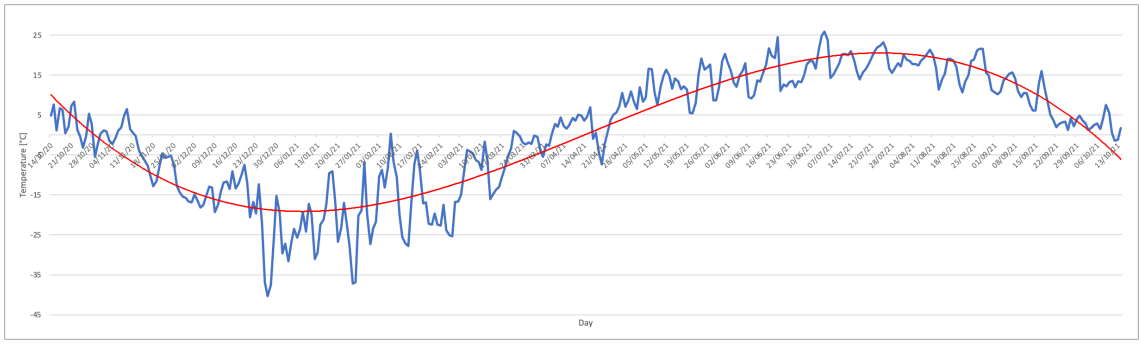

Figure 5.1: Mean daily temperatures between 14/10/2020 and 14/10/2021 in Tomsk

Figure 5.2 shows the temperature data between 5/12/2020 and 5/12/2021 for Salekhard; again, it is possible to see that a complete cycle lasts for about one year.

The average air temperature is equal to -5,517 °C; from the trend line plot, we can assume an amplitude of 25 °C and January 25 as the day in which the minimum air temperature is reached, hence, t_{shift}=25.

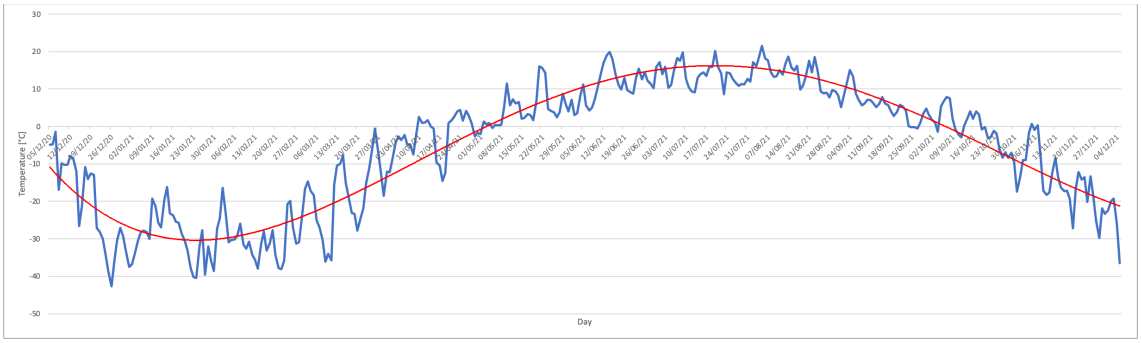

Figure 5.2: Mean daily temperatures between 5/12/2020 and 5/12/2021 in Salekhard

Finally, the thermal diffusivity α is defined as follows:

$$\alpha = \frac{k}{\rho \cdot c_p}$$

where:

- k [J/(s·m·K)] is the thermal conductivity;
- ρ [kg/m^3] is the density;
- c_p [J/(kg·K)] is the specific heat capacity.

Some reference values may be assumed for the materials under analysis. **Table 5.5** shows the input data for determining the thermal diffusivity (the density of both granular layers and subgrade has been estimated from laboratory tests conducted in the Road Construction Faculty of TSUAB).

Table 5.5: Some reference values for the materials under analysis

Type of soil	**k [J/(s·m·K)]**	**c_p [J/(kg·K)]**	**ρ [kg/m^3]**	**α [cm^2/day]**
Crushed stone	1,6	880	1600	981,82

Gravel and sand mix	0,25	780	1800	153,85
Clayey soil	0,9	878	2100	421,74
Sand	1,125	830	1600	731,93

At this point, it is possible to compare the results obtained from Kasuda's equation with the information available from the sensors; **Figure 5.3** shows the two data sets for the case of Tomsk.

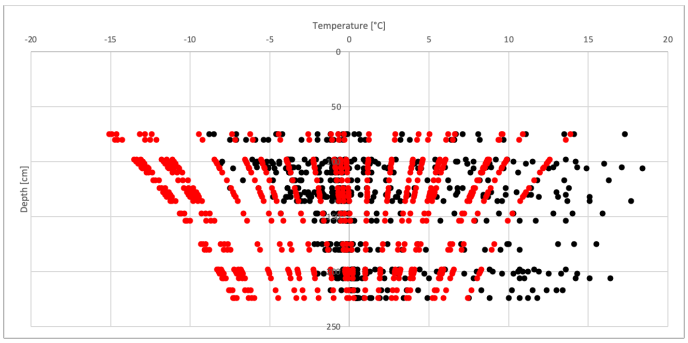

Figure 5.3: Comparison between measured (black) and calculated (red) subgrade temperatures in Tomsk

It is possible to note that the sensors data are slightly shifted towards the right: this is mainly due to the fact that Kasuda's formula was developed for homogeneous soils without considering the contribution of the asphalt layers.

The subgrade temperature changes slowly because of its large mass and heat capacity and because it is insulated from changes in air temperature by the overlying pavement. Moreover, it should be noted that minimum surface temperatures occurring during warming periods are unduly affected by the low subgrade temperatures resulting from the previous cooling period due to its large heat capacity, therefore, warming more slowly than air.

In addition, it has also been observed that in this case, the temperature data do not highly depend on the pavement thickness, rather on the day in which these values have been collected, with an optimal superimposition in correspondence of March 30. Interestingly, this day corresponds to the end of the cold season defined by Ryynänen.

The least-squares method has been therefore applied in order to link the results obtained from Kasuda's equation and the day of measurement with respect to March 30;

calculations showed that only the data belonging to the cold season, namely, from October 16 to March 30, are suitable to perform this kind of assessment.

The following trial equation has been hypothesized:

$$T_{soil} = T_{Kasuda} + (167 - d) \cdot k$$

being T_{soil} [°C] the modified subgrade temperature, T_{Kasuda} [°C] the soil temperature derived from Kasuda's equation, d is the analyzed day of the year with respect to the cold season (d=1 for October 16, d=23 for November 7, etc.) and k is the parameter to be derived using the least-squares method; the coefficient 167 is referred to March 30, being the 167th day of the period under analysis. By using the Microsoft Excel solver, a value of k=0,124 has been found.

The calculated data have then been compared to the temperature information available from the sensors; **Figure 5.4** to **Figure 5.11** show the plotted data; a 45° straight line passing through the origin was drawn to show the distribution among measured and predicted results: the calculated values are allocated close to this line.

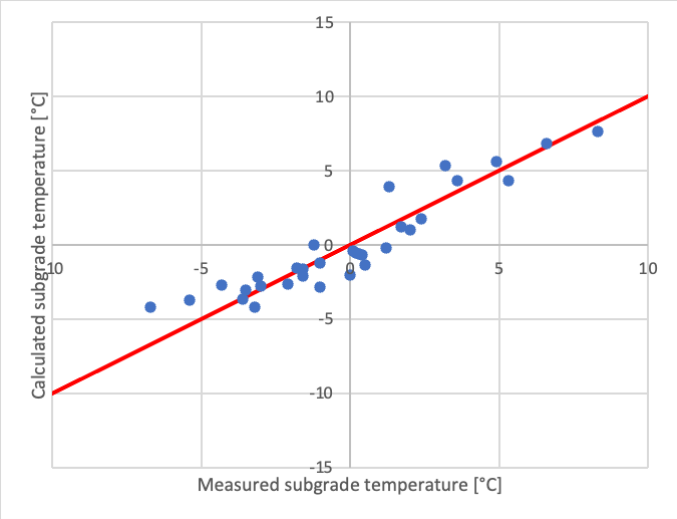

Figure 5.4: Comparison between calculated and measured subgrade temperatures (Tomsk-section 1)

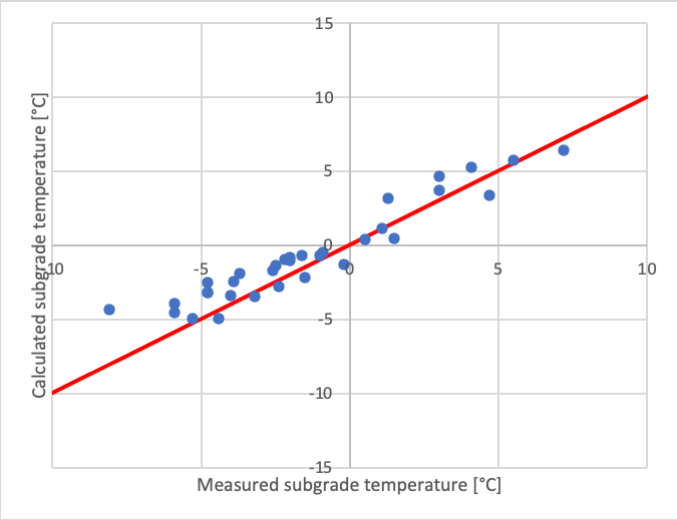

Figure 5.5: Comparison between calculated and measured subgrade temperatures (Tomsk-section 2)

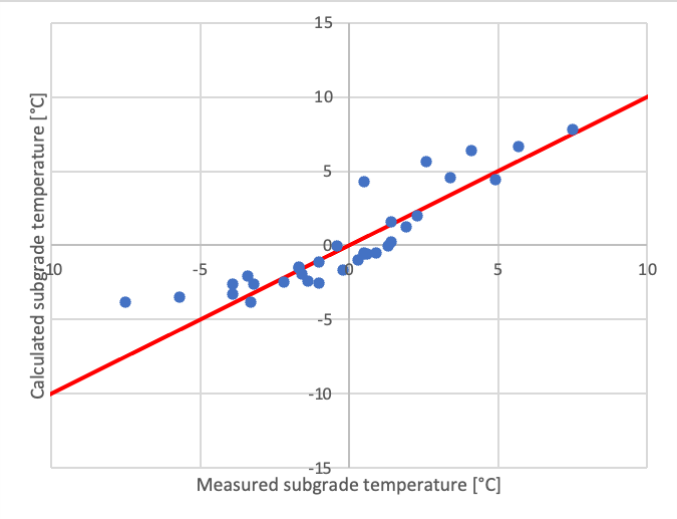

Figure 5.6: Comparison between calculated and measured subgrade temperatures (Tomsk-section 3)

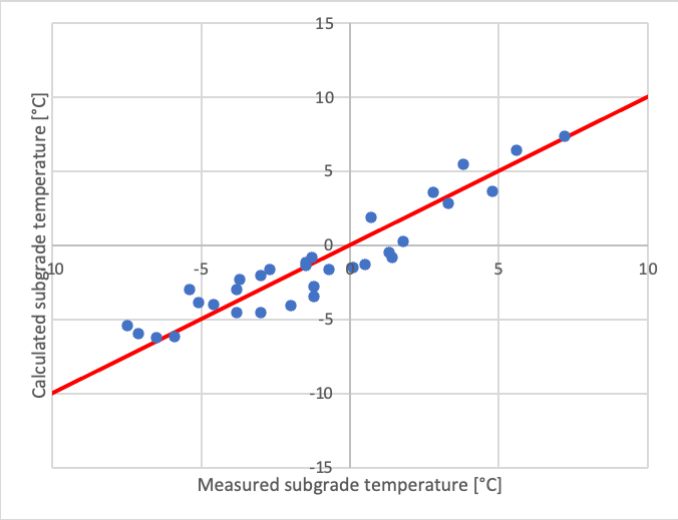

Figure 5.7: Comparison between calculated and measured subgrade temperatures (Tomsk-section 4)

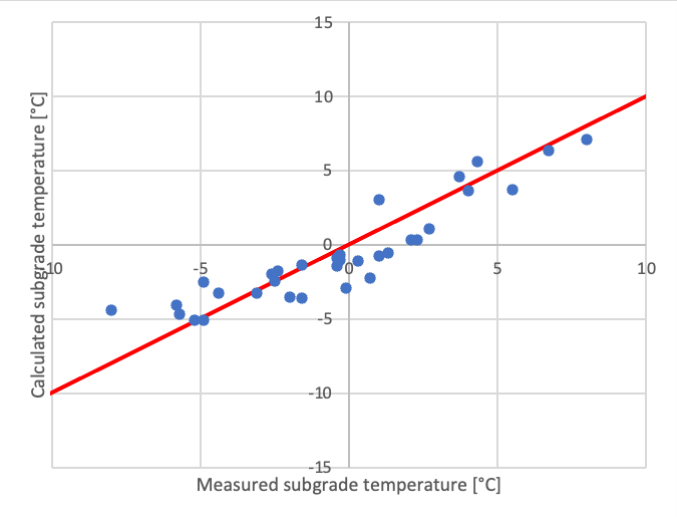

Figure 5.8: Comparison between calculated and measured subgrade temperatures (Tomsk-section 5)

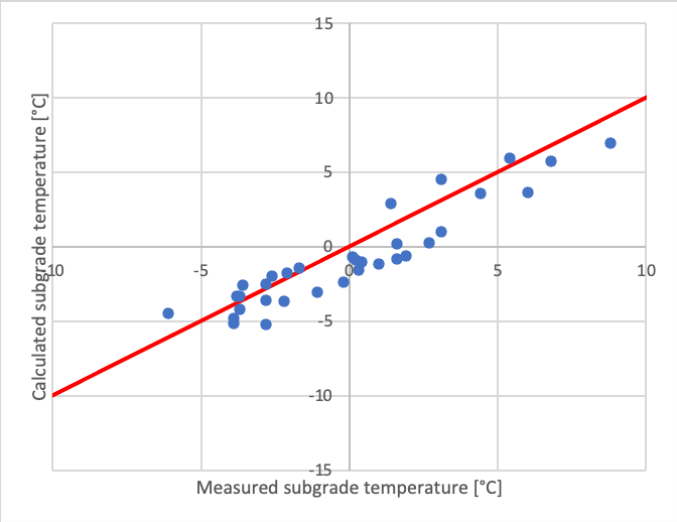

Figure 5.9: Comparison between calculated and measured subgrade temperatures (Tomsk-section 6)

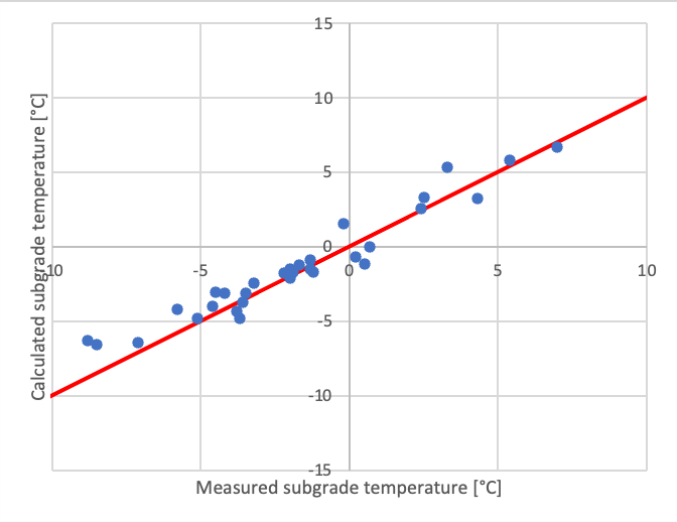

Figure 5.10: Comparison between calculated and measured subgrade temperatures (Tomsk-section 7)

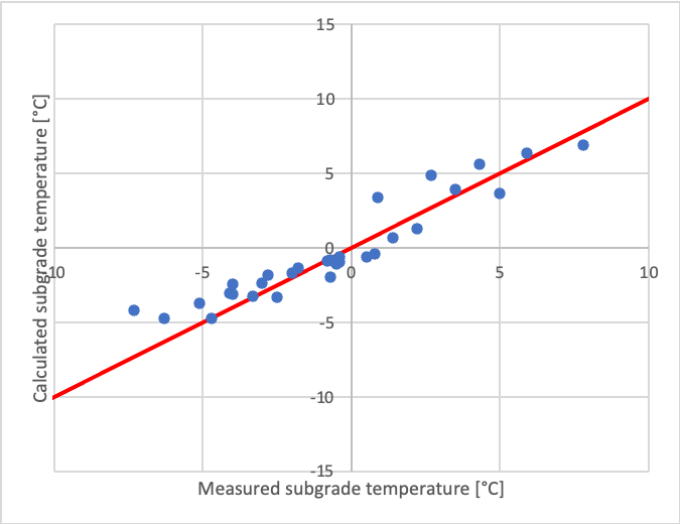

Figure 5.11: Comparison between calculated and measured subgrade temperatures (Tomsk-section 8)

Residuals (namely, the difference between the sensors and the calculated data) have also been plotted in **Figure 5.12** to examine their randomness, which is fundamental to define the reliability of the model; the error is randomly scattered, which entails that the derived equation can be used for the test sections with good approximation.

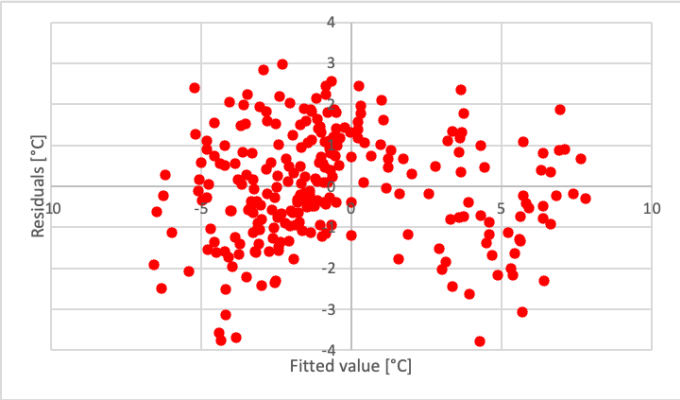

Figure 5.12: Residuals for Tomsk results

In particular, a maximum difference of 3,79 °C has been obtained.

Similar considerations can be applied to the Salekhard test sections; since temperature information is referred to November/December, all the available data have been considered for the assessment.

It should be noted that even in this case, Kasuda's equation must be modified by means of the least-squares method. However, the optimal solution is shown to be:

$$T_{soil} = T_{Kasuda} + k$$

where k=11,08; hence, no contribution of the day number is present.
A maximum residual of 3,93 °C has been obtained.

At this point, it is possible to plot all the different temperature data through depth obtained by combining the previously described models, namely:

- pavement surface temperature: Khan et al. and Diefenderfer et al.;
- asphalt layers temperature: Park et al.;
- granular materials and subgrade: modified Kasuda.

Temperature trend plots for the test sections in Tomsk and Salekhard are reported in *annex 1*.

REFERENCES

BIBLIOGRAPHY

- Asefzadeh A., Hashemian L., Bayat A. – *Development of Statistical Temperature Prediction Models for a Test Road in Edmonton, Alberta, Canada*, International Journal of Pavement Research and Technology, Canada, 2017;
- Diefenderfer B., Al-Qadi I. L., Diefenderfer S. D. – *Model to Predict Pavement Temperature Profile: Development and Validation*, Journal of Transportation Engineering, United States, 2006;
- Dorè G., Zubech H. K. – *Cold Regions Pavement Engineering*, McGraw Hill, United States, 2009;
- Florides G., Kalogirou S. – *Measurements of ground Temperature at Various Depths*, 3rd International Conference on Sustainable Energy Technologies, United Kingdom, 2004;
- Kasuda T., Archenbach P. R. – *Earth Temperature and Thermal Diffusivity at Selected Stations in the United States*, U.S. Department of Commerce, National Bureau of Standards, United States, 1965;
- Khan Z. H., Islam M. R., Tarefder R. A. – *Determining Asphalt Surface Temperature Using Weather Parameters*, Journal of Traffic and Transportation Engineering, United States, 2019;
- Park D. Y., Buch N., Chatti K. – *Effective Layer Temperature Prediction Model and Temperature Correction Via Falling Weight Deflectometer Deflections*, Transportation Research Record Journal of the Transportation Research Board, United States, 2001;
- Robertson W. – *Determining the Winter Design Temperature for Asphalt Pavements*, Transportation Association of Canada, Canada, 1997;
- Williams G. P., Gold L. W. – *Ground Temperatures*, NRC Publications Archive, Canadian Building Digest, Division of Building Research, National Research Council Canada, Canada, 1976.

SITOGRAPHY

- http://matweb.com/search/datasheet.aspx?matguid=7f7a7cc7496c4dfeb3075850ec777fbe;
- http://www.matweb.com/search/datasheet.aspx?matguid=1bb54fa6ce614e218f906c4cd50d9541;
- http://www.pogodaiklimat.ru/monitor.php?id=23330 (in Russian);
- http://www.pogodaiklimat.ru/monitor.php?id=29430 (in Russian);
- https://www.chegg.com/homework-help/questions-and-answers/-1-thermal-diffusivity-given-material-given-following-equation-k-pc-k-thermal-conductivity-q64961459;
- https://www.civillead.com/density-of-cement-sand-and-aggregate/;
- https://theengineeringmindset.com/specific-heat-capacity-of-materials/specific-heat-capacity-tablepsd/;
- https://www.engineeringtoolbox.com/specific-heat-capacity-d_391.html;
- https://www.engineeringtoolbox.com/thermal-conductivity-d_429.html;
- https://www.ncei.noaa.gov/access/past-weather/Salekhard;
- https://www.ncei.noaa.gov/access/past-weather/Tomsk;
- https://www.rfcafe.com/references/general/density-building-materials.htm.

FROST DEPTH ANALYSIS

This chapter aims to provide a general yet accurate overview regarding frost action in pavement systems.
First of all, a summarized description of the factors that influence the frost susceptibility of soil is presented, as well as a characterization of the main parameters that are fundamental for understanding and performing a complete and detailed cold region pavement analysis.
The second part is instead dedicated to describing the heat transfer problem that governs the process of ice formation within the soil, including a general overview of the main models proposed in the literature that allow determining the freezing depth. In particular, one of these equations has been used to compare the data available from the sensors installed in the test sections.

6.1 AN OVERVIEW

Before the 1920s and the rapid development of automobile traffic, roads were left snow-covered. Due to the excellent insulation, frost penetration depths were limited and frost heave was rarely considered a problem. Moreover, since traffic loads were light, few issues arose during spring thaw as well.
With the need for snow removal, frost heave was initially attributed merely to the 10% volumetric expansion of water upon freezing, even though nowadays we can say that frost action is a rather complicated heat diffusion (hence, thermodynamic) and pore water chemistry problem, which is related to the soil-water potential and the water movement in frozen soils.

Pavement design in cold regions requires special consideration; the damaging effects of frost action can include uneven uplifts and loss of soil strength during warm periods and spring thaw.

Other detrimental consequences include possible loss of compaction, pavement roughness development, drainage restriction and cracking and deterioration of the pavement surface.

For a harmful frost action, three conditions must exist at the same time:

- the soil must be frost-susceptible;
- freezing temperatures must penetrate the soil;
- free moisture must be available in sufficient quantities to form ice lenses.

Soils frost susceptibility depends mainly on the size and the distribution of voids in them: specifically, they must be of an ideal critical size for the development of ice lenses. In addition, the soil must be fine enough for relatively high capillary pressures to develop and yet not so fine so that water flow is not restricted.

Soils are subdivided into four categories (the higher the frost group number, the more susceptible the material), listed in **Table 6.1**.

Table 6.1: Soil frost groups

Frost group	**Soil type**	**Percentage finer than 0,02 mm by weight**
FG-1	Gravelly soils	3 to 10
FG-2	Gravelly soils	10 to 20
	Sands	3 to 5
FG-3	Gravelly soils	>20
	Sands (except very fine silty sands)	>15
	Clays with *PI*>12	-

FG-4	Very fine silty sands	>15
	All silts	-
	Clays with $PI \leq 12$	-
	Varved clays and other fine-grained banded sediments	-

Freezing temperatures depend on climatic conditions at the site: ground cover, topography, presence of snow, thermal properties and surface temperature of the pavement and soil mass at the start of the freezing season, as well as many other factors, locally affect the rate and depth of frost penetration.

There must be free water in the soil mass for frost action to occur that can freeze and form ice lenses.

Water can enter the soil from many different sources, for instance, by infiltration from the surface of the sides of the pavement structure, by condensation of atmospheric vapor, or taken from considerable depths by capillarity; in general, if the degree of soil saturation is greater or equal to 70%, frost heave will probably occur.

6.2 FREEZING INDEX

Frost severity in a specific area may be described in terms of the so-called freezing index, expressed in degree days.

This parameter can be defined as the area between the mean daily air temperature curve and the 0 °C line over a given period; mathematically, it is possible to define the following equation:

$$FI = \int_0^t -T\_dt$$

or

$$FI = \sum_{0}^{t} -MDAT\_$$

where $T\_$ and $MDAT\_$ are the temperature and the mean daily air temperature below 0 °C, respectively.

Another critical parameter in most road engineering applications is surface temperature, as it represents the boundary condition on the surface of the pavement system; however, this information is rarely available. Thus, it must be estimated from another quantity: air temperature.

The mean air temperature for a given period can be obtained by averaging the mean daily temperatures over the considered time:

$$MAT = \frac{1}{n} \cdot \sum_{1}^{n} MDAT$$

where n is the number of days in the examined period.

However, it should be noted that, due to the difficulty of obtaining site-specific information, to determine such parameters as radiation balance, convective heat transfer coefficients, etc., a complete surface energy balance analysis is impractical.

It is, therefore, more convenient to use empirical approaches to convert the freezing index of the air into the freezing index of the surface.

Two different methods have been proposed in the literature: the n-factor and the radiation index approach.

The freezing n-factor is defined as follows:

$$n_f = \frac{FI_s}{FI_a}$$

where FI_s and FI_a are the surface and air freezing index, respectively.

Generally, n_f varies with:

- surface characteristics: albedo, latent heat of fusion/evaporation, thermal conductivity and thermal capacity of the soil;
- radiation balance on the pavement: latitude, season, cloud cover, presence of shading obstacles, slope and direction of the slope;
- convective heat transfer: difference in temperature between air and surface and wind speed;
- damping effects by large water bodies.

Typical values of the *n*-factor for different conditions are reported in **Table 6.2**.

Table 6.2: Typical values of the *n*-factor

	n_f		n_t
Material	**Range**	**Suggested Practical Range**	**Range**
Asphalt concrete	0.25–2.50	0.8–0.95	1.60–3.00
Gravel	0.60–1.50	0.9–1.0	1.10–2.00
Trees and bushes, moss, and peat soil	0.25–0.50	0.30–0.35	0.37–0.80
Snow		1.00	

Radiation index values can be derived from different tables available in the literature by retrieving total radiation data from weather stations or by simply assessing the pavement exposure to sunlight.

6.3 FROST DEPTH

Frost and thaw extent directly affect the design of all infrastructures, including pavements, retaining structures, buildings and bridges foundations and utility lines. Frost depth is a function of the material type, soil thermal properties, water content and climatic conditions such as temperature, wind speed, precipitations and solar radiation.

In geotechnical engineering, freezing effects are overcome by installing the foundations below the frost line. In the road field, non-frost susceptible soils such as granular materials are used to mitigate the effects of freezing and heave; nevertheless, soils over time become frost susceptible due to migration of fines from the lower strata.

Frost penetration in soils and pavements results from a heat extraction process. The generated thermal gradient will activate a heat flow directed towards the pavement surface when the surface temperature is below the freezing one. If it turns out to be larger than the geothermal gradient, it will force the overall system to regain balance by releasing energy.

A sustained cold temperature at the surface will consume the heat stored in the pavement system and will eventually fall below the freezing threshold: the ice front will initially progress rapidly in the pavement since the temperature gradient is steeper at shallow depths and because the pavement materials in the top portion of the pavement are drier and have thus less accumulated heat.

When reaching the lower strata and eventually the subgrade, the frost front progresses more slowly since the thermal gradient is gentler due to the larger quantity of moisture available in the subgrade soil (**Figure 6.1**).

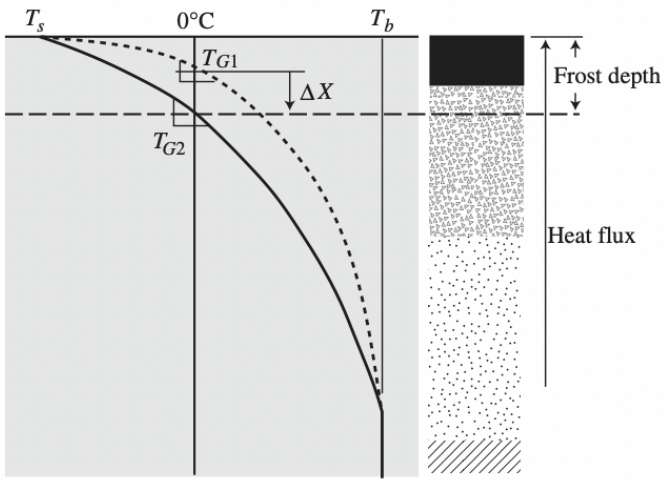

Figure 6.1: Frost front progression in a pavement system

6.3.1 HEAT TRANSFER PROBLEM

Frost penetration analysis involves fundamental relationships among specific thermal properties paramount to all heat transfer problems.

In nature, every physical object releases a portion of thermal energy when cooled.

Considering a generic soil sample containing water, with reference to **Figure 6.2**, it is clear that when a body is cooled, starting from a generic point A, its thermal energy decreases by an amount C_u for each degree of temperature drop.

As the soil starts to freeze (point B), a thermal energy equal to L is released, while its temperature remains almost constant.

When all the water in the soil voids has frozen (point C), the temperature falls below the freezing one, as heat is withdrawn from the sample at a rate of C_f per degree change in temperature.

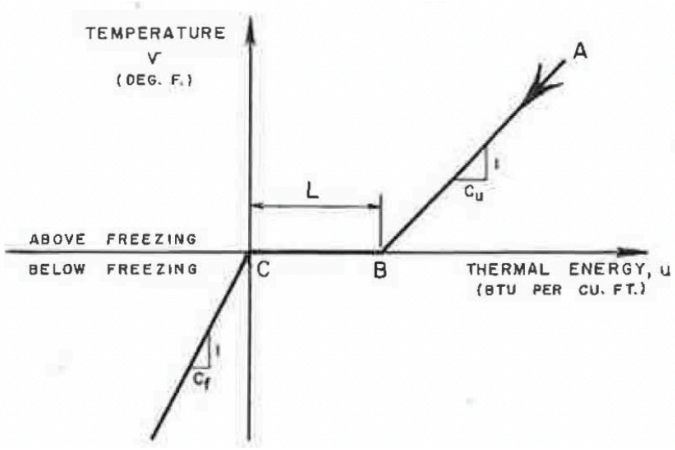

Figure 6.2: Ideal diagram for thermal energy changes

In the absence of freezing or thawing, the change of thermal energy is expressed as:

$$U_1 - U_2 = C \cdot (T_1 - T_2)$$

or, more generically,

$$\frac{\partial U}{\partial t} = C \cdot \frac{\partial T}{\partial t}$$

where U is the thermal energy, C is the volumetric heat and T is the temperature.

Conduction, convection and radiation represent the three methods of transferring energy within an object or from one object to another.
In particular, conduction is defined as the transfer of heat arising from temperature differences between adjacent parts of a body; this phenomenon is described in Fourier's equation:

$$Q = k \cdot i \cdot A = k \cdot \frac{T_1 - T_2}{l} \cdot A$$

where Q is the rate of heat flow, k is the thermal conductivity, i is the thermal gradient, function of the temperature difference $T_1 - T_2$ and the length l and A is the area.
Another expression of the same equation is:

$$q = -k \cdot \frac{\partial T}{\partial x}$$

where q is the heat conducted per unit area per unit time in the x direction.
In the absence of freezing or thawing, the time rate at which the thermal energy U of an element of soil changes plus the net rate of heat transfer into the element must equal zero, according to the conservation of thermal energy:

$$\frac{\partial U}{\partial t} + \frac{\partial q}{\partial x} = 0$$

From the previous equations, it is, therefore, possible to write:

$$C \cdot \frac{\partial T}{\partial t} = k \cdot \frac{\partial^2 T}{\partial x^2}$$

or also

$$\frac{\partial T}{\partial t} = a \cdot \frac{\partial^2 T}{\partial x^2}$$

being a the thermal diffusivity of the soil.

In correspondence of the interface between the frozen and unfrozen soil, the following continuity equation must be satisfied:

$$L \cdot \frac{dz}{dt} = q_u - q_f = k_f \cdot \frac{\partial T_f}{\partial x} - k_u \cdot \frac{\partial T_u}{\partial x}$$

in which L is the latent heat, z is the depth of frost penetration and $q_u - q_f$ is the net rate of heat flow away from the interface (subscripts u and f for unfrozen and frozen soil, respectively).

The last two formulas constitute the basic differential equations that must be solved for different initial and boundary conditions to retrieve an expression for the depth of frost penetration.

6.3.2 FROST DEPTH MODELS

Depending on the availability of the input data and the required accuracy, frost depth can be estimated by means of numerical, empirical or mechanistic-empirical models.

Neumann proposed one of the first solutions to the heat transfer phase-change problem in the 1869s; he studied the case of a one-dimensional heat transfer in a semi-infinite region with uniform properties at an initial temperature T_0 above the freezing one (**Figure 6.3**).
As the temperature decreases, formation of ice starts to propagate through the liquid phase according to the following equation:

$$z = \mu \cdot \sqrt{4 \cdot \alpha_f \cdot t}$$

where z [m] is the frost depth, α [m/s²] is the thermal diffusivity and t [s] is the time since freezing starts. The coefficient μ can be derived from the following equation:

$$\frac{e^{-\mu^2}}{erf\mu} - \sqrt{\frac{\alpha_f}{\alpha_u}} \cdot \frac{k_u}{k_f} \cdot \frac{T_0}{T_s} \cdot \frac{e^{-\frac{\mu^2 \cdot \alpha_f}{\alpha_u}}}{1 - erf\left(\sqrt{\frac{\alpha_f}{\alpha_u}} \cdot \mu\right)} = \frac{\sqrt{\pi} \cdot \mu \cdot l}{c_{pf} \cdot T_s}$$

where:

- erf is the Gauss error function;
- k [W/(°C·m)] is the thermal conductivity of the soil;
- T_0 [°C] is the initial ground temperature;
- T_s [°C] is the applied constant surface temperature;
- l [J/kg] is the latent heat of fusion;
- c_{pf} [J/(kg·°C)] is the specific heat of frozen soil at constant pressure.

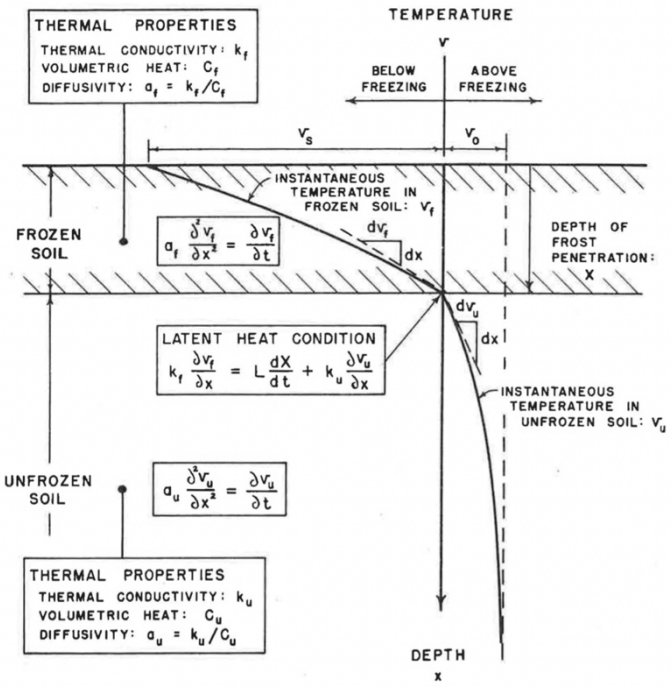

Figure 6.3: Thermal conditions hypothesized by Neumann

Later, Stefan modified Neumann's formula and solved the problem for a particular case in which no heat transfer in the liquid layer is considered.

Thermal conditions assumed in the derivation of Stefan's equation are reported in **Figure 6.4**.

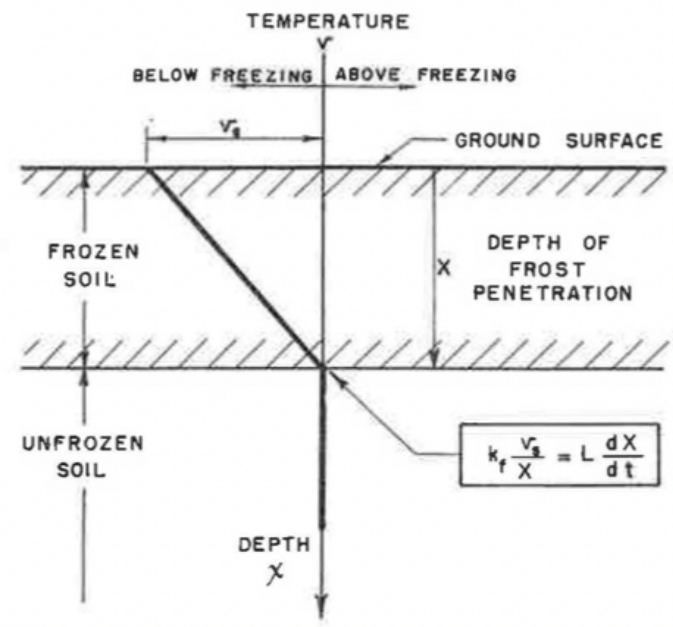

Figure 6.4: Thermal conditions assumed for Stefan's formula

It is supposed that the latent heat of soil moisture is the only heat that must be removed when the soil freezes; hence, the thermal energy which is stored in the form of volumetric heat and released as the soil temperatures drop to and below the freezing point is not taken into account: this assumption is equivalent to shifting the sloping lines in **Figure 6.2** to the vertical position.

Under these hypotheses, the only equation that governs the problem is:

$$L \cdot \frac{dz}{dt} = k_f \cdot \frac{T_s}{z}$$

where T_s is the difference between the ground surface and the freezing temperature of soil moisture at any time.

This means that the latent heat supplied by the soil moisture as it freezes is equal to the rate at which heat is conducted to the ground surface.

By integrating:

$$z = \sqrt{\frac{2 \cdot k_f \cdot \int T_s \, dt}{L}}$$

in which z [ft] is the depth of frost penetration, k_f [BTU/(h·ft·°F)] is the thermal conductivity of the frozen soil, L [BTU/ft³] is the latent heat and $\int T_s \, dt$ is the cumulative surface freezing index CFI in degree Fahrenheit-hour.

If we want to express this parameter in degree Fahrenheit-day, it is possible to write:

$$z = \sqrt{\frac{48 \cdot k_f \cdot CFI}{L}}$$

One of the shortcomings of Stefan's equation is that it does not consider the volumetric heat capacity of the frozen and unfrozen soil; hence the accuracy of the results is debatable.

Consequently, various studies have been conducted to develop more realistic predictions.

One of the most common equations is the modified Berggren's formula, initially proposed by Berggren and later implemented by Aldrich and Paynter. The boundary conditions are the same hypothesized by Neumann in his studies (**Figure 6.3**) and the equation is written in the form of:

$$z = \lambda \cdot \sqrt{\frac{2 \cdot k_f \cdot n_f \cdot T_s \cdot t}{L}} = \lambda \cdot \sqrt{\frac{48 \cdot k_f \cdot n_f \cdot CFI}{L}}$$

where n_f is the n-factor used to convert the air temperature into the surface temperature and λ is a dimensionless correction coefficient that is a function of the thermal ratio α and the fusion parameter μ and can be derived from **Figure 6.5**:

$$\alpha = \frac{T_0}{T_s} = \frac{T_0 \cdot t}{n_f \cdot CFI}$$

$$\mu = \frac{C}{L} \cdot T_s = \frac{C \cdot n_f \cdot CFI}{L \cdot t}$$

being T_0 [°F] the initial ground temperature, t [days] the duration of the freezing period and C [BTU/(ft³·°F)] the volumetric heat.

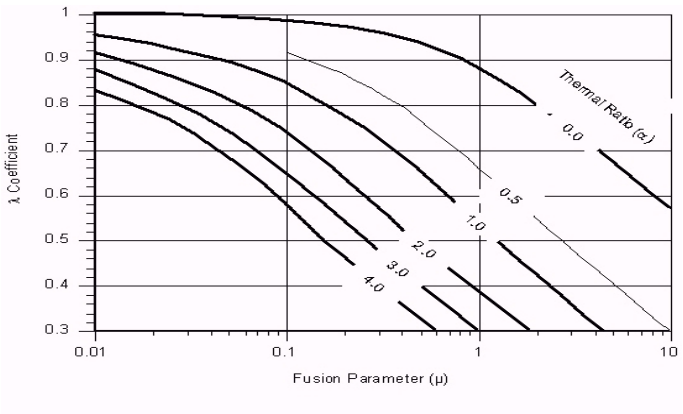

Figure 6.5: Correction coefficient values for the modified Berggren's formula

It is possible to see that the correction coefficient λ is basically a term introduced to correct Stefan's formula for the effects of volumetric heat; since the values calculated using this approach are almost often too deep, λ is always less than unity.

It should be noted that in the pavement engineering field, most of the assessments are related to the case of multi-layered systems: reasonable assumptions must therefore be hypothesized in order to apply the different frost depth models.
The modified Berggren's formula can also be adapted to the case of pavement layouts constituted by different strata; in particular, the following steps must be applied:

- determine the pavement cumulative freezing index CFI and the n-factor n_f;
- determine the duration of the freezing period t and the mean air temperature;
- knowing the mass water content w and the dry density γ_d [lb/ft³], determine the thermal properties k, C and L for each stratum:

$$k = \frac{k_f + k_u}{2}$$

$$L = 1{,}434 \cdot \gamma_d \cdot w$$

$$C = \frac{C_f + C_u}{2}$$

where k_f and k_u can be derived from tables or charts available in the literature, $C_u = \gamma_d \cdot \left(0{,}17 + \frac{w}{100}\right)$ and $C_u = \gamma_d \cdot \left(0{,}17 + \frac{0{,}5 \cdot w}{100}\right)$;

- compute an effective $\frac{L}{k}$ from the following equation:

$$\left(\frac{L}{k}\right)_{eff} = \frac{2}{z'} \cdot \left[\frac{d_1}{k_1} \cdot \left(\frac{L_1 \cdot d_1}{2} + L_2 \cdot d_2 + \cdots + L_n \cdot d_n\right) + \frac{d_2}{k_2} \cdot \left(\frac{L_2 \cdot d_2}{2} + L_3 \cdot d_3 + \cdots + L_n \cdot d_n\right) + \cdots + \frac{d_n}{k_n} \cdot \frac{L_n \cdot d_n}{2}\right]$$

being z' the estimated depth of frost penetration and d_i the thickness of the generic layer within the depth. z' can be derived from experimental results or charts available in the literature;

- compute the weighted values of C and L within the estimated depth of frost penetration:

$$C_{wt} = \frac{C_1 \cdot d_1 + C_2 \cdot d_2 + \cdots + C_n \cdot d_n}{z'}$$

$$L_{wt} = \frac{L_1 \cdot d_1 + L_2 \cdot d_2 + \cdots + L_n \cdot d_n}{z'}$$

- compute the effective values of thermal ratio and fusion parameter and derive the λ coefficient:

$$\alpha = \frac{T_0 \cdot t}{n_f \cdot CFI}$$

$$\mu = \frac{C_{wt} \cdot n_f \cdot FI}{L_{wt} \cdot t}$$

- compute the depth of frost penetration from:

$$z = \lambda \cdot \sqrt{\frac{48 \cdot n_f \cdot CFI}{\left(\frac{L}{k}\right)_{eff}}}$$

The cycle must be repeated if the computed value appreciably differs from the assumed depth.

6.3.3 DATA ANALYSIS

The scope of this study is to find a valid model that can be used to retrieve past frost depth information, since no experimental results are available for these years.
To do so, temperature data from the sensors installed in the test sections were used to derive the freezing depths during several cold season days, which were then compared to the values calculated using the modified Berggren's equation.
Due to the lack of water content information regarding the bituminous and granular course, the subgrade volumetric heat C and latent heat L have been considered. Moreover, according to Aldrich, the pavement freezing index can be conservatively assumed to be equal to the air freezing index.
It should be noted that only data related to Tomsk have been analyzed, since no information regarding the calibrated VWC is available for Salekhard.
Thermal conductivity values have been derived from laboratory tests and are reported in **Table 6.3** (for the granular layers and the subgrade, the values in **Table 5.4** have been used)

Table 6.3: Thermal conductivity values for different materials constituting the test sections

Material	**Thermal conductivity [BTU/(h·ft·°F)]**
Asphalt concrete	0,81
RAP	0,72

RCC	1

Only the days of the cold period in which it was possible to observe a transition from negative to positive subgrade temperatures have been analyzed. In this way, the experimental and the calculated data could be compared.

By plotting the mean daily air temperatures for the cold season, it is possible to observe that the freezing index is defined between 12/11/2020 and 31/03/2021 (**Figure 6.6**); hence, the following dates were included in the analysis: 05/11/2020, 26/12/2020, 15/01/2021, 23/01/2021, 06/02/2021, 11/02/2021 and 27/02/2021 (March data have been discarded due to the fact that the air temperature rise has caused a water migration outside the sensors range, leading to non-realistic water content readings).

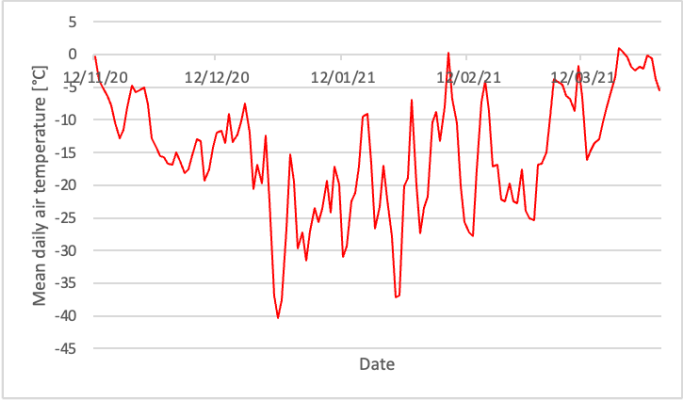

Figure 6.6: Mean daily air temperature for the cold season in Tomsk

For each day, the available information from the sensor is reported from **Table 6.5** to **Table 6.11**.

The mass water content w has been derived from the volumetric water content VWC, knowing that:

$$w = \frac{VWC}{\gamma_{dry}}$$

where γ_{dry} is the dry density of the soil (derived from laboratory tests conducted in the Road Construction Faculty of TSUAB and the results of which are listed in **Table 5.4**).

The depth of frost penetration can instead be derived by retrieving the depth at which the sensor output gives a temperature value equal to 0 °C.

Table 6.4: Dry density values for Tomsk subgrade

Section	γ_{dry} **[g/cm³]**
1	2,01
2	1,39
3	1,7
4	1,42
5	1,4
6	1,69
7	1,64
8	1,71

Table 6.5: Tomsk sensors data (05/10/2020)

Section	VWC **[%]**	w **[%]**
1	38,3	19,1
2	35,8	25,8
3	40,8	24
4	40,6	28,6
5	39,7	28,4
6	42,5	25,1
7	38,9	23,7
8	38,8	22,7

Table 6.6: Tomsk sensors data (26/12/2020)

Section	VWC **[%]**	w **[%]**
1	38,3	19,1
2	31,2	22,4
3	31	18,2
4	32,3	22,7

5	32	22,9
6	42,4	25,1
7	31,4	19,1
8	32,1	18,8

Table 6.7: Tomsk sensors data (15/01/2021)

Section	$\boldsymbol{VWC}$ **[%]**	$\boldsymbol{w}$ **[%]**
1	26,6	13,2
2	26,9	19,4
3	25,2	14,8
4	31,6	22,3
5	26,7	19,1
6	31,8	18,8
7	32,3	19,7
8	29,8	17,4

Table 6.8: Tomsk sensors data (23/01/2021)

Section	$\boldsymbol{VWC}$ **[%]**	$\boldsymbol{w}$ **[%]**
1	26,5	13,2
2	26,6	19,1
3	28,5	16,8
4	31,2	22
5	30,2	21,6
6	30,8	18,2
7	32,4	19,8

Table 6.9: Tomsk sensors data (06/02/2021)

Section	$\boldsymbol{VWC}$ **[%]**	$\boldsymbol{w}$ **[%]**
1	26,1	13
2	27,4	19,7
3	28,8	16,9

4	29,7	20,9
5	30,5	21,8
6	29,4	17,4
7	32,2	19,6
8	28,6	16,7

Table 6.10: Tomsk sensors data (11/02/2021)

Section	$\boldsymbol{VWC}$ **[%]**	$\boldsymbol{w}$ **[%]**
1	26,9	13,4
2	27,5	19,8
3	27,5	16,2
4	30,8	21,7
5	28,6	20,4
6	29,9	17,7
7	32,4	19,8
8	28,7	16,8

Table 6.11: Tomsk sensors data (27/02/2021)

Section	$\boldsymbol{VWC}$ **[%]**	$\boldsymbol{w}$ **[%]**
1	26,4	13,1
2	27,1	19,5
3	26,9	15,8
4	31,8	22,4
5	28	20
6	29,6	17,5
7	31,9	19,5
8	30,2	17,7

The obtained frost depth values have then been compared in **Figure 6.7**; a 45° straight line passing through the origin was drawn to show the distribution among measured and predicted results: the calculated values are distributed close to this line.

Moreover, the residuals (namely, the difference between the sensors and the Berggren's data) have been plotted in **Figure 6.8** to examine their randomness, which is fundamental to define the reliability of the model; the error is randomly scattered, which entails that Berggren's approach can be used for the test sections with good approximation.

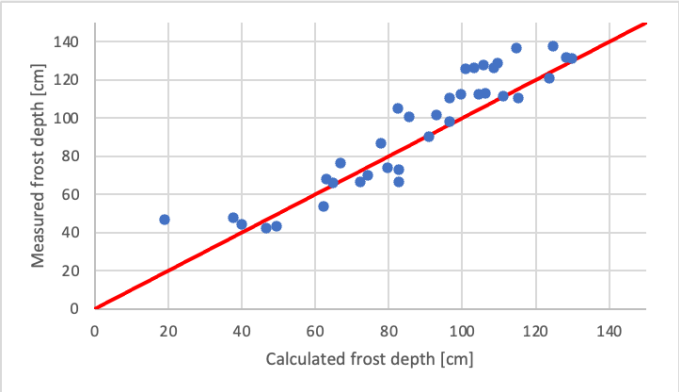

Figure 6.7: Comparison between measured and calculated frost depth values in Tomsk

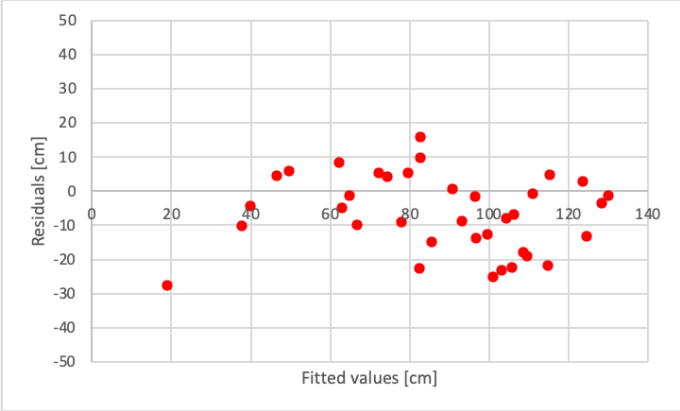

Figure 6.8: Residuals for frost depth data in Tomsk

REFERENCES

BIBLIOGRAPHY

- Advisory Circular n°150/5320-6F: *Airport Pavement Design and Evaluation*, U.S. Department of Transportation Federal Aviation Administration, United States, 2016;
- Aldrich H. P. – *Frost Penetration Below Highway and Airfield Pavements*, Massachusetts Institute of Technology, United States, 1956;
- Dorè G., Zubech H. K. – *Cold Regions Pavement Engineering*, McGraw Hill, United States, 2009;
- Holtz R. D., Kovacs W. D. – *An Introduction to Geotechnical Engineering*, Prentice Hall, United States, 1981;
- Rajaei P., Baladi G. Y. – *Frost Depth-A General Prediction Model*, 94th Transportation Research Board Annual Meeting, United States, 2015;
- Rajaei P., Baladi G. Y. – *Predictive Modeling of Freezing and Thawing of Frost-Susceptible Soils*, Michigan Department of Transportation, United States, 2015.

SITOGRAPHY

- https://pavementinteractive.org/reference-desk/design/design-parameters/modified-berggren-formula/;
- https://www.britannica.com/science/thermal-conduction.

TREND ANALYSES FOR CLIMATE CHANGE

This chapter aims to provide a statistical analysis of past meteorological data related to Tomsk and Salekhard to find a trend in weather parameters and perform a climate change assessment.

Two different reference periods have been investigated and the impact of temperature and precipitations variations has been studied over the last 50 and 100 years.

The available information and analyzed periods are reported in **Table 7.1** and **Table 7.2**; all data have been collected from the National Centers for Environmental Information (missing ones were derived by means of a Russian database).

Table 7.1: Available information for Tomsk

TOMSK	
Information	**Period under analysis**
Annual minimum temperature	1920-2020, 1970-2020
Annual maximum temperature	1922-2020, 1970-2020
Average annual temperature	1920-2020, 1970-2020
Total annual precipitations	1920-2020, 1970-2020

Table 7.2: Available information for Salekhard

SALEKHARD	
Information	**Period under analysis**
Annual minimum temperature	1922-2020, 1970-2020
Annual maximum temperature	1930-2020, 1970-2020
Average annual temperature	1920-2020, 1970-2020
Total annual precipitations	1930-2020, 1970-2020

Different parametric and non-parametric methodologies and statistical tests have been applied to the time series data and results have been compared to be sure that the obtained outcomes are acceptable and suitable to be employed for climate change considerations.

Specifically, the following approaches have been adopted (**Figure 7.1**):

- linear regression analysis followed by F-test;
- Mann-Kendall (MK) test and Sen's slope (SS) estimate, preceded by trend-free pre-whitening (TFPW);
- innovative trend analysis (ITA).

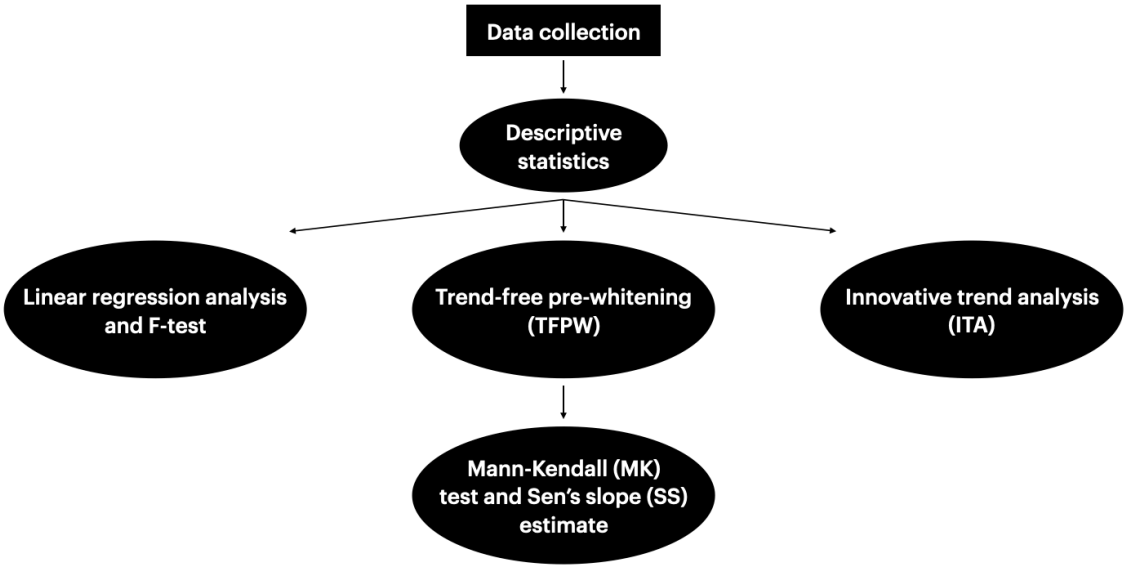

Figure 7.1: Flow-chart of the adopted approach

In the climate change field, time series modeling is one of the most common tools used to predict short- and long-term variations in meteorological data; these analyses are often employed for monitoring, forecasting and feedback by fitting a suitable model to the available information.

Overall, results show a positive increase in temperatures and precipitations for both Tomsk and Salekhard, with very few exceptions.

However, time series analysis turned out to be statistically significant only over a 100-year period for Tomsk and over a 50-year period for Salekhard.
Furthermore, the obtained data are coherent to what was stated by Groisman et al. in their document, which main conclusions are listed in *chapter 2*.

Finally, in the second part, a frost depth assessment has been performed for both sites, taking into account an analysis period of 100 years for Tomsk and 50 years for Salekhard. These results are necessary to carry out a pavement design for frost resistance, as described in *chapter 8*.

It is expected that the following outcomes will constitute a valid starting point for climate change considerations and more detailed time series analyses, which tasks go beyond this master's thesis level.

7.1 AN INTRODUCTION TO STATISTICAL TESTING

Hypothesis testing (or significance testing) is a method used to study hypotheses about a parameter in a population, using data measured in a sample.
The methodology can be summarized in four main steps:

- state the hypotheses;
- set the criteria for a decision;
- compute the test statistics;
- make a decision.

We begin by stating the so-called null hypothesis H_0, i.e., a statement about a population parameter assumed to be true.
An alternative hypothesis H_1 is then defined, namely, an assertion that directly contradicts the null hypothesis by affirming that the actual value of a population parameter is less than, greater than or not equal to the one previously described.

The second step is to set a level of significance, which refers to a criterion of judgment upon which a decision is made regarding the value stated in the null hypothesis.

Typically, the level of significance is set at 5%; when the probability of obtaining a sample mean is less than 5%, if the null hypothesis were true, the null hypothesis is rejected.

Subsequently, test statistics is performed; namely, we apply a mathematical formula that allows researchers to determine the likelihood of obtaining sample outcomes if the null hypothesis were true.

Finally, a decision has to be made; in sum, there are two choices a researcher can make:

- reject the null hypothesis: the tested parameter is associated with a low probability of occurrence when the null hypothesis is true;
- accept the null hypothesis: the tested parameter is associated with a high probability of occurrence when the null hypothesis is true.

The probability of obtaining a given parameter, provided that the value stated in the null hypothesis is true, is described by the *p*-value, which is compared to the level of significance: when the *p*-value is less than 5%, the null hypothesis is rejected and vice-versa.

The decision to reject or retain the null hypothesis is called significance: significance is reached when the *p*-value is less than 0,05.

Figure 7.2 shows a schematization of the process.

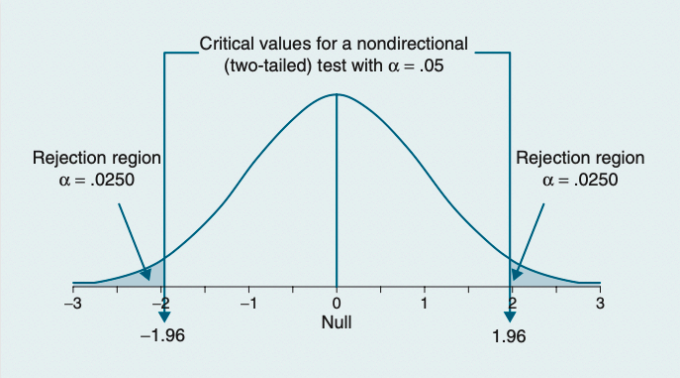

Figure 7.2: Statistical testing scheme

7.2 DESCRIPTIVE STATISTICS

First of all, the available time series have been plotted and the main statistical parameters have been calculated in order to have an overall knowledge of the climatic situation in both Tomsk and Salekhard.

Tomsk results for the last 100 years are plotted in **Figure 7.3** to **Figure 7.6**. The mean annual temperature is shown to be 0,3 °C, with a minimum of -2,2 °C in 1969 and a maximum of 3,6 °C in 2020, indicating that the past year was the hottest over the last 100 years.

The mean minimum temperature is -41,5 °C, with a minimum of -55 °C on January 6, 1931, and a maximum of -27,8 °C on February 5, 1983, while the mean maximum temperature is 31,5 °C, with a minimum of 25,9 °C on July 3, 1924, and a maximum of 35,6 °C on July 15, 2014.

As regards precipitations, the mean total annual precipitation is 554 mm, with a minimum of 396 mm in 1935 and a maximum of 745 mm in 1987.

Overall statistical parameters are reported in **Table 7.3**.

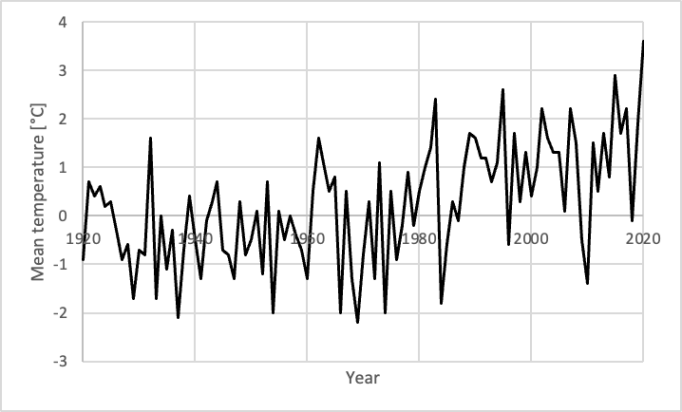

Figure 7.3: Tomsk annual average temperatures (1920-2020)

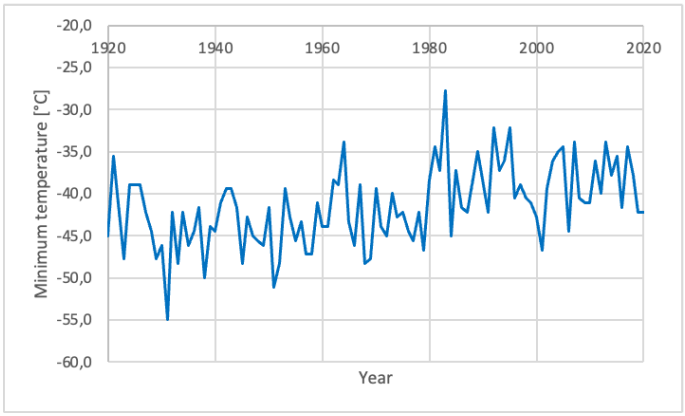

Figure 7.4: Tomsk annual minimum temperatures (1920-2020)

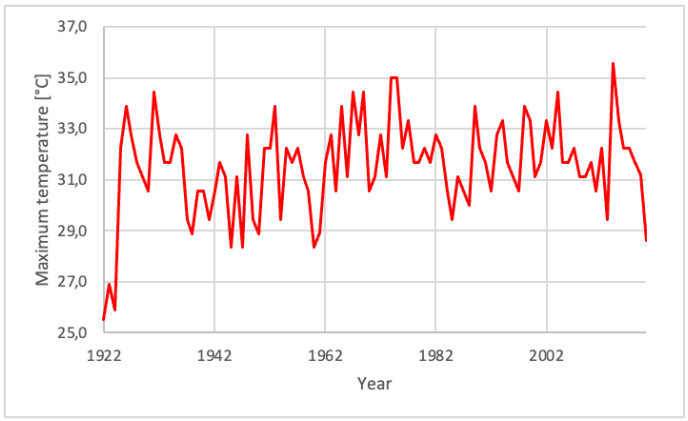

Figure 7.5: Tomsk annual maximum temperatures (1922-2020)

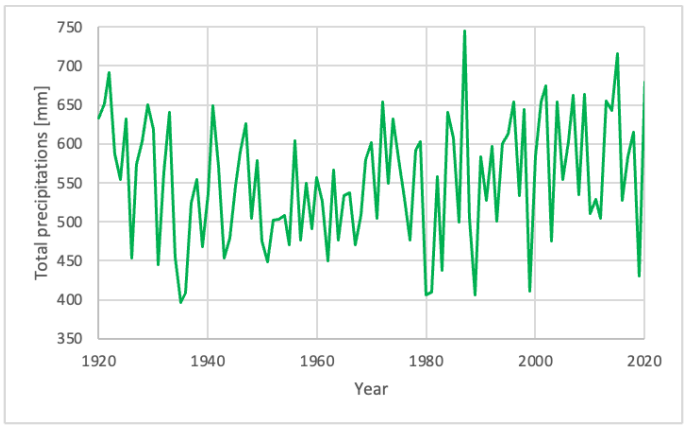

Figure 7.6: Tomsk total annual precipitations (1920-2020)

Table 7.3: Tomsk results (last 100 years)

Information	N° of observations	Average	Minimum	Maximum	Variance	Standard deviation
Average annual temperature	101	0,2 °C	-2,2 °C	3,6 °C	1,5 °C^2	1,2 °C
Minimum annual temperature	101	-41,5 °C	-55 °C	-27,8 °C	21,3 °C^2	4,6 °C
Maximum annual temperature	99	31,5 °C	25,9 °C	35,6 °C	3,3 °C^2	1,8 °C
Total annual precipitations	101	554 mm	396 mm	745 mm	6192 mm^2	78,7 mm^2

Tomsk results for the last 50 years are plotted in **Figure 7.7** to **Figure 7.10**. The mean annual temperature is shown to be 0,8 °C, with a minimum of -2 °C in 1974 and a maximum of 3,6 °C in 2020.

The mean minimum temperature is -39,4 °C, with a minimum of -46,7 °C on December 8, 1979, and a maximum of -27,8 °C on February 5, 1983, while the mean maximum temperature is 31,9 °C, with a minimum of 28,6 °C on July 7, 2020, and a maximum of 35,6 °C on July 15, 2014.

As regards precipitations, the mean total annual precipitation is 570 mm, with a minimum of 406 mm in 1980 and a maximum of 745 mm in 1987.

Overall statistical parameters are reported in **Table 7.4**.

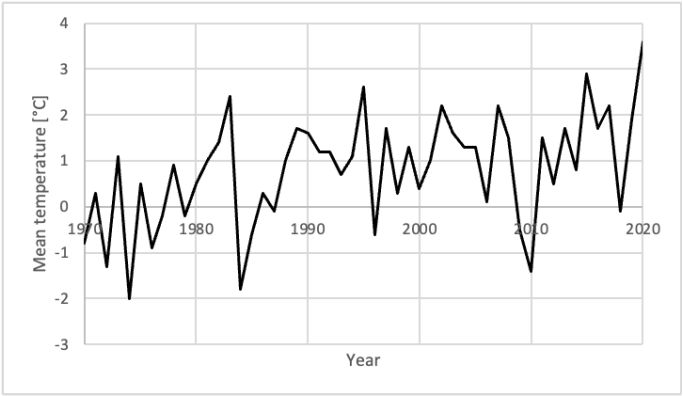

Figure 7.7: Tomsk annual average temperatures (1970-2020)

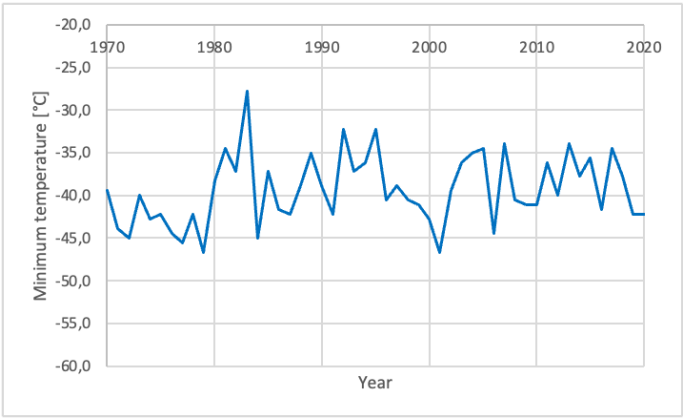

Figure 7.8: Tomsk annual minimum temperatures (1970-2020)

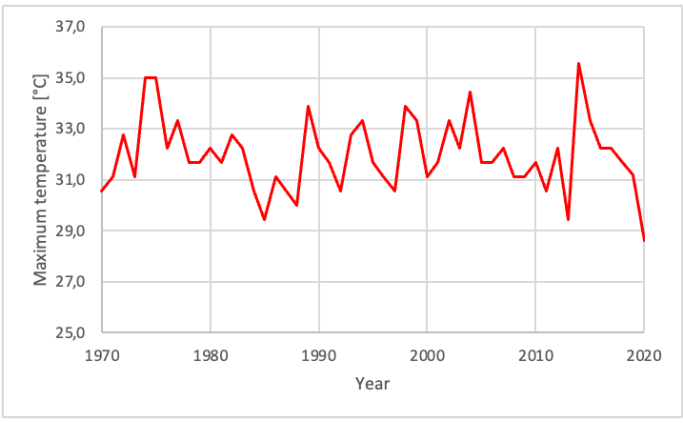

Figure 7.9: Tomsk annual maximum temperatures (1970-2020)

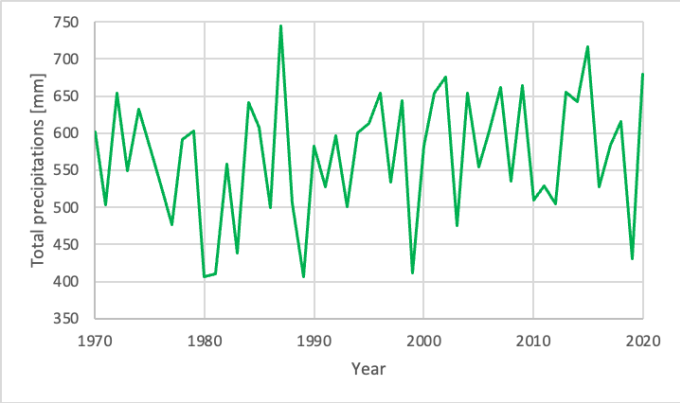

Figure 7.10: Tomsk total annual precipitations (1970-2020)

Table 7.4: Tomsk results (last 50 years)

Information	N° of observations	Average	Minimum	Maximum	Variance	Standard deviation
Average annual temperature	51	0,8 °C	-2 °C	3,6 °C	1,4 °C²	1,2 °C
Minimum annual temperature	51	-39,4 °C	-46,7 °C	-27,8 °C	16,7 °C²	4,1 °C
Maximum annual temperature	51	31,9 °C	28,6 °C	35,6 °C	2 °C²	1,4 °C
Total annual precipitations	51	570 mm	406 mm	745 mm	6940 mm²	83,3 mm²

Salekhard results for the last 100 years are plotted in **Figure 7.11** to **Figure 7.14**. The mean annual temperature is shown to be -5,8 °C, with a minimum of -8,8 °C in 1968 and a maximum of -1,2 °C in 2020, again indicating that the past year was the hottest over the last 100 years.

The mean minimum temperature is -43,6 °C, with a minimum of -51,3 °C on January 28, 1973, and a maximum of -35,5 °C on December 13, 2012, while the mean maximum temperature is 28,2 °C, with a minimum of 22,2 °C on July 4, 1980, and a maximum of 32,8 °C on July 13, 1990.

As regards precipitations, the mean total annual precipitation is 458 mm, with a minimum of 282 mm in 1935 and a maximum of 730 mm in 1960.

Overall statistical parameters are reported in **Table 7.5**.

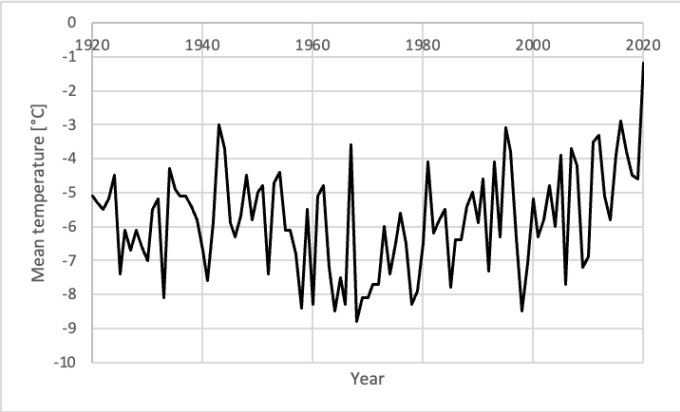

Figure 7.11: Salekhard annual average temperatures (1920-2020)

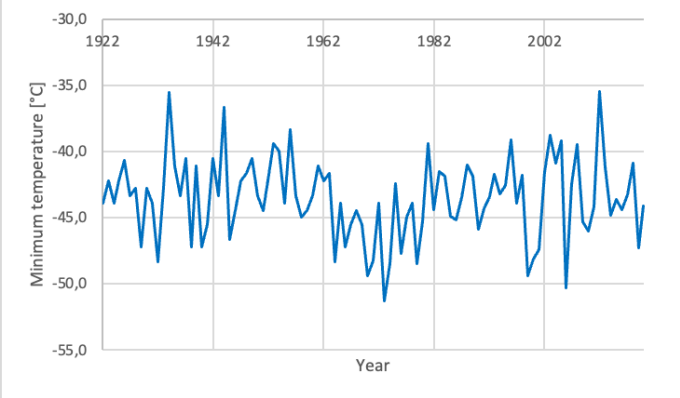

Figure 7.12: Salekhard annual minimum temperatures (1922-2020)

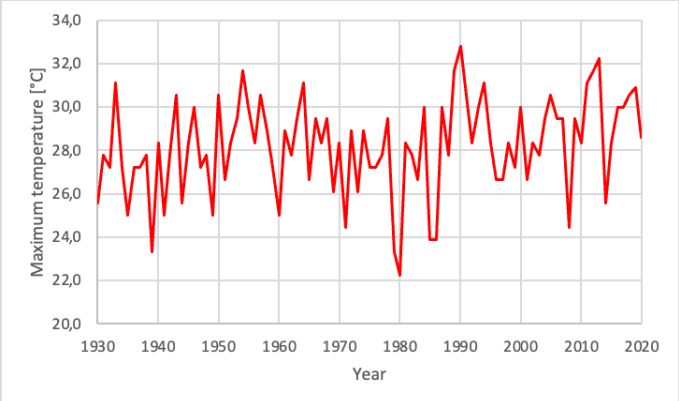

Figure 7.13: Salekhard annual maximum temperatures (1930-2020)

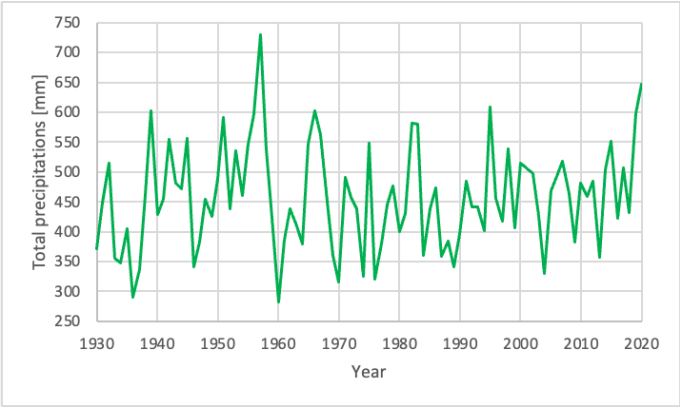

Figure 7.14: Salekhard total annual precipitations (1930-2020)

Table 7.5: Salekhard results (last 100 years)

Information	N° of observations	Average	Minimum	Maximum	Variance	Standard deviation
Average annual temperature	101	-5,8 °C	-8,8 °C	-1,2 °C	2,3 °C²	1,5 °C
Minimum annual temperature	99	-43,6 °C	-51,3 °C	-35,5 °C	9,3 °C²	3 °C
Maximum annual temperature	91	28,2 °C	22,2 °C	32,8 °C	4,8 °C²	2,2 °C
Total annual precipitations	91	458 mm	282 mm	730 mm	7403 mm²	86 mm²

Salekhard results for the last 50 years are plotted in **Figure 7.15** to **Figure 7.18**. The mean annual temperature is shown to be -5,6 °C, with a minimum of -8,5 °C in 1998 and a maximum of -1,2 °C in 2020.

The mean minimum temperature is -44 °C, with a minimum of -51,3 °C on January 28, 1973, and a maximum of -35,5 °C on December 13, 2012, while the mean maximum temperature is 28,4 °C, with a minimum of 22,2 °C on July 4, 1980, and a maximum of 32,8 °C on July 13, 1990.

As regards precipitations, the mean total annual precipitation is 455 mm, with a minimum of 316 mm in 1970 and a maximum of 647 mm in 2020.

Overall statistical parameters are reported in **Table 7.6**.

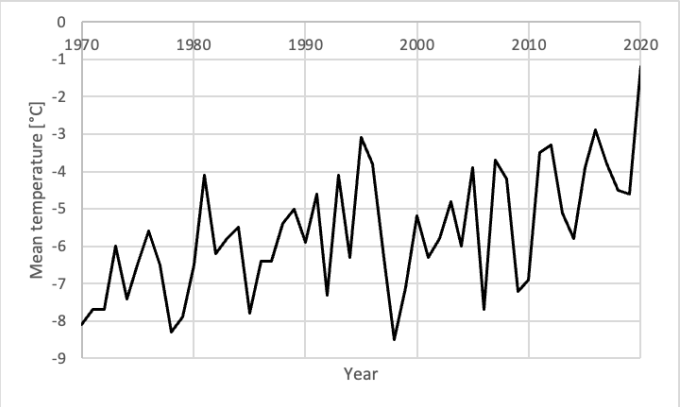

Figure 7.15: Salekhard annual average temperatures (1970-2020)

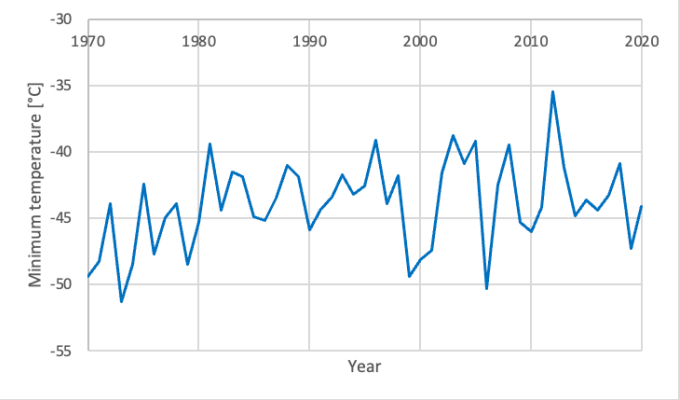

Figure 7.16: Salekhard annual minimum temperatures (1970-2020)

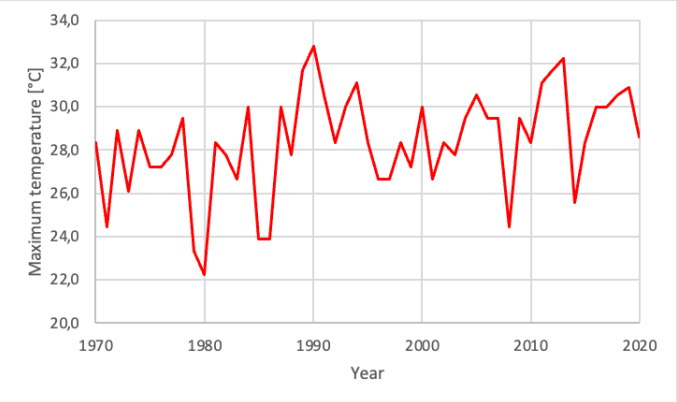

Figure 7.17: Salekhard annual maximum temperatures (1970-2020)

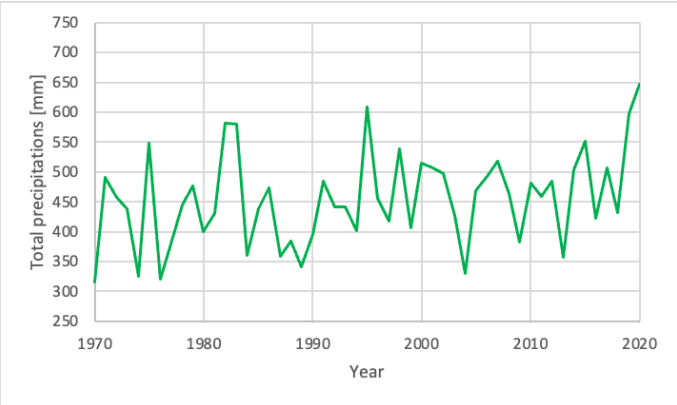

Figure 7.18: Salekhard total annual precipitations (1970-2020)

Table 7.6: Salekhard results (last 50 years)

Information	N° of observations	Average	Minimum	Maximum	Variance	Standard deviation
Average annual temperature	51	-5,6 °C	-8,5 °C	-1,2 °C	2,6 °C²	1,6 °C
Minimum annual temperature	51	-44 °C	-51,3 °C	-35,5 °C	10,6 °C²	3,3 °C
Maximum annual temperature	51	28,4 °C	22,2 °C	32,8 °C	5,5 °C²	2,3 °C
Total annual precipitations	51	455 mm	316 mm	647 mm	5964 mm²	77 mm²

7.3 LINEAR REGRESSION ANALYSIS

Linear regression is probably the most frequently used statistical method. A distinction is generally made between simple (with only one explanatory variable) and multiple (with several explanatory variables) regression, although the overall concept and calculation methods are identical.

The principle of linear regression is to model a quantitative dependent variable Y through a linear combination of p qualitative independent variables X_1, X_2,…, X_p. The determinist model (randomness is not taken into account) is written for observation i as follows:

$$y_i = \beta_0 + \sum_{j=1}^{p} \beta_j \cdot x_{ij} + \epsilon_i$$

where y_i is the dependent variable for observation i, x_{ij} is the value taken by variable j for observation i and ϵ_i is the error.

According to the linear regression hypotheses, the errors follow the same normal distribution $N(0, \sigma)$ and are independent, hence y_i express random variables with mean μ_i and variance σ^2, being

$$\mu_i = \beta_0 + \sum_{j=1}^{p} \beta_j \cdot x_{ij}$$

As regards the β-coefficients, these can be obtained from the followings:

$$\hat{\beta} = (X^t \cdot X)^{-1} \cdot X^t \cdot Y$$

$$\sigma^2(\hat{\beta}) = \hat{\sigma}^2 (X^t \cdot X)^{-1}$$

Linear regression analysis was then coupled with the F-test; this statistical tool indicates whether the specified model (in our case, linear regression) provides a better fit to the data with respect to the one that contains no independent variables.

The null hypothesis is that the fit of the intercept-only model is similar to the specified one, while the alternative hypothesis is that the investigated model better fits the data with respect to the one with no independent variables.

Consequently, the null hypothesis can be rejected if the p-value is less than the fixed significance level and the F-test is statistically significant. In this study, a 95% confidence interval was used.

All the results were obtained through Microsoft Excel and Addinsoft XLSTAT 2021.

Tomsk results for the last 100 years are listed in **Table 7.7**. It is possible to note that in all cases, there is a positive tendency, indicating an increase of 0,022 °C/year (with a 28% significance), 0,074 °C/year (with a 22% significance) and 0,017 °C/year (with a 7% significance) for mean, minimum and maximum temperature, respectively, and 0,41 mm/year (with a 2% significance) for precipitations.

Moreover, the F-test showed to be statistically significant in all cases, except for the overall annual precipitations.

Figure 7.19 to **Figure 7.26** show the linear fit results and the corresponding residuals.

Table 7.7: Linear regression outcomes for Tomsk (last 100 years)

Information	**Linear regression equation**	R^2	p**-value**	**F-test result**
Average annual temperature	$y = -42{,}94 + 0{,}02 \cdot x$	0,28	<0,0001	**ACCEPTED**
Minimum annual temperature	$y = -186{,}45 + 0{,}07 \cdot x$	0,22	<0,0001	**ACCEPTED**
Maximum annual temperature	$y = -1{,}39 + 0{,}02 \cdot x$	0,07	0,009	**ACCEPTED**
Total annual precipitations	$y = -255{,}53 + 0{,}41 \cdot x$	0,02	0,129	**REJECTED**

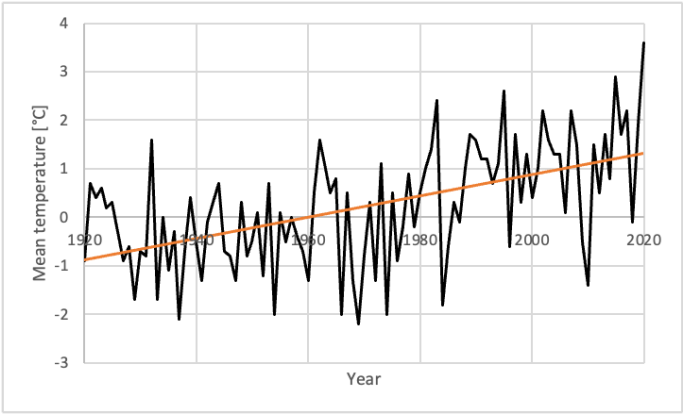

Figure 7.19: Linear regression analysis for Tomsk mean temperatures (1920-2020)

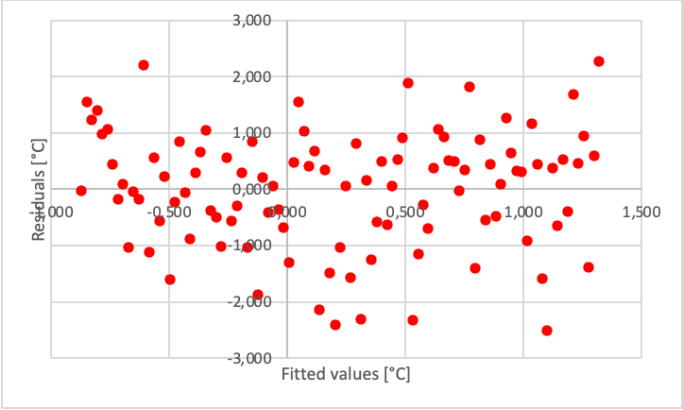

Figure 7.20: Residuals for Tomsk mean temperatures (1920-2020)

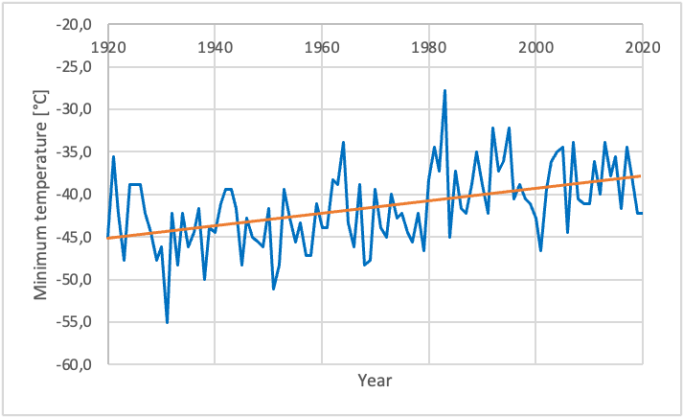

Figure 7.21: Linear regression analysis for Tomsk minimum temperatures (1920-2020)

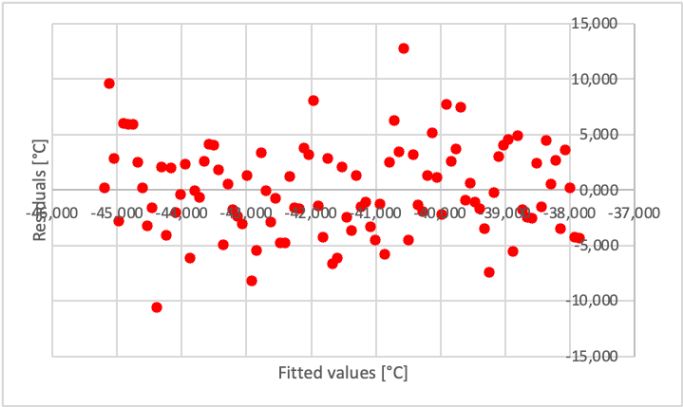

Figure 7.22: Residuals for Tomsk minimum temperatures (1920-2020)

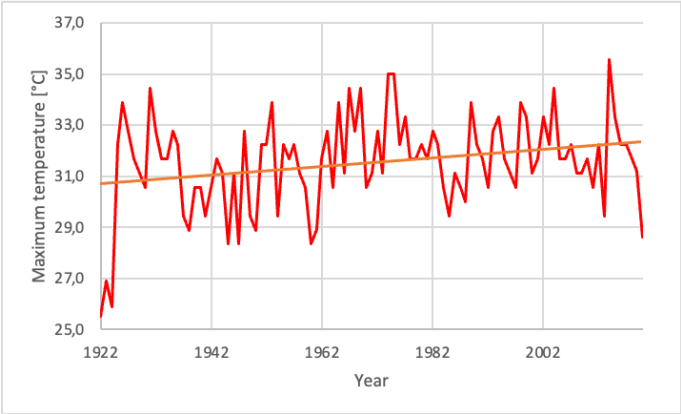

Figure 7.23: Linear regression analysis for Tomsk maximum temperatures (1922-2020)

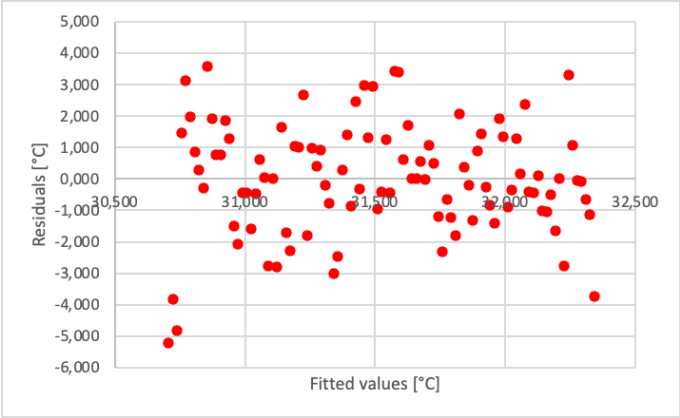

Figure 7.24: Residuals for Tomsk maximum temperatures (1922-2020)

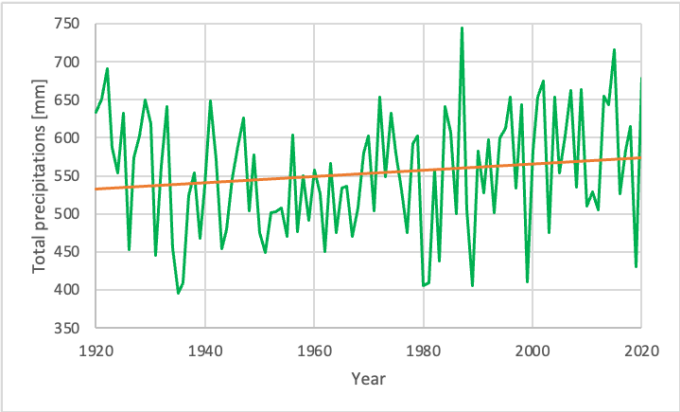

Figure 7.25: Linear regression analysis for Tomsk total precipitations (1920-2020)

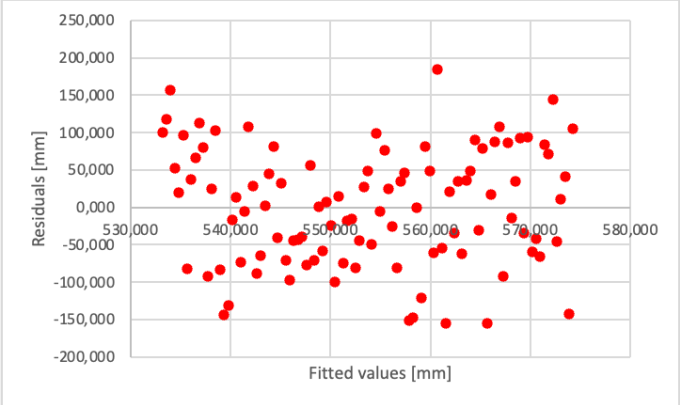

Figure 7.26: Residuals for Tomsk total precipitations (1920-2020)

Tomsk results for the last 50 years are listed in **Table 7.8**. It is possible to note that there is a positive tendency for mean and minimum temperatures, indicating an increase of 0,038 °C/year (with a 22% significance) and 0,066 °C/year (with a 6% significance), respectively, and a negative trend for maximum temperatures, with a decrease of 0,0091 °C/year (with a 0,9% significance). There is a positive tendency of 1,04 mm/year (with a 3% significance) regarding precipitations.

In this case, the F-test was statistically significant only for the mean annual temperature data.

Figure 7.27 to **Figure 7.34** show the linear fit results and the corresponding residuals.

Table 7.8: Linear regression outcomes for Tomsk (last 50 years)

Information	**Linear regression equation**	R^2	***p*-value**	**F-test result**
Average annual temperature	$y = -75{,}19 + 0{,}04 \cdot x$	0,22	0,001	**ACCEPTED**
Minimum annual temperature	$y = -170{,}85 + 0{,}07 \cdot x$	0,06	0,093	**REJECTED**
Maximum annual temperature	$y = 50{,}02 - 0{,}01 \cdot x$	0,009	0,513	**REJECTED**
Total annual precipitations	$y = -1503{,}75 + 1{,}04 \cdot x$	0,03	0,197	**REJECTED**

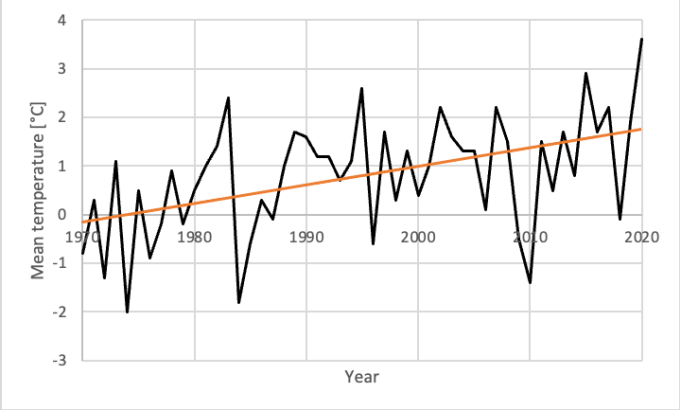

Figure 7.27: Linear regression analysis for Tomsk mean temperatures (1970-2020)

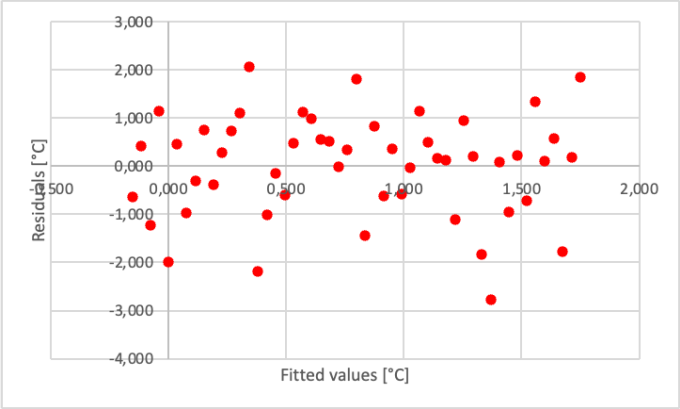

Figure 7.28: Residuals for Tomsk mean temperatures (1970-2020)

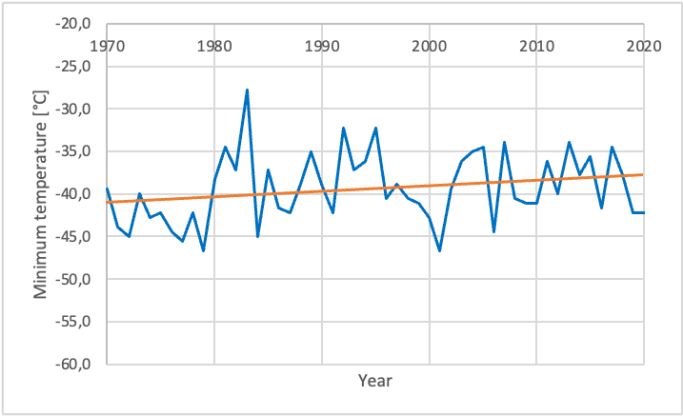

Figure 7.29: Linear regression analysis for Tomsk minimum temperatures (1970-2020)

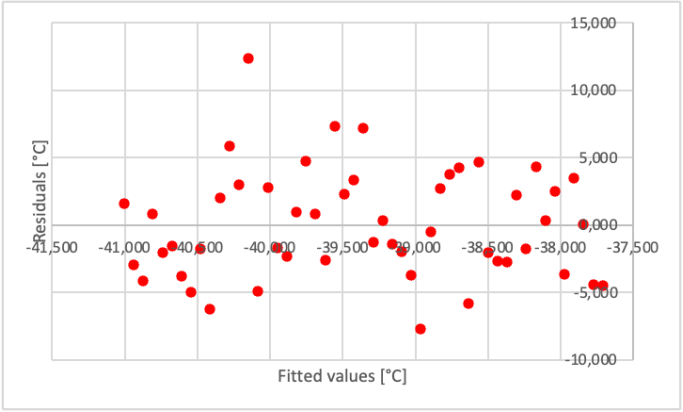

Figure 7.30: Residuals for Tomsk minimum temperatures (1970-2020)

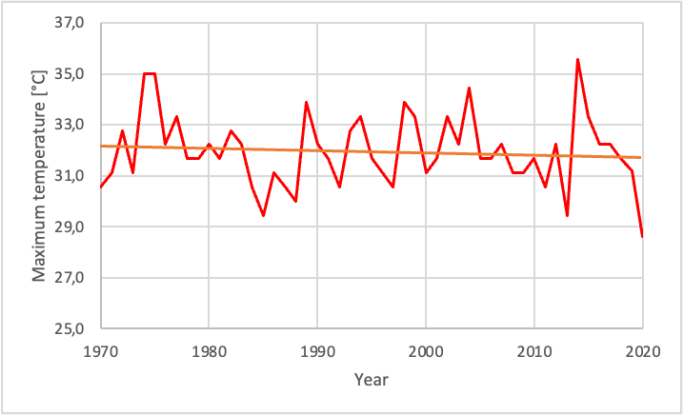

Figure 7.31: Linear regression analysis for Tomsk maximum temperatures (1970-2020)

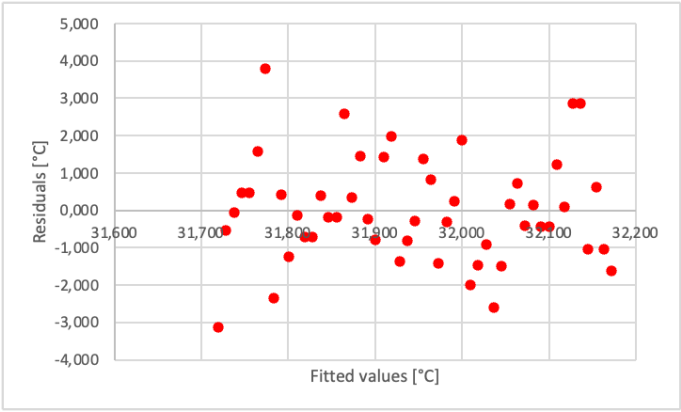

Figure 7.32: Residuals for Tomsk maximum temperatures (1970-2020)

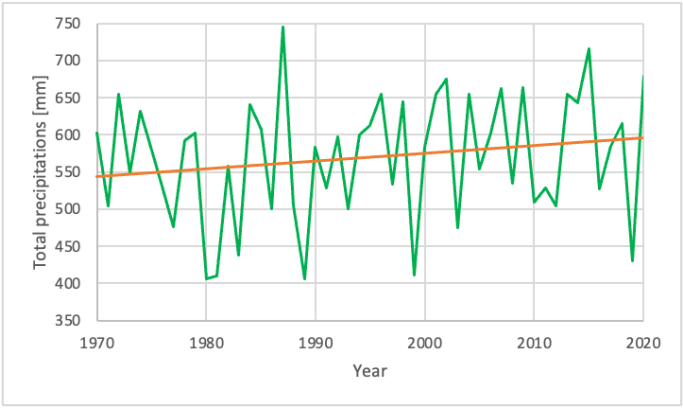

Figure 7.33: Linear regression analysis for Tomsk total precipitations (1970-2020)

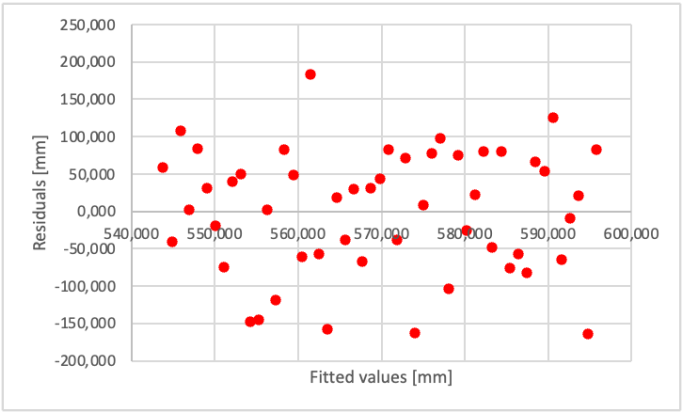

Figure 7.34: Residuals for Tomsk total precipitations (1970-2020)

Salekhard results for the last 100 years are listed in **Table 7.9**. It is possible to note that there is a positive tendency for mean and maximum temperatures, indicating an increase of 0,0099 °C/year (with a 4% significance) and 0,021 °C/year (with a 6% significance), respectively, and a negative trend for minimum temperatures, with a decrease of 0,0063

°C/year (with a 0,4% significance). There is a positive tendency of 0,35 mm/year (with a 1% significance) regarding precipitations.

In this case, the F-test was statistically significant only for the maximum annual temperature data.

Figure 7.35 to **Figure 7.42** show the linear fit results and the corresponding residuals.

Table 7.9: Linear regression outcomes for Salekhard (last 100 years)

Information	**Linear regression equation**	R^2	***p*-value**	**F-test result**
Average annual temperature	$y = -25{,}33 + 0{,}01 \cdot x$	0,04	0,056	**REJECTED**
Minimum annual temperature	$y = -31{,}09 - 0{,}01 \cdot x$	0,004	0,559	**REJECTED**
Maximum annual temperature	$y = -13{,}36 + 0{,}02 \cdot x$	0,06	0,015	**ACCEPTED**
Total annual precipitations	$y = -239{,}04 + 0{,}35 \cdot x$	0,01	0,31	**REJECTED**

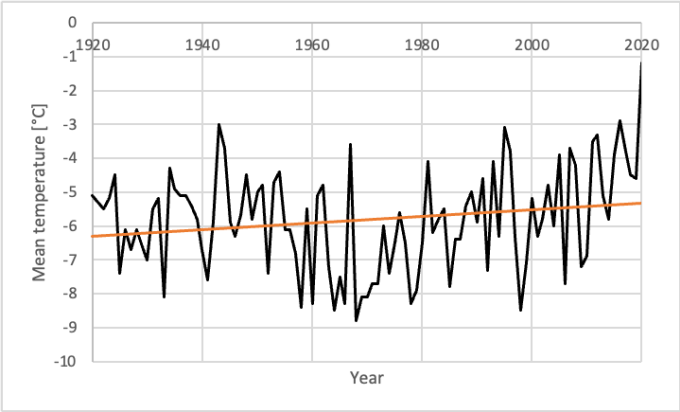

Figure 7.35: Linear regression analysis for Salekhard mean temperatures (1920-2020)

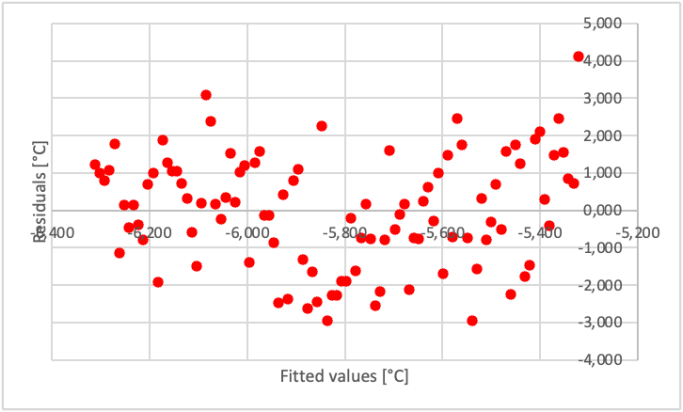

Figure 7.36: Residuals for Salekhard mean temperatures (1920-2020)

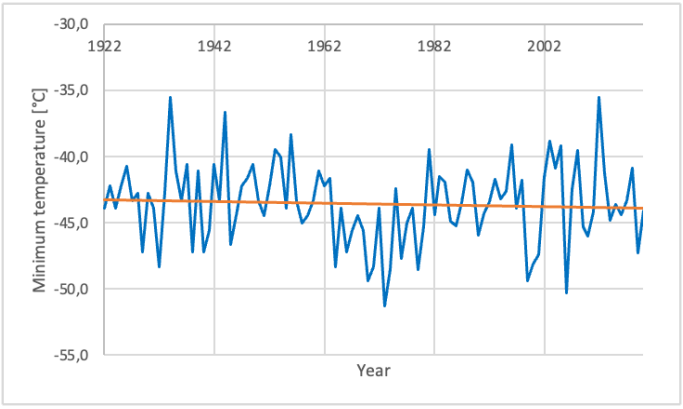

Figure 7.37: Linear regression analysis for Salekhard minimum temperatures (1922-2020)

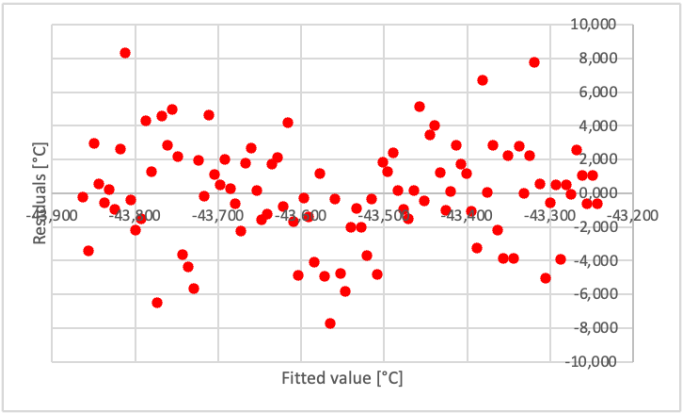

Figure 7.38: Residuals for Salekhard minimum temperatures (1922-2020)

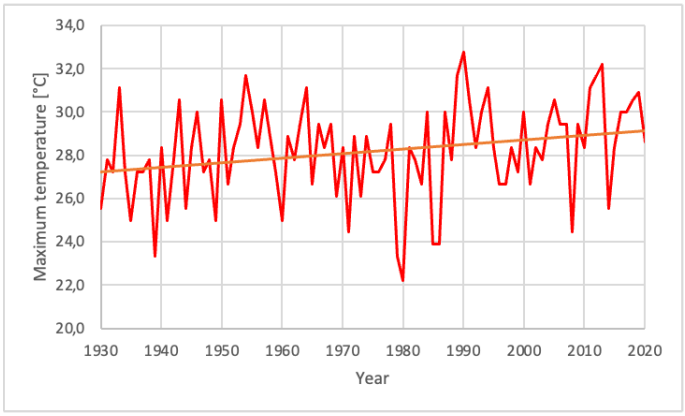

Figure 7.39: Linear regression analysis for Salekhard maximum temperatures (1930-2020)

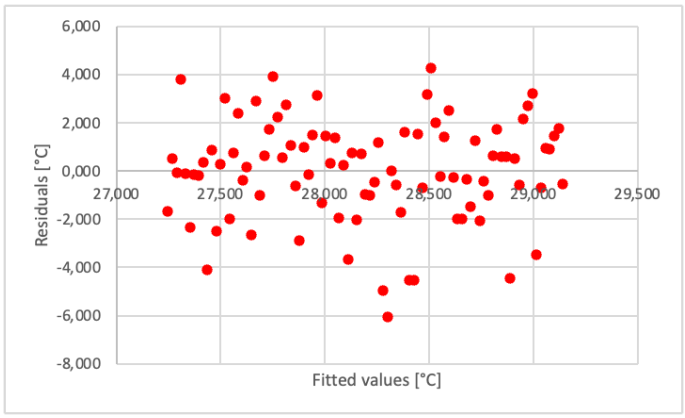

Figure 7.40: Residuals for Salekhard maximum temperatures (1930-2020)

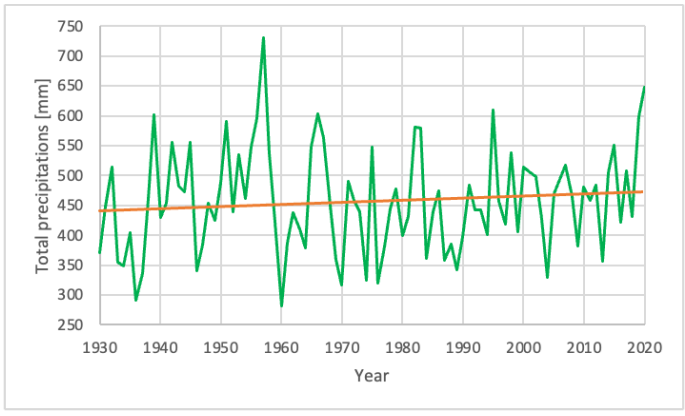

Figure 7.41: Linear regression analysis for Salekhard total precipitations (1930-2020)

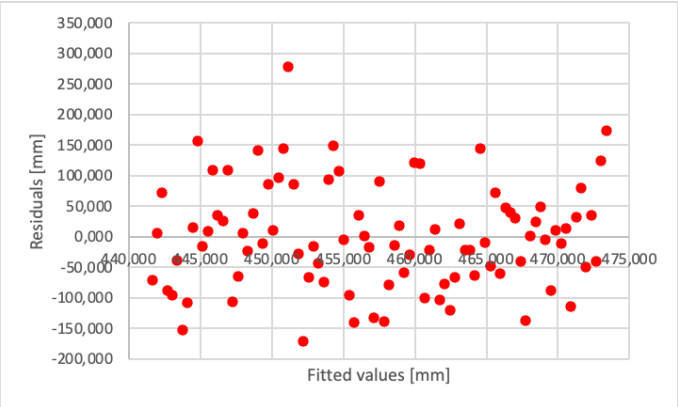

Figure 7.42: Residuals for Salekhard total precipitations (1930-2020)

Salekhard results for the last 50 years are listed in **Table 7.10**. It is possible to note that in all cases, there is a positive tendency, indicating an increase of 0,064 °C/year (with a 3% significance), 0,066 °C/year (with a 1% significance) and 0,06 °C/year (with a 15% significance) for mean, minimum and maximum temperature, respectively, and 1,04 mm/year (with an 11% significance) for precipitations.

Moreover, the F-test showed to be statistically significant in all cases.

Figure 7.43 to **Figure 7.50** show the linear fit results and the corresponding residuals.

Table 7.10: Linear regression outcomes for Salekhard (last 50 years)

Information	**Linear regression equation**	R^2	***p*-value**	**F-test result**
Average annual temperature	$y = -132{,}5 + 0{,}06 \cdot x$	0,03	<0,0001	**ACCEPTED**
Minimum annual temperature	$y = -176{,}58 + 0{,}07 \cdot x$	0,01	0,032	**ACCEPTED**
Maximum annual temperature	$y = -92{,}08 + 0{,}06 \cdot x$	0,15	0,006	**ACCEPTED**
Total annual precipitations	$y = -2964{,}88 + 1{,}71 \cdot x$	0,11	0,019	**ACCEPTED**

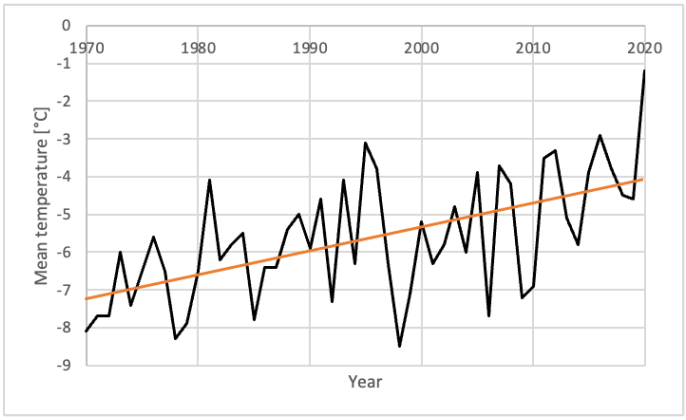

Figure 7.43: Linear regression analysis for Salekhard mean temperatures (1970-2020)

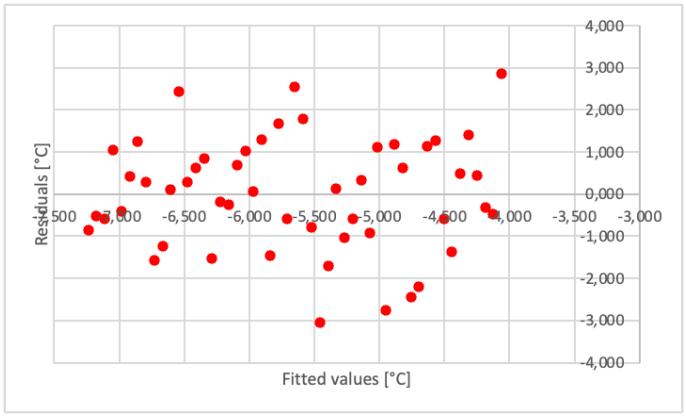

Figure 7.44: Residuals for Salekhard mean temperatures (1970-2020)

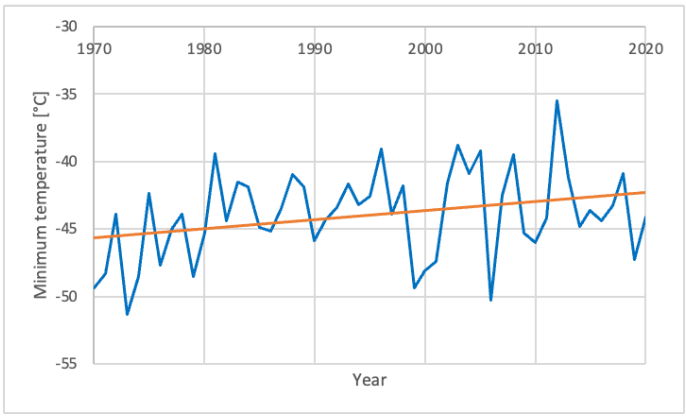

Figure 7.45: Linear regression analysis for Salekhard minimum temperatures (1970-2020)

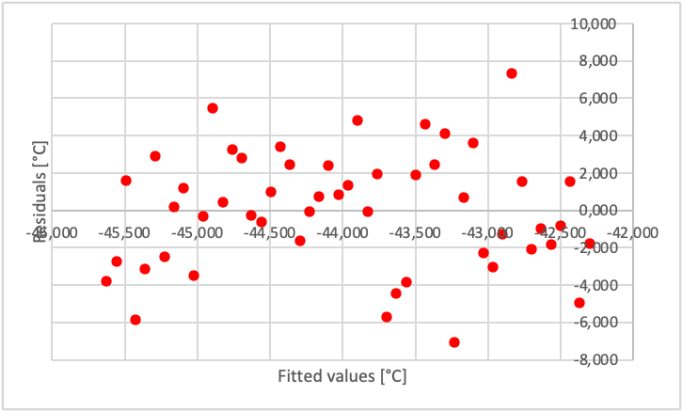

Figure 7.46: Residuals for Salekhard minimum temperatures (1970-2020)

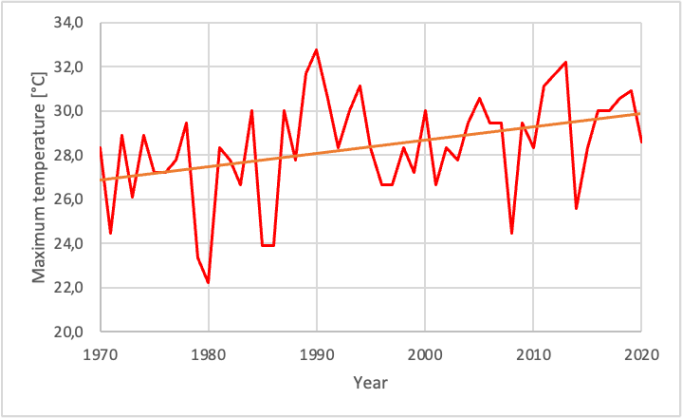

Figure 7.47: Linear regression analysis for Salekhard maximum temperatures (1970-2020)

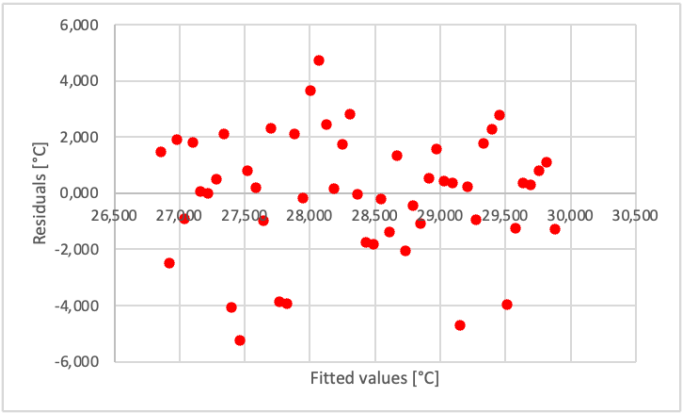

Figure 7.48: Residuals for Salekhard maximum temperatures (1970-2020)

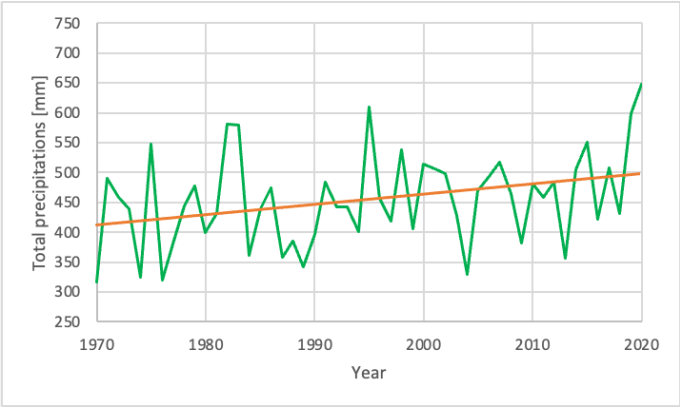

Figure 7.49: Linear regression analysis for Salekhard total precipitations (1970-2020)

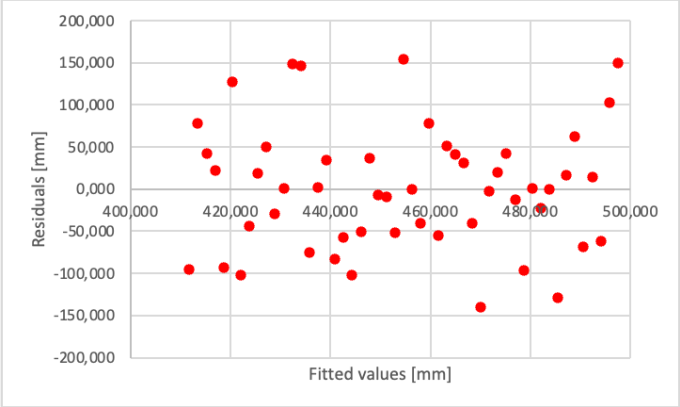

Figure 7.50: Residuals for Salekhard total precipitations (1970-2020)

Broadly speaking, it should be noted that simple linear regression analysis can give us an overall idea about the collected data in terms of trend, but it is not suitable for a deep climate change analysis; hence, further statistical models must be implemented.

7.4 MANN-KENDALL TEST AND SEN'S SLOPE ESTIMATOR

The non-parametric Mann-Kendall (MK) test is usually used to detect an upward or downward (i.e., monotonic) trend in a series of hydrological and environmental data. Even though parametric methods are more powerful, their applications are limited to normally distributed time series. Therefore, since most climatic data do not fulfill normality requirements, non-parametric approaches are most frequently applied in

trend analysis. Moreover, such methodologies are considered more robust against outliers.

The null hypothesis H_0 indicates no trend in the series and data that come from an independent population are identically distributed; the alternative hypothesis H_1 states that the values follow a monotonic trend.

The time series $x_1, x_2, \ldots, x_n$ represents n data points; statistic S can be obtained from:

$$S = \sum_{k=1}^{n-1} \sum_{j=k+1}^{n} sgn(x_j - x_k)$$

where

$$sgn(x_j - x_k) = \begin{cases} 1 & if\ x_j - x_k > 0 \\ 0 & if\ x_j - x_k = 0 \\ -1 & if\ x_j - x_k < 0 \end{cases}$$

in which k=1, 2,…, n-1 and j=k+1,…, n.

A positive value of S means that later observations in the time series tend to be larger than those that appear earlier, indicating an increasing trend, while S<0 is characteristic of a negative tendency.

When n>8, S approximates to the normal distribution: its mean is equal to 0 and the variance is determined as follows:

$$\sigma^2(S) = \frac{n \cdot (n-1) \cdot (2 \cdot n - 5)}{18}$$

Finally, the test statistic Z is obtained from:

$$Z = \begin{cases} \dfrac{S-1}{\sqrt{\sigma^2(S)}} & if\ S > 0 \\ 0 & if\ S = 0 \\ \dfrac{S+1}{\sqrt{\sigma^2(S)}} & if\ S < 0 \end{cases}$$

Hence, given a confidence level α, the sequential data would be supposed to experience a statistically significant trend if $|Z| > Z\left(1-\frac{\alpha}{2}\right)$, where $Z\left(1-\frac{\alpha}{2}\right)$ is the corresponding value of $P=\frac{\alpha}{2}$ following the standard normal distribution. In this study, a 0,05 confidence level was used.

Hamed suggested that there will be a decrease or an increase in the S value when autocorrelation is positive or negative, which is underestimated or overestimated by the variance $\sigma^2(S)$; therefore, the Mann-Kendall test may lead to uncorrected results. Applying the trend-free pre-whitening (TFPW) process can overcome this problem.
To check whether TFPW is necessary, we need to calculate the $lag-1$ autocorrelation coefficient $r1$:

$$r1=\frac{\frac{1}{n-k}\cdot\sum_{i=1}^{n-k}[(x_i-\bar{x})\cdot(x_{i+k}-\bar{x})]}{\frac{1}{n}\cdot\sum_{i=1}^{n}(x-\bar{x})^2}$$

where $\bar{x}$ is the mean value of the time series.
If the following condition

$$\frac{-1-1{,}96\cdot\sqrt{n-2}}{n-1}\leq r1\leq\frac{-1+1{,}96\cdot\sqrt{n-2}}{n-1}$$

is satisfied, then the series is assumed to be independent at a 5% significance level and there is no need for TFPW.
If this is not the case, the Mann-Kendall test must be applied to the trend-free pre-whitened data, defined as follows:

$$\begin{Bmatrix} x_2-r1\cdot x_1 \\ x_3-r1\cdot x_2 \\ \dots \\ x_n-r1\cdot x_{n-1} \end{Bmatrix}$$

TFPW results for Tomsk and Salekhard data for the last 100 years are reported in **Table 7.11** and **Table 7.12**.

Table 7.11: Trend-free pre-whitening results for Tomsk (last 100 years)

Information	r_{min}	$r1$	r_{MAX}	Need of TFPW?
Average annual temperature	-0,205	0,271	0,185	**YES**
Minimum annual temperature	-0,205	0,316	0,185	**YES**
Maximum annual temperature	-0,207	0,302	0,187	**YES**
Total annual precipitations	-0,205	0,052	0,185	**NO**

Table 7.12: Trend-free pre-whitening results for Salekhard (last 100 years)

Information	r_{min}	$r1$	r_{MAX}	Need of TFPW?
Average annual temperature	-0,205	0,243	0,185	**YES**
Minimum annual temperature	-0,207	0,142	0,187	**NO**
Maximum annual temperature	-0,217	0,153	0,194	**NO**
Total annual precipitations	-0,217	0,262	0,194	**YES**

TFPW results for Tomsk and Salekhard data for the last 50 years are reported in **Table 7.13** and **Table 7.14**.

Table 7.13: Trend-free pre-whitening results for Tomsk (last 50 years)

Information	r_{min}	$r1$	r_{MAX}	Need of TFPW?
Average annual temperature	-0,298	0,108	0,257	**NO**
Minimum annual temperature	-0,298	0,131	0,257	**NO**

Maximum annual temperature	-0,298	0,121	0,257	**NO**
Total annual precipitations	-0,298	-0,169	0,257	**NO**

Table 7.14: Trend-free pre-whitening results for Salekhard (last 50 years)

Information	r_{min}	$r1$	r_{MAX}	**Need of TFPW?**
Average annual temperature	-0,298	0,292	0,257	**YES**
Minimum annual temperature	-0,298	0,182	0,257	**NO**
Maximum annual temperature	-0,298	0,291	0,257	**YES**
Total annual precipitations	-0,298	0,262	0,257	**NO**

The statistical analysis was divided into two parts. First, the Mann-Kendall test and the Sen's slope estimator were applied to the time series data without TFPW; later, those sets which needed pre-whitening were modified and the statistical tests were again applied. All the results were obtained by means of Microsoft Excel and Addinsoft XLSTAT 2021.

7.4.1 MANN-KENDALL TEST WITHOUT TREND-FREE PRE-WHITENING

Results for Tomsk for the last 100 years are reported in **Table 7.15**. It is possible to highlight a positive trend in all the cases, which is in accordance with the outcomes of the linear regression analysis; in particular, a 0,023 °C/year, 0,071 °C/year, 0,009 °C/year and 0,494 mm/year increase is observed for mean, minimum and maximum temperature and precipitations, respectively.

On the other hand, the test was statistically significant at a 0,05 confidence level only for the first two indicators.

Table 7.15: Mann-Kendall test and Sen's slope estimator outcomes for Tomsk (without trend-free pre-whitening, last 100 years)

Information	S	p-value	MK result	Sen's slope
Average annual temperature	1855	<0,0001	**ACCEPTED**	0,023
Minimum annual temperature	1571	<0,0001	**ACCEPTED**	0,071
Maximum annual temperature	610	0,064	**REJECTED**	0,009
Total annual precipitations	594	0,082	**REJECTED**	0,494

Results for Tomsk for the last 50 years are reported in **Table 7.16**. It is possible to highlight a positive trend in all the cases, except for the annual T_{MAX}, which is in accordance with the outcomes of the linear regression analysis; in particular, a 0,038 °C/year, 0,071 °C/year and 1,053 mm/year increase is observed for mean and minimum temperature and precipitations, respectively, whereas no trend is observed for maximum temperature.

On the other hand, the test was statistically significant at a 0,05 confidence level only for the first indicator.

Table 7.16: Mann-Kendall test and Sen's slope estimator outcomes for Tomsk (without trend-free pre-whitening, last 50 years)

Information	S	p-value	MK result	Sen's slope
Average annual temperature	15124	0,0003	**ACCEPTED**	0,038
Minimum annual temperature	221	0,073	**REJECTED**	0,071
Maximum annual temperature	-50	0,688	**REJECTED**	0

Total annual precipitations	200	0,106	**REJECTED**	1,053

Results for Salekhard for the last 100 years are reported in **Table 7.17**. Also in this case, the results are consistent with the one obtained in the linear regression analysis; in particular, an increase of 0,01 °C/year, 0,023 °C/year and 0,459 mm/year was observed for mean and maximum temperature and precipitations, respectively. In contrast, a decrease of 0,004 °C/year is characteristic of the minimum temperature.
Mann-Kendall test was statistically significant at a 0,05 confidence level only for T_{MAX} time series.

Table 7.17: Mann-Kendall test and Sen's slope estimator outcomes for Salekhard (without trend-free pre-whitening, last 100 years)

Information	S	p**-value**	**MK result**	**Sen's slope**
Average annual temperature	569	0,095	**REJECTED**	0,01
Minimum annual temperature	-204	0,539	**REJECTED**	-0,004
Maximum annual temperature	789	0,007	**ACCEPTED**	0,023
Total annual precipitations	374	0,201	**REJECTED**	0,459

Results for Salekhard for the last 50 years are reported in **Table 7.18**. Also in this case, the results are consistent with the one obtained in the linear regression analysis; in particular, an increase of 0,046 °C/year, 0,069 °C/year, 0,044 °C/year and 1,75 mm/year was observed for mean, minimum and maximum temperature and precipitations, respectively.
Mann-Kendall test was statistically significant at a 0,05 confidence level for all time series.

Table 7.18: Mann-Kendall test and Sen's slope estimator outcomes for Salekhard (without trend-free pre-whitening, last 50 years)

Information	S	p-value	MK result	Sen's slope
Average annual temperature	541	<0,0001	**ACCEPTED**	0,068
Minimum annual temperature	262	0,034	**ACCEPTED**	0,069
Maximum annual temperature	349	0,005	**ACCEPTED**	0,058
Total annual precipitations	292	0,018	**ACCEPTED**	1,75

7.4.2 MANN-KENDALL TEST WITH TREND-FREE PRE-WHITENING

Results for Tomsk for the last 100 years are reported in **Table 7.19**. In this case, a positive trend of 0,016 °C/year, 0,048 °C/year and 0,006 °C/year was observed for average, minimum and maximum temperature, respectively: it is possible to note that in this case, the increasing rates are lower with respect to the non-pre-whitened time series. Mann-Kendall test is still not statistically significant at a 0,05 confidence level for T_{MAX}.

Table 7.19: Mann-Kendall test and Sen's slope estimator outcomes for Tomsk (with trend-free pre-whitening, last 100 years)

Information	S	p-value	MK result	Sen's slope
Average annual temperature	1410	<0,0001	**ACCEPTED**	0,016
Minimum annual temperature	1030	0,002	**ACCEPTED**	0,048
Maximum annual temperature	306	0,349	**REJECTED**	0,006

Results for Salekhard for the last 100 years are reported in **Table 7.20**. In this case, the Mann-Kendall test is still not statistically significant at a 0,05 confidence level for both indicators.

An increase of 0,008 °C/year and 0,31 mm/year was observed for mean temperature and total precipitations, respectively.

Table 7.20: Mann-Kendall test and Sen's slope estimator outcomes for Salekhard (with trend-free pre-whitening, last 100 years)

Information	***S***	***p*-value**	**MK result**	**Sen's slope**
Average annual temperature	499	0,138	**REJECTED**	0,008
Total annual precipitations	339	0,403	**REJECTED**	0,31

Results for Salekhard for the last 50 years are reported in **Table 7.21**. In this case, the Mann-Kendall test is still statistically significant at a 0,05 confidence level for both indicators.

An increase of 0,068 °C/year and 0,058 °C/year was observed for mean and maximum temperature, respectively.

Table 7.21: Mann-Kendall test and Sen's slope estimator outcomes for Salekhard (with trend-free pre-whitening, last 50 years)

Information	***S***	***p*-value**	**MK result**	**Sen's slope**
Average annual temperature	351	0,003	**ACCEPTED**	0,046
Maximum annual temperature	245	0,041	**ACCEPTED**	0,044

7.5 INNOVATIVE TREND ANALYSIS

Şen proposed the innovative trend analysis (ITA) to detect trends in time series. In this approach, data are equally divided into two segments between the first to the last date and arranged in ascending order; the two vectors are then plotted in the Cartesian coordinate system (the first one in the x-axis and the second in the y-axis) together with the bisector 1:1 line (45°), dividing the area into two equal regions: if the data points exist on the top triangle, it is indicative of a positive trend and vice-versa, whereas if the values lay on the bisector, no trend is observed.

Compared with the Mann-Kendall test, this approach has some advantages; in particular, it allows a more detailed interpretation of trend detection, which has benefits for identifying hidden variations of climatic data such as precipitations and temperatures, and the graphical illustration is helpful to analyze the trend variability of extreme events, which cannot be discovered by applying traditional methods.

Results of Tomsk for the last 100 years data are reported in **Figure 7.51** to **Figure 7.54**. It is possible to observe that in this case, all the points are located above the bisecting line, indicating a positive trend: this is especially clear for the mean annual temperatures. However, low precipitation values show a slightly decreasing pattern.

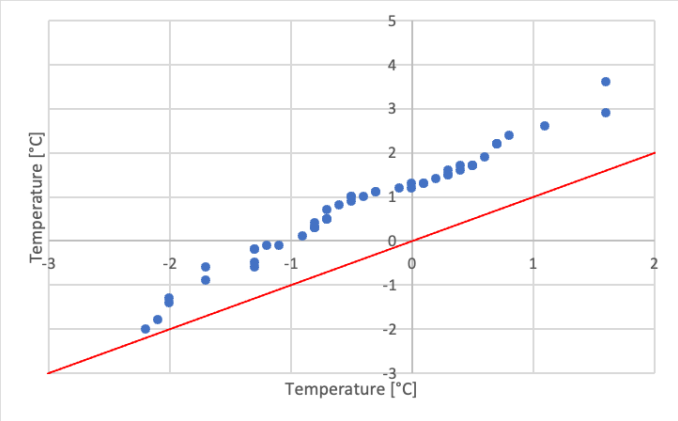

Figure 7.51: Innovative trend analysis for Tomsk mean temperatures (1920-2020)

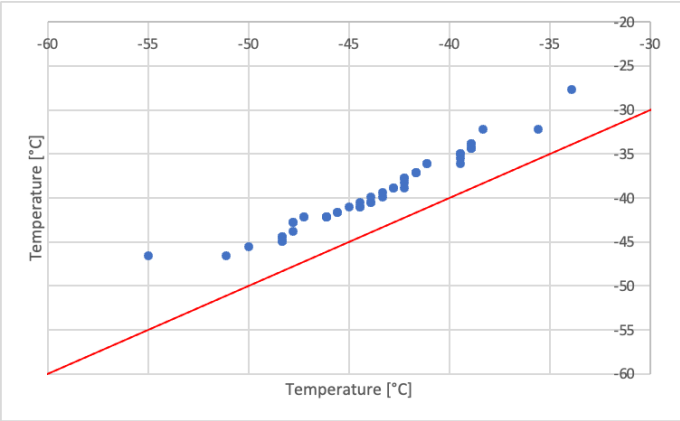

Figure 7.52: Innovative trend analysis for Tomsk minimum temperatures (1920-2020)

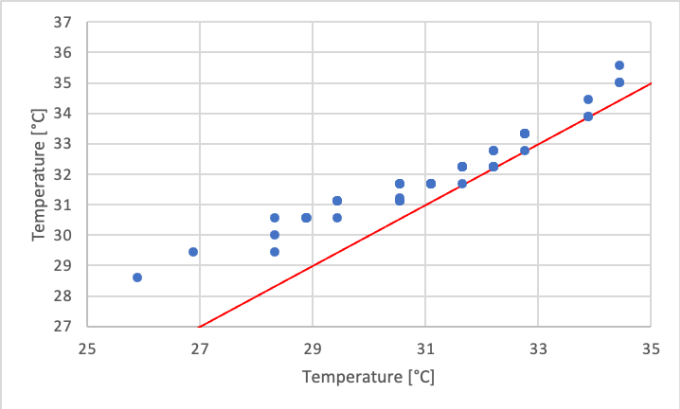

Figure 7.53: Innovative trend analysis for Tomsk maximum temperatures (1922-2020)

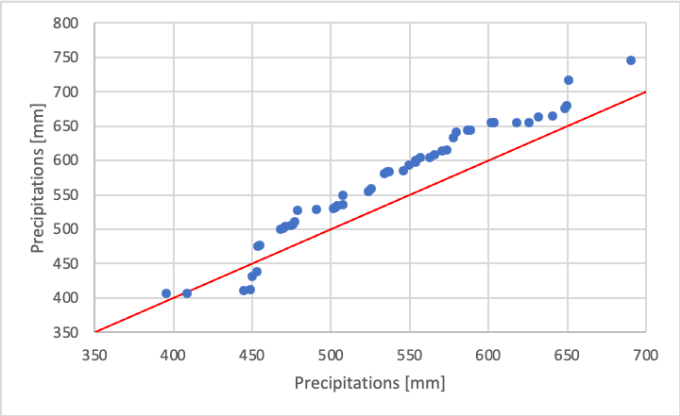

Figure 7.54: Innovative trend analysis for Tomsk total precipitations (1920-2020)

Results of Tomsk for the last 50 years data are reported in **Figure 7.55** to **Figure 7.58**. In this case, it is possible to evidence an increasing trend for mean temperatures and

precipitations, whereas T_{min} points are located close to the 45° line, which means that there is still an upward trend, but with a lower level of confidence.

Maximum temperature values are located more or less on the 45° line; therefore, no significant trend is detectable.

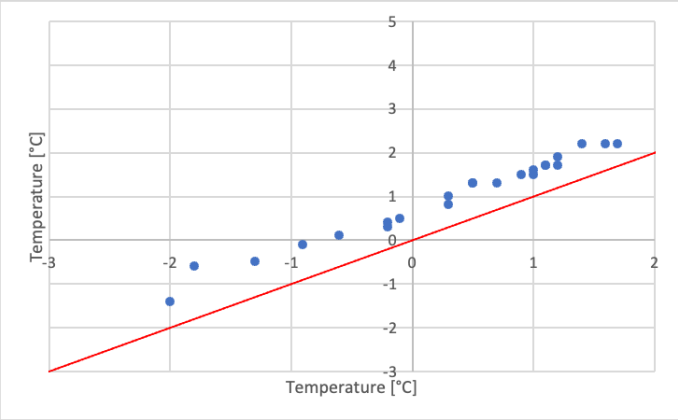

Figure 7.55: Innovative trend analysis for Tomsk mean temperatures (1970-2020)

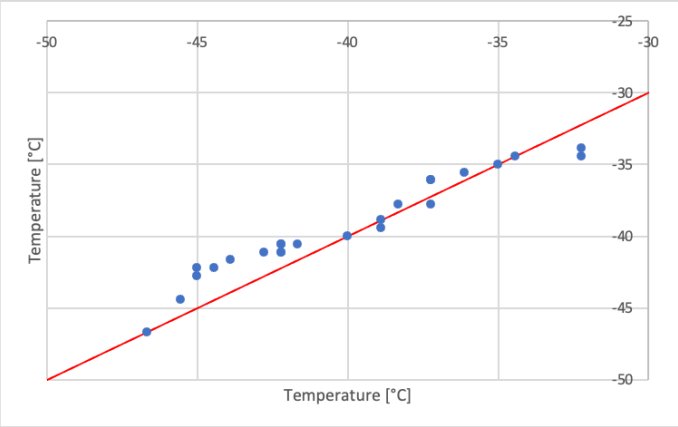

Figure 7.56: Innovative trend analysis for Tomsk minimum temperatures (1970-2020)

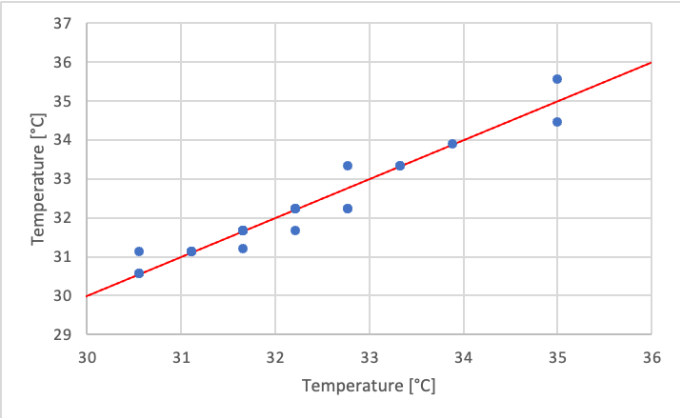

Figure 7.57: Innovative trend analysis for Tomsk maximum temperatures (1970-2020)

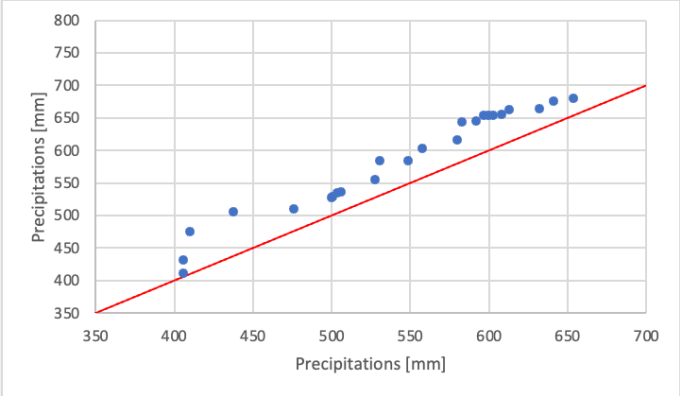

Figure 7.58: Innovative trend analysis for Tomsk total precipitations (1970-2020)

Results of Salekhard data for the last 100 years are reported in **Figure 7.59** to **Figure 7.62**. In this case, it is possible to see that points are closer to the 45° line, which indicates that there is still a tendency, but with a lower level of confidence.

Minimum temperatures show a decreasing trend, in line with the results of both linear regression analysis and Mann-Kendall test, whereas for T_{mean} and T_{MAX} we can observe an increasing pattern.

No significant trend is detectable for precipitations values.

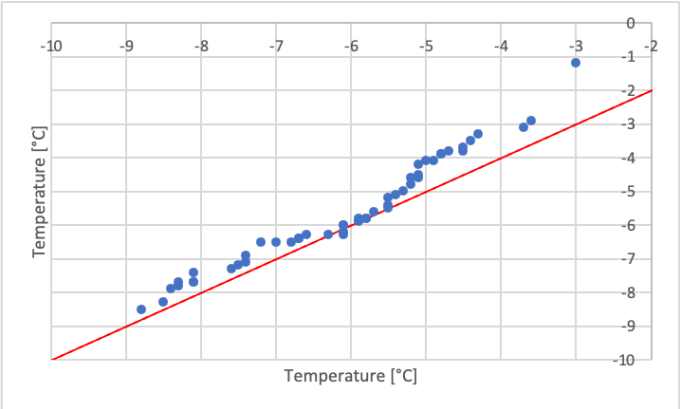

Figure 7.59: Innovative trend analysis for Salekhard mean temperatures (1920-2020)

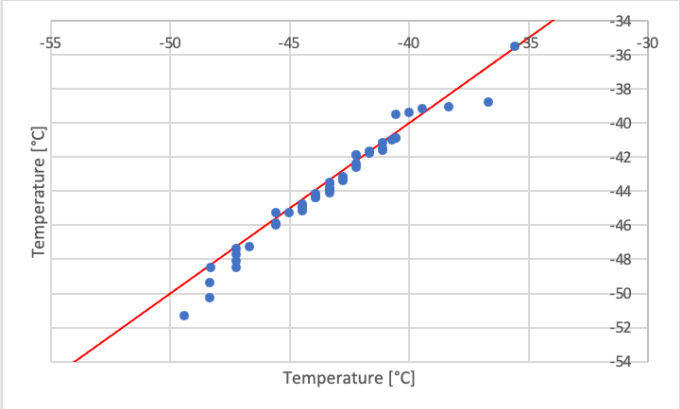

Figure 7.60: Innovative trend analysis for Salekhard minimum temperatures (1922-2020)

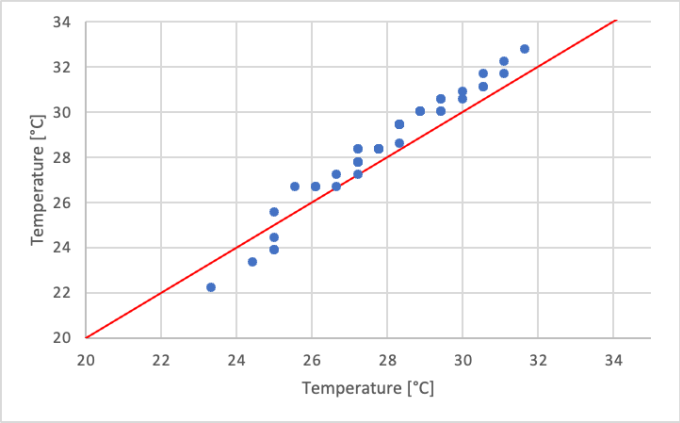

Figure 7.61: Innovative trend analysis for Salekhard maximum temperatures (1930-2020)

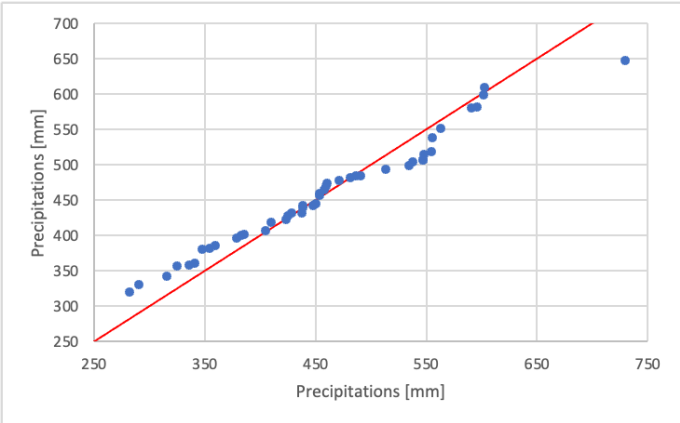

Figure 7.62: Innovative trend analysis for Salekhard total precipitations (1930-2020)

Results of Salekhard for the last 50 years data are reported in **Figure 7.63** to **Figure 7.66**. It is possible to observe that in this case, all the points are overall located above the bisecting line, indicating a positive trend: this is especially clear for the mean annual temperatures.

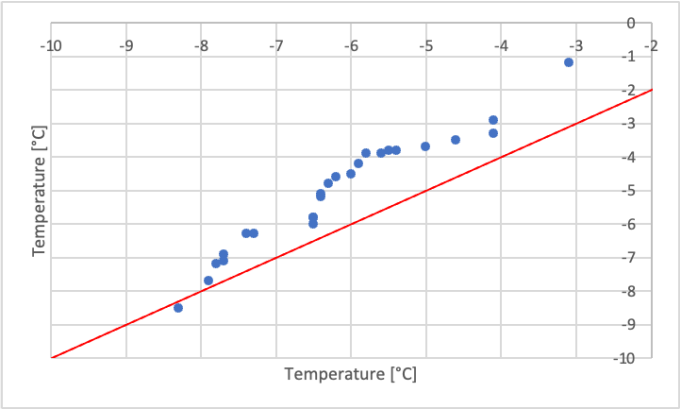

Figure 7.63: Innovative trend analysis for Salekhard mean temperatures (1970-2020)

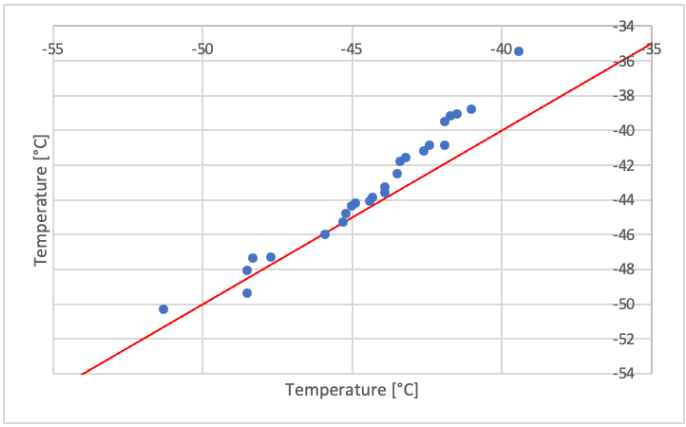

Figure 7.64: Innovative trend analysis for Salekhard minimum temperatures (1970-2020)

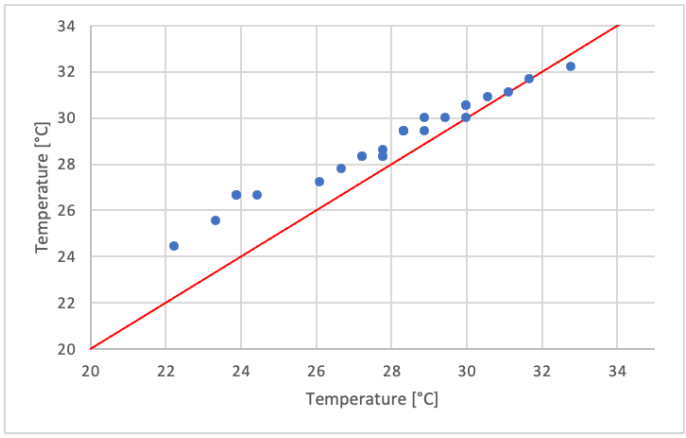

Figure 7.65: Innovative trend analysis for Salekhard maximum temperatures (1970-2020)

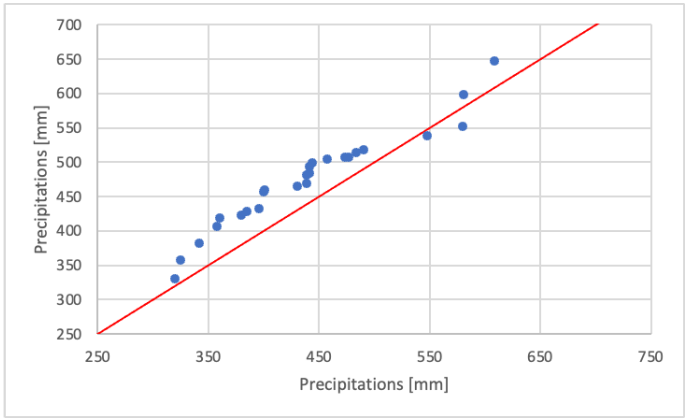

Figure 7.66: Innovative trend analysis for Salekhard total precipitations (1970-2020)

7.6 FROST DEPTH ASSESSMENT

The following analysis is devoted to studying frost depth variations for the two sites under consideration over the past years. In *chapter 6* it has been shown that the modified Berggren's formula allows determining the freezing depth with a good approximation; hence, for the calculations below, this approach will be adopted.

It should be noted that, due to the lack of sufficient information for Salekhard test section (in particular, no data regarding the calibrated volumetric water content are available), it is not possible to apply the modified Berggren's formula to this site; hence, another solution has to be implemented.
Considering that the evaluation of the freezing depth is a pretty cumbersome process, the following approach will be observed:

- calculation of the freezing depth over the last 50 years through the modified Berggrens's formula for Tomsk test sections;
- evaluation of a relationship between freezing depth and freezing index;
- apply the equation in order to evaluate frost depth variations in Tomsk and Salekhard.

Considering the results obtained above, the analysis will be applied over the last 100 years for Tomsk and over the last 50 years for Salekhard; for the calculations, two reference days have been chosen, namely, January 15 for Tomsk and December 12 for Salekhard.
Frost depth values determined through the modified Berggren's formula were evaluated by assuming a constant water content over the years.

Freezing depth results for the eight test sections in Tomsk are reported in **Figure 7.67**.

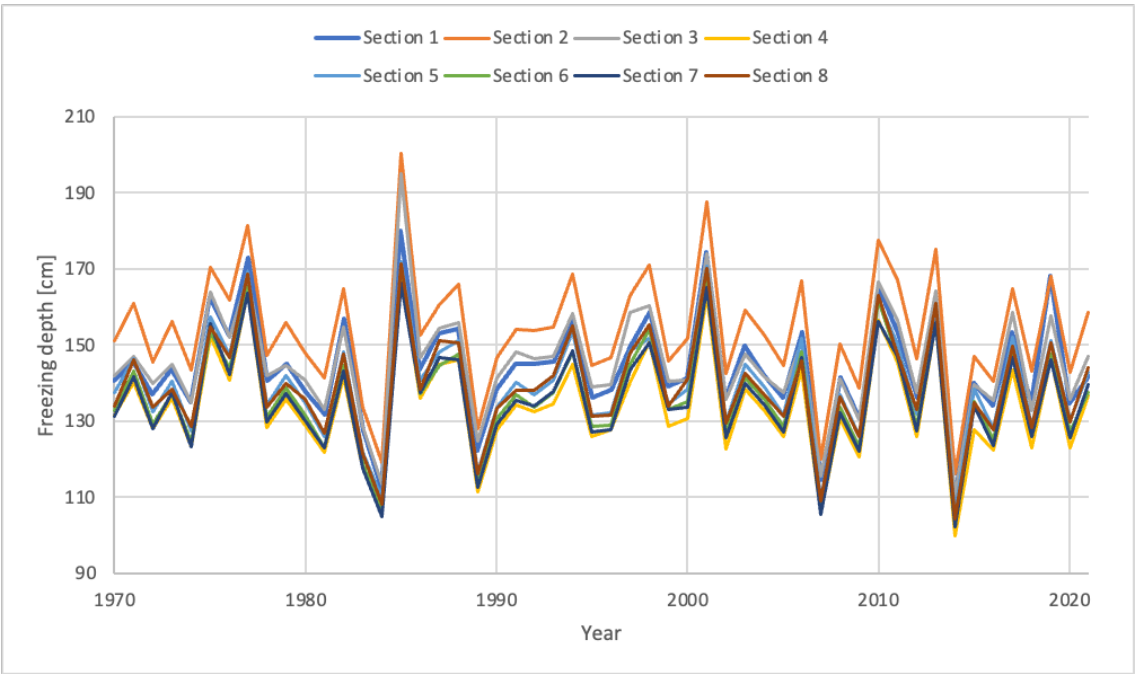

Figure 7.67: Frost depth values for the last 50 years in the eight test sections in Tomsk

As already underlined, frost depth calculation is quite a long process; hence, to reduce the computational time, freezing index values have been analyzed to see if a correlation between the two data sets can be found.

By observing **Figure 7.68**, it is possible to highlight the same trend for the two series; hence, climate change considerations can be made in terms of the freezing index.

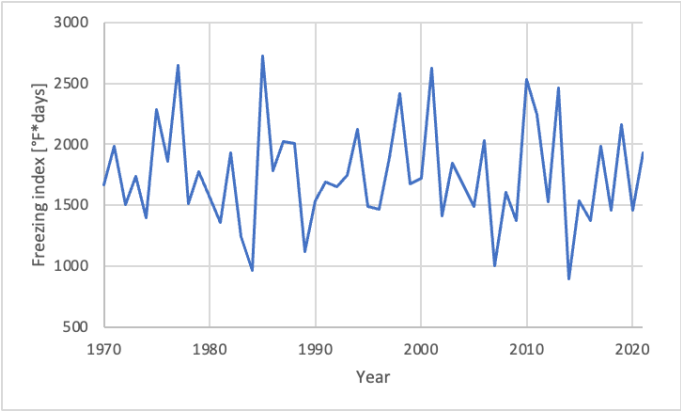

Figure 7.68: Freezing index for the last 50 years in Tomsk

The interpolating equation can be derived by plotting the freezing index versus freezing depth values for each test section; **Figure 7.69** to **Figure 7.76** show the obtained results.

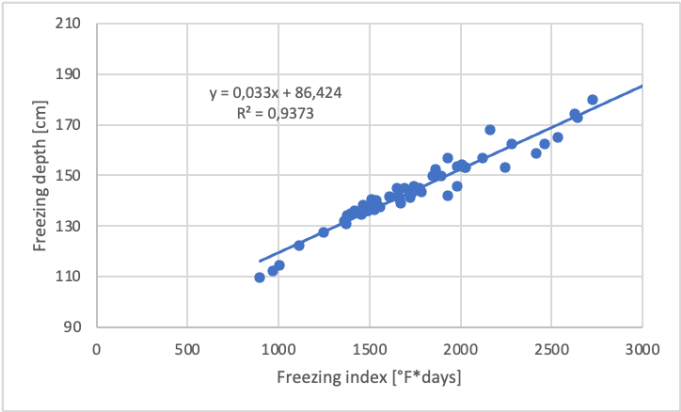

Figure 7.69: Freezing index vs. freezing depth values for section 1 in Tomsk

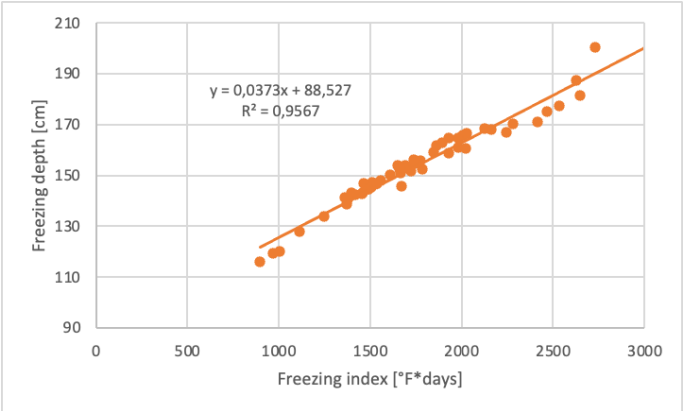

Figure 7.70: Freezing index vs. freezing depth values for section 2 in Tomsk

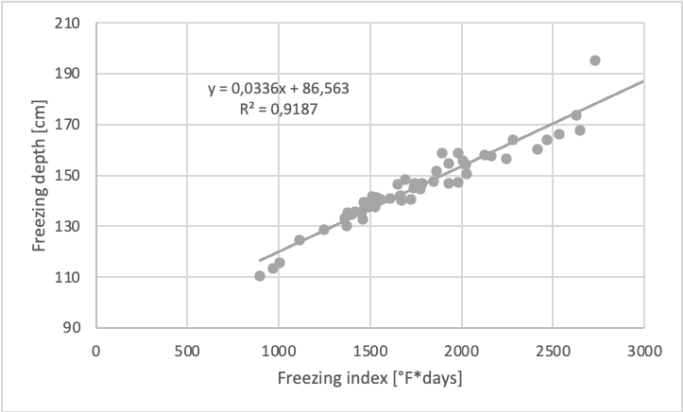

Figure 7.71: Freezing index vs. freezing depth values for section 3 in Tomsk

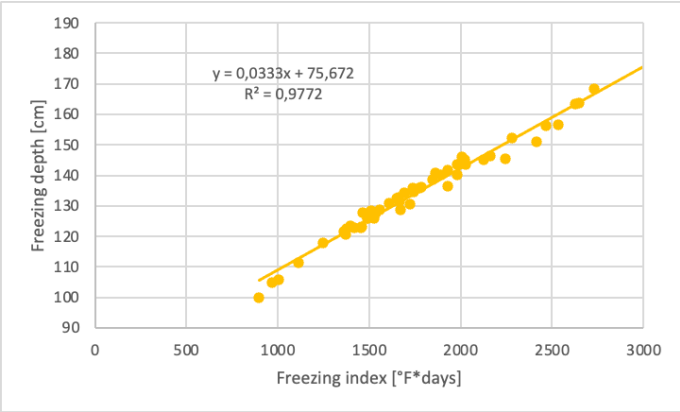

Figure 7.72: Freezing index vs. freezing depth values for section 4 in Tomsk

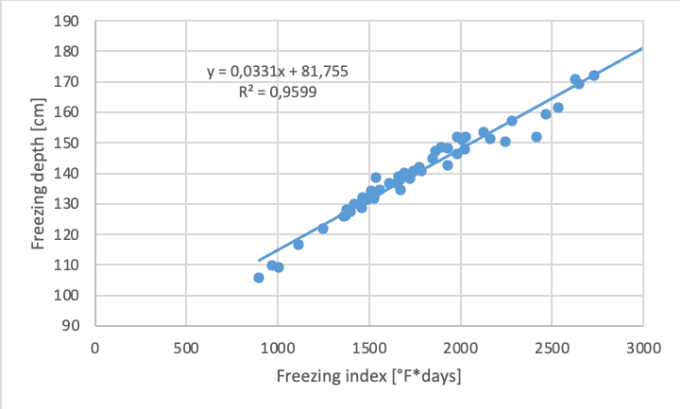

Figure 7.73: Freezing index vs. freezing depth values for section 5 in Tomsk

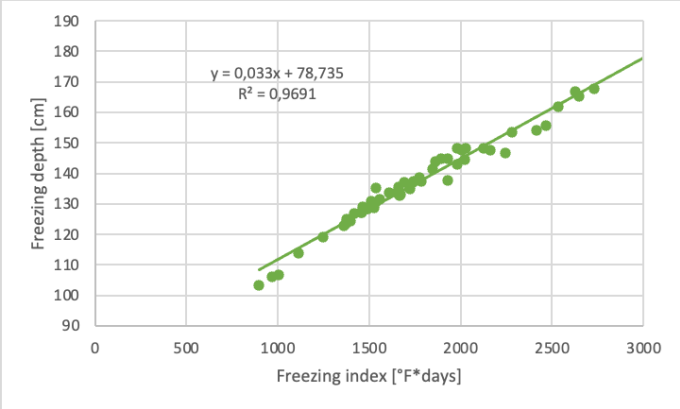

Figure 7.74 Freezing index vs. freezing depth values for section 6 in Tomsk

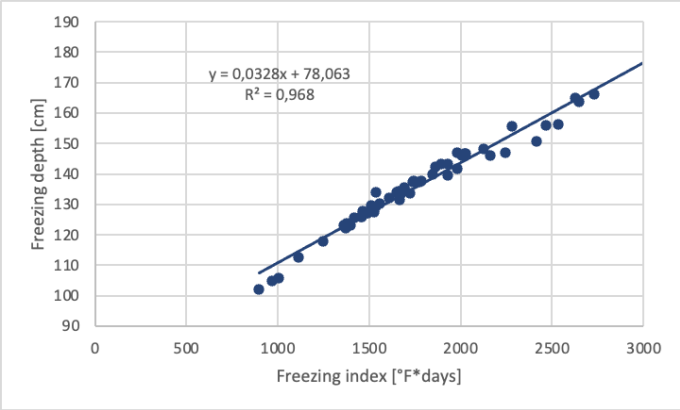

Figure 7.75: Freezing index vs. freezing depth values for section 7 in Tomsk

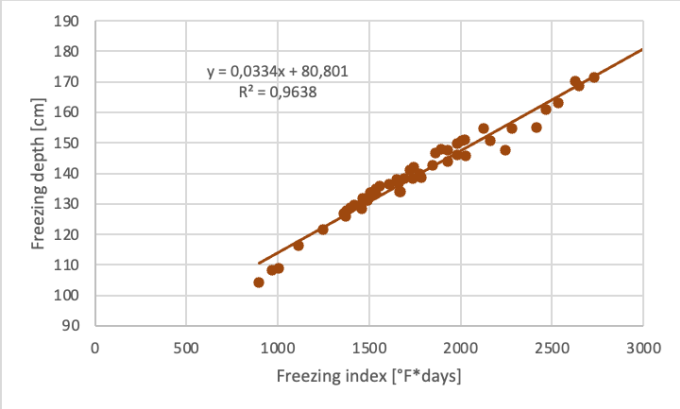

Figure 7.76: Freezing index v.s freezing depth values for section 8 in Tomsk

The following generic equation may be derived:

$$FD = 0{,}0337 \cdot FI + 82{,}0685$$

where FD is the freezing depth in centimeters and FI is the freezing index in degrees Fahrenheit.

It should be noted that all the equations above have been obtained for freezing index values comprised between 800 °F and 3000 °F; hence, it is suggested to adopt a different approach in the case data are outside this range.

In order to study the evolution of the freezing depth over time for the two sites under investigation, freezing index values for the last 100 and 50 years must be derived for Tomsk and Salekhard, respectively. **Figure 7.77** and **Figure 7.78** show the results and the

linear regression equation (for Tomsk test section, daily temperature data were only available from 1925): it is possible to observe a negative trend, indicating a decrease of about 4,5 °F/year in Tomsk and 8 °F/year in Salekhard.

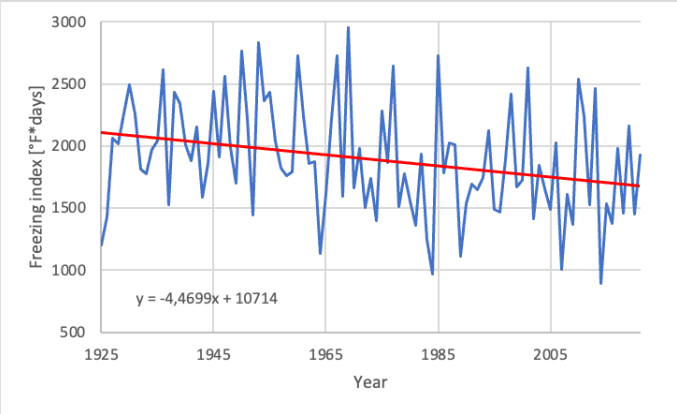

Figure 7.77: Freezing index for the last 100 years in Tomsk

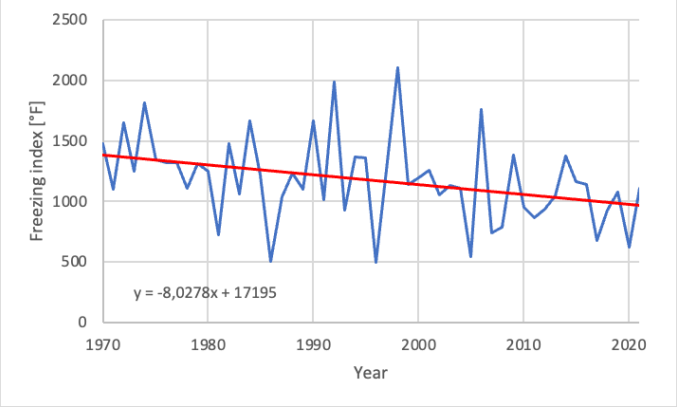

Figure 7.78: Freezing index for the last 50 years in Salekhard

In conclusion, it is possible to observe a decrease of the freezing index of 429,44 °F and 409,41 °F for Tomsk and Salekhard, respectively, with a subsequent reduction of the freezing depth as well, as reported in **Table 7.22**.

Table 7.22: Freezing depth outcomes

TOMSK (15/01)	
1925	**2021**
FI=2109,44 °F	*FI*=1680 °F
FD=153,16 cm	*FD*=1380,7 cm

ΔFD=19,46 cm	
SALEKHARD (05/12)	
1970	**2021**
FI=1380,23 °F	FI=970,82 °F
FD=128,58 cm	FD=114,79 cm
ΔFD=13,79 cm	

REFERENCES

BIBLIOGRAPHY

- Alemu Z. A., Dioha M. O. – *Climate Change and Trend Analysis of Temperature: the Case of Addis Ababa, Ethiopia*, Environmental System Research, Ethiopia, 2020;
- Alifujiang Y., Abuduwaili J., Maihemuti B., Emin B., Groll M. – *Innovative Trend Analysis of Precipitation in the Lake Issyk-Kul Basin, Kyrgyzstan*, MDPI, China, 2020;
- Mahmood R., Jia S., Zhu W., *Analysis of Climate Variability, Trends and Prediction in the Most Active Parts of the Lake Chad Basin, Africa*, Scientific Reports, China, 2019;
- Privitera G. J. – *Statistics for the Behavioral Sciences*, SAGE Publications, United States, 2018;
- *XLSTAT 2021 user's manual*, Addinsoft, United States, 2021.

SITOGRAPHY

- https://statisticsbyjim.com/regression/interpret-f-test-overall-significance-regression/;
- https://www.statisticshowto.com/probability-and-statistics/f-statistic-value-test/;
- https://www.youtube.com/watch?v=lOuQ9Trte74.

Part 4:

Structural Analysis

PAVEMENT DESIGN ACCORDING TO RUSSIAN REGULATIONS

The following chapter is devoted to the assessment of two road sections (one in Tomsk and one in Salekhard) following the Russian standards for the design of flexible pavements.
In particular, two reference documents are now available: ODN 218.046-01: *Design of Flexible Road Pavements* and the new version PNST 542-2021: *Automobile Roads of General Use. Flexible Pavement. Design Rules*, which contains updates and corrections of the previous regulations.

The goal of the analysis is to study the effects of climate change on pavement design by taking into account climatic effects such as rise in temperatures, precipitations increase and reduction of the freezing depth.
Results in Tomsk show that in the future, there will be a need for a thickness increase of the asphalt layer by approximately 9 cm and of the drainage stratum by a minimum value of 2 cm up to a maximum of 24 cm, as well as a reduction of the frost-protective layer by 4 cm.
In Salekhard, the most important outcome is the introduction of a drainage layer with a thickness varying between 22 cm and 30 cm, depending on the draining principle.

The main issue of the assessment was related to the fact that to date, there is no official English version of the Russian standards; therefore, the first step was to translate this document by means of online supports such as Google Translate, together with the help of the International Scientific Department of TSUAB.
A personally realized English version of the ODN 218.046-01 standards is reported in *annex 2*; it is hoped that this document will also be helpful for future investigations.

8.1 DESCRIPTION OF THE ROAD SECTIONS

Two simple cross-sections (one in Tomsk and one in Salekhard) have been analyzed; layers material and thickness are listed in **Table 8.1** and **Table 8.2**. Both pavements are of capital type, category IV (Tomsk) and III (Salekhard); according to **Figure P.2.2** and **Table P.2.7**, the corresponding road-climatic zone is II and I for Tomsk and Salekhard, respectively.

It is important to note that according to Russian regulations, pavement design is based on the verification of different conditions starting from a configuration in which the layers have the minimum thickness. If the requirements are not satisfied, the thicknesses are increased accordingly.
These minimum values are reported in the standard GOST R 59120-2021: *Automobile Roads of General Use. Road Pavement. General Requirements* and are equal to 3 cm for asphalt concrete layers and 8 cm for a crushed stone stratum.

Table 8.1: Analyzed cross-section in Tomsk

Layer	Material	Thickness [cm]
1	Dense asphalt concrete BND 100/130	3
2	High-porosity asphalt concrete BND 100/130	3
3	Crushed stone	8
4	Clayey soil	-

Table 8.2: Analyzed cross-section in Salekhard

Layer	Material	Thickness [cm]
1	Dense asphalt concrete BND 100/130	3
2	Crushed stone	8
3	Medium sand	-

8.2 COLLECTION OF TRAFFIC INFORMATION

The first step necessary to perform a pavement analysis is to retrieve traffic information on the sections under consideration.

For the case of Tomsk, data have been derived from an experimental investigation conducted by researchers of the Road Construction Faculty of TSUAB, who performed a monthly visual inspection of the passing vehicles over the period 2020-2021 for two different cross-sections, as shown in **Figure 8.1**. To stay conservative, the highest traffic values have been taken into account for the analysis, namely, data corresponding to section n° 1 (km 1+000) for the year 2021. The results are reported in **Table 8.3**.

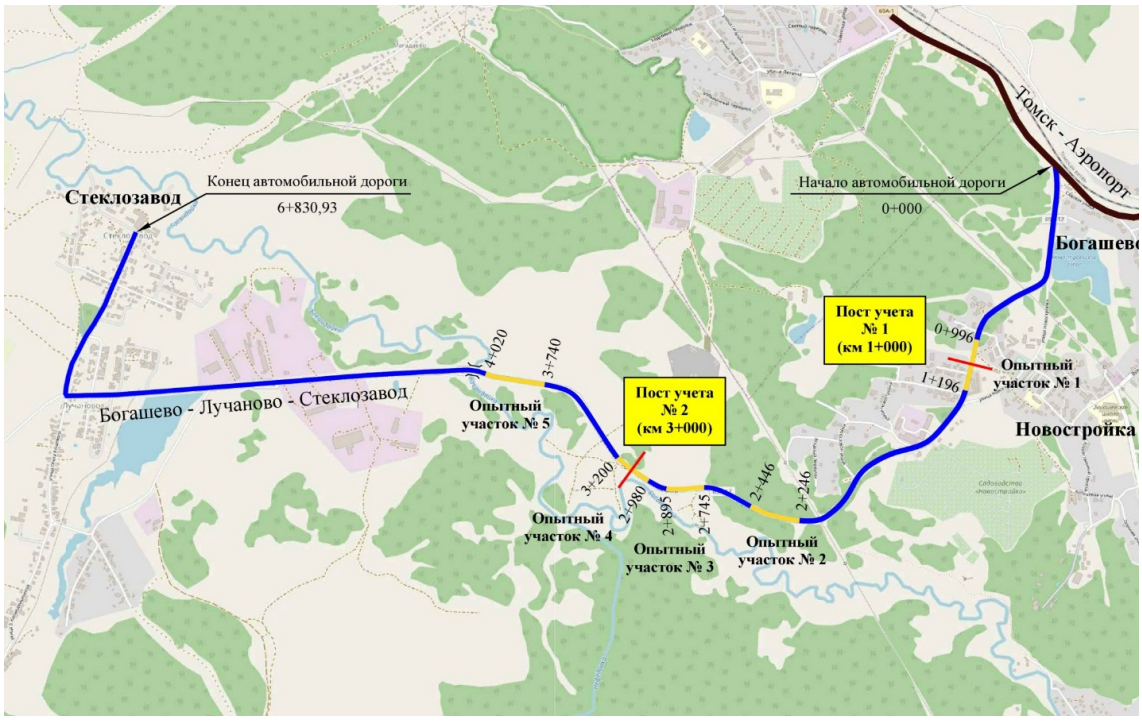

Figure 8.1: Location of the test sections for the collection of traffic information

For the case of Salekhard, traffic information has been provided by the local road organization of the Yamalo-Nenets autonomous okrug (ГКУ "Дорожная дирекция ЯНАО"). Average daily traffic flow data are available for years 2015, 2017, 2018 and 2020; also in this case, to stay conservative, the year with the highest value has been taken into account, i.e., 2020. A detailed traffic description is reported in **Table 8.4**.

It should be noted that, in order to perform a pavement design according to ODN and PNST standards, prospective traffic information at the end of the service life is necessary; due to the lack of sufficient data, values in **Table 8.3** and **Table 8.4** have been used in the calculations, by supposing them to occur at the end of the pavement life (15 years).

The next step is traffic load conversion. Following the indications in the Russian standards, a single-tire axle with a total load of 110 kN is taken as the reference one; hence, the wheel load is 55 kN, the transmitted pressure is 0,6 MPa and the imprint diameter is equal to 39 cm and 34 cm for a moving and stationary wheel, respectively, as reported in **Table P.1.1**.
Total reduction coefficients are taken according to **Table P.1.3**.

Table 8.3: Traffic information for Tomsk cross-section

Vehicle type	N_t **[vehicles/day]**	$N_t \cdot S_{t,sum}$ **[vehicles/day]**
Passenger cars	1011	1,52
Single-unit two-axle trucks	17	25,67
Single-unit three-axle trucks	23	53,59
Single-unit five-axle trucks	3	8,49
Single-unit six-axle trucks	14	29,68
Buses	23	0,035

Table 8.4: Traffic information for Salekhard cross-section

Vehicle type	N_t **[vehicles/day]**	$N_t \cdot S_{t,sum}$ **[vehicles/day]**
Passenger cars	1893	2,84
Single-unit two-axle trucks	563	850,13
Single-unit three-axle trucks	254	591,82
Single-unit five-axle trucks	237	670,71
Single-unit six-axle trucks	35	74,2
Buses	225	0,34

The average daily number of passages of the design vehicle within one lane of the carriageway at the end of the service life is calculated as (Tomsk and Salekhard, respectively):

$$N_r = f_{pol} \cdot \sum_{t=1}^{p} (N_t \cdot S_{t,sum})$$
$$= 0{,}55 \cdot (1{,}52 + 25{,}67 + 53{,}59 + 8{,}49 + 29{,}68 + 0{,}035)\ vehicles/day$$
$$= 66\ vehicles/day$$

$$N_r = 0{,}55 \cdot (2{,}84 + 850{,}13 + 591{,}82 + 670{,}71 + 74{,}2 + 0{,}34)\ vehicles/day$$
$$= 1205\ vehicles/day$$

where f_{pol} is taken according to **Table A.3.2**.

To perform the final step of traffic conversion, some parameters must be preliminarily defined, which are listed in **Table 8.5** and **Table 8.6**; traffic growth factor q was assumed equal to 1,04.

Table 8.5: Reference coefficients for Tomsk cross-section

T_{sl}	15 years (from **Table P.6.2**)
K_s	20 (from **Table P.6.3**)
T_{rdg}	130 days (from **Figure P.6.1** and **Table P.6.1**)
k_p	1,31 (from **Table A.3.3**)

Table 8.6: Reference coefficients for Salekhard cross-section

T_{sl}	15 years (from **Table P.6.2**)
K_s	20 (from **Table P.6.3**)
T_{rdg}	150 days (from **Figure P.6.1** and **Table P.6.1**)
k_p	1,38 (from **Table A.3.3**)

Finally, the total design number of passages of the design vehicle within one lane of the carriageway during the service life is determined as follows (Tomsk and Salekhard, respectively):

$$\sum N_r = 0{,}7 \cdot N_r \cdot \frac{K_s}{q^{T_{sl}-1}} \cdot T_{rdg} \cdot k_p = 0{,}7 \cdot 66 \ \frac{vehicles}{day} \cdot \frac{20}{1{,}04^{15\ years-1}} \cdot 130\ days \cdot 1{,}31$$
$$= 90099\ vehicles$$

$$\sum N_r = 0{,}7 \cdot 1205 \ \frac{vehicles}{day} \cdot \frac{20}{1{,}04^{15\ years-1}} \cdot 150\ days \cdot 1{,}38 = 2015793\ vehicles$$

8.3 PAVEMENT DESIGN FOR STRENGTH

Following the Russian regulations, there are three main criteria according to which pavements are designed: strength, frost resistance and drainage. Strength verification, in turn, is divided into three further assessments: elastic deflection of the whole structure, shear stability of the granular layers and fatigue of the asphalt concrete surface stratum; the analyses must be performed in this order.

8.3.1 PAVEMENT DESIGN FOR ELASTIC DEFLECTION

First of all, layers material properties must be defined; **Table 8.7** and **Table 8.8** report the values of the soil elastic modulus to be used in the design for elastic deflection. For the relative humidity $\frac{W}{W_t}$, a reference value equal to 0,7 has been assumed.

Table 8.7: Materials elastic moduli for elastic deflection design (Tomsk)

Material	***E* [MPa] for elastic deflection**
Dense asphalt concrete BND 100/130	2400 (from **Table P.3.2**)
High-porosity asphalt concrete BND 100/130	1400 (from **Table P.3.2**)
Crushed stone	450 (from **Table P.3.9**)
Clayey soil	41 (from **Table P.2.5**)

Table 8.8: Materials elastic moduli for elastic deflection design (Salekhard)

Material	***E* [MPa] for elastic deflection**
Dense asphalt concrete BND 100/130	2400 (from **Table P.3.2**)
Crushed stone	450 (from **Table P.3.9**)
Medium sand	120 (from **Table P.2.5**)

The following verification must be checked:

$$\frac{E_{ob}}{E_{min}} \geq K_{pr}^{tr}$$

where K_{pr}^{tr} is equal to 1,17, according to **Table A.3.1**.

The minimum required total modulus elasticity of the structure is determined as (Tomsk and Salekhard, respectively):

$$E_{min} = 98{,}65 \cdot \left(log \sum N_r - c\right) = 98{,}65 \cdot [\log 90099 - 3{,}25] = 168{,}17\ MPa$$

$$E_{min} = 98{,}65 \cdot [\log 2015793 - 3{,}25] = 301{,}32\ MPa$$

Both values are acceptable, according to the indications in **Table A.3.4**.

The design modulus of elasticity of the structure, instead, is determined using the nomogram in **Figure A.3.1** by reducing the multi-layer layout to an equivalent single-layer configuration: in this case, a bottom-up approach has been adopted.

Results show that the minimum thicknesses proposed at the beginning of the design process are not enough to satisfy the verification; hence, calculations have been performed stepwise by gradually increasing the depth of the layers until the condition was checked.

Tomsk calculations are reported in **Table 8.9** to **Table 8.13**.

Table 8.9: Pavement design for elastic deflection (Tomsk, 1st iteration)

$\frac{E_4}{E_3} = \frac{41\ MPa}{450\ MPa} = 0{,}091$

$\frac{h_3}{D} = \frac{8\ cm}{39\ cm} = 0{,}21$	
$\frac{E_{3+4}}{E_3}$	0,13 (from **Figure A.3.1**)
$E_{3+4} = 0{,}13 \cdot E_3 = 0{,}13 \cdot 450\ MPa = 58{,}5\ MPa$	
$\frac{E_{3+4}}{E_2} = \frac{58{,}5\ MPa}{1400\ MPa} = 0{,}042$	
$\frac{h_2}{D} = \frac{3\ cm}{39\ cm} = 0{,}077$	
$\frac{E_{2+3+4}}{E_2}$	0,06 (from **Figure A.3.1**)
$E_{2+3+4} = 0{,}06 \cdot E_2 = 0{,}06 \cdot 1400\ MPa = 84\ MPa$	
$\frac{E_{2+3+4}}{E_1} = \frac{84\ MPa}{2400\ MPa} = 0{,}035$	
$\frac{h_1}{D} = \frac{3\ cm}{39\ cm} = 0{,}077$	
$\frac{E_{ob}}{E_1}$	0,05 (from **Figure A.3.1**)
$E_{ob} = 0{,}05 \cdot E_1 = 0{,}05 \cdot 2400\ MPa = 120\ MPa$	
$K_{pr}^{tr} = \frac{120\ MPa}{168{,}17\ MPa} = 0{,}71 < 1{,}17$ **NOT VERIFIED**	

Table 8.10: Pavement new stratigraphy (Tomsk, 2nd iteration)

Material	**Thickness [cm]**
Dense asphalt concrete BND 100/130	6
High-porosity asphalt concrete BND 100/130	6
Crushed stone	16
Clayey soil	-

Table 8.11: Pavement design for elastic deflection (Tomsk, 2nd iteration)

$\frac{E_4}{E_3} = \frac{41\ MPa}{450\ MPa} = 0{,}091$	
$\frac{h_3}{D} = \frac{16\ cm}{39\ cm} = 0{,}41$	
$\frac{E_{3+4}}{E_3}$	0,2 (from **Figure A.3.1**)
$E_{3+4} = 0{,}2 \cdot E_3 = 0{,}2 \cdot 450\ MPa = 90\ MPa$	

$\frac{E_{3+4}}{E_2} = \frac{90\ MPa}{1400\ MPa} = 0{,}064$	
$\frac{h_2}{D} = \frac{6\ cm}{39\ cm} = 0{,}15$	
$\frac{E_{2+3+4}}{E_2}$	0,08 (from **Figure A.3.1**)
$E_{2+3+4} = 0{,}08 \cdot E_2 = 0{,}08 \cdot 1400\ MPa = 112\ MPa$	
$\frac{E_{2+3+4}}{E_1} = \frac{112\ MPa}{2400\ MPa} = 0{,}047$	
$\frac{h_1}{D} = \frac{6\ cm}{39\ cm} = 0{,}15$	
$\frac{E_{ob}}{E_1}$	0,05 (from **Figure A.3.1**)
$E_{ob} = 0{,}05 \cdot E_1 = 0{,}05 \cdot 2400\ MPa = 120\ MPa$	
$K_{pr}^{tr} = \frac{120\ MPa}{168{,}17\ MPa} = 0{,}71 < 1{,}17$ **NOT VERIFIED**	

Table 8.12: Pavement new stratigraphy (Tomsk, 3rd iteration)

Material	**Thickness [cm]**
Dense asphalt concrete BND 100/130	9
High-porosity asphalt concrete BND 100/130	9
Crushed stone	19
Clayey soil	-

Table 8.13: Pavement design for elastic deflection (Tomsk, 3rd iteration)

$\frac{E_4}{E_3} = \frac{41\ MPa}{450\ MPa} = 0{,}091$	
$\frac{h_3}{D} = \frac{19\ cm}{39\ cm} = 0{,}49$	
$\frac{E_{3+4}}{E_3}$	0,2 (from **Figure A.3.1**)
$E_{3+4} = 0{,}2 \cdot E_3 = 0{,}2 \cdot 450\ MPa = 90\ MPa$	
$\frac{E_{3+4}}{E_2} = \frac{90\ MPa}{1400\ MPa} = 0{,}064$	
$\frac{h_2}{D} = \frac{9\ cm}{39\ cm} = 0{,}23$	
$\frac{E_{2+3+4}}{E_2}$	0,095 (from **Figure A.3.1**)

$E_{2+3+4} = 0{,}095 \cdot E_2 = 0{,}095 \cdot 1400\ MPa = 133\ MPa$	
$\frac{E_{2+3+4}}{E_1} = \frac{133\ MPa}{2400\ MPa} = 0{,}055$	
$\frac{h_1}{D} = \frac{9\ cm}{39\ cm} = 0{,}23$	
$\frac{E_{ob}}{E_1}$	0,082 (from **Figure A.3.1**)
$E_{ob} = 0{,}082 \cdot E_1 = 0{,}05 \cdot 2400\ MPa = 196{,}8\ MPa$	
$K_{pr}^{tr} = \frac{196{,}8\ MPa}{168{,}17\ MPa} = 1{,}17$ **VERIFIED**	

It should be noted that the final configuration gives a factor of safety equal to 1,17; hence, these are the minimum thicknesses that satisfy the condition for elastic deflection.
The same rationale is applied to Salekhard cross-section (**Table 8.14** to **Table 8.18**).

Table 8.14: Pavement design for elastic deflection (Salekhard, 1st iteration)

$\frac{E_3}{E_2} = \frac{120\ MPa}{450\ MPa} = 0{,}27$	
$\frac{h_2}{D} = \frac{8\ cm}{39\ cm} = 0{,}21$	
$\frac{E_{2+3}}{E_2}$	0,31 (from **Figure A.3.1**)
$E_{2+3} = 0{,}31 \cdot E_2 = 0{,}31 \cdot 450\ MPa = 139{,}5\ MPa$	
$\frac{E_{2+3}}{E_1} = \frac{139{,}5\ MPa}{2400\ MPa} = 0{,}077$	
$\frac{h_1}{D} = \frac{3\ cm}{39\ cm} = 0{,}077$	
$\frac{E_{ob}}{E_1}$	0,08 (from **Figure A.3.1**)
$E_{ob} = 0{,}08 \cdot E_1 = 0{,}08 \cdot 2400\ MPa = 192\ MPa$	
$K_{pr}^{tr} = \frac{192\ MPa}{301{,}32\ MPa} = 0{,}64 < 1{,}17$ **NOT VERIFIED**	

Table 8.15: Pavement new stratigraphy (Salekhard, 2nd iteration)

Material	**Thickness [cm]**
Dense asphalt concrete BND 100/130	10
Crushed stone	20

Medium sand	-

Table 8.16: Pavement design for elastic deflection (Salekhard, 2nd iteration)

$\frac{E_3}{E_2} = \frac{120\ MPa}{450\ MPa} = 0{,}27$	
$\frac{h_2}{D} = \frac{20\ cm}{39\ cm} = 0{,}51$	
$\frac{E_{2+3}}{E_2}$	0,43 (from **Figure A.3.1**)
$E_{2+3} = 0{,}43 \cdot E_2 = 0{,}43 \cdot 450\ MPa = 193{,}5\ MPa$	
$\frac{E_{2+3}}{E_1} = \frac{193{,}5\ MPa}{2400\ MPa} = 0{,}081$	
$\frac{h_1}{D} = \frac{10\ cm}{39\ cm} = 0{,}26$	
$\frac{E_{ob}}{E_1}$	0,13 (from **Figure A.3.1**)
$E_{ob} = 0{,}13 \cdot E_1 = 0{,}13 \cdot 2400\ MPa = 312\ MPa$	
$K_{pr}^{tr} = \frac{312\ MPa}{301{,}32\ MPa} = 1{,}04 < 1{,}17$ **NOT VERIFIED**	

Table 8.17: Pavement new stratigraphy (Salekhard, 3rd iteration)

Material	**Thickness [cm]**
Dense asphalt concrete BND 100/130	12
Crushed stone	28
Medium sand	-

Table 8.18: Pavement design for elastic deflection (Salekhard, 3rd iteration)

$\frac{E_3}{E_2} = \frac{120\ MPa}{450\ MPa} = 0{,}27$	
$\frac{h_2}{D} = \frac{28\ cm}{39\ cm} = 0{,}72$	
$\frac{E_{2+3}}{E_2}$	0,44 (from **Figure A.3.1**)
$E_{2+3} = 0{,}44 \cdot E_2 = 0{,}44 \cdot 450\ MPa = 198\ MPa$	
$\frac{E_{2+3}}{E_1} = \frac{198\ MPa}{2400\ MPa} = 0{,}0825$	
$\frac{h_1}{D} = \frac{12\ cm}{39\ cm} = 0{,}31$	

$\frac{E_{ob}}{E_1}$	0,147 (from **Figure A.3.1**)
$E_{ob} = 0{,}147 \cdot E_1 = 0{,}147 \cdot 2400\ MPa = 352{,}8\ MPa$	
$K_{pr}^{tr} = \frac{352{,}8\ MPa}{301{,}32\ MPa} = 1{,}17$ **VERIFIED**	

Also in this case, the proposed thicknesses are the minimum values that satisfy the requirement for elastic deflection.

8.3.2 PAVEMENT DESIGN FOR SHEAR STABILITY

As before, layers material properties must be defined. **Table 8.19** and **Table 8.20** show the reference values for the elastic modulus, adhesion and angle of internal friction under the action of a dynamic load to be used in the analysis for shear stability (asphaltic material properties are derived following the indications of **Table A.3.5**).

Table 8.19: Material properties for shear stability design (Tomsk)

Material	***E* [MPa] for shear stability**
Dense asphalt concrete BND 100/130	1200 (from **Table P.3.2**)
High-porosity asphalt concrete BND 100/130	800 (from **Table P.3.2**)
Crushed stone	450 (from **Table P.3.9**)
Clayey soil	41 (from **Table P.2.5**)
c=0,007 MPa (from **Table P.2.4**)	
φ=6,5° (from **Table P.2.4**)	

Table 8.20: Material properties for shear stability design (Salekhard)

Material	***E* [MPa] for shear stability**
Dense asphalt concrete BND 100/130	1200 (from **Table P.3.2**)
Crushed stone	450 (from **Table P.3.9**)
Medium sand	120 (from **Table P.2.5**)
c_N=0,002 MPa (from **Table P.2.4**)	

φ=22° (from **Table P.2.4**)

The following verification must be checked:

$$\frac{T_{pr}}{T} \geq K_{pr}^{tr}$$

where K_{pr}^{tr} is equal to 1, according to **Table A.3.1**.

In this case, calculations are carried out by reducing the multi-layer structure to an equivalent two-layer configuration (pavement+subgrade); the elastic modulus of the upper stratum of the model is calculated as a weighted average (Tomsk and Salekhard, respectively):

$$E_v = \frac{1200\ MPa\ \cdot 9\ cm + 800\ MPa \cdot 9\ cm + 450\ MPa \cdot 19\ cm}{9\ cm + 9\ cm + 19\ cm} = 717{,}57\ MPa$$

$$E_v = \frac{1200\ MPa\ \cdot 12\ cm + 450\ MPa \cdot 28\ cm}{12\ cm + 28\ cm} = 675\ MPa$$

The limiting active shear stress depends on the weighted average specific gravity of the structural layers located above the tested one, as shown in **Table 8.21** and **Table 8.22**.

Table 8.21: Calculation of the weighted average specific gravity for Tomsk section

Material	**ρ [kg/m³] (from Table P.5.1)**
Dense asphalt concrete BND 100/130	2400
High-porosity asphalt concrete BND 100/130	2200
Crushed stone	1800
$\gamma_{sr} = \frac{2400\ \frac{kg}{m^3} \cdot 9\ cm + 2200\ \frac{kg}{m^3} \cdot 9\ cm + 1800\ \frac{kg}{m^3} \cdot 19\ cm}{9\ cm + 9\ cm + 19\ cm} \cdot 10^{-6} = 0{,}002\ kg/cm^3$	

Table 8.22: Calculation of the weighted average specific gravity for Salekhard section

Material	**ρ [kg/m³] (from Table P.5.1)**
Dense asphalt concrete BND 100/130	2400

Crushed stone	1800
$\gamma_{sr} = \frac{2400\ \frac{kg}{m^3} \cdot 12\ cm + 1800\ \frac{kg}{m^3} \cdot 28\ cm}{12\ cm + 28\ cm} \cdot 10^{-6} = 0{,}002\ kg/cm^3$	

Results show that the thicknesses proposed in the previous step (design for elastic deflection) are not enough to satisfy the verification for shear stability; hence, an iterative approach must be adopted.

For the calculation of the limiting active shear stress, the value of the angle of internal friction under static conditions has been derived from **Table P.2.4**.

Tomsk results are reported in **Table 8.23**, **Table 8.24** and **Table 8.25**.

Table 8.23: Pavement design for shear stability (Tomsk, 1st iteration)

$\frac{E_v}{E_4} = \frac{717{,}57\ MPa}{41\ MPa} = 17{,}5$	
$\frac{h_{1+2+3}}{D} = \frac{9\ cm + 9\ cm + 19\ cm}{39\ cm} = 0{,}95$	
$\bar{\tau}_h$	0,044 (from **Figure A.3.2**)
$T = \bar{\tau}_H \cdot p = 0{,}044 \cdot 0{,}6\ MPa = 0{,}026\ MPa$	
$T_{pr} = c_N \cdot k_d + 0{,}1 \cdot \gamma_{sr} \cdot z_{op} \cdot tan\varphi_{st}$ $= 0{,}007\ MPa \cdot 1 + 0{,}1 \cdot 0{,}002\ \frac{kg}{cm^3} \cdot 37\ cm \cdot tan18° = 0{,}0095\ MPa$	
$K_{pr}^{tr} = \frac{0{,}0095\ MPa}{0{,}026\ MPa} = 0{,}37 < 1$ **NOT VERIFIED**	

Table 8.24: Pavement new stratigraphy (Tomsk, 2nd iteration)

Material	**Thickness [cm]**
Dense asphalt concrete BND 100/130	10
High-porosity asphalt concrete BND 100/130	25
Crushed stone	27
Clayey soil	-

Considering the change in the thicknesses, the new values of E_v and γ_{sr} are equal to:

$$E_v = \frac{1200\ MPa\ \cdot 10\ cm + 800\ MPa \cdot 25\ cm + 450\ MPa \cdot 27\ cm}{10\ cm + 25\ cm + 27\ cm} = 712{,}1\ MPa$$

$$\gamma_{sr} = \frac{2400\ \frac{kg}{m^3} \cdot 10\ cm + 2200\ \frac{kg}{m^3} \cdot 25\ cm + 1800\ \frac{kg}{m^3} \cdot 27\ cm}{10\ cm + 25\ cm + 27\ cm} \cdot 10^{-6} = 0{,}0021\ kg/cm^3$$

Table 8.25: Pavement design for shear stability (Tomsk, 2nd iteration)

$\frac{E_v}{E_4} = \frac{711{,}1\ MPa}{41\ MPa} = 17{,}37$	
$\frac{h_{1+2+3}}{D} = \frac{10\ cm + 25\ cm + 27\ cm}{39\ cm} = 1{,}59$	
$\bar{\tau}_h$	0,018 (from **Figure A.3.2**)
$T = \bar{\tau}_H \cdot p = 0{,}018 \cdot 0{,}6\ MPa = 0{,}0108\ MPa$	
$T_{pr} = 0{,}007\ MPa \cdot 1 + 0{,}1 \cdot 0{,}0021\ \frac{kg}{cm^3} \cdot 62\ cm \cdot tan18° = 0{,}0111\ MPa$	
$K_{pr}^{tr} = \frac{0{,}0111\ MPa}{0{,}0108\ MPa} = 1{,}03 > 1$ **VERIFIED**	

It is possible to note that the factor of safety is very close to one; hence, the proposed thicknesses are the minimum values that satisfy the requirement for shear stability.
The same approach is applied to Salekhard (**Table 8.26**, **Table 8.27** and **Table 8.28**).

Table 8.26: Pavement design for shear stability (Salekhard, 1st iteration)

$\frac{E_v}{E_3} = \frac{675\ MPa}{120\ MPa} = 5{,}63$	
$\frac{h_{1+2}}{D} = \frac{12\ cm + 28\ cm}{39\ cm} = 1{,}03$	
$\bar{\tau}_h$	0,049 (from **Figure A.3.2**)
$T = \bar{\tau}_H \cdot p = 0{,}049 \cdot 0{,}6\ MPa = 0{,}029\ MPa$	
$T_{pr} = 0{,}002\ MPa \cdot 4 + 0{,}1 \cdot 0{,}002\ \frac{kg}{cm^3} \cdot 40\ cm \cdot tan32° = 0{,}013\ MPa$	
$K_{pr}^{tr} = \frac{0{,}013\ MPa}{0{,}029\ MPa} = 0{,}45 < 1$ **NOT VERIFIED**	

Table 8.27: Pavement new stratigraphy (Salekhard, 2nd iteration)

Material	**Thickness [cm]**
Dense asphalt concrete BND 100/130	20
Crushed stone	34
Medium sand	-

Considering the change in the thicknesses, the new values of E_v and γ_{sr} are equal to:

$$E_v = \frac{1200\ MPa\ \cdot 20\ cm + 450\ MPa \cdot 34\ cm}{20\ cm + 34\ cm} = 727{,}78\ MPa$$

$$\gamma_{sr} = \frac{2400\ \frac{kg}{m^3} \cdot 20\ cm + 1800\ \frac{kg}{m^3} \cdot 34\ cm}{20\ cm + 34\ cm} \cdot 10^{-6} = 0{,}002\ kg/cm^3$$

Table 8.28: Pavement design for shear stability (Salekhard, 2nd iteration)

$\frac{E_v}{E_3} = \frac{727{,}78\ MPa}{120\ MPa} = 6{,}06$	
$\frac{h_{1+2}}{D} = \frac{20\ cm + 34\ cm}{39\ cm} = 1{,}38$	
$\bar{\tau}_h$	0,024 (from **Figure A.3.2**)
$T = \bar{\tau}_H \cdot p = 0{,}024 \cdot 0{,}6\ MPa = 0{,}014\ MPa$	
$T_{pr} = 0{,}002\ MPa \cdot 4 + 0{,}1 \cdot 0{,}002\ \frac{kg}{cm^3} \cdot 54\ cm \cdot tan32° = 0{,}015\ MPa$	
$K_{pr}^{tr} = \frac{0{,}015\ MPa}{0{,}014\ MPa} = 1{,}03 > 1$ **VERIFIED**	

Also in this case, the factor of safety is very close to one, so the proposed configuration is the minimum one that satisfies the verification for shear stability.

8.3.3 PAVEMENT DESIGN FOR FATIGUE

New material properties must be defined; **Table 8.29** and **Table 8.30** show the elastic modulus values to be used in the calculations for fatigue failure.

Table 8.29: Materials elastic moduli for elastic deflection design (Tomsk)

Material	***E* [MPa] for fatigue failure**
Dense asphalt concrete BND 100/130	3600 (from **Table P.3.1**)
High-porosity asphalt concrete BND 100/130	1700 (from **Table P.3.1**)
Crushed stone	450 (from **Table P.3.9**)
Clayey soil	41 (from **Table P.2.5**)

Table 8.30: Materials elastic moduli for elastic deflection design (Salekhard)

Material	***E* [MPa] for fatigue failure**
Dense asphalt concrete BND 100/130	3600 (from **Table P.3.1**)
Crushed stone	450 (from **Table P.3.9**)
Medium sand	120 (from **Table P.2.5**)

The following verification must be checked:

$$\frac{R_N}{\sigma_r} > K_{pr}^{tr}$$

where K_{pr}^{tr} is equal to 1, according to **Table A.3.1**.

Calculations are carried out by reducing the multi-layer structure to an equivalent two-layer configuration (asphalt concrete layers+granular mixtures and subgrade). The elastic modulus of the upper stratum is determined as a weighted average, as shown below (Tomsk and Salekhard, respectively), whereas for the lower one, an equivalent stiffness is derived from the nomogram in **Figure A.3.1**.

$$E_v = \frac{3600\ MPa\ \cdot 10\ cm + 1700\ MPa \cdot 25\ cm}{10\ cm + 25\ cm} = 2242{,}86\ MPa$$

$$E_v = \frac{3600\ MPa\ \cdot 20\ cm}{20\ cm} = 3600\ MPa$$

For the calculations, the parameters in **Table 8.31** must be preliminary defined:

Table 8.31: Reference values for calculations according to fatigue failure)

Material	**R_0 (from Table P.3.1)**	**α (from Table P.3.1)**	**t (from Table P.3.1)**
Dense asphalt concrete BND 100/130	9,5	5,4	5
High-porosity asphalt concrete BND 100/130	5,5	6,5	3,8

For Tomsk cross-section, results are reported in **Table 8.32**. The coefficient of variation of the tensile strength ν_R and the standard deviation t were assumed equal to 0,1 (from **Table P.4.1**) and 1,71 (from **Table P.4.2**), respectively.

Table 8.32: Pavement design for fatigue failure (Tomsk)

E_h	90 MPa (from **Figure A.3.1**, see *subparagraph 8.3.1*)
$\frac{E_v}{E_h} = \frac{2242{,}86\ MPa}{90\ MPa} = 24{,}92$	
$\frac{h_v}{D} = \frac{10\ cm + 25\ cm}{39\ cm} = 0{,}9$	
$\bar{\sigma}_r$	0,95 (from **Figure A.3.4**)
$\sigma_r = \bar{\sigma}_r \cdot p \cdot k_v = 0{,}95 \cdot 0{,}6\ MPa \cdot 0{,}85 = 0{,}48\ MPa$	
$k_1 = \frac{\alpha}{\sqrt[t]{\sum N_r}} = \frac{6{,}5}{\sqrt[3{,}8]{90099}} = 0{,}32$	
k_2	0,8 (from **Table A.3.6**)
$R_N = R_0 \cdot k_1 \cdot k_2 \cdot (1 - \nu_R \cdot t) = 5{,}5\ MPa \cdot 0{,}32 \cdot 0{,}8 \cdot (1 - 0{,}1 \cdot 1{,}71) = 1{,}18\ MPa$	
$K_{pr}^{tr} = \frac{1{,}18\ MPa}{0{,}48\ MPa} = 2{,}43 > 1$ **VERIFIED**	

It is possible to note that the configuration proposed in the previous step (design for shear stability) is sufficient to verify the fatigue failure criterion.

For Salekhard, we obtain similar results (**Table 8.33**); ν_R and t assume the same values as above.

Table 8.33: Pavement design for fatigue failure (Salekhard)

E_h	198 MPa (from **Figure A.3.1**, see *subparagraph 8.3.1*)
$\frac{E_v}{E_h} = \frac{3600\ MPa}{198\ MPa} = 18{,}18$	
$\frac{h_v}{D} = \frac{20\ cm}{39\ cm} = 0{,}51$	
$\bar{\sigma}_r$	1,59 (from **Figure A.3.4**)
$\sigma_r = \bar{\sigma}_r \cdot p \cdot k_v = 1{,}59 \cdot 0{,}6\ MPa \cdot 0{,}85 = 0{,}81\ MPa$	
$k_1 = \frac{\alpha}{\sqrt[t]{\sum N_r}} = \frac{5{,}4}{\sqrt[5]{2015792{,}26}} = 0{,}3$	
k_2	0,9 (from **Table A.3.6**)

$R_N = R_0 \cdot k_1 \cdot k_2 \cdot (1 - \nu_R \cdot t) = 9{,}5\ MPa \cdot 0{,}3 \cdot 0{,}81 \cdot (1 - 0{,}1 \cdot 1{,}71) = 2{,}1\ MPa$
$K_{pr}^{tr} = \frac{2{,}1\ MPa}{0{,}81\ MPa} = 2{,}59 > 1$ **VERIFIED**

Also in this case, the thicknesses evaluated in the design for shear stability satisfy the requirement for fatigue failure.

8.4 PAVEMENT DESIGN FOR FROST RESISTANCE

For pavement design according to frost resistance, the following condition must be satisfied:

$$\frac{l_{dop}}{l_{puc}} \geq 1$$

where l_{dop} is taken from **Table A.4.3** (equal to 4 cm for both sites).
The design frost heave of the subgrade soil is given in the following equation:

$$l_{puc} = l_{puc,sr} \cdot K_{UGV} \cdot K_{pl} \cdot K_{gr} \cdot K_{nagr} \cdot K_{vl}$$

where $l_{puc,sr}$, since in both cases the freezing depth z_{pr} is greater than 2 m, is determined according to the following formula:

$$l_{puc,sr} = l_{puc,sr2.0} \cdot [a + b \cdot (z_{pr} - c)]$$

For Tomsk, the results are listed in **Table 8.34**. According to **Table A.4.2**, we are in the case of soil group III.

Table 8.34: Reference coefficients to be used in the determination of l_{puc} (Tomsk)

$l_{puc,sr2.0}$	6 cm (from **Figure A.4.3**)
a	1
b	0,16

c	2
z_{pr}	2,25 m
$l_{puc,sr} = 6\ cm \cdot [1 + 0{,}16 \cdot (2{,}25\ m - 2)] = 6{,}24\ cm$	
K_{UGV}	0,65 (from **Figure A.4.1**, the depth of the groundwater level is equal to 1,5 m)
K_{pl}	1 (from **Table A.4.4**, by assuming a sealing factor between 1,01 and 0,98)
K_{gr}	1,5 (from **Table A.4.5**)
K_{nagr}	0,875 (from **Figure A.4.2**)
K_{vl}	1,1 (from **Table A.4.6**)
$l_{puc} = 6{,}24\ cm \cdot 0{,}65 \cdot 1 \cdot 1{,}5 \cdot 0{,}875 \cdot 1{,}1 = 5{,}86\ cm > 4\ cm$ **NOT VERIFIED**	

Since the verification is not satisfied, a frost-protective layer must be designed. To determine its thickness, the average value of frost heave considering the allowable one is equal to:

$$l_{puc,sr} = \frac{l_{dop}}{K_{UGV} \cdot K_{pl} \cdot K_{gr} \cdot K_{nagr} \cdot K_{vl}} = \frac{4\ cm}{0{,}65 \cdot 1 \cdot 1{,}5 \cdot 0{,}875 \cdot 1{,}1} = 4{,}26\ cm$$

and from **Figure A.4.3**, we obtain the total pavement depth h_{od}=85 cm.
The thickness of the frost-protective layer will therefore be equal to:

$$h_{mz} = 85\ cm - 10\ cm - 25\ cm - 27\ cm = 23\ cm$$

It should be noted that since the pavement stratigraphy has been modified due to the additional frost-protective layer, strength verifications must be again performed. However, the introduction of this stratum will surely increase the value of E_{ob} (see *subparagraph 8.3.1*) and, therefore, the factor of safety for elastic deflection and will not influence the design calculations for fatigue failure; hence, only the condition for shear stability must be checked (**Table 8.35**).
A fine sand frost-protective layer with a modulus of elasticity equal to 100 MPa (**Table P.2.5**) and a density of 1850 kg/m^3 (**Table P.5.1**) has been chosen for the calculations.

The new values of E_v and γ_{sr} are equal to:

$$E_v = \frac{1200\ MPa\ \cdot 10\ cm + 800\ MPa \cdot 25\ cm + 450\ MPa \cdot 27\ cm + 100\ MPa \cdot 13\ cm}{10\ cm + 25\ cm + 27\ cm + 23\ cm} = 546{,}47\ MPa$$

$$\gamma_{sr} = \frac{2400\ \frac{kg}{m^3} \cdot 10\ cm + 2200\ \frac{kg}{m^3} \cdot 25\ cm + 1800\ \frac{kg}{m^3} \cdot 27\ cm + 1850\ \frac{kg}{m^3} \cdot 13\ cm}{10\ cm + 25\ cm + 27\ cm + 13\ cm} \cdot 10^{-6} = 0{,}002\ kg/cm^3$$

Table 8.35: Pavement design for shear stability considering the frost-protective layer (Tomsk)

$\frac{E_v}{E_4} = \frac{546{,}47\ MPa}{41\ MPa} = 13{,}33$	
$\frac{h_{1+2+3}}{D} = \frac{10\ cm + 25\ cm + 27\ cm + 23\ cm}{39\ cm} = 2{,}18$	
$\bar{\tau}_h$	0,0135 (from **Figure A.3.2**)
$T = \bar{\tau}_H \cdot p = 0{,}0135 \cdot 0{,}6\ MPa = 0{,}0081$	
$T_{pr} = 0{,}007\ MPa \cdot 1 + 0{,}1 \cdot 0{,}002\ \frac{kg}{cm^3} \cdot 85\ cm \cdot tan18° = 0{,}013\ MPa$	
$K_{pr}^{tr} = \frac{0{,}013\ MPa}{0{,}0081\ MPa} = 1{,}55 > 1$ **VERIFIED**	

Calculations for Salekhard cross-section (**Table 8.36**) have been performed similarly (soil group II, according to **Table A.4.2**); a 1st moistening scheme of the active layer of the subgrade has been used for the analysis, with reference to **Table A.5.1**.

Table 8.36: Reference coefficients to be used in the determination of l_{puc} (Salekhard)

$l_{puc,sr2.0}$	2 cm (from **Figure A.4.3**)
a	1,08
b	0,08
c	2,5
z_{pr}	2,5 m
$l_{puc,sr} = 2\ cm \cdot [1{,}08 + 0{,}08 \cdot (2{,}5\ m - 2{,}5)] = 2{,}16\ cm$	
K_{UGV}	0,45 (from **Figure A.4.1**, the depth of the groundwater level is equal to 2 m)

K_{pl}	1 (from **Table A.4.4**, by assuming a sealing factor between 1,01 and 0,98)
K_{gr}	1 (from **Table A.4.5**)
K_{nagr}	0,72 (from **Figure A.4.2**)
K_{vl}	1,1 (from **Table A.4.6**)
$l_{puc} = 2{,}16\ cm \cdot 0{,}45 \cdot 1 \cdot 1 \cdot 0{,}72 \cdot 1{,}1 = 0{,}77\ cm < 4\ cm$ **VERIFIED**	

In this case, the verification is satisfied with a pretty large margin of safety (the factor of safety is, in fact, equal to 5,2): this is due to the fact that, with respect to Tomsk subgrade, Salekhard soil is constituted by a medium sand, hence, it will be less prone to frost heave phenomena.

8.5 PAVEMENT DESIGN FOR DRAINAGE

In all pavements (with the exception of those located in road-climatic zone I), a drainage layer must also be included in the pavement layout. The preliminary design is carried out by considering that the frost-protective stratum (if present) will also work as a draining one and, eventually, its thickness will be increased depending on the case. According to ODN and PNST standards, there are four principles according to which a drainage layer can work:

- simple drainage;
- absorption;
- edge drainage;
- drainage with a lag period.

All four cases have been separately studied to find the most economical solution and eventually analyze which option is the most impactful taking into account climate change effects.

As indicated in *paragraph 8.4*, a fine sand layer has been adopted; the filtration coefficient K_ϕ has been assumed equal to 2,1 m/day and the slope i equal to 0,02.

It should be noted that, since Salekhard is located in RCZ I, design for drainage is not necessary.

For Tomsk, a 1st moistening scheme of the active layer of the subgrade is suggested for the calculations.

8.5.1 SIMPLE DRAINAGE

The thickness of a drainage layer is given as:

$$h_p = h_{nas} + h_{zap}$$

where h_{zap} is equal to 0,19 m and h_{nas} is determined from **Figure A.5.1**, which is dependent on the quantity q':

$$q' = 0{,}5 \cdot q_r \cdot B$$

$$q_r = \frac{q \cdot K_p \cdot K_g \cdot K_{vog} \cdot K_r}{1000}$$

The coefficients in **Table 8.37** have been defined:

Table 8.37: Coefficients to evaluate the thickness of the drainage layer working on the simple drainage principle

B	7 m
q	2 L/(m²·day) (from **Table A.5.3**)
K_p	1,5 (from **Table A.5.4**)
K_g	1 (from **Table A.5.4**)
K_{vog}	1*
K_r	1*

**assuming the absence of cracks in the longitudinal profile, as well as special measures to reduce the water inflow.*

Hence, we derive the following results (**Table 8.38**).

Table 8.38: Calculation of h_{nas}

q_r	0,003 m³/(m²·day)
q'	0,0053 m³/m²
$\frac{q'}{K_\phi}$	0,0025
$L = \frac{B}{2} = \frac{7\ m}{2} = 3{,}5\ m$	
$3{,}5 \cdot \frac{h_{nas}}{L}$	0 (from **Figure A.5.1**)
$h_{nas} = \frac{0 \cdot 3{,}5\ m}{3{,}5} = 0\ m$	

The drainage layer working with the simple drainage principle will have a thickness of 0,19 m, which must be increased to 0,2 m according to the minimum requirements.

8.5.2 ABSORPTION

In this case, the total thickness of the drainage layer is calculated as:

$$h_p = \frac{\frac{Q}{1000 \cdot n} + 0{,}3 \cdot h_{zap}}{1 - \varphi_{zim}}$$

where Q=20 L/m² (from **Table A.5.3**), n is the porosity, assumed equal to 0,32, and φ_{zim}=0,6 (from **Table A.5.6**). We obtain a total thickness of 0,3 m.

8.5.3 EDGE DRAINAGE

The thickness of a drainage layer working on the edge drainage principle is determined graphically from the nomogram in **Figure A.5.4**. We derive a thickness of 0,25 m.

8.5.4 DRAINAGE WITH A LAG PERIOD

In this case, the total thickness is equal to:

$$h_p = \frac{\frac{q_r \cdot T_{zap}}{n} + 0{,}3 \cdot h_{zap}}{1 - \varphi_{zim}}$$

where T_{zap} is equal to 5 days. We obtain h_p=0,26 m.

To sum up, for the case of Tomsk cross-section, a drainage layer is mandatory, which thickness varies between 20 cm and 30 cm, depending on the case.
At this point, pavement design for strength (and, in particular, for shear stability, as explained in *paragraph 8.4*) must be performed again, due to the change in the stratigraphy; however, it is possible to conclude that a thickness increase of the fine sand stratum will undoubtedly be beneficial in terms of factor of safety for shear stability calculations.

8.6 EFFECTS OF CLIMATE CHANGE ON PAVEMENT DESIGN

The objective of this second part is to study how Russian pavement design is affected by climate change, taking into account the results and provisions listed in *chapter 2* and *chapter 7*.

It should be underlined the fact that these types of analyses are always a quite delicate process, since they are based on hypotheses, data that are always coupled with a level of uncertainty, future forecasts that may sometimes be either too much or too little conservative, etc.; hence, it is hoped that the following study will provide helpful information and will constitute a good point of debate for professionals and researchers in further investigations, even though its results may show some deviations from actual future conditions, despite the fact that are based on books and papers published by respected scholars, professors and academics.

The main issue of the assessment is to understand how to take into account climate change effects in the pavement design, since all the parameters that are employed in the calculations depend on several factors such as temperature, soil freezing depth, moisture content, etc., all summarized in the so-called road-climatic zone. A detailed description of how the Russian Federation territory is subdivided is reported in **Figure P.2.2** and **Table P.2.7**.

Having said that, a good solution for the analysis would be to consider a shift in the RCZ in both sites: this approach has been already adopted by researchers of the Road Construction Faculty of TSUAB, especially for the case of Salekhard, and constitutes one of the most precautionary options to study climate change impacts.

To sum up, a new pavement design will be carried out for both cross-sections according to ODN and PNST regulations starting from the minimum thickness configuration by considering Tomsk in RCZ III and Salekhard in RCZ II.

The general parameters affected by this shift are listed in **Table 8.39** (for Salekhard test section, the values remain unchanged).

Table 8.39: Modified parameters considering climate change effects

T_{sl}	16 years (from **Table P.6.2**)
K_s	21,96 (from **Table P.6.3**)
$\sum N_r = 0{,}7 \cdot 66 \ \frac{vehicles}{day} \cdot \frac{21{,}96}{1{,}04^{16\ years-1}} \cdot 130\ days \cdot 1{,}31 = 95123\ vehicles$	
$E_{min} = 98{,}65 \cdot [\log(95123\ vehicles) - 3{,}25] = 170{,}5\ MPa$	

The value for the minimum required total modulus of elasticity is acceptable, according to the indications in **Table A.3.4**.

8.6.1 PAVEMENT DESIGN FOR STRENGTH

Despite the change in the RCZ, Salekhard pavement design for strength does not show any modification in the final results; therefore, all the calculations below will be only referred to Tomsk.

Outcomes show that the stratigraphy proposed in the previous analysis for elastic deflection (see **Table 8.12**) gives a value of the factor of safety equal to 1,15 (previously, 1,17); hence, the configuration must be modified:

$$K_{pr}^{tr} = \frac{196{,}8\ MPa}{170{,}5\ MPa} = 1{,}15$$

Calculations are reported in **Table 8.40** and **Table 8.41** (for the first two steps, see **Table 8.9**, **Table 8.10** and **Table 8.11**).

Table 8.40: Layers thickness assumed for elastic deflection analysis considering climate change effects (1st iteration)

Material	Thickness [cm]
Dense asphalt concrete BND 100/130	10
High-porosity asphalt concrete BND 100/130	9
Crushed stone	19
Clayey soil	-

Table 8.41: Pavement design for elastic deflection considering climate change effects (2nd iteration)

$\frac{E_4}{E_3} = \frac{41\ MPa}{450\ MPa} = 0{,}091$

$\frac{h_3}{D} = \frac{19\ cm}{39\ cm} = 0{,}49$	
$\frac{E_{3+4}}{E_3}$	0,2 (from **Figure A.3.1**)
$E_{3+4} = 0{,}2 \cdot E_3 = 0{,}2 \cdot 450\ MPa = 90\ MPa$	
$\frac{E_{3+4}}{E_2} = \frac{90\ MPa}{1400\ MPa} = 0{,}064$	
$\frac{h_2}{D} = \frac{9\ cm}{39\ cm} = 0{,}23$	
$\frac{E_{2+3+4}}{E_2}$	0,095 (from **Figure A.3.1**)
$E_{2+3+4} = 0{,}095 \cdot E_2 = 0{,}095 \cdot 1400\ MPa = 133\ MPa$	
$\frac{E_{2+3+4}}{E_1} = \frac{133\ MPa}{2400\ MPa} = 0{,}055$	
$\frac{h_1}{D} = \frac{10\ cm}{39\ cm} = 0{,}26$	
$\frac{E_{ob}}{E_1}$	0,085 (from **Figure A.3.1**)
$E_{ob} = 0{,}085 \cdot E_1 = 0{,}085 \cdot 2400\ MPa = 204\ MPa$	
$K_{pr}^{tr} = \frac{204\ MPa}{170{,}5\ MPa} = 1{,}2$ **VERIFIED**	

For the design according to shear stability, new material properties must be defined (**Table 8.42**).

Table 8.42: New elastic moduli for shear stability of the asphalt concrete layers considering climate change effects

Material	***E* [MPa] for shear stability**
Dense asphalt concrete BND 100/130	550 (from **Table P.3.2**)
High-porosity asphalt concrete BND 100/130	510 (from **Table P.3.2**)

Using the same thicknesses adopted in the previous analysis for shear stability, a factor of safety equal to 0,79 (**Table 8.43**) is obtained (previously, 1,03); therefore, the thicknesses must be increased, as shown in **Table 8.44** and **Table 8.45**.

The elastic modulus of the upper stratum is calculated as:

$$E_v = \frac{550\ MPa \cdot 10\ cm + 510\ MPa \cdot 25\ cm + 450\ MPa \cdot 27\ cm}{10\ cm + 25\ cm + 27\ cm} = 490{,}32\ MPa$$

Table 8.43: Pavement design for shear stability considering climate change effects (1st iteration)

$\frac{E_v}{E_4} = \frac{490{,}32\ MPa}{41\ MPa} = 11{,}96$	
$\frac{h_{1+2+3}}{D} = \frac{10\ cm + 25\ cm + 27\ cm}{39\ cm} = 1{,}59$	
$\bar{\tau}_h$	0,0235 (from **Figure A.3.2**)
$T = \bar{\tau}_H \cdot p = 0{,}0235 \cdot 0{,}6\ MPa = 0{,}014\ MPa$	
$T_{pr} = 0{,}007\ MPa \cdot 1 + 0{,}1 \cdot 0{,}0021\ \frac{kg}{cm^3} \cdot 62\ cm \cdot tan18° = 0{,}011\ MPa$	
$K_{pr}^{tr} = \frac{0{,}011\ MPa}{0{,}014\ MPa} = 0{,}79 < 1$ **NOT VERIFIED**	

Table 8.44: Pavement new stratigraphy considering climate change effects (2nd iteration)

Material	**Thickness [cm]**
Dense asphalt concrete BND 100/130	15
High-porosity asphalt concrete BND 100/130	29
Crushed stone	27
Clayey soil	-

Considering the change in the thicknesses, the new values of E_v and γ_{sr} are equal to:

$$E_v = \frac{550\ MPa \cdot 15\ cm + 510\ MPa \cdot 29\ cm + 450\ MPa \cdot 27\ cm}{15\ cm + 29\ cm + 27\ cm} = 495{,}63\ MPa$$

$$\gamma_{sr} = \frac{2400\ \frac{kg}{m^3} \cdot 15\ cm + 2200\ \frac{kg}{m^3} \cdot 29\ cm + 1800\ \frac{kg}{m^3} \cdot 27\ cm}{15\ cm + 29\ cm + 27\ cm} \cdot 10^{-6} = 0{,}0021\ kg/cm^3$$

Table 8.45: Pavement design for shear stability considering climate change effects (2nd iteration)

$\frac{E_v}{E_4} = \frac{495{,}63\ MPa}{41\ MPa} = 12{,}09$	
$\frac{h_{1+2+3}}{D} = \frac{15\ cm + 29\ cm + 27\ cm}{39\ cm} = 1{,}82$	
$\bar{\tau}_h$	0,0195 (from **Figure A.3.2**)
$T = \bar{\tau}_H \cdot p = 0{,}0195 \cdot 0{,}6\ MPa = 0{,}0117\ MPa$	

$T_{pr} = 0{,}007\ MPa \cdot 1 + 0{,}1 \cdot 0{,}0021\ \frac{kg}{cm^3} \cdot 71\ cm \cdot tan18° = 0{,}0118\ MPa$
$K_{pr}^{tr} = \frac{0{,}0118\ MPa}{0{,}0117\ MPa} = 1{,}01 > 1$ **VERIFIED**

For pavement design according to fatigue, the only parameter that is changed is α, equal to 6,3 and 7,9 for a dense and a high-porosity asphalt concrete mixture, respectively (according to **Table P.3.1**).

By performing the calculations using the stratigraphy found in the analysis for shear stability, a factor of safety equal to 4,61 is found, as reported in **Table 8.46**.

$$E_v = \frac{3600\ MPa\ \cdot 15\ cm + 1700\ MPa \cdot 29\ cm}{15\ cm + 29\ cm} = 2347{,}73\ MPa$$

Table 8.46: Pavement design for fatigue failure considering climate change effects

E_h	90 MPa (from **Figure A.3.1**, see design for elastic deflection)
$\frac{E_v}{E_h} = \frac{2347{,}73\ MPa}{90\ MPa} = 26{,}09$	
$\frac{h_v}{D} = \frac{15\ cm + 29\ cm}{39\ cm} = 1{,}13$	
$\bar{\sigma}_r$	0,6 (from **Figure A.3.4**)
$\sigma_r = \bar{\sigma}_r \cdot p \cdot k_v = 0{,}6 \cdot 0{,}6\ MPa \cdot 0{,}85 = 0{,}48\ MPa$	
$k_1 = \frac{\alpha}{\sqrt[t]{\sum N_r}} = \frac{6{,}5}{\sqrt[3{,}8]{90099}} = 0{,}31$	
k_2	0,8 (from **Table A.3.6**)
$R_N = 5{,}5\ MPa \cdot 0{,}31 \cdot 0{,}8 \cdot (1 - 0{,}1 \cdot 1{,}71) = 1{,}41\ MPa$	
$K_{pr}^{tr} = \frac{1{,}41\ MPa}{0{,}48\ MPa} = 4{,}61 > 1$ **VERIFIED**	

8.6.2 PAVEMENT DESIGN FOR FROST RESISTANCE

Pavement design for frost resistance does not depend on the RCZ; in this case, calculations are carried out by considering how a reduction of the freezing depth will

influence the outcomes: a reference value of 15 cm, following the considerations introduced in *chapter 7*, has been assumed.

Results for Tomsk are reported in **Table 8.47**; we obtain a thickness of the frost-protective layer equal to 19 cm (previously, 23 cm).

Table 8.47: Pavement design for frost resistance considering climate change effects (Tomsk)

$l_{puc,sr2.0}$	5 cm (from **Figure A.4.3**)
a	1
b	0,16
c	2
z_{pr}	2,1 m
$l_{puc,sr} = 5\ cm \cdot [1 + 0{,}16 \cdot (2{,}1\ m - 2)] = 5{,}08\ cm$	
K_{UGV}	0,65 (from **Figure A.4.1**, the depth of the groundwater level is equal to 1,5 m)
K_{pl}	1 (from **Table A.4.4**, by assuming a sealing factor between 1,01 and 0,98)
K_{gr}	1,5 (from **Table A.4.5**)
K_{nagr}	0,9 (from **Figure A.4.2**)
K_{vl}	1,1 (from **Table A.4.6**)
$l_{puc} = 5{,}08\ cm \cdot 0{,}65 \cdot 1 \cdot 1{,}5 \cdot 0{,}9 \cdot 1{,}1 = 4{,}9\ cm > 4\ cm$ **NOT VERIFIED**	

Since the verification is not satisfied, a frost-protective layer must be designed. To determine its thickness, the average value of frost heave considering the allowable one is equal to:

$$l_{puc,sr} = \frac{4\ cm}{0{,}65 \cdot 1 \cdot 1{,}5 \cdot 0{,}9 \cdot 1{,}1} = 4{,}14\ cm$$

and from **Figure A.4.3**, we obtain the total pavement depth h_{od}=90 cm.

The thickness of the frost-protective layer will therefore be equal to:

$$h_{mz} = 90\ cm - 15\ cm - 29\ cm - 27\ cm = 19\ cm$$

Also in this case, calculations for shear stability must again be performed due to the introduction of an additional layer (**Table 8.48**).

The new values of E_v and γ_{sr} are equal to:

$$E_v = \frac{550\ MPa\ \cdot 15\ cm + 510\ MPa \cdot 29\ cm + 450\ MPa \cdot 27\ cm + 100\ MPa \cdot 19\ cm}{15\ cm + 29\ cm + 27\ cm + 19\ cm}$$
$$= 412{,}11\ MPa$$

$$\gamma_{sr} = \frac{2400\ \frac{kg}{m^3} \cdot 15\ cm + 2200\ \frac{kg}{m^3} \cdot 29\ cm + 1800\ \frac{kg}{m^3} \cdot 27\ cm + 1850\ \frac{kg}{m^3} \cdot 19\ cm}{15\ cm + 29\ cm + 27\ cm + 19\ cm} \cdot 10^{-6}$$
$$= 0{,}002\ kg/cm^3$$

Table 8.48: Pavement design for shear stability with the frost-protective layer considering climate change effects (Tomsk)

$\frac{E_v}{E_4} = \frac{412{,}11\ MPa}{41\ MPa} = 10{,}05$	
$\frac{h_{1+2+3}}{D} = \frac{15\ cm + 29\ cm + 27\ cm + 19\ cm}{39\ cm} = 2{,}31$	
$\bar{\tau}_h$	0,0149 (from **Figure A.3.2**)
$T = \bar{\tau}_H \cdot p = 0{,}0149 \cdot 0{,}6\ MPa = 0{,}0089\ MPa$	
$T_{pr} = 0{,}007\ MPa \cdot 1 + 0{,}1 \cdot 0{,}002\ \frac{kg}{cm^3} \cdot 90\ cm \cdot tan18° = 0{,}013\ MPa$	
$K_{pr}^{tr} = \frac{0{,}013\ MPa}{0{,}0089\ MPa} = 1{,}45 > 1$ **VERIFIED**	

Calculations for Salekhard are reported in **Table 8.49**; for the analysis, a 2nd moistening scheme of the active layer of the subgrade has been used (see *subparagraph 8.6.3*).

Table 8.49: Reference coefficients to be used in the determination of l_{puc} considering climate change effects (Salekhard)

$l_{puc,sr2.0}$	4 cm (from **Figure 4.3**)
a	1
b	0,16
c	2
z_{pr}	2,35 m
$l_{puc,sr} = 2\ cm \cdot [1 + 0{,}16 \cdot (2{,}5\ m - 2)] = 4{,}22\ cm$	

K_{UGV}	0,5 (from **Figure A.4.1**, the depth of the groundwater level is equal to 2 m)
K_{pl}	1 (from **Table A.4.4**, by assuming a sealing factor between 1,01 and 0,98)
K_{gr}	1 (from **Table A.4.5**)
K_{nagr}	0,75 (from **Figure 4.2**)
K_{vl}	1,1 (from **Table A.4.6**)
$l_{puc} = 4{,}22\ cm \cdot 0{,}5 \cdot 1 \cdot 1 \cdot 0{,}75 \cdot 1{,}1 = 1{,}74\ cm < 4\ cm$ **VERIFIED**	

It is interesting to note that in this case, the factor of safety is equal to 2,3 (previously, 5,2); although this significant decrease, no frost-protective layer is needed. However, it is expected that this outcome will help future researchers to stress the importance of studying frost heave effects in Salekhard road pavements.

8.6.3 PAVEMENT DESIGN FOR DRAINAGE

Taking into account precipitations increase is a more complex procedure, since road-climatic zoning is influenced, rather than in water and snowfalls, on the moisture degree. For this reason, two different analyses have been performed in order to offer two possible future scenarios:

- pavement design considering a shift in both the RCZ and the moistening scheme of the active layer of the subgrade;
- pavement design considering only a shift in the moistening scheme of the active layer of the subgrade.

The shift in the moistening principle has been carried out according to the provisions listed in *chapter 2*, the outcomes in *chapter 7* and the indications of the Road Construction Faculty of TSUAB; for a detailed description of the schemes, see **Table A.5.1**.

Results of the first analysis for Tomsk are reported below, considering the values listed in **Table 8.50** and **Table 8.51**.

Table 8.50: Coefficients to evaluate the thickness of the drainage layer working on the simple drainage principle considering climate change effects (Tomsk, 1st analysis)

q	2 L/(m²·day) (from **Table A.5.3**)
K_p	1,4 (from **Table A.5.4**)
K_g	1 (from **Table A.5.4**)
K_{vog}	1*
K_r	1*

** assuming the absence of cracks in the longitudinal profile, as well as special measures to reduce the water inflow*

Hence, we derive:

Table 8.51: Calculation of h_{nas} considering climate change effects (Tomsk, 1st analysis)

q_r	0,0028 m³/(m²·day)
q'	0,0049 m³/m²
$\frac{q'}{K_\phi}$	0,0023
$3{,}5 \cdot \frac{h_{nas}}{L}$	0 (from **Figure A.5.1**)
$h_{nas} = \frac{0 \cdot 3{,}5\ m}{3{,}5} = 0\ m$	

The drainage layer working with the simple drainage principle will have a thickness of 0,19 m, which must be increased to 0,2 m according to the minimum requirements.
For the case of absorption:

$$h_p = \frac{\frac{25\ L/m^2}{1000 \cdot 0{,}32} + 0{,}3 \cdot 0{,}19\ m}{1 - 0{,}48} = 0{,}26\ m$$

For the edge drainage option, we obtain a thickness of 0,23 m (from **Figure A.5.4**), while for the case of drainage with a lag period:

$$h_p = \frac{\frac{0{,}0028 \cdot 3{,}5\ days}{0{,}32} + 0{,}3 \cdot 0{,}19\ m}{1 - 0{,}48} = 0{,}17\ m$$

Instead, for the second analysis, the following thicknesses are derived, following the values reported in **Table 8.52** and **Table 8.53**.

Table 8.52: Coefficients to evaluate the thickness of the drainage layer working on the simple drainage principle considering climate change effects (Tomsk, 2nd analysis)

q	3 L/(m²·day) (from **Table A.5.3**)
K_p	1,5 (from **Table A.5.4**)
K_g	1 (from **Table A.5.4**)
K_{vog}	1*
K_r	1*

** assuming the absence of cracks in the longitudinal profile, as well as special measures to reduce the water inflow*

Hence, we derive:

Table 8.53: Calculation of h_{nas} considering climate change effects (Tomsk, 2nd analysis)

q_r	0,0045 m³/(m²·day)
q'	0,0079 m³/m²
$\frac{q'}{K_\phi}$	0,0038
$3{,}5 \cdot \frac{h_{nas}}{L}$	0,03 (from **Figure A.5.1**)
$h_{nas} = \frac{0{,}03 \cdot 3{,}5\ m}{3{,}5} = 0{,}03\ m$	

The drainage layer working with the simple drainage principle will have a thickness of 0,22 m.

For the case of absorption:

$$h_p = \frac{\frac{50\ L/m^2}{1000 \cdot 0{,}32} + 0{,}3 \cdot 0{,}19\ m}{1 - 0{,}6} = 0{,}54\ m$$

For the edge drainage option, we obtain a thickness of 0,3 m (from **Figure A.5.4**), while for the case of drainage with a lag period:

$$h_p = \frac{\frac{0{,}0045 \cdot 5\ days}{0{,}32} + 0{,}3 \cdot 0{,}19\ m}{1 - 0{,}6} = 0{,}32\ m$$

For Salkehard test section, the design considering only a shift in the soil moistening scheme does not have any effects since we are still in RCZ I.

For the second analysis, the results are reported below, considering the values reported in **Table 8.54** and **Table 8.55**.

Table 8.54: Coefficients to evaluate the thickness of the drainage layer working on the simple drainage principle considering climate change effects (Salekhard, 1st analysis)

q	3 L/(m²·day) (from **Table A.5.3**)
K_p	1,5 (from **Table A.5.4**)
K_g	1 (from **Table A.5.4**)
K_{vog}	1*
K_r	1*

** assuming the absence of cracks in the longitudinal profile, as well as special measures to reduce the water inflow*

Hence, we derive:

Table 8.55: Calculation of h_{nas} considering climate change effects (Salekhard, 2nd analysis)

q_r	0,0045 m³/(m²·day)
q'	0,0079 m³/m²

$\frac{q'}{K_\phi}$	0,0038
$3{,}5 \cdot \frac{h_{nas}}{L}$	0,03 (from **Figure A.5.1**)
$h_{nas} = \frac{0{,}03 \cdot 3{,}5\ m}{3{,}5} = 0{,}03\ m$	

The drainage layer working with the simple drainage principle will have a thickness of 0,22 m.

For the case of absorption:

$$h_p = \frac{\frac{25\ L/m^2}{1000 \cdot 0{,}32} + 0{,}3 \cdot 0{,}19\ m}{1 - 0{,}5} = 0{,}28\ m$$

For the edge drainage option, we obtain a thickness of 0,3 m (from **Figure A.5.4**), while for the case of drainage with a lag period:

$$h_p = \frac{\frac{0{,}0045 \cdot 5\ days}{0{,}32} + 0{,}3 \cdot 0{,}19\ m}{1 - 0{,}5} = 0{,}26\ m$$

8.7 FINAL CONSIDERATIONS

A summary of the results for Tomsk and Salekhard is reported in **Table 8.56** and **Table 8.57**.

Table 8.56: Summary of the outcomes for Tomsk section considering climate change effects

Material	**Thickness [cm]**
Dense asphalt concrete BND 100/130	15 (previously, 10)
High-porosity asphalt concrete BND 100/130	29 (previously, 25)
Crushed stone	27
Clayey soil	-

Frost-protective layer with a thickness h_{mz} equal to 19 cm (previously, 23 cm)			
Drainage layer			
Principle	**Thickness [cm]**		
	Shift in RCZ and moistening scheme	*Shift in moistening scheme*	*Analysis without considering climate change*
Simple drainage	20	22	20
Absorption	26	54	30
Edge drainage	23	30	25
Drainage with a lag period	17	32	26

In this case, the main outcomes are an increase of 9 cm of the surface course, a decrease of 4 cm of the frost-protective layer and a change in the thickness of the fine sand drainage stratum.

It is possible to note that in the case of analysis considering both a shift in the RCZ and in the moistening scheme of the active layer of the subgrade, there is a reduction in the thickness of the drainage layer up to 9 cm, depending on the draining principle. This result is due to the fact that we are increasing the overall pavement thickness (in particular, the surface course), which reflects pavement design calculations for drainage. On the other hand, by performing the analysis considering only a shift in the moistening scheme, the asphalt concrete layer is not enough to ensure a proper draining; hence, the thickness of the fine sand drainage stratum must be modified (depending on the principle, the increase varies between 2 cm and 24 cm).

Table 8.57: Summary of the outcomes for Salekhard section considering climate change effects

Material	**Thickness [cm]**
Dense asphalt concrete BND 100/130	20
Crushed stone	34
Medium sand	-
No need for a frost-protective layer	

Drainage layer			
Principle	**Thickness [cm]**		
	Shift in RCZ and moistening scheme	*Shift in moistening scheme*	*Analysis without considering climate change*
Simple drainage	22	-	-
Absorption	28	-	-
Edge drainage	30	-	-
Drainage with a lag period	26	-	-

In this case, climate change effects reflect on the introduction of a drainage layer with a thickness varying between 17 cm and 26 cm: this applies to the case of analysis considering both a shift in the RCZ and in the soil moistening scheme. Since we are still in RCZ I, no drainage layer is needed for the second assessment.

REFERENCES

BIBLIOGRAPHY

- Efimenko S. V., Efimenko V. N., Badina M. V., Sukhorukov A. V., Churilin V. S., Afinogenov A. O. – *Standardization of Estimated Values of Clayey Soil Properties for the Quality Assurance in Road Design in Kuzbass*, Publishing House of Tomsk State University of Architecture and Building, Russian Federation, 2015 (in Russian);
- GOST R 59120-2021: *Automobile Roads of General Use. Road Pavement. General Requirements*; National Standard of the Russian Federation, Russian Federation, 2021 (in Russian);
- ODN 218.046-01: *Design of Flexible Road Pavements*, Industry Road Regulations, State Road Service of the Ministry of Transport of the Russian Federation, Russian Federation, 2001;
- PNST 542-2021: *Automobile Roads of General Use. Flexible Pavement. Design Rules*, Preliminary National Standard of the Russian Federation, Russian Federation, 2021 (in Russian).

CONCLUSIONS

The following master's thesis project was carried out with the aim to study how climate change will influence the design of road pavements in areas characterized by continental and subarctic climates in a period of fifty years.

Calculations have, in fact, shown statistically significant results in both reference sites, Tomsk and Salekhard, for annual average, minimum and maximum temperature, as well as total precipitations. In particular, linear regression analysis highlighted an increase of 2,2 °C, 7,4 °C and 1,7 °C for T_{mean}, T_{min} and T_{MAX}, respectively, over 100 years in Tomsk and of 3,2 °C, 3,3 °C and 3 °C in 50 years in Salekhard, as well as a rise of 52 mm in total precipitations. Mann-Kendall test and Sen's slope estimate showed an increase of 1,6 °C and 4,8 °C for T_{mean} and T_{min}, respectively, over 100 years in Tomsk and of 2,3 °C, 3,45 °C and 2,2 °C for T_{mean}, T_{min} and T_{MAX}, respectively, in 50 years in Salekhard, as well as a rise of 87,5 mm in total precipitations.

Frost penetration assessment revealed a lowering of the freezing depth of 19,46 cm in 100 years in Tomsk and of 13,79 cm in 50 years in Salekhard.

Taking into account the conclusions above, pavement design following the Russian regulations was carried out considering a shift in the road-climatic zone, a reduction of the freezing depth of 15 cm and a change in the soil moistening scheme.

Results for Tomsk show the need to increase the asphalt layer thickness of 9 cm and the drainage stratum of a value ranging between 2 cm and 24 cm, depending on the draining typology, indicating that, in the future, the leading failure criteria in road pavement design will be constituted by the shear stability of the granular layers and drainage. In contrast, the influence of frost heave will be slight.

In Salekhard, the introduction of a draining layer will be necessary, with a depth varying between 22 cm and 30 cm, again indicating the importance of the contribution of precipitations increase in future analyses.

An English version of the abovementioned regulations is included in *annex 2*.

Additionally, a temperature trend model has been validated for past and future assessments.

ANNEX 1

Temperature trend plots for the test sections in Tomsk on December 5, 2020.

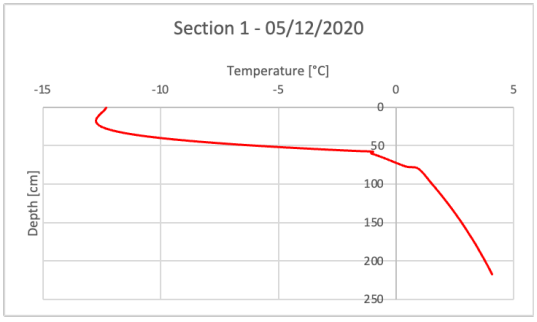

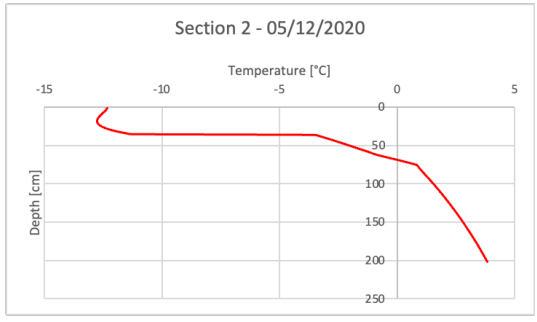

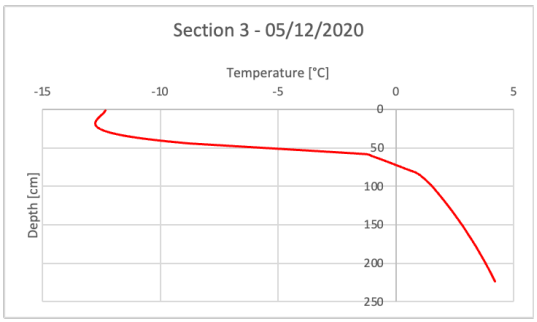

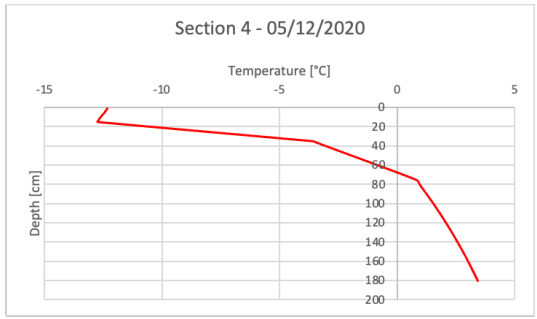

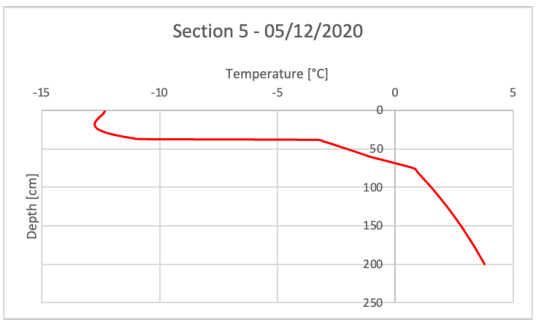

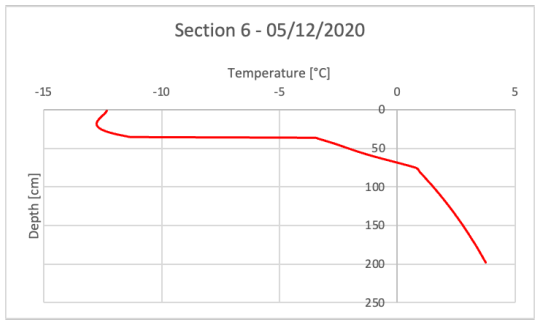

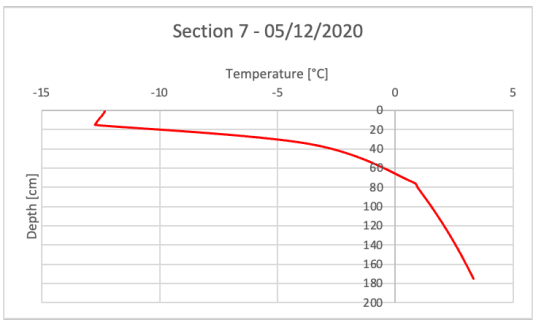

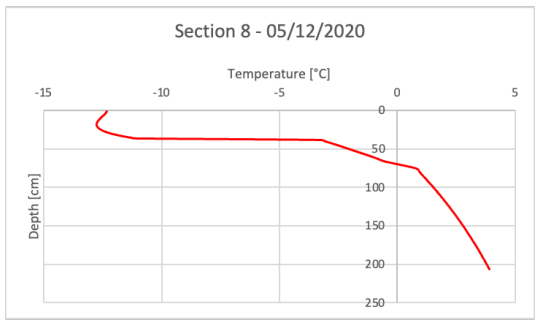

Temperature trend plots for the test sections in Tomsk on January 23, 2021.

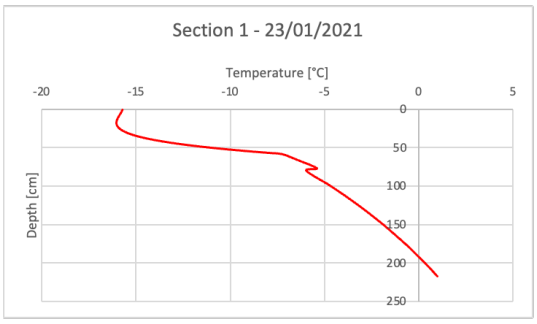

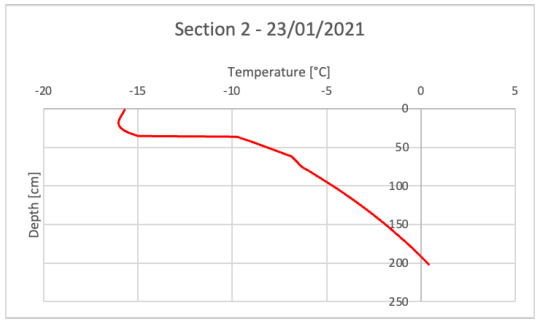

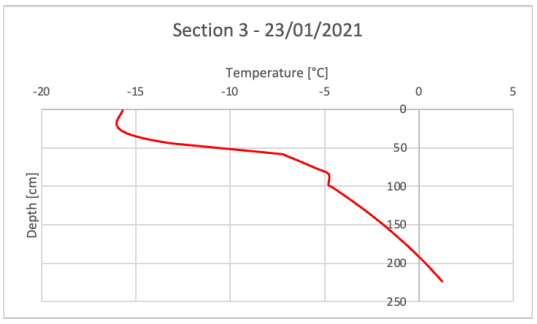

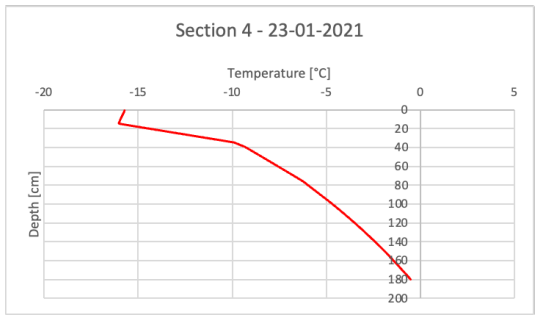

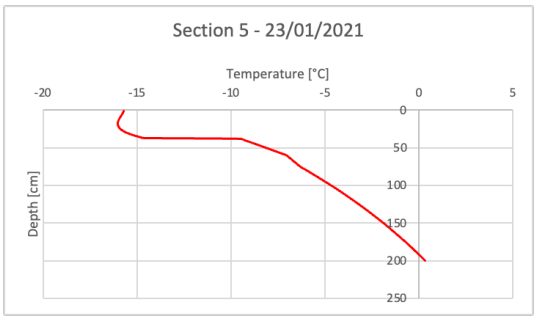

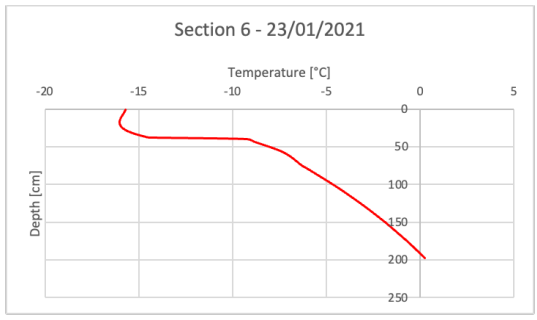

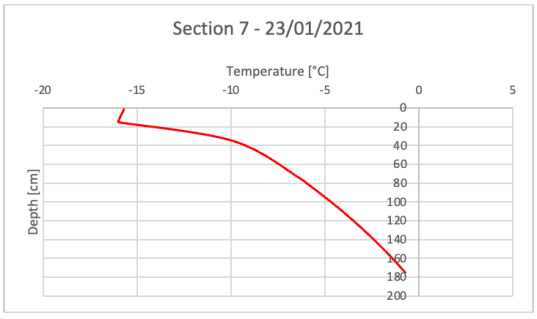

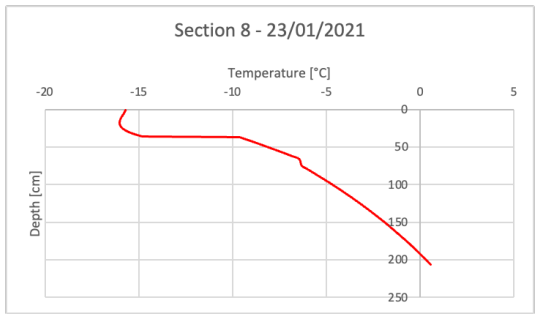

Temperature trend plots for test section 1 in Salekhard on different days of the analyzed period

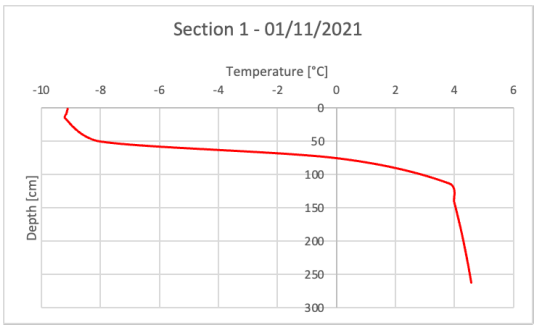

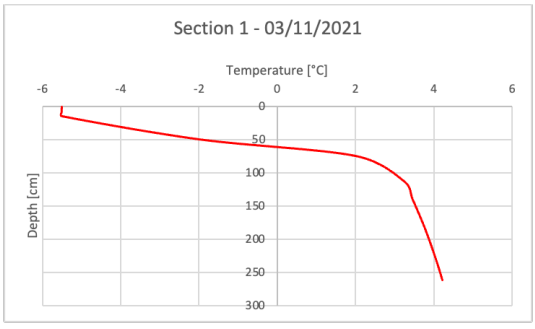

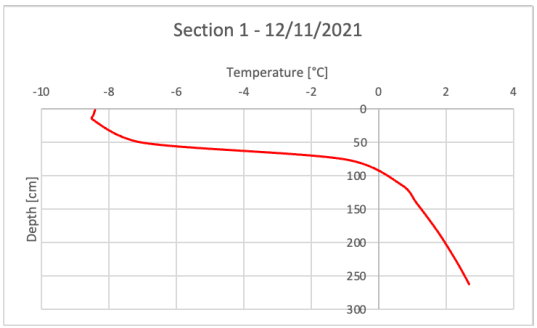

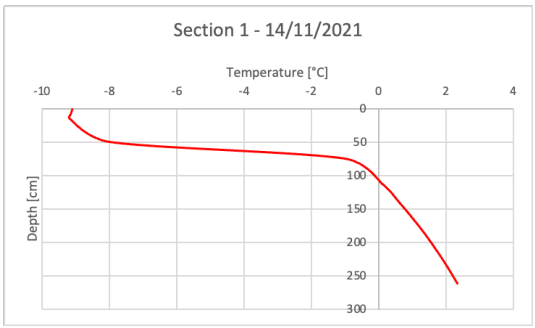

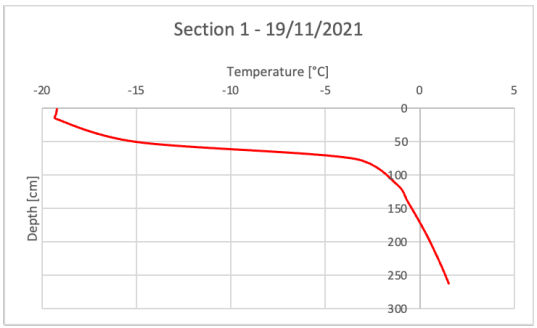

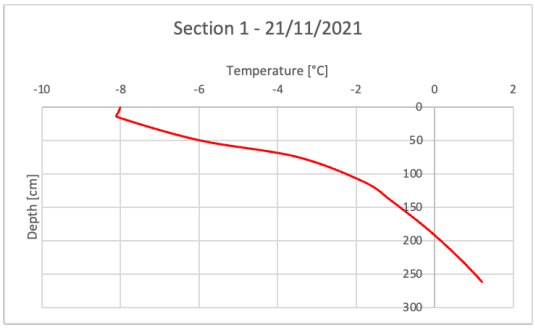

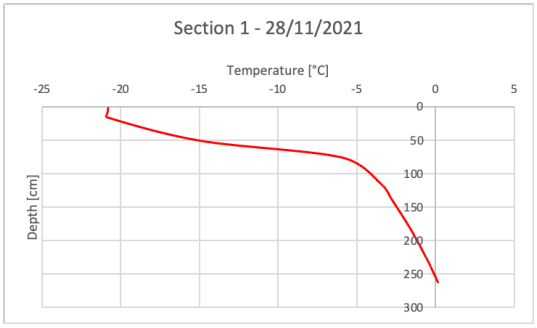

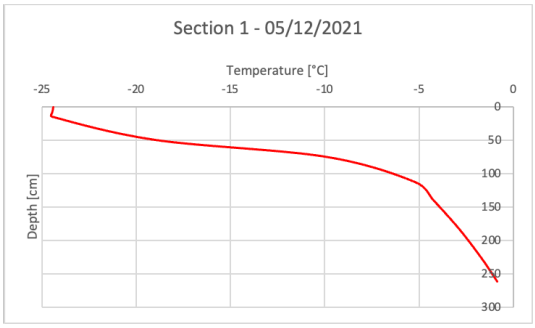

Temperature trend plots for test section 1 in Salekhard on different days of the analyzed period

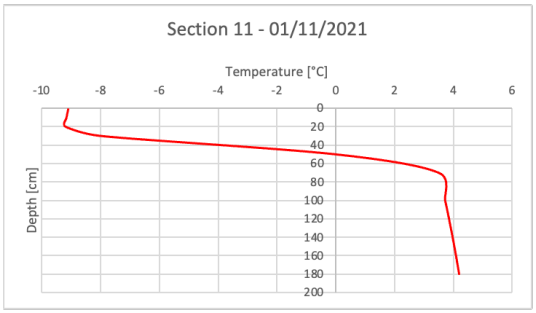

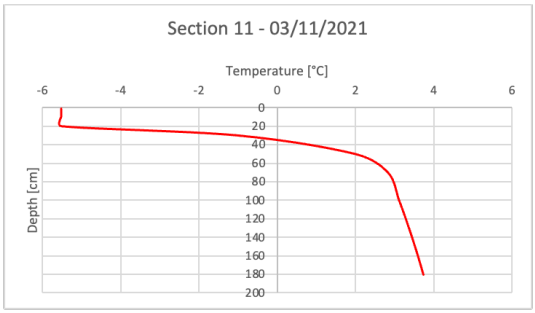

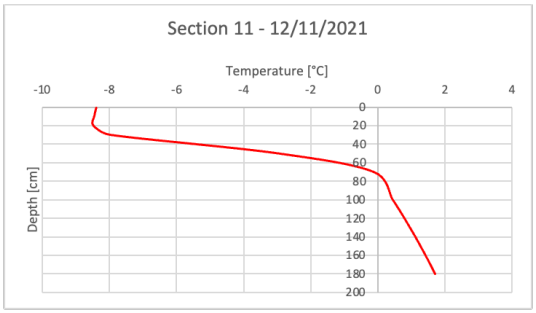

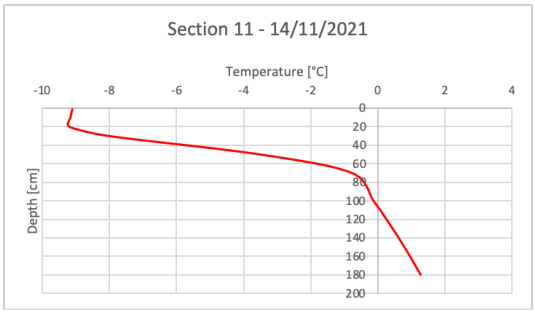

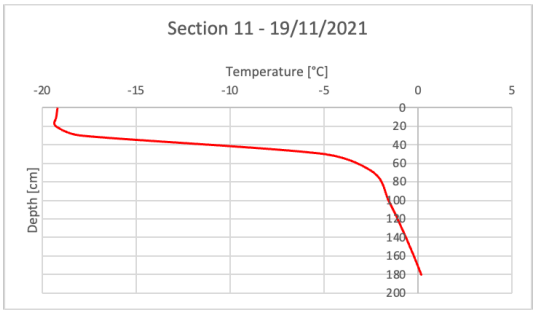

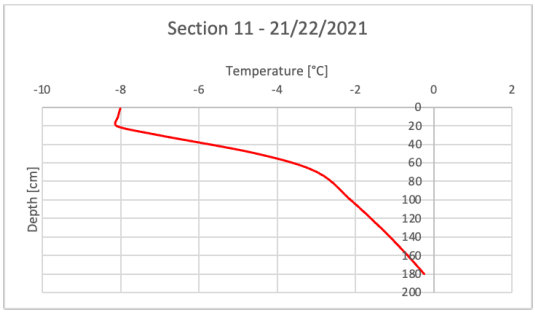

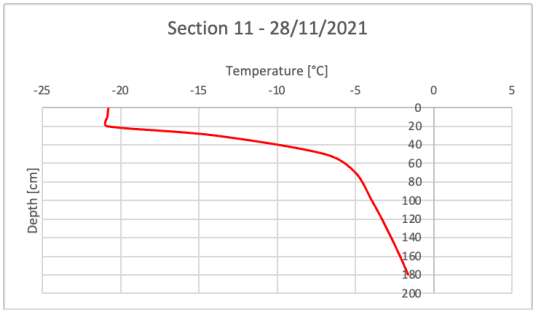

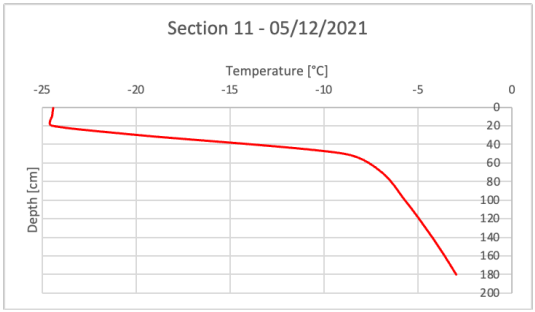

ANNEX 2

ODN 218.046-01: DESIGN OF FLEXIBLE ROAD PAVEMENTS

Sources:

https://znaytovar.ru/gost/2/ODN_21804601_Proektirovanie_ne.html

https://docs.cntd.ru/document/1200179561

1. GENERAL PROVISIONS

1.1. ODN are applicable for the design of newly constructed pavements, new sections of reconstructed roads, the development of standard design albums and can also be used to assess the strength and the design of reinforcement of pavements of existing roads.

1.2. Flexible pavements include roads with layers made of different types of asphalt concrete (tar concrete), materials and soils reinforced with bitumen, cement, lime, complex binders and others, as well as loosely cohesive granular materials (crushed stone, slag, gravel, etc.).

1.3. The following elements are distinguished:

- surface: the upper part of the pavement that receives the loads from the wheels of the vehicles and is directly exposed to atmospheric factors. On the pavement, layers of surface treatments for various purposes (increase of roughness, protective films, etc.) can be placed;
- base: a part of the pavement located under the surface and providing the redistribution of stresses in the structure and a decrease in their value in the soil

of the active layer of the subgrade (underlying soil), as well as frost resistance and drainage.

A distinction should be made between the load-bearing part of the base and additional base layers. The first one must ensure the strength of the pavement and be frost-resistant;

- additional base layers: layers between the bearing base and the underlying soil, provided in the presence of unfavorable weather, climatic and hydrogeological conditions. Together with the surface and the base, they must provide the necessary frost resistance and drainage of the structure and create conditions for reducing the thickness of the overlying layers of expensive materials.

According to the primary function, it can be frost-protective, heat-insulating and draining. Additional layers also include hydro- and vapor-insulating, capillary-interrupting, anti-silting, etc.

Additional layers are made of sand and other local materials in their natural state or reinforced with organic, mineral or complex binders from local soils.

When using additional layers in the project, it is necessary to consider the technological problems associated with the movement of construction vehicles along them.

Pavements classification is given in **Table A.1.1**;

Table A.1.1: Pavements classification

Type of pavement	**Type of surface, materials and method of installation**
Improved coatings	
Capital	Hot asphalt mixes
Lightweight	- Hot asphalt mixes - Cold asphalt concrete mixtures - Organic-mineral mixtures with liquid organic binders (with or without minerals), with viscous binders (including emulsified organic binders with or without minerals); stone materials treated with organic binders by impregnation; black

	crushed stone; porous and highly porous asphalt mixes with surface treatment; durable crushed stone with double surface treatment
Transitional coatings	
Transitional	Crushed solid rocks, arranged according to the wedge method without the use of binders; low-strength stone materials, reinforced with binders; cobblestone and chipped stone
Inferior	Crushed stone-gravel-sand mixtures; low-strength stone materials and slags; soils reinforced or improved with various local materials; wood materials

- active layer of the subgrade (underlying soil): the upper part of the roadbed within the range from the bottom of the pavement to 2/3 of the freezing depth, but not less than 1,5 m from the surface of the pavement.

1.4. Capital and lightweight pavements with an improved surface are designed in such a way that during the overhaul period, no damage and residual deformations that are unacceptable from the point of view of the requirements for the evenness of the surface of the residual deformations provided for by the current regulatory documents are present, as well as the effect of natural factors do not lead to unacceptable changes in its elements.

Lightweight pavements with an improved surface are expected to have a shorter overhaul than capital ones: this allows less durable and expensive materials and lighter construction.

When designing transitional pavements, the leveling of which is not associated with significant costs (crushed stone, gravel and similar surfaces), allow the possibility of a more significant accumulation of residual deformations under the action of motion.

In all cases, the solutions of the theory of elasticity are used to assess the stress state of the structure.

1.5. In areas with a humid and cold climate and with unfavorable soil and hydrological conditions, measures should be taken to drain and ensure frost resistance of the pavement and subgrade.

1.6. The designed pavement must be not only durable and reliable in operation, but also economical and possibly less material intensive, especially in terms of consumption of scarce materials and energy, and must also comply with environmental requirements.
The design efficiency is determined by comparing the options with the assessment of the comparative economic efficiency of capital investments according to the current regulatory documents. A feasibility study substantiates the choice of the type of pavement and its design.

1.7. When designing pavements for specific objects and developing standard (unified) solutions for road structures, along with the provisions of these ODN, data from regional scientific and practical experience should be taken into account (also in terms of the use of local materials, clarification of the design values of characteristics, etc.), reflected in the current regional technical conditions, norms, rules for the production of work and other technical documents approved in the prescribed manner.
When developing regional standard pavement designs, one should also consider the specialization of road-building organizations, the region provisions with road-building materials, provide for the maximum mechanization and industrialization of construction processes and strive to reduce the labor intensity and costs of manual labor.

1.8. The design service life of the projected pavement and the design required level of reliability must be assigned on the basis of the norms adopted by the administrative authorities in agreement with the regional road organizations.

1.9. These ODN do not apply to the design of road pavements in the permafrost zone, where the nature of permafrost soils, their temperature and water regime, as well as the effect of the thickness of the active layer and permafrost (rigid base) on the strength of the pavement must be taken into account.

2. DESIGN OBJECTIVES AND PRINCIPLES

2.1. Pavement design is a single process of designing and calculating the road structure (pavement system+active layer of the subgrade) for strength, frost resistance and drainage with a feasibility study of options in order to choose the most economical solution in the given conditions.

2.2. The pavement design procedure includes:

- the choice of the type of coating;
- the appointment of the number of structural layers and materials, their placement in the structure and their approximate thicknesses;
- a preliminary assessment of the need to assign additional frost protection measures, taking into account the road-climatic zone, the type of soil of the active layer of the subgrade and its moistening scheme in different areas;
- preliminary assessment of the need for the appointment of measures to drain the structure, as well as to increase the crack resistance;
- assessment of the feasibility of strengthening or improving the upper part of the active layer of the subgrade;
- preliminary selection of competitive options, taking into account local natural and design working conditions.

2.3. When designing pavements, it is necessary to be guided by the following principles:

- the design must meet the transport and operational requirements for the road of the corresponding category and the composition and traffic intensity expected in the future, taking into account the change in traffic intensity during the specified overhaul periods and the expected conditions of repair and maintenance;
- the design can be adopted as standard or developed individually for each section or several sections of the road, characterized by similar natural conditions (soil of the active layer of the subgrade, its moisture conditions, climate, provision of

local road-building materials, etc.) with the same design loads. When choosing a pavement design for these conditions, preference should be given to a typical design tested in practice under the same circumstances;

- in areas that are insufficiently provided with standard stone materials, it is allowed to use local stone materials, industrial by-products and soils, the properties of which can be improved by processing them with binders (cement, bitumen, lime, active fly ash, etc.). At the same time, engineers must strive to create a structure that is as material intensive as possible;
- the design must be technologically advanced and ensure the possibility of maximum mechanization and industrialization of road construction processes. To achieve this goal, the number of layers and types of materials in the structure should be minimized;
- when designing, it is necessary to take into account the actual conditions of construction work (summer or winter technology, etc.).

2.4. When assigning the types of coatings for different options for the construction of road pavements, one should be guided by the provisions of the current standards and norms for road building materials and products and the norms for designing highways.

2.5. When choosing materials for paving layers, the following provisions should be taken into account.

The pavement and top layers of the base must comply with the design impact loads and be water-, frost- and heat-resistant.

For the top layer of the asphalt concrete pavement, choose the material in accordance with the current GOST "*Mixes Asphalt Road, Airfield and Asphalt Concrete. Technical conditions*" and SNiP "*Highways*".

With a prospective traffic intensity in physical units of up to 3000 vehicles/day and during stage-by-stage construction, it is allowed to realize a pavement from porous asphalt concrete with a surface treatment or from highly porous asphalt concrete with a double surface treatment.

The pavement design at public transport stops, at regulated intersections and in other places where speed changes or traffic is at reduced speeds, increased shear stability at high summer temperatures must be provided. To meet this requirement, the coating provides for the use of asphalt concrete mixtures of type A and B, high-density mixtures and, at the base, coarse-grained asphalt concrete mixtures or stone materials reinforced with cement.

The main challenges when designing asphalt layers are to optimize the thickness of the top layer of dense or high-density asphalt concrete and to reduce the number of layers. Asphalt concrete pavement should, as a rule, be a single layer. The minimum structural thickness of the pavement is assigned according to the norms of the current SNiP and strength calculations determine the thickness of the layer of the asphalt concrete base.

When designing transitional pavements, one option is provided without using an asphalt concrete base; in this case, the required coating thickness is assigned according to the strength calculation.

With stage-by-stage construction or a possible prospective increase in the capital of the pavement with a special feasibility study, the use of cold asphalt concrete is allowed.

When choosing a material for the top layer of the base, it is necessary to consider the type of pavement, the type of coating and the deformation and thermophysical properties of materials and soils reinforced with organic and inorganic binders.

Asphalt concrete part of the bearing base should be provided, as a rule, a single layer. A two-layer asphalt concrete base can only be adopted if it is necessary to use asphalt concrete with a low shear resistance (highly porous, sandy) in the lower base layer. In this case, the total thickness of asphalt concrete layers with increased shear resistance (pavement with a coarse-grained asphalt concrete base) should not be less than 12 cm.

When choosing the type of material for constructing a base made of mineral materials, one should be guided by experience in constructing and operating roads in the region. Materials must meet the requirements of the current SNiP or local technological conditions, approved in the prescribed manner.

In areas that are insufficiently provided with standard stone materials, it is advisable to widely use local stone materials (including low-strength and substandard ones) and soils reinforced with an inorganic binder (cement, lime, active fly ash, etc.).

A base made of granular materials should, as a rule, be a double layer: a supporting layer made of rigid and shear-resistant materials (crushed stone, gravel, gravel-sand mixtures, materials and soils reinforced with an inorganic binder) and an additional layer that performs frost protection and drainage functions.

2.6. If a homogeneous sand with a degree of heterogeneity (according to GOST 25100-2011) less than 3 is used in an additional base layer, a protective layer of crushed stone (gravel) sand mixtures, screenings of crushing of igneous rocks, gravelly or coarse sands of optimal composition and cement sand are provided for. With a degree of sand heterogeneity from 2 to 3, the thickness of the protective layer is taken to be 10 cm; with a degree of heterogeneity of less than 2, a protective layer with a thickness of 15-20 cm is set. In calculating the strength of the pavement, the thickness of the protective layer is included in the thickness of the additional base layer. When installing a protective layer, geotextiles can be used.

2.7. In the case of using local low-strength stone materials at the base (crushed stone with a strength grade of at least 200, gravel and crushed stone from gravel with a crushing capacity not lower than D_r. 24, sand and gravel mixtures, gravelly sands and other shear-resistant materials with a modulus of elasticity less than 250 MPa) provide the supporting layer of the base with strong crushed stone or reinforced with inorganic binders with a minimum structural thickness provided for by SNiP.

2.8. The location of unreinforced granular materials between layers of materials or soils treated with binders, as a rule, is not allowed.

Together with the top layers and the coating, additional base layers should provide the necessary structural strength, frost resistance and drainage capacity. The lower layers of the base, especially those of granular materials, must resist shear stresses.

The foundations should be made mainly of reinforced materials on main roads with heavy and high-speed traffic.

2.9. The thickness of layers made of materials containing an organic binder and laid on the top layer of a base made of materials reinforced with cement, in order to limit the appearance of reflected cracks on the pavement, should be taken, as a rule, not less than the thickness of layers reinforced with cement. In this case, the minimum thickness of layers with organic binders should correspond to the data in **Table A.2.1**.

Table A.2.1: Minimum thickness specifications

Road pavement type	*Capital*	*Lightweight*
The smallest thickness of layers of materials containing organic binder [cm]	18	12

In the case of using materials reinforced with complex binders, as well as slowly hardening hydraulic binders, the layer thickness can be reduced by 20% and in hot and dry regions of road-climatic zones IV-V by 30%.

To increase the crack resistance of the coating, special crack-breaking interlayers can be provided, including those based on geogrids and geotextiles, the use of modified binders in the coating material and other special solutions.

2.10. The thickness of an individual layer is pre-assigned in the range from the minimum structural thickness, regulated by the current SNiP, to practically accepted values (for example, in typical projects) for a given region.

The total thickness of the pavement and the thickness of the individual structural layers are finally determined according to the calculation for strength, frost resistance and drainage in accordance with sections 3, 4 and 5 of this instruction.

In the design of pavements, it is necessary to provide as few layers of different materials as possible (2-4 without taking into account additional layers).

2.11. To significantly reduce the inflow of surface water into the base of the pavement and reduce the design moisture content of the subgrade soil, it is necessary to provide for such measures as strengthening the shoulders, ensuring their proper lateral slope and water tightness, arranging curbs and trays, as well as ensuring a safe distance from

the edge of the subgrade to the edge long-term stagnant surface water, increased compaction (up to K_y=1,03-1,05) of the upper part of the active layer in road-climatic zones III-V, etc.

2.12. In areas with unfavorable climatic and soil hydrological conditions, in order to limit the migration of moisture from the lower layers of the subgrade to the upper ones, measures should be taken to artificially regulate the water-thermal regime designed in accordance with the current SNiP and special documents for their development.

2.13. To ensure the possibility of assigning the same type of pavement structure on sections of great length, it is necessary to strengthen the upper part of the roadbed at different depths.

2.14. In order to ensure favorable working conditions for the edge parts of the pavement, the base should be 0,6 m wider than the roadway and the reinforcing strip and an additional bottom layer of sand or other granular material should be 1 m wider than the base or it should be arranged over the entire width of the roadbed. In addition, the installation of side stones, slabs or a monolithic side can be provided for road pavements of the capital type.

Strengthening of roadsides is performed in accordance with the instructions of the SNiP "*Highways. Design Standards*" and recommendations of special documents.

CONSTRUCTION OF PAVEMENTS AND FOUNDATIONS OF CAPITAL ROAD PAVEMENTS

2.15. The type and brand of asphalt concrete for the pavement is assigned in accordance with the provisions of the current SNiP "*Highways*" and GOST "*Asphaltic Concrete Mixtures for Roads and Aerodromes and Asphaltic Concrete*".

2.16. The bearing layer of the base of capital road pavements should be made of durable materials (from porous asphalt concrete, tar concrete, crushed stone mixtures treated with bitumen emulsion, fractionated crushed stone treated with viscous bitumen according to the impregnation method, as well as from fractionated crushed stone laid according to the principle of wedging with fine crushed stone or slag, strengthened by the method of impregnation with a cement-sand mixture, etc.). On roads intended for the movement of vehicles with a carrying capacity of 8 and more tons, when paving with a thickness of 3-5 cm, the upper part of the supporting base should be provided from asphalt concrete.

For the device of the lower part of the supporting base, depending on the design conditions of movement, monolithic (hardened soils and stone materials), as well as granular materials that meet the requirements of the current SNiP and GOST, can be used.

In the structures of road pavements for roads with heavy traffic, at the contact of layers of coarse-grained or gravel materials with sandy layers of the base or with the subgrade soil, it is necessary to provide for separating layers of geotextile in order to prevent the interpenetration of materials of adjacent layers and reduce the durability of the structure.

CONSTRUCTION OF PAVEMENTS AND BASES OF LIGHTWEIGHT AND TRANSITIONAL ROAD PAVEMENTS

2.17. Lightweight road pavements with improved coatings (asphalt concrete, tar concrete, black crushed stone, crushed stone treated with binders according to the impregnation method, coarse-grained materials, sandy or sandy loamy soils treated in an installation with bitumen emulsion together with cement) are advisable to be used on roads of category III and IV, as well as in the stage-by-stage construction of pavements on roads of category II.

2.18. Preliminary, the thickness of the asphalt concrete layer of lightweight road pavements should be set equal to 4-6 cm and, when using other materials specified in *point 2.17*, equal to 6-8 cm. Finally, the thickness of the pavement is set by calculation.

2.19. Bearing bases for lightweight road pavements with an improved surface are provided from monolithic or granular materials. At the same time, on roads of categories III and IV, it is advisable to arrange the base of the pavement from gravel porous asphalt concrete, gravel-sand mixtures treated with emulsion, tar and other organic binders, various materials, soils and industrial by-products treated with inorganic or complex binders, crushed stone and crushed stone-gravel mixtures.

2.20. Road pavements of transitional type (crushed stone and gravel from strong rocks, from low-strength stone materials and soils reinforced with organic, inorganic or complex binders, pavements from cobblestone and crushed stone) can be provided on roads of categories IV and V, as well as in stage construction on roads of category III.
When designing pavements with a transitional surface type, one should strive for the surface to consist of one or two layers.
For coatings arranged by the method of wedging or when fractionated crushed stone of natural rocks, crushed stone from mining waste and crushed stone from low-activity metallurgical slags are used, which meet the current GOST "*Crushed Natural Stone for Construction Work*" and "*Crushed Stone Blast-Furnace and Steelmaking for Road Construction*".

2.21. It is allowed to use simplified structures to reduce initial costs with an appropriate feasibility study, the movement along which in an unfavorable period of the year should be limited in terms of the axle load of vehicles, speed and intensity.

2.22. Frost-protective layers are arranged from stable granular materials, such as sand, sand and gravel mixture, gravel, crushed stone, slags, etc., as well as from soils reinforced with binders or hydrophobized soils or from other non-porous materials. An indicator of the suitability of a material for frost resistance is its degree of heaving, determined in laboratory conditions in accordance with the current GOST. It is allowed to take values of the degree of heaving according to **Table A.4.1** and **Table A.4.2**.

2.23. In the case of a frost-protective layer made of granular materials with a filtration coefficient of at least 1-2 m/day, it can also act as a drainage layer, which must be confirmed by an appropriate calculation. In this case, the frost-protective layer must be arranged over the entire width of the subgrade with access to the embankment slopes or with the laying of tubular drains or other drainage devices.
The thickness of the frost-protective layer is established by calculation in accordance with the provisions of *chapter 4* of these ODN. The width of the frost protection layer must exceed the width of the overlying layer by at least 0,5 m on each side.

2.24. In places where different structures of the pavement abut, it is necessary to provide for a transition zone, within which the pavement structure must change in such a way that at the ends of this zone, the heaving of soils would be equal to the values of the winter rise in the adjacent sections. The length of the transition zone is established by calculation in accordance with *chapter 4*.

2.25. In heaving-hazardous areas where it is technically impossible or economically inexpedient for traditional measures to ensure the frost resistance of the structure, heat-insulating layers of special materials should be provided to partially or wholly prevent the freezing of the subgrade. For the installation of heat-insulating layers in especially unfavorable soil hydrological conditions (wet excavations, subgrade at zero marks, low embankments where the freezing depth is greater than the distance from the surface of the coating to the groundwater level or long-term stagnant surface water), the option of

using foam plastics should be considered. The choice of the required grade of foam should be made in accordance with *chapter 4*.

Lightweight concrete, heat-insulating compositions made of local materials (soils) or industrial waste and porous aggregates (expanded clay, perlite, aggloporite, polystyrene granules, crushed foam waste, etc.), can also be used as a heat insulator.

The distance from the surface of the coating to the heat-insulating foam layer must be at least 0,5 m (to exclude the increased risk of ice formation). The heat-insulating layer should be 0,5-1,5 m wider than the roadway on each side, depending on the depth of freezing of the subgrade, and when calculating to prevent freezing of soils under the pavement, by 1,0-2,0 m. The sand layer should be at least 0,2 m in a compacted state with foam plastic plates.

A thermal calculation determines the thickness and location of the heat-insulating layer in the structure. The deformation and strength characteristics of the layer material, as well as its thickness, should be taken into account when calculating the strength of the road structure.

The abovementioned minimum depth of the heat insulator from the coating surface is specified according to the data of the regional operating experience of structures with heat-insulating layers.

The optimal design and type of thermal insulation materials must be selected on the basis of a technical and economic comparison of options that are equivalent in terms of frost resistance.

2.26. Drainage layers are arranged in areas with a subgrade of non-draining soils in all cases with the 3rd scheme of moistening the active layer of the subgrade, with the 1st and 2nd humidification schemes in areas with a large amount of precipitations (RCZ II-III), as well as in areas at the base of the carriageway of which water may accumulate penetrating from the surface (areas with long longitudinal slopes, with relatively easy permeable soils of roadsides, on open fractures of the longitudinal profile, near green spaces and lawns adjacent to the carriageway, etc.).

Drainage layers should be made of sand, gravel materials, sorted slag and other filter materials. In structures where the drainage layer is higher than the freezing depth, the

layers must be frost-resistant and robust enough. The required filtration coefficient of the drainage layer material is determined by calculation, taking into account the geometric parameters of the roadway and other conditions. Regardless of the calculation results, it should be at least 1 m/day and 2 m/day, respectively, on road sections passing in an embankment and a low embankment or excavation.

When choosing a material for the drainage layer, the strength properties that affect the strength of the pavement are taken into account.

In most cases, especially in heaving-hazardous areas, it is rational to construct the upper part of the subgrade made of drainage material without special drainage devices. If the amount of water to be diverted is more than 0.007 m/day per 1 m of the carriageway, as well as in recesses and in places with zero marks, the option of arranging longitudinal tubular drains (made of various materials, as well as flat geosynthetic drains, etc.) with transverse outlets at the edges of the carriageway is considered, as well as the use of longitudinal drainage from a largely porous material.

The drainage structure should be selected based on a feasibility study of the options.

2.27. In areas with long slopes, where the longitudinal slope is greater than the transverse one, for interception and drainage of water moving in the drainage layer along the road, it is envisaged to arrange small slots in the soil base with the laying of perforated pipes, pipe filters or crushed stone with anti-silt insulation in them.

2.28. To reduce moisture accumulation in the upper part of the subgrade, waterproof layers (of various materials) can be provided for the entire width of the subgrade. If the width of the roadbed is more than 15 m and the waterproof cover is allowed, the device of closed layers (clips) for the width of the carriageway is allowed. The depth of the layer from the pavement surface depends on the road-climatic zone and should be more than 90 cm in road-climatic zone II, 80 cm in RCZ III, 70 cm in RCZ IV and 65 cm in RCZ V zone.

2.29. Capillary-interrupting layers 10-15 cm thick from coarse sand or gravel are provided for the entire width of the roadbed. To protect the interlayer of granular

materials from rapid contamination, under and above it, it is necessary to provide interlayers that play the role of filters.

2.30. In the southern regions, a significant decrease in the volume of migrating, mainly vaporous moisture, can be achieved by installing vapor barrier layers from polymer roll materials, soil treated with an organic binder or from a layer of carefully compacted soil in a cage.

2.31. If a coarse-grained material (such as crushed stone, gravel, slag) is laid directly on the soil of the subgrade, an interlayer is provided to prevent the interpenetration of materials from adjacent layers. As interlayer materials, it is possible to use fine crushed stone, seeding (0-10 mm), gravel-sand mixtures, coarse and medium-sized sands, non-dusty slags, non-porous ash and slags, synthetic textile materials, etc. A layer of soil reinforced with binders can serve as a protective layer (5-8 cm thick). The thickness of the interlayer of granular material should be taken from 5 to 20 cm, depending on the degree of moistening of the subgrade soil. An interlayer of geotextile materials should also be provided when laying largely porous materials on a sand layer on roads of categories I-III.

FEATURES OF THE DESIGN OF PAVEMENTS WITH LAYERS OF LOW-STRENGTH MATERIALS AND INDUSTRIAL BY-PRODUCTS

2.32. The possibility of using soft limestones, flasks, gravel materials, grit, shell rock, artificial stone materials, etc., without processing with binders, is determined by the compliance of their properties with the requirements of the current GOST. If the properties do not meet the standard requirements, the materials must be processed. In areas with unfavorable soil and hydrological conditions, it is not allowed to use in the base (even for the lower layers) untreated materials that do not meet the requirements of the current GOST in terms of grain size composition, as well as materials in which the plasticity index of particles less than 0,16 mm exceeds 7.

2.33. Road surfaces coated with binder-treated or untreated low-strength materials on a sandy, gravel and crushed stone base, or on a base made of hardened soil, may be used in climatic zones IV and V with a traffic intensity of no more than 100 vehicles/day with an axle load of no more than 70 kN. With a greater traffic intensity, it is always necessary to provide for the processing of low-strength materials with organic and inorganic binders.

For the construction of foundations for improved pavements or pavements on roads of IV-V categories, it is possible to use lean cement concrete based on weak limestone crushed stone, shell rock, river sandstones, etc., as well as gravel materials reinforced with an inorganic binder.

2.34. Crushed slag from highly active and active slags can be used for paving on roads of IV-V categories and for bases (from improved and unimproved slags) of roads of II-IV categories.

To increase the solidity and strength of layers of acidic low-activity slags with a basicity modulus of less than 1, it is necessary to provide for the addition of fine particles from active slags and 2-3% of slaked lime or ground granulated slag in the amount of 20-25% of the mass of crushed stone to the crushed slag. For the arrangement of layers of road pavements, which should have improved strength and deformation qualities, crushed slag treated with organic and mineral binders should be used.

It is advisable to process acidic metallurgical slags with coal tar (taking into account the requirements of GOST for tar), which have higher adhesion properties than petroleum bitumen. They can also be treated with bitumen emulsion with lime, active fly ash, etc.

MEASURES TO INCREASE THE STRENGTH AND STABILITY OF THE ACTIVE LAYER OF THE SUBGRADE

2.35. To increase the strength and stability of the active layer of the subgrade, it is necessary to provide for various measures: its construction from non-porous, low-

porous and low-swelling soils, protection of soil from moisture by surface and underground waters, etc.

In road-climatic zones III and IV, in areas with the 1st moistening scheme, it is allowed to provide for the compaction of the upper part of the active layer (30-50 cm thick) to a compaction coefficient of 1,0-1,05. A layer of increased density soil should be considered an independent structural layer. The design deformation and strength characteristics of the soil in this layer are taken in accordance with reference *appendix 2*.

When constructing a layer of increased density from cohesive (swelling) soil, measures are taken to protect it from moisture.

2.36. When the design relative humidity of the soil is more than 0,7, among the possible measures to increase the stability of the active layer, one should consider strengthening its upper part with a small number of binders (for example, 3-4% cement, 10-15% fly ash or granular slags, lime, etc.).

REGIONAL PECULIARITIES

2.37. When designing pavements in various specific regions, along with considering general regulations and these standards, one should be guided by the instructions of special regional regulatory and technical documents approved in the prescribed manner. In the absence of such documents, one should be guided by these standards.

2.38. Design temperatures, deformation and strength characteristics of soils and road building materials in the absence of regional standards should be assigned in accordance with the recommendations of *appendix 2* and *appendix 3*.

2.39. In areas where permafrost soils are spread, road pavements are designed taking into account the principles of regulating the permafrost state on the basis of heat engineering calculations performed according to special regulatory and technical documents.

When designing roads in areas of irrigated land, it is necessary to take into account the adverse impact on the operation of the road structure of an increased level of groundwater during irrigation of agricultural land, a local rise in groundwater near the irrigation network, flooding of reserves and drainage ditches as a result of irrigation of lands.

When designing pavements on roads in sandy deserts, it is necessary to provide for strengthen the surface of the sand under the pavement. It can be in the form of a layer of cohesive soil 15 cm thick, from an optimal mixture of sand and loam, from sand treated with a bitumen emulsion using geotextiles, etc.

Protective layers of hardened or unreinforced materials on a dune sand subgrade should be considered as structural elements of the pavement.

PRINCIPLES OF THE DESIGNATION OF PAVEMENT STRUCTURES IN THE DESIGN, RECONSTRUCTION OF EXISTING ROADS

2.40. On the sections of the reconstructed roads where new pavement is arranged, the pavement design is carried out according to these ODN. On reconstructed areas where old pavement is retained or used, the design is carried out in accordance with the provisions of special regulatory documents on the basis of detailed data on the structure of the existing pavement, the state of its structural layers and the assessment of the ability of these layers to perform their functions. To obtain the initial data, the existing pavement and the active layer of the subgrade must be examined in detail with the performance of drilling and other works and tests that allow obtaining the necessary information. Quantitative assessments of the strength and frost resistance of the structure are carried out according to the methods described in these ODN.

When developing a design solution, the following issues should be considered:

- the expediency of using the existing pavement or its individual structural layers without prior destruction;
- the expediency of using materials of structural layers after their processing;

- the need to strengthen the existing structure;
- the need to increase the frost resistance of the existing structure;
- the need to improve the drainage of the existing structure;
- the need to change the design of strengthening the shoulders;
- the need to broaden the pavement and the broadening method.

3. PAVEMENT DESIGN FOR STRENGTH

3.1. The strength of the pavement is defined as the ability to resist the process of development of residual deformations and fractures under the influence of tangential and normal stresses arising in the structural layers and the underlying soil from the design load (short-term or single/multiple long-term) applied to the pavement surface.

3.2. The method for assessing the strength of a structure includes both an analysis considering the system as a whole (using the empirical dependence of the permissible elastic deflection and the number of load applications) and an assessment taking into account the stresses arising in individual structural layers and established using the solutions of elasticity theory.

3.3. Roads should be designed with the required level of reliability, which is defined as the probability of failure-free operation during the overhaul period. Failure of a structure in terms of strength can be physically characterized by the formation of longitudinal and transverse unevenness of the pavement surface associated with the resistance of the structure (transverse irregularities and fatigue cracks), with the subsequent development of other types of deformations (frequent cracks, networks of cracks, potholes, subsidence, breaks, etc.). The nomenclature of defects and the method for quantifying them is determined by particular standards used in roads maintenance. As a quantitative indicator of the pavement failure intended as an element of linear nature of an engineering structure, the limiting coefficient of destruction K_r^{pr} is used, which is the ratio of the total length (or total area) of the road sections requiring repair due to insufficient pavement strength to the road total length (or total area) between the corresponding points. The K_r^{pr} values for the last year of service, depending on the road category, should be taken in accordance with **Table A.3.1**.

Table A.3.1: Suggested values of pavement design parameters

Pavement type		*Capital*										
Road category		*I*		*II*		*III*			*IV*			
Limiting coefficient of destruction K_r^{pr}		0,05				0,1						
Specified reliability K_n		0,98	0,95	0,98	0,95	0,98	0,95	0,9	0,95	0,9	0,85	0,8
Required strength factor K_{pr}^{tr}	**Elastic deflection**	1,5	1,3	1,38	1,2	1,29	1,17	1,1	1,17	1,1	1,06	1,02
	Bending shear	1,1	1	1,1	1	1,1	1	0,94	1	0,94	0,9	0,87

Pavement type		*Lightweight*										
Road category		*III*			*IV*				*V*			
Limiting coefficient of destruction K_r^{pr}		0,15										
Specified reliability K_n		0,98	0,95	0,9	0,95	0,9	0,85	0,8	0,95	0,9	0,8	0,7
Required strength factor K_{pr}^{tr}	**Elastic deflection**	1,29	1,17	1,1	1,17	1,1	1,06	1,02	1,13	1,06	0,98	0,9
	Bending shear	1,1	1	0,94	1	0,94	0,9	0,87	1	0,94	0,87	0,8

Pavement type		*Transitional*							
Road category		*IV*				*V*			
Limiting coefficient of destruction K_r^{pr}		0,4							
Specified reliability K_n		0,95	0,9	0,85	0,8	0,95	0,9	0,8	0,7
Required strength factor K_{pr}^{tr}	**Elastic deflection**	1,17	1,1	1,06	1,02	1,13	1,06	0,98	0,9
	Bending shear*	1	0,94	0,9	0,87	1	0,94	0,87	0,8

**pavements of transitional type for roads of category V are not designed according to the criterion of elongation in bending.*

3.4. The structural strength is quantified by the value of the so-called strength factor. When assessing the resistance of a system as a whole based on the permissible elastic deflection, this value is generally determined by the formula:

$$K_{pr} = \frac{l_{dop}}{l} = \frac{E_{ob}^{tr}}{E_{ob}}$$

When assessing the strength of a structure by layers according to the allowable stresses, the strength factor is determined by the formula:

$$K_{pr} = \frac{\sigma_{dop}}{\sigma_{rasc}}$$

where:

- l_{dop} is the total allowable deflection of the structure under the design load;
- l is the design total deflection of the structure under the design load;
- E_{ob}^{tr} is the required total modulus of elasticity of the structure, determined at the design load;
- E_{ob} is the design total modulus of elasticity of the structure, determined at the design load;
- σ_{dop} is the allowable stress (normal or tangential) from the design load;
- σ_{rasc} is the design effective stress (normal or tangential) from the design load.

3.5. The strength factor of a newly designed structure should be such that, in a given overhaul period, a failure in strength does not occur with a probability greater than a given one, i.e., to ensure the specified reliability.

3.6. To ensure the specified reliability, the strength factor of the calculated structure for each of the design criteria should not be lower than the minimum required value determined from **Table A.3.1**.

3.7. The calculation task includes the determination of the thickness of the pavement layers in the options outlined during the design or the choice of the materials with the appropriate deformation and strength characteristics.

3.8. Pavement failure (in the forms specified in *point 3.3*) associated with its insufficient strength may result from:

- accumulation of unacceptable residual deformations with loss of evenness of the pavement surface and a corresponding decrease in the traveling speed until the expiration of the specified service life of the structure under the influence of shear stresses arising in the structural layers and the underlying soil from the transport load;
- fatigue fractures of the asphaltic layers of the structure under the influence of tensile stresses from repeated applications of the transport load, followed by an intensive loss of the operational properties in the road pavement before the end of the specified service life.

In accordance with this, the calculation of the strength in the layers is carried out according to the permissible shear stress, with a reduced shear resistance, and the tensile bending in asphaltic strata.
The calculation of the strength of the structure as a whole is carried out according to the permissible elastic deflection (or the required total modulus of elasticity).

3.9. Pavements rely on short-term repeated action of moving loads. The accepted values of the parameters of the strength and deformation characteristics of materials must correspond to the specified nature of the load application.
Roads at stops, crossroads, at the approaches to intersections with railway tracks, etc. must be additionally checked for single loading with a load duration of at least ten minutes.
Pavements in parking lots and roadsides should be designed for continuous loading (more than ten minutes). The calculation is carried out for a single load. In this case, the static values of the design parameters are used and the coefficients for repetition are not entered. The calculation is carried out according to the criteria of shear in the subgrade, in loosely bound materials, as well as in layers treated with an organic binder.

3.10. When studying structures with layers of bitumen-mineral materials, the effect of temperature on their properties is taken into account. When designing pavement layers of asphalt concrete in tension during bending, their characteristics should correspond to low spring temperatures (see *appendix 3*, **Table P.3.1**). When assessing layers of weakly connected materials, as well as the subgrade for shear strength, the modulus of elasticity of the asphalt concrete pavement must correspond to high spring temperatures (see *point 3.31* and *appendix 3*, **Table P.3.2**).

3.11. The required level of reliability in each specific case must be indicated when issuing a design assignment.

For most design cases, the values of the required strength factor for various calculation criteria can be taken depending on the specified level of reliability, the pavement type and the road category according to **Table A.3.1**.

3.12. The design values of the strength characteristics (characteristic shear and tensile strength in bending) of the structural layers are determined using the relationship:

$$M_r = \bar{M}_r \cdot (1 - \nu_t \cdot t)$$

where:

- M_r is the design value of the strength characteristics;
- $\bar{M}_r$ is the normative value of this characteristic (see *appendix 3*);
- t is the normalized deviation coefficient at an acceptable level of reliability (see *appendix 4*);
- ν_t is the coefficient of variation (see *appendix 4*).

For the design values of the structural layers' deformation characteristics (elastic moduli), it is allowed to take their standard values (see *appendix 3*).

For the design values of the strength (shear) and deformation (elastic moduli) characteristics of the soil of the active layer, it is allowed to take their standard values

(see *appendix 2*), which correspond to the design value of the relative humidity of the soil, as described in *appendix 2*.

GENERAL PROCEDURE AND CRITERIA FOR STRENGTH CALCULATION

3.13. Calculation sequence:

3.13.1. Design of the pavement by the criterion of elastic deflection based on the dependence of the required total modulus of elasticity of the structure on the total number of load applications.

As a result of this calculation, the thickness of the structural layers and their elastic moduli are assigned so that the total modulus of elasticity of the pavement is not less than the required one, taking into account the corresponding strength factor (**Table A.3.1**).

3.13.2. Design of the pavement that meets the criterion of elastic deflection, taking into account the mechanism of breaking strength in its individual structural layers according to two independent criteria:

- the criterion of compliance with the shear stability of the materials of the structural layers and the subgrade to the tangential stresses arising in them, reflecting the condition for limiting the accumulation of residual shear deformations under the influence of repeated short-term loads;
- the criterion of compliance of the resistance of the materials of asphaltic structural layers to the tensile stresses arising in them from multiple movable loads, reflecting the strength of these layers against fatigue processes that cause the development of microcracks, the loss of their continuity and a decrease in the distribution capability.

Strength factors for these criteria must not be less than the values indicated in **Table A.3.1**; if this is not the case, the design is repeated by either increasing the thickness of the layers or using materials with higher elastic moduli.

3.14. Pavements of transitional and lower types are designed according to elastic deflection and shear stability.

Structures intended for the movement of special heavy vehicles (with a static axle load of 120 kN and more) are not designed according to elastic deflection.

CALCULATION OF STRESSES AND STRAINS

3.15. Stresses in the structural layers and the underlying soil from the effect of the transport load are calculated by the formulas of the theory of elasticity for a layered medium loaded with a uniformly distributed load through a flexible round stamp, taking into account the conditions at the layers contact.

In this case, approximate methods are used based on simplified design schemes and nomograms.

A simplified design scheme is selected depending on the design criterion under consideration.

When performing calculations, actual multi-layer road structures lead to one- or two-layer models using the methods described in *point 3.27*, *point 3.32* and *point 3.39*.

3.16. The main stresses from the dead weight of the structure are determined based on the hydrostatic scheme, according to the formula:

$$\sigma_{sv} = \gamma_{sr} \cdot z_{op}$$

where:

- γ_{cr} is the weighted average specific gravity of the structure located above the design point;
- z_{op} is the distance from the pavement surface to the design point.

3.17. When assessing the characteristics of the pavement stress-strain state, the nomograms of these ODN (referred to multi-layer structures) lead to one- and two-layer design schemes.

DESIGN PARAMETERS OF THE MOVING LOAD

3.18. As a design scheme for loading a structure with a car wheel, a flexible circular stamp with a diameter D is considered, which transfers a uniformly distributed load p.
The values of the design specific pressure of the wheel p and the design diameter D of the imprint on the pavement surface reduced to a circle are assigned taking into account the parameters of the different types of vehicles.
For the design, the heaviest car of those systematically circulating on the road is considered, the share of which is at least 10% (taking into account the prospect of changing the composition of traffic by the end of the overhaul period).
The value of p is taken to be equal to the air pressure in the tires. The diameter of the design tire imprint D is determined from the dependence:

$$D = \sqrt{\frac{40 \cdot Q_{rasc}}{\pi \cdot p}}$$

where:

- Q_{rasc} is the design value of the load transmitted by the wheel to the surface of the pavement;
- p is the pressure.

For the D and p values of the design load of type A, see *appendix 1*.

3.19. Taking into account the nature of the acting load (short-term multiple loading and static loading) is carried out by adopting the corresponding design values of the characteristics of the structural layers and by introducing the dynamic factor when assigning the value of the load.

3.20. Depending on the type of design calculation, various characteristics are used, reflecting the intensity of the effect of a moving load:

- N is the prospective (at the end of the service life) total average daily traffic intensity;
- N_r is the average daily (at the end of the service life) number of passages of all wheels of the design vehicle, reduced to the design load, within one lane of the carriageway;
- $\sum N_r$ is the total design number of applications of the design load within one lane of the carriageway during the service life.

3.21. N is established according to economic surveys' analyses of traffic volume and intensity patterns changes.

3.22. The value of N_r of the reduced intensity for the last year of the service life is determined by the formula:

$$N_r = f_{pol} \cdot \sum_{t=1}^{p} \left(N_t \cdot S_{t,sum} \right)$$

where:

- f_{pol} is a coefficient taking into account the number of traffic lanes and the distribution of traffic along them, determined from **Table A.3.2;**

Table A.3.2: Suggested values of f_{pol}

Number of lanes	**f_{pol} for each lane starting from the curb**		
	1	*2*	*3*
1	1	-	-
2	0,55	-	-
3	0,5	0,5	-
4	0,35	0,2	-
6	0,3	0,2	0,05

Note:

1. *The lane number is considered with respect to the travel direction.*
2. *For the shoulders, take f_{pol}=0,01.*
3. *On multi-lane roads, it is allowed to perform the design of thicknesses varying along the width of the carriageway, designing the pavement within different lanes taking into account the value of N_r.*
4. *At intersections (places where the cars flow is reorganized), when designing pavements within all traffic lanes, f_{pol}=0,5 should be taken if the total number of lanes of the carriageway is greater than three.*

- p is the total number of the different vehicle types in the traffic flow;
- N_t is the number of passages per day in both directions of vehicles of the tth type;
- $S_{t,sum}$ is the total reduction coefficient of the impact on the road surface of the vehicle of the tth type to the design load Q_{rasc} (see *appendix 1*).

3.23. The total estimated number of applications of the design load on a point on the pavement surface during the service life is determined by the formula:

$$\sum N_r = f_{pol} \cdot \sum_{t=1}^{p} \left(N_{1t} \cdot K_s \cdot T_{rdg} \cdot 0{,}7 \cdot S_{tsum} \cdot k_p \right)$$

or by the formula:

$$\sum N_r = 0{,}7 \cdot N_r \cdot \frac{K_s}{q^{T_{sl}-1}} \cdot T_{rdg} \cdot k_p$$

where:

- p is the number of vehicle types;
- N_{1t} is the daily traffic intensity of vehicles of the t[th] type in the first year of service (in both directions);
- K_s is the summation coefficient, determined by the formula:

$$K_s = \frac{q^{T_{sl}} - 1}{q - 1}$$

  where T_{sl} is the estimated service life (see *appendix 6*, **Table P.6.4**) and q is an indicator of the change in the traffic intensity of a given type of vehicle over the years;
- T_{rdg} is the estimated number of design days in a year corresponding to a particular state of deformability of the structure (see *appendix 6*);
- k_p is a coefficient that takes into account the probability of deviation of the total movement from the average expected (**Table A.3.3**).

Table A.3.3: Suggested values of k_p

Pavement type	**k_p for different road categories**				
	I	*II*	*III*	*IV*	*V*
Capital	1,49	1,49	1,38	1,31	-
Lightweight	-	1,47	1,32	1,26	1,06
Transitional	-	-	1,19	1,16	1,04

CALCULATION OF THE STRUCTURE AS A WHOLE FOR THE PERMISSIBLE ELASTIC DEFLECTION

3.24. The structure of the pavement as a whole meets the requirements of strength and reliability in terms of amount of elastic deflection, provided that:

$$E_{ob} \geq E_{min} \cdot K_{pr}^{tr}$$

where:

- E_{ob} is the design modulus of elasticity of the structure;
- E_{min} is the minimum required total modulus of elasticity of the structure;
- K_{pr}^{tr} is the required coefficient of strength of the pavement according to the criterion of elastic deflection, taken depending on the required level of reliability (see *point 3.6* and **Table A.3.1**).

3.25. The value of the minimum required total modulus of elasticity of the structure is calculated using the empirical equation:

$$E_{min} = 98{,}65 \cdot \left[log \sum N_r - c\right]$$

where:

- $\sum N_r$ is the total estimated number of load applications for the service life of the pavement, established in accordance with *point 3.23*;
- c is an empirical parameter taken for the design axle load of 100 kN equal to 3,55, for 110 kN equal to 3,25 and for 130 kN equal to 3,05.

Note:

1. *The formula should be used when* $\sum N_r > 4 \cdot 10^4$ *vehicles.*
2. *For roads in RCZ V, the required modulus should be reduced by 15%.*

3.26. Regardless of the result obtained by the formula, the required total modulus of elasticity must be at least as indicated in **Table A.3.4**.

Table A.3.4

Road category	**Required total modulus of elasticity [MPa]**		
	Capital	*Lightweight*	*Transitional*
I	230	-	-
II	220	210	-
III	200	200	-
IV	-	150	100
V	-	100	50

3.27. The general design modulus of elasticity of the structure is determined using the nomogram in **Figure A.3.1**, constructed according to the solution of the theory of elasticity for the model of a multi-layer medium.

The reduction of a multi-layered structure to an equivalent single one is carried out stepwise, either from top to bottom or from bottom to top.

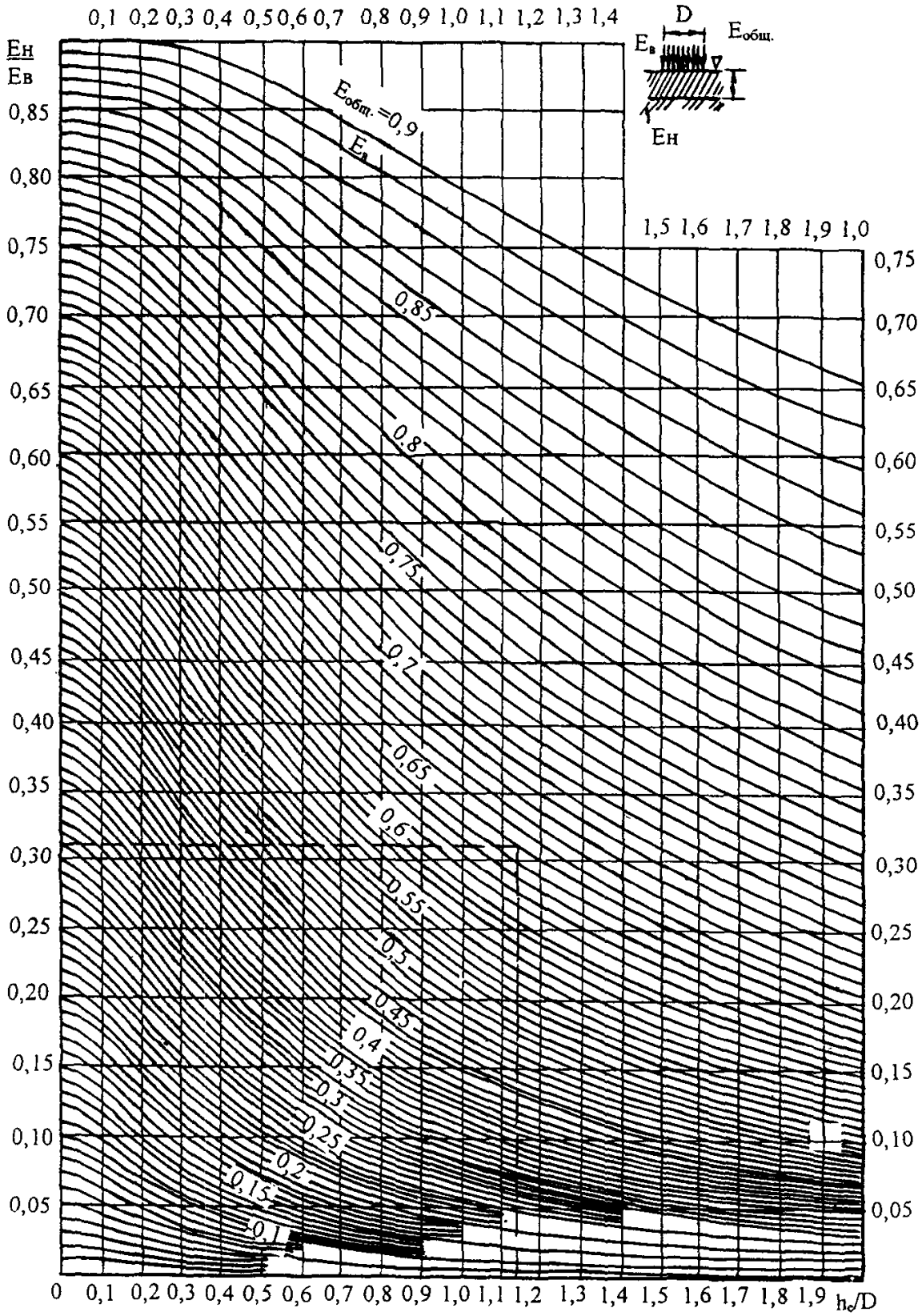

Figure A.3.1: Nomogram for pavement design according to elastic deflection

3.28. The design values of the moduli of elasticity of different soils and materials may be taken according to the indications in *appendix 2* and *appendix 3*.
The elastic modulus of materials containing organic binder must be taken in all climatic zones at a temperature of +10 °C, according to *appendix 3* (**Table P.3.2**).

3.29. The calculation for the permissible elastic deflection (for the required modulus of deformation) is carried out in the following sequence:

- determine the required minimum total modulus of elasticity according to the formula;
- assign moduli and pre-thicknesses of the layers of the structure (except for the thickness of the subgrade);
- set using the nomogram in **Figure A.3.1** the total modulus of elasticity of each structural layer either from top to bottom or vice-versa;
- check the fulfillment of the strength condition; if the verification is not satisfied, change the thickness of one or more structural layers or use materials with a higher elastic modulus.

CALCULATION ACCORDING TO THE CONDITION OF SHEAR STABILITY OF THE UNDERLYING SOIL AND POORLY CONNECTED STRUCTURAL LAYERS

3.30. Pavements are designed so that under the action of short-term and long-term loads in the underlying soil and poorly connected layers, unacceptable residual deformations do not accumulate over the entire service life. Inadmissible shear strains in the structure will not arise if the following condition is satisfied:

$$T \leq \frac{T_{pr}}{K_{pr}^{tr}}$$

where:

- T is the design active shear stress (part of the shear stress not extinguished by internal friction) at the design point of the structure from the current short- or long-term load (*point 3.34*);
- T_{pr} is the limiting value of the active shear stress (at the same point), the excess of which causes a breach of the shear strength (*point 3.35*);
- K_{pr}^{tr} is the required minimum value of the strength factor, determined taking into account the given level of reliability (see **Table A.3.1**).

3.31. In practical calculations, a multi-layer structure leads to a two-layer design model. When designing a pavement for the shear stability of the subgrade, the soil (with its characteristics) is taken as the lower one and all pavement strata are taken as the upper one. The thickness of the top layer h_v is equal to the sum of the thicknesses of the layers of the pavement $\sum_{i=1}^{p} h_i$.
The elastic modulus of the upper stratum of the model is calculated as a weighted average by the formula:

$$E_v = \frac{\sum_{i=1}^{p}(E_i \cdot h_i)}{\sum_{i=1}^{p} h_i}$$

where p is the number of the pavement layers, E_i is the modulus of elasticity of the ith layer and h_i is the thickness of the ith layer.

3.32. When designing according to the condition of shear stability, the typical characteristics of the granular material (c_p, φ_p) are assigned to the lower layer and the elastic modulus is taken equal to the modulus on its top, as explained in *point 3.27*; the depth of the upper stratum of the model is equal to the total thickness of the layers lying above the granular one and the modulus of elasticity E_v is calculated as a weighted average.

3.33. When designing for shear stability, the values of the elastic moduli of materials containing an organic binder are taken so that they correspond to the temperatures indicated in **Table A.3.5**.

Table A.3.5: Design temperature for shear stability

Road climatic zone	*I-II*	*III*	*IV*	*V*
Design temperature [°C]	20	30	40	50

3.34. Active shear stresses (T) acting in the subgrade or in the granular layer are calculated by the formula:

$$T = \bar{\tau}_H \cdot p$$

where $\bar{\tau}_H$ is the specific active shear stress from a unit load, determined using nomograms (**Figure A.3.2** and **Figure A.3.3**), and p is the design pressure from the wheel to the surface.

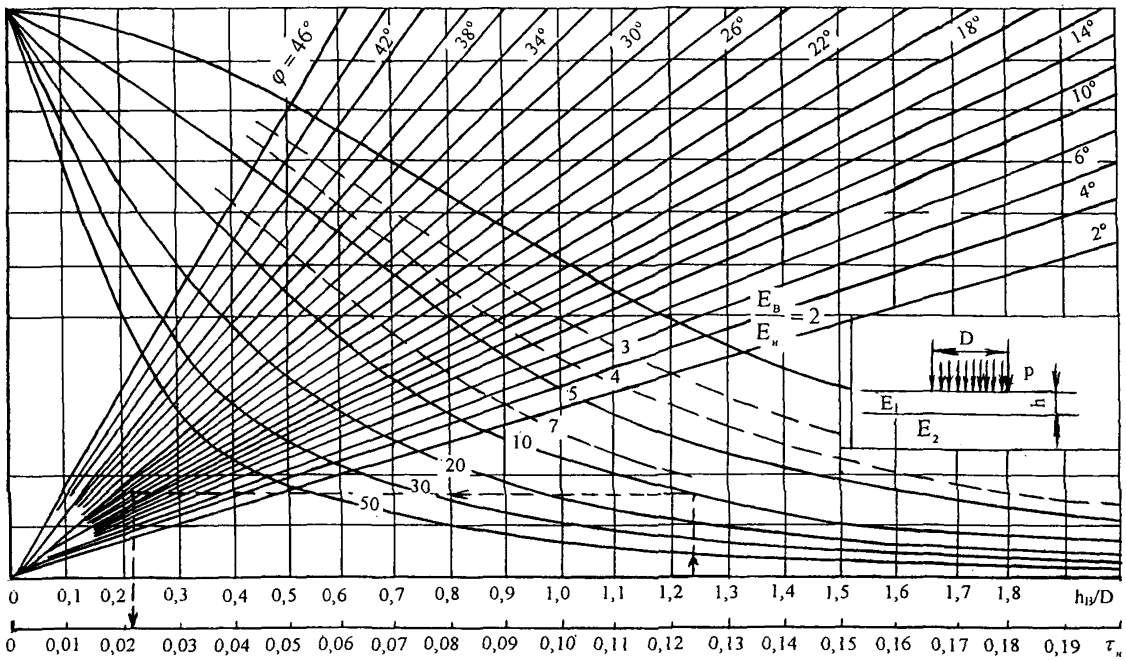

Figure A.3.2: Nomogram for pavement design according to shear stability (1)

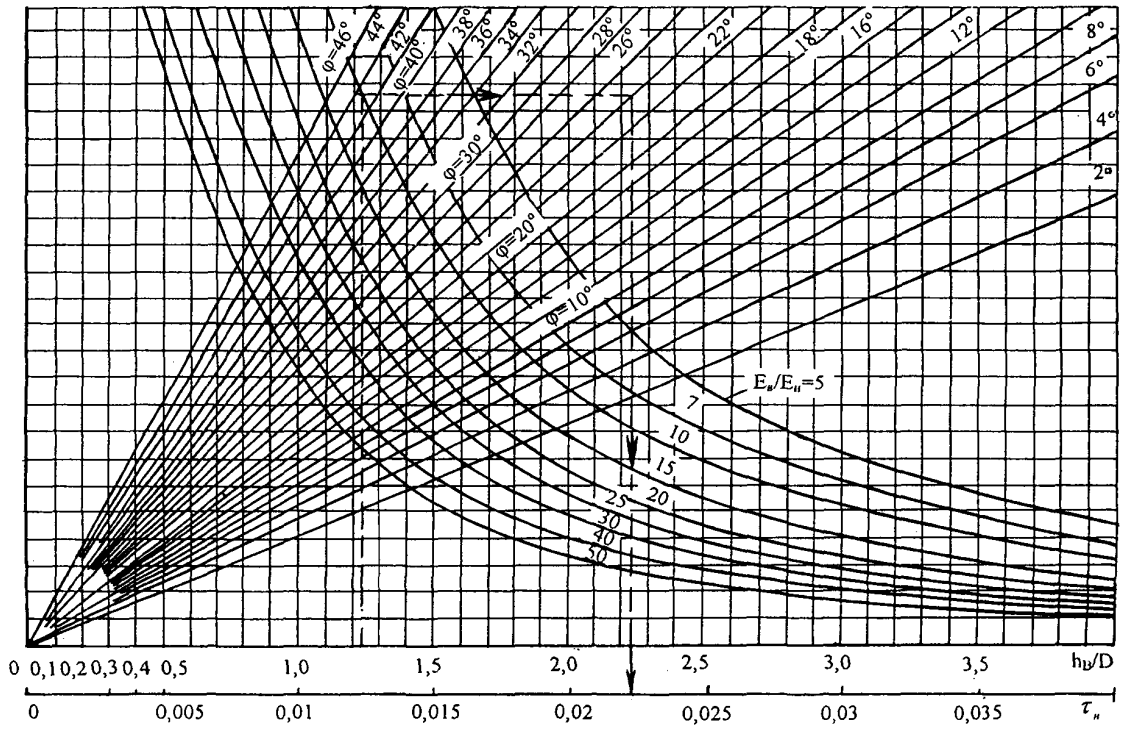

Figure A.3.3: Nomogram for pavement design according to shear stability (2)

Note: when using the nomogram to determine the value of $\bar{\tau}_H$, φ is taken for the case of the effect of a dynamic load (taking into account the number of applications) (see appendix 2, ***Table P.2.6*** *and* ***Table P.2.8****).*

3.35. The limiting active shear stress T_{pr} in the soil of the active layer (or in the granular material of the intermediate layer) is determined by the formula:

$$T_{pr} = c_N \cdot k_d + 0{,}1 \cdot \gamma_{sr} \cdot z_{op} \cdot tan\varphi_{st}$$

where:

- c_N is the cohesion in the subgrade soil (or in the intermediate granular layer) depending on the design moisture content and the load repetition (see *appendix 2,* **Table P.2.6** and **Table P.2.8**);
- k_d is a coefficient that takes into account the features of the structure at the boundary between the granular layer and the lower one of the subgrade. When constructing with reinforced materials, as well as when inserting a separating

geotextile layer at the boundary base-subgrade, the values of k_d should be taken equal to:

- 4,5, when used in a sandy layer of coarse sand;
- 4, when used in a sand layer of medium-size sand;
- 3, when used in a sandy layer of fine sand;
- 1, in all other cases.

- γ_{sr} is the weighted average specific gravity of the structural layers located above the tested one;
- z_{op} is the depth of the location of the surface of the layer tested for shear resistance from the top of the structure;
- φ_{st} is the design value of the angle of internal friction of the material of the tested layer under the static action of the load.

3.36. As design values of the angle of internal friction of the soil and weakly connected layers, the one that corresponds to the design total number of load effects for the overhaul period $\sum N_r$ equal to one is used. In this case, the value of design days in a year corresponding to the design state of strength and deformability of the structure T_{rdg} is determined according to special regional reference data (see *appendix 6*, **Figure P.6.1** and **Table P.6.1**).

3.37. Pavement design for shear resistance in the subgrade soil, as well as in the granular materials of the intermediate layers of the pavement, is carried out in the following sequence:

- according to **Table P.3.2**, designate the design moduli of elasticity for layers of asphalt concrete, corresponding to the maximum possible temperatures in the early spring (design) period (according to *point 3.33*); assign, according to **Table P.2.4** and **Table P.2.6** (taking into account the design moisture content and the total number of load effects), the design strength characteristics φ and c from

the soil of the subgrade and granular material of the intermediate layer (if any), considering the requirements of *point 3.36*. The rest of the design characteristics of the soil and materials remain the same as in the calculation for elastic deflection;

- according to **Figure A.3.2** or **Figure A.3.3**, determine the active shear stresses $\bar{\tau}_H$ from a unit time load. For this, the multi-layer structure is brought to a two-layer model (*point 3.31* and *point 3.32*);
- calculate the design shear stress in the soil of the subgrade or in the granular layer of the pavement;
- calculate the limiting shear stress;
- check the strength condition (taking into account the required reliability);
- if necessary, changing the thickness of the structural layers, select a structure that meets the condition of *point 3.30*.

STRUCTURAL ANALYSIS OF THE RESISTANCE OF MONOLITHIC LAYERS TO FATIGUE FAILURE FROM TENSILE BENDING

3.38. In monolithic layers (made of asphalt concrete, tar concrete, materials and soils reinforced with complex and inorganic binders, etc.), the stresses arising from the deflection of the pavement under the action of repeated short-term loads should not lead to the formation of cracks from fatigue failure during a given service life. For this, the following condition must be met:

$$\sigma_r < \frac{R_N}{K_{pr}^{tr}}$$

where σ_r is the largest tensile stress in the considered layer, established by calculation, K_{pr}^{tr} is the required strength factor, taking into account the given level of reliability (**Table A.3.1**), and R_N is the tensile strength of the layer material in bending, considering fatigue phenomena.

3.39. The greatest tensile stress σ_r in bending of a monolithic layer is determined using a nomogram (**Figure A.3.4**), bringing the actual structure into a two-layer model.

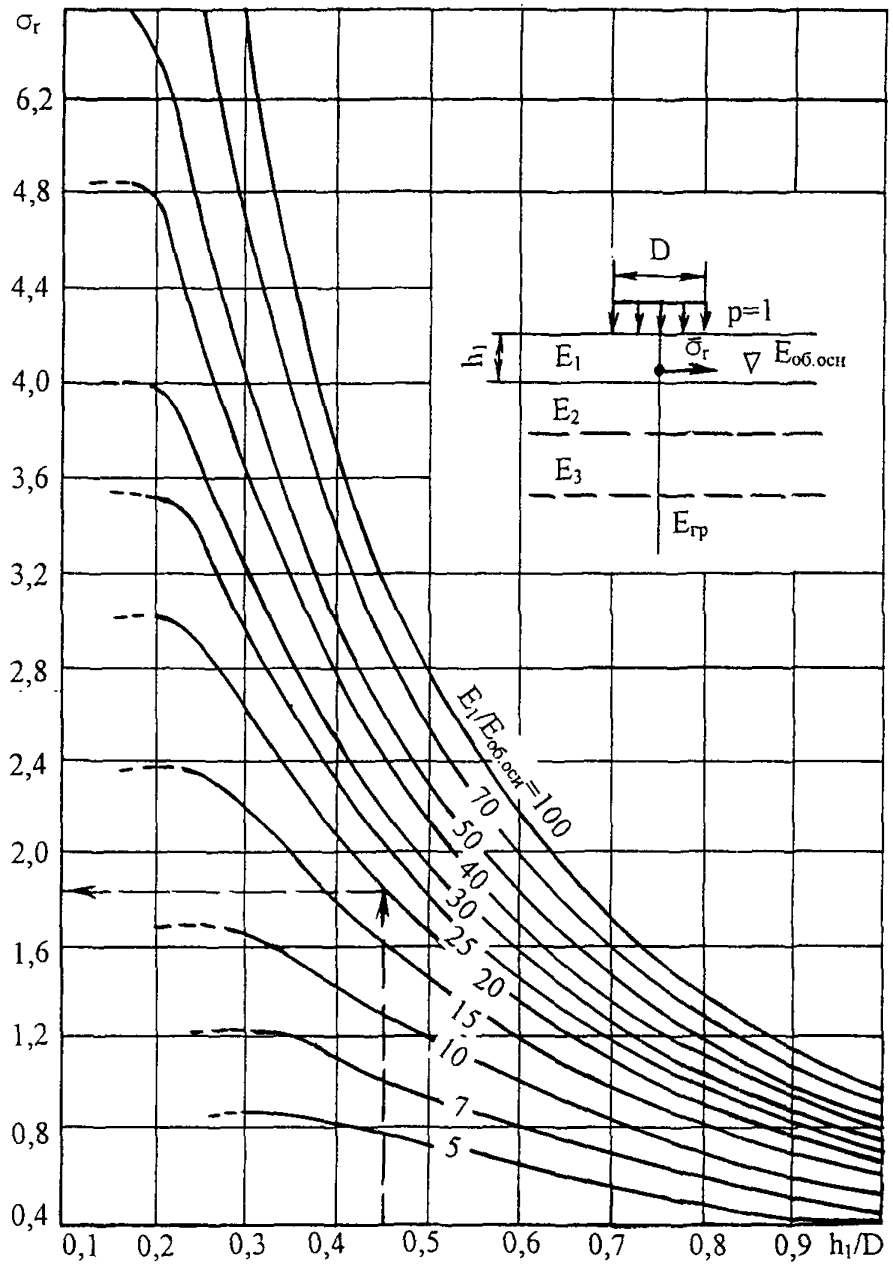

Figure A.3.4: Nomogram for pavement design according to fatigue

The top layer includes all asphalt concrete strata. Its depth h_v is taken equal to the sum of the thicknesses included in the package of asphalt concrete $\sum h_i$.

The value of the modulus of elasticity is set as the weighted average of the monolithic strata.

The model lower (semi-infinite) layer is the part of the structure located below the asphalt concrete system, including the soil of the active layer of the subgrade.
The modulus of elasticity is calculated by determining an equivalent stiffness using the nomogram in **Figure A.3.1**.

3.40. When using the nomogram in **Figure A.3.4**, the design tensile stress is determined by the formula:

$$\sigma_r = \bar{\sigma}_r \cdot p \cdot k_v$$

where $\bar{\sigma}_r$ is the tensile stress from a unit load, determined from the nomogram in **Figure A.3.4**, p is the design pressure, according to *appendix 1*, **Table P.1.1,** and k_v is a coefficient depending on the stress-strain features of the monolithic layer, equal to 0,85.

3.41. The strength of the material of a monolithic layer under repeated stretching in bending is determined by the formula:

$$R_N = R_0 \cdot k_1 \cdot k_2 \cdot (1 - v_R \cdot t)$$

where:

- R_0 is the standard value of the ultimate tensile strength in bending at the design low spring temperature with a single load application, taken according to *appendix 3*, **Table P.3.1;**
- k_1 is a coefficient that takes into account the decrease in strength due to fatigue phenomena with repeated application of the load;
- k_2 is a coefficient that takes into account the decrease in strength over time from the impact of weather and climatic factors (**Table A.3.6**);

Table A.3.6: Suggested values of k_2

Material of the computational layer		$\boldsymbol{k_2}$
Asphalt concrete	*Highly dense*	1
	Dense:	
	I mark	0,95
	II mark	0,9
	III mark	0,8
	Porous and highly porous	0,8
Organomineral mixtures		0,8

- v_R is the coefficient of variation of the tensile strength (see *appendix 4*);
- t is the standard deviation (see *appendix 4*).

3.42. The coefficient k_1, reflecting the effect of fatigue processes on the strength, is calculated by the expression:

$$k_1 = \frac{\alpha}{\sqrt[t]{\sum N_r}}$$

where $\sum N_r$ is the estimated total number of applications of the design load for the service life of the monolithic layer, taking into account the number of design days (see *appendix 6*), t is an exponent depending on the material properties (see *appendix 3*, **Table P.3.1**) and α is a coefficient that takes into account the difference in real and laboratory conditions of stretching by repeated loading, determined from **Table. P.3.1**.

3.43. Fatigue strength calculations are performed in the following order:

- derive to the two-layer structure model and determine the relationship $\frac{h_v}{D}$, $\frac{E_v}{E_{pr}}$;
- according to the obtained parameters, using the nomogram in **Figure A.3.4**, find the value $\bar{\sigma}_r$ and calculate the design tensile stress;

- calculate the ultimate tensile stress. In a package of asphalt concrete layers, the tensile strength R_N is taken as the value corresponding to the material of the lower layer;
- check the condition and adjust the design if necessary.

4. CHECKING THE ROAD STRUCTURE FOR FROST PENETRATION

4.1. In areas of seasonal freezing of the subgrade under unfavorable soil and hydrological conditions, along with the required strength and stability, sufficient frost resistance of road pavements must be ensured.

For this purpose, various special measures are used:

- the use of non-porous or slightly porous soils (**Table A.4.1** and **Table A.4.2**) for the construction of the upper part of the subgrade located in the freezing zone;

Table A.4.1: Classification of soils according to the degree of frost heave during freezing

Soil group by frost heave	Degree of frost heave	Relative frost heave
I	Non-porous	<1
II	Weakly bumpy	From 1 to 4
III	Puffy	From 4 to 7
IV	Heavily puffy	From 7 to 10
V	Overly puffy	>10

Table A.4.2: Soil groups according to the degree of frost heave

Soil	Group
Gravelly, coarse-, or medium-sized sand with particles content finer than 0,05 up to 2%	I
Gravelly, coarse-, medium-, or fine-sized sand with particles content finer than 0,05 up to 15%, light coarse sandy loam	II
Light sandy loam, light and heavy loam, clay	III
Dusty sand, silty sandy loam, heavy silty loam	IV
Heavy silty sandy loam, light silty loam	V

- drainage of the active layer of the subgrade (see *chapter 5*), including the device for increasing the distance from the bottom of the pavement to the groundwater level, waterproofing and capillary interlayers for the transition from the 2nd or 3rd moistening scheme of the active layer of the subgrade to the 1st one;
- a frost-protective layer made of non-porous mineral materials, fortified with small doses of mineral or organic binders;
- arrangement of heat-insulating layers that reduce the depth or completely exclude soil freezing under the road surface;
- installation of a monolithic pavement base (realized with lean concrete or other granular materials treated with a mineral or organic binder).

4.2. The structure is considered frost-resistant if the following condition is met:

$$l_{puc} \leq l_{dop}$$

where l_{puc} is the design (expected) frost heave of the subgrade soil and l_{dop} is the allowed frost heave for a given structure (**Table A.4.3**).

Table A.4.3: Values of the allowed soil frost heave according to the pavement type

Pavement type	**Coating type**	$\boldsymbol{l_{dop}}$ **[cm]**
Capital	*Asphalt concrete*	4
Lightweight	*Asphalt concrete*	6
Transitional	*Transitional*	10

Note: in road-climatic zones II and III, l_{dop} values should be increased by 20-40% (larger values for lightweight and transitional road pavements).

4.3. The calculation for frost resistance must be performed for distinct sections or groups of characteristic sections of the road, similar in soil-hydrological conditions, having the same pavement structure and the moistening scheme of the active layer of the subgrade.

4.4. During a preliminary check for frost resistance, the amount of possible frost heave should be determined by the formula:

$$l_{puc} = l_{puc,sr} \cdot K_{UGV} \cdot K_{pl} \cdot K_{gr} \cdot K_{nagr} \cdot K_{vl}$$

where:

- $l_{puc,sr}$ is the amount of frost heave under averaged conditions, depending on the pavement thickness (including additional layers of the base), the group of soil according to the degree of frost heave (**Table A.4.1**) and the freezing depth z_{pr} (determined from **Figure A.4.4**);
- K_{UGV} is a coefficient that takes into account the influence of the estimated depth of the level of groundwater or long-term standing surface water (h_γ) (**Figure A.4.1**); if the effect is null, the following values should be taken: for heavy silty sandy loam and loam K_{UGV}=0,53, for sand and sandy loam, light and large K_{UGV}=0,43;

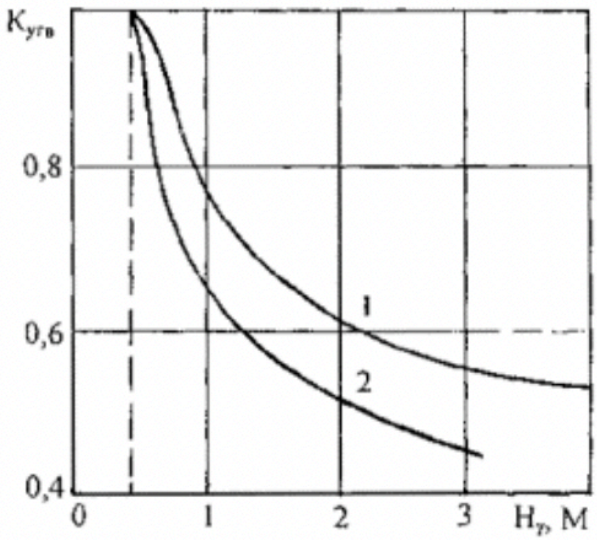

Figure A.4.1: Dependence of the K_{UGV} coefficient on the distance from the bottom of the road pavement to the groundwater level

Note: 1-heavy silty sandy loam, 2-sand, sandy loam.

- K_{pl} is a coefficient depending on the degree of soil compaction of the active layer (**Table A.4.4**);

Table A.4.4: Reference values of K_{pl}

Sealing factor K_{upl}	**K_{pl}**	
	Silty sand, light and silty sandy loam, clay	*Sands other than silty sands, light coarse sandy loam*
1,03-1	0,8	1
1,01-0,98	1	1
0,97-0,95	1,2	1,1
0,94-0,9	1,3	1,2
<0,9	1,5	1,3

- K_{gr} is a coefficient taking into account the influence of the granulometric composition of the soil at the base of the embankment or excavation (**Table A.4.5**);

Table A.4.5: Reference values of K_{gr}

Soil	**K_{gr}**
Sands	1
Sandy loams	1,1
Loams	1,3
Clays	1,5

- K_{nagr} is a coefficient that depends on the freezing depth (**Figure A.4.2**);

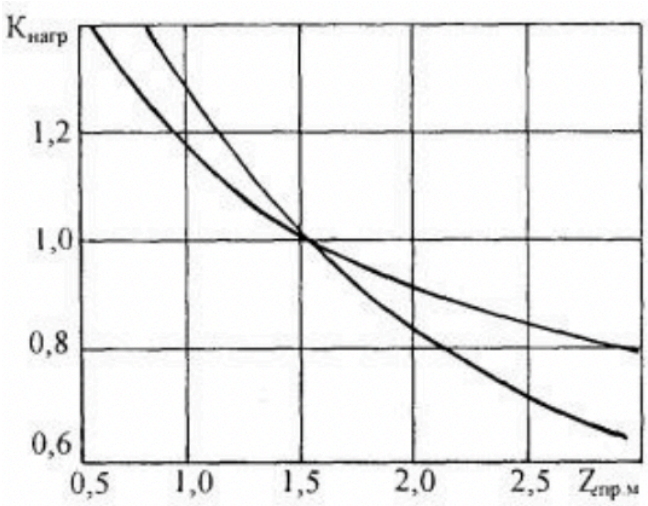

Figure A.4.2: Dependence of the K_{nagr} coefficient on the freezing depth from the surface

Note: 1-heavy silty sandy loam, 2-sand, sandy loam.

- K_{vl} is a coefficient depending on the soil moisture (**Table A.4.6**).

Table A.4.6: Reference values of K_{vl}

Relative humidity W/W_t	*0,6*	*0,7*	*0,8*	*0,9*
$\boldsymbol{K_{vl}}$	1	1,1	1,2	1,3

4.5. If there are no field observations, the freezing depth of the road structure may be determined by the formula:

$$z_{pr} = z_{pr(cp)} \cdot 1{,}38$$

where $z_{pr(cp)}$ is the average freezing depth for a given area, established using contour maps (**Figure A.4.4**).

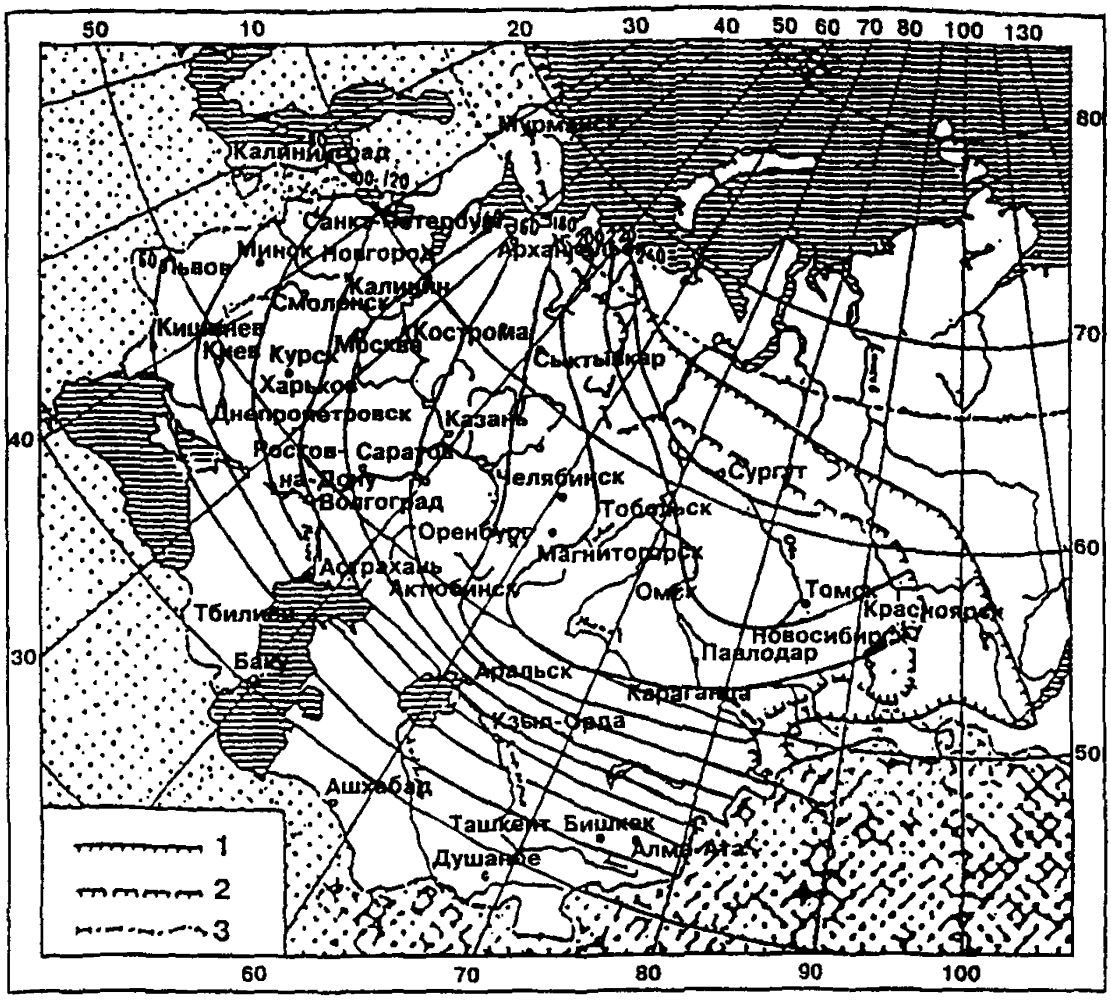

Figure A.4.4: Map of isolines of freezing depth $z_{pr(cp)}$ in the CSI countries

4.6. With a freezing depth of the road structure z_{pr} up to 2 m, $l_{puc,sr}$ is set according to the graphs in **Figure A.4.3**.

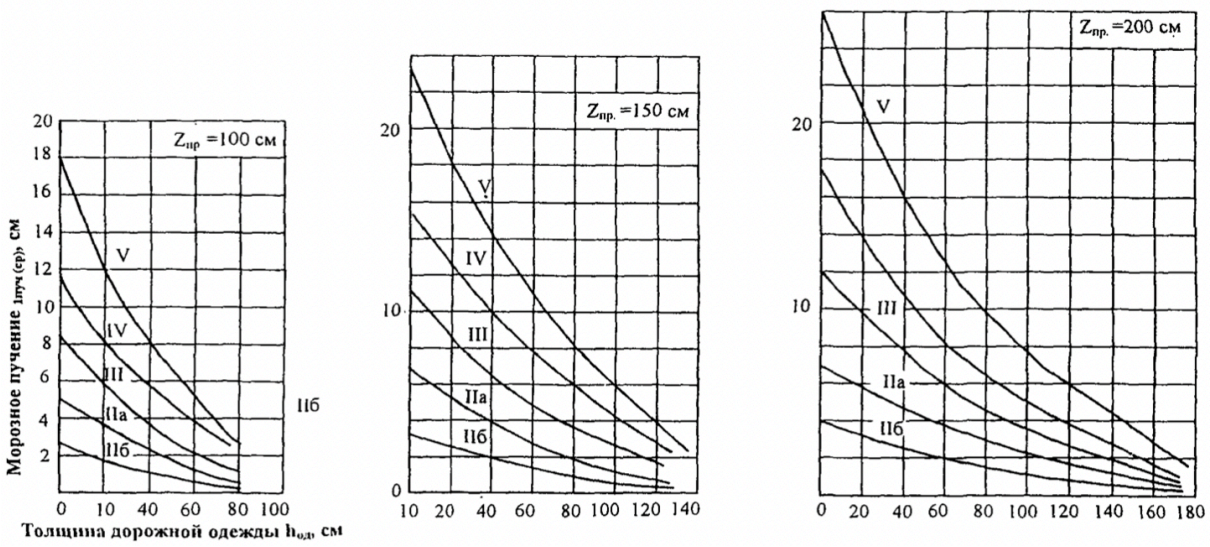

Figure A.4.3: Graphs for determining the average value of frost heave $l_{puc,sr}$

Note:

1. *Curve II to V is selected according to* ***Table A.4.2****.*
2. *Curve IIa is selected for the 2nd and 3rd moistening scheme of the active layer, curve IIb for the 1st.*

When z_{pr} is between 2 and 3 m, $l_{puc,sr}$ is calculated by the formula:

$$l_{puc,sr} = l_{puc,sr2.0} \cdot [a + b \cdot (z_{pr} - c)]$$

where:

- $l_{puc,sr2.0}$ is the amount of frost heave at z_{pr}=2 m;
- a=1, b=0,16 and c=2 if 2<z_{pr}<2,5;
- a=1,08, b=0,08 and c=2,5 if 2,5<z_{pr}<3.

4.7. If, with a design life of up to ten years, the obtained value of possible frost heave will exceed the required one (**Table A.4.3**) and, with a service life of more than ten years, it will exceed 80% of its value, it is necessary to consider the option of a frost-protective layer. In this case, the roughly required thickness of the frost-resistant pavement structure is preliminarily determined using the graphs in **Figure A.4.3**. To do this, knowing the permissible value of frost heave l_{dop}, calculate the average value of frost heave $l_{puc,sr}$ by the formula:

$$l_{puc,sr} = \frac{l_{dop}}{K_{UGV} \cdot K_{pl} \cdot K_{gr} \cdot K_{load} \cdot K_{vl}}$$

Then, according to the graph in **Figure A.4.3,** depending on the soil group and the degree of frost heave, h_{od} is determined.

4.8. A refined calculation of the thickness of the frost-protective layer (h_{mz}) is performed according to the thermal resistance of the structure. To do this, the following initial data are necessary:

- the geographic location of the road section under consideration;
- the structure of the pavement (material and thickness of the layers), required for the conditions of strength and drainage;
- moistening scheme of the active layer of the subgrade (1st, 2nd or 3rd) and the estimated groundwater depth from the pavement surface;
- the type of the subgrade soil;
- the estimated service life of the pavement.

4.9. The thickness of the frost-protective layer h_{mz} is determined by the formula:

$$h_{mz} = (R_{od(tr)} - R_{od(o)}) \cdot \lambda_{mz}$$

where:

- $R_{od(tr)}$ is the thermal resistance of the structure required under the given conditions;
- $R_{od(o)}$ the thermal resistance of the considered pavement;
- λ_{mz} is the thermal conductivity coefficient of the frost-protective layer, equal to the mean of the values in the thawed and frozen states.

In the absence of measured data, it is allowed to include tabular values of λ_{mz} in the calculation (**Table P.5.1**).

$R_{od(tr)}$ is determined depending on the number of isolines on the map (**Figure A.4.5**), corresponding to the geographical position of the considered section of the road. When the site is located between the isolines, two values of $R_{od(tr)}$ are determined and two values of h_{mz} corresponding to these lines are calculated. The required thickness of the frost-protective layer is determined by the interpolation method depending on the distance from the considered road section to the neighboring isolines.

Figure A.4.5: Map with contour lines to determine the required values of thermal resistance of pavement

4.10. The theoretical resistance of the road pavement $R_{od(o)}$ is calculated by the formula:

$$R_{od(o)} = \sum_{i=1}^{n_{od}} \frac{h_{od(i)}}{\lambda_{od(i)}}$$

where n_{od} is the number of structural layers of the pavement without a frost-protective layer, $h_{od(i)}$ is the thickness of the i[th] stratum and $\lambda_{od(i)}$ is the coefficient of thermal conductivity of individual layers in the frozen state.

4.11. The value of the required thermal resistance $R_{od(tr)}$ is calculated by the formula:

$$R_{od(tr)} = R_{pr} \cdot K_{od} \cdot K_{uvl} \cdot \delta$$

where:

- R_{pr} is the reduced thermal resistance, determined using a nomogram (see *point 4.12*);
- K_{od} is a coefficient taking into account the service life of the pavement between major repairs (**Table A.4.7**);

Table A.4.7: Reference values for K_{od}

Contour line on the map (Figure A.4.5)	**K_{od} depending on the time between major repairs**		
	<10 years	*10 years*	*20 years*
I-II	0,7	0,85	1
III-X	0,8	0,9	1

- K_{uvl} is a coefficient that takes into account the moistening scheme of the active layer of the subgrade, taken for the 2[nd] and 3[rd] type equal to 1 and with the 1[st] one according to **Table A.4.8**;

Table A.4.8: Reference values for K_{uvl}

Contour line on the map (Figure A.4.5)	**K_{uvl}**
I	0,8

II	0,65
III	0,55
IV	0,45
V	0,4
VI	0,35
VII	0,3
VIII	0,3
IX	0,25
X	0,25

- δ is a reduction factor, taken for road-climatic sub-zones II_1, II_3 and II_5 equal to 1, for sub-zones II_2, II_4 and II_6 equal to 0,95, for RCZ III equal to 0,9 and for RCZ IV equal to 0,85 (see *appendix 2*).

4.12. R_{pr} is determined using the nomogram (**Figure A.4.6**) by the iteration method through the ratio $\frac{l_{dop}}{C_{puc} \cdot C_r}$ (horizontal axis of the graph). The values of l_{dop}, C_{puc} and C_r are determined, respectively, according to the **Table A.4.3**, **Table A.4.9** and **Table A.4.10**.

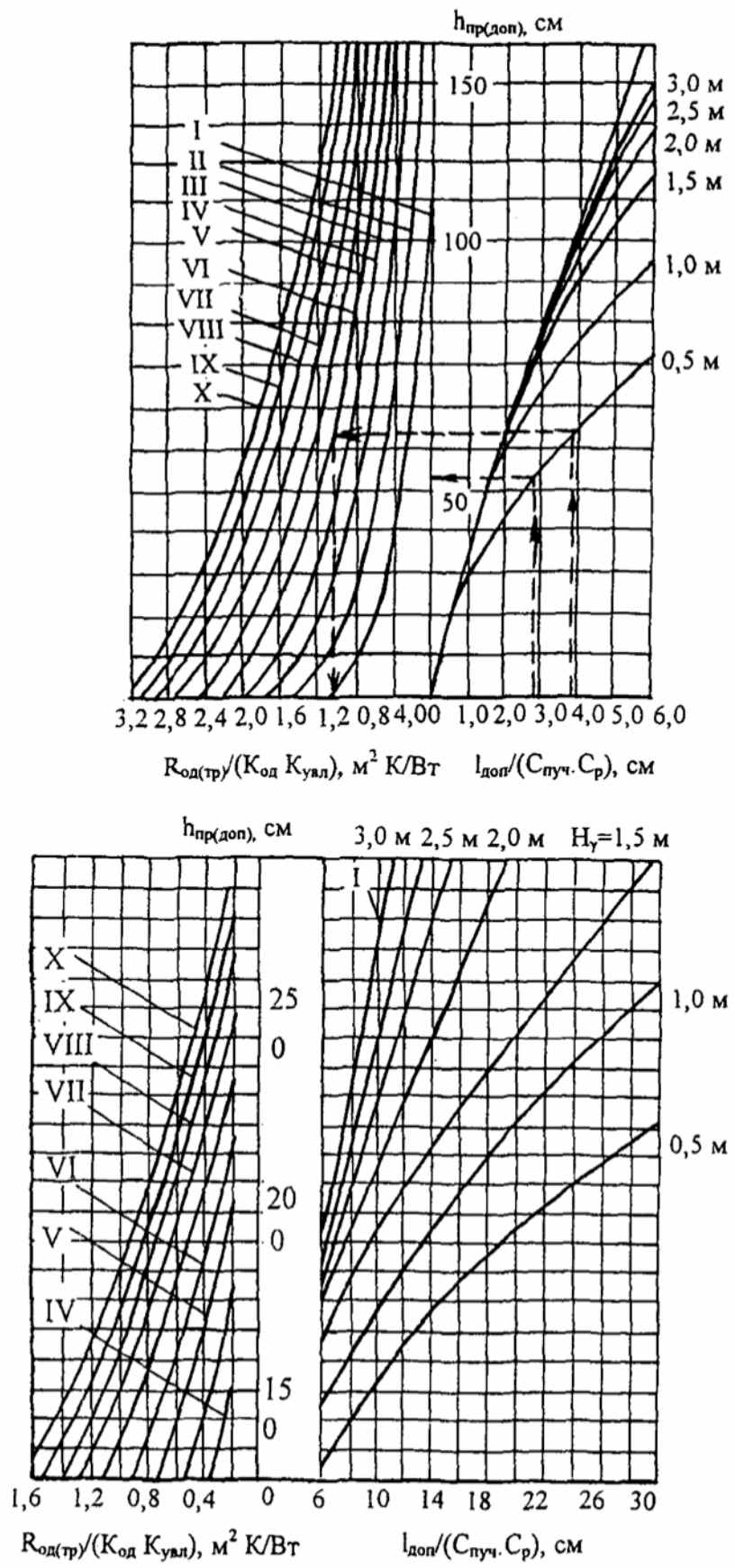

Figure A.4.6: Nomogram for determining the required thermal resistance $R_{od(tr)}$ of the pavement

Note:

1. *I-X: number of isolines on the map (**Figure A.4.5**).*
2. *The first chart is used in calculations for the 1st and 2nd moistening scheme of the active layer of the subgrade.*
3. *H_γ is the groundwater level depth from the bottom of the pavement, including frost-protective layers.*

Table A.4.9: Reference values of C_{puc}

Contour line on the map (Figure 4.5)	C_{puc}			
	Weakly bumpy	*Puffy*	*Heavily puffy*	*Overly puffy*
I	0,7	1,4	2,1	2,8
II	0,6	1,25	1,85	2,5
III	0,55	1,1	1,65	2,2
IV	0,5	1	1,5	2
V	0,45	0,9	1,35	1,8
VI	0,4	0,8	1,2	1,6
VII	0,35	0,7	1,05	1,4
VIII	0,3	0,6	0,9	1,2
IX	0,25	0,5	0,75	1
X	0,2	0,4	0,6	0,8

*Note: the soil group according to the degree of frost heave is determined through **Table A.4.1** and **Table A.4.2**.*

Table A.4.10: Reference values of C_r

Subgrade soil	**C_r depending on the pavement thickness h_{od} [m] and the permissible freezing depth $h_{pr(dop)}$ [cm]**								
	h_{od}=0,5			h_{od}=1		h_{od}=1,5		h_{od}=2	
	$h_{pr(dop)}$			$h_{pr(dop)}$		$h_{pr(dop)}$		$h_{pr(dop)}$	
	0-50	51-100	>100	0-100	>100	0-100	>100	0-100	>100

Dusty sand	0,6	0,55	0,5	0,5	0,45	0,45	0,4	0,4	0,35
Light sandy loam	0,7	0,65	0,6	0,6	0,55	0,55	0,5	0,5	0,45
Silt sandy loam	0,75	0,7	0,65	0,65	0,6	0,6	0,55	0,55	0,5
Light loam, light silty loam	0,8	0,75	0,7	0,7	0,65	0,65	0,6	0,6	0,55
Heavy loam, heavy silty loam, clay	0,85	0,8	0,75	0,75	0,7	0,7	0,65	0,65	0,6

Note: at intermediate values of the pavement thickness, C_r should be taken by interpolation of the corresponding values.

When assigning the value of C_r according to **Table A.4.10**, select the permissible freezing depth $h_{pr(dop)}$ in such a way that the obtained value of the ratio $\frac{l_{dop}}{C_{puc} \cdot C_r}$ corresponds to the $h_{pr(dop)}$ on the vertical axis of the nomogram, equal to that adopted in determining C_r. The selection must begin with the value of $h_{pr(dop)}$ corresponding to the smallest permissible freezing depth.

The distance H_γ from the bottom of the pavement to the groundwater level, necessary for using the nomogram, is determined by taking as initial value, obtained in accordance with *point 4.6*, the approximate thickness of the frost-protective layer h_{mz} and calculating the total thickness of the pavement h_{od} for a given h_{mz}.

When the groundwater depth on the road section differs from those indicated on the nomogram, two values of R_{pr} must be determined: one when the value of H_γ on the nomogram is greater and the other when the value of H_γ on the nomogram is less than this one. The desired value of R_{pr} is set by interpolation between the corresponding values.

4.13. After completing the calculation of the thickness of the frost-protective layer, the obtained value of h_{mz} is compared with the previously assigned value h_{mz}. The difference should not be more than 5 cm; otherwise, the calculation must be repeated.

4.14. The calculation of the thickness of the insulating layer is carried out in the same way as for the frost protection. The analysis should include the thickness of the pavement required for the conditions to ensure strength and drainage, as well as the values of the soil frost heave index C_{puc} (**Table A.4.11**); the thickness of the insulating layer should be determined according to the graph (**Figure A.4.7**) depending on $R_{od(tr)}$ and $R_{od(o)}$.

Table A.4.11: Reference values of C_{puc}

C_{puc}			
Weakly bumpy	*Puffy*	*Heavily puffy*	*Overly puffy*
0,5	1	1,5	2

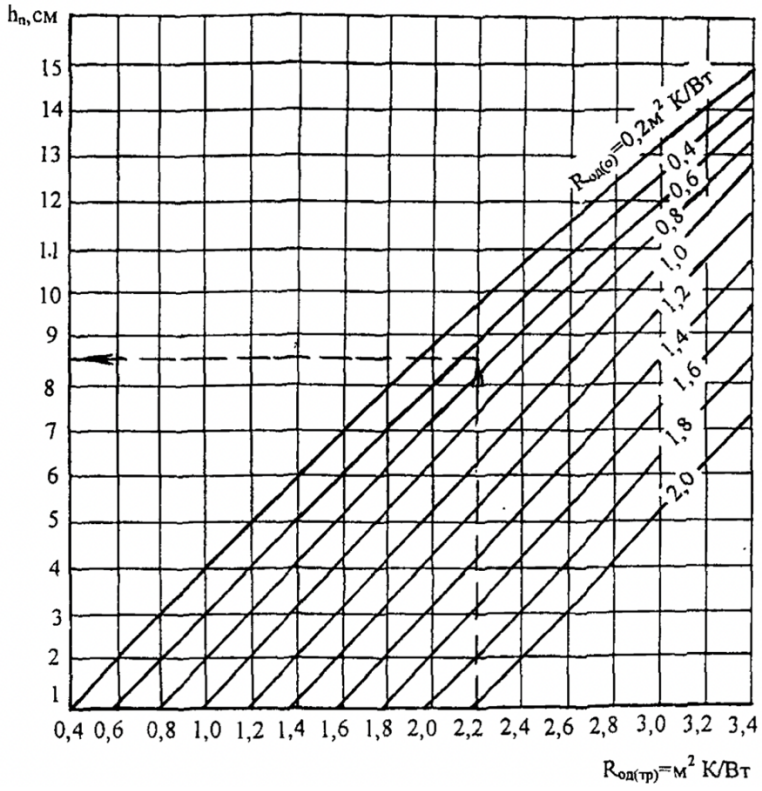

Figure A.4.7: Chart for determining the required thickness of the foam insulating layer

4.15. The foam used for the construction of the heat-insulating layer must meet the following requirements: compressive strength at 10% linear deformation of at least 0,4 MPa, ultimate strength in bending of at least 0,7 MPa, water absorption by volume no more than 0,45, thermal conductivity no more than 0,032 W/(m·K) (with test methods according to the current GOST). The choice of the correct grade of foam should be carried out taking into account the pilot test results on roads.

4.16. If the active layer of the subgrade includes two layers of soils with different frost heave, the thickness of the frost-protective layer at the top of the active layer should be calculated from the equation:

$$h_{mz} = h_{mz1} + \frac{(h_{mz2} - h_{mz1}) \cdot (h_{mz1} + h_{pr(dop)} - \Delta\vartheta_{gr})}{h_{mz1} + h_{pr(dop)}}$$

where:

- h_{mz1} is the thickness of the frost protective layer necessary in the case of complete replacement of the local soils with a less heaving one;
- h_{mz2} is the thickness of the frost protective layer necessary for the case of a single-layer subgrade from local soil;
- $h_{pr(dop)}$ is the permissible freezing depth of the subgrade in the case of complete replacement of local soil with a less heaving one;
- $\Delta\vartheta_{gr}$ is the thickness of the replaced layer from the bottom of the pavement (without a frost protective layer).

The calculation of h_{mz1}, h_{mz2} and $h_{pr(dop)}$ is carried out according to *point 4.9* to *point 4.13*. The maximum value of $\Delta\vartheta_{gr}$ is equal to $h_{mz1} + h_{pr(dop)}$.
The calculation of the thickness of the heat-insulating layer when replacing the upper layer of the subgrade with less heaving soil should be carried out in the same way as for the frost-protective layer.

4.17. To determine the amount of frost heave, a technique based on determining the coefficient of soil moisture conductivity K_{vl} can also be used.

5. PAVEMENT DESIGN FOR DRAINAGE

5.1. A drainage structure (drainage layer and drainage devices) is necessary for traditional road pavements with layers of granular materials in areas with weakly filtering soils (dusty sands, non-dusty sands with a filtration coefficient less than 0,5 m/day and clayey soils) in road-climatic zone II with all moistening schemes of the active layer of the subgrade, in RCZ III with the 2nd and 3rd schemes and in RCZ IV and V with only the 3rd scheme (**Table A.5.1**).

Table A.5.1: Moistening schemes

Subgrade active layer moistening scheme	**Moisture sources**	**Conditions**
1-Dry	Precipitations	For embankments in areas of the 1st type of soil moisture conditions. For embankments in areas of the 2nd and 3rd type of soil moisture conditions when the pavement surface rises above the level of water or earth surface more than 1,5 times the value specified in **Table A.5.2**. For embankments in areas of the 2nd type with a distance from the edge of the surface water (absent for at least 2/3 of the summer period) greater than 5-10 m for sandy loams, 2-5 m for light silty loams and 2 m for heavy silty loams and clays (lower values should be taken for soils

		with a large plasticity index); when various soils are deposited, take the larger values. In cuts in sandy and clayey soils with ditch slopes greater than 20‰ (in RCZ I-III) and when the pavement surface rises above the groundwater level more than 1,5 times the value specified in **Table A.5.2**. When using special methods for regulating the thermal water regime (capillary-interrupting, waterproofing, heat-insulating and reinforcing layers, drainage, etc.) assigned according to special calculations.
2-Damp places with excessive moisture in certain periods of the year	Short-term (up to 30 days) water surface, precipitations	For embankments in areas of the 2nd type of soil moisture conditions with a pavement elevation not less than that required according to **Table A.5.2** and not greater than two times these values, with a steepness slope of at least 1:1,5 and a simple (without berms) transverse profile. For embankments in areas of the 3rd type of soil moisture conditions with the use of special measures to protect against groundwater (capillary-interrupting layers, drainage), assigned according to special calculations, in the absence of long-term (more than 30 days) standing water surface. In cuts in sandy and clayey soils with ditch slopes less than 20‰ (in RCZ I-II) and when the

		pavement surface rises above the groundwater level more than 1,5 times the value specified in **Table A.5.2**.
3-Wet places with constant excessive moisture	Ground or long-term (more than 30 days) standing water surface, precipitations	For embankments in areas of the 3rd type of soil moisture conditions with a pavement elevation not less than that required according to **Table A.5.2** and not greater than 1,5 times these values. The same for excavations, at the base of which a groundwater surface is present, the location of which in depth does not exceed the requirements of **Table A.5.2** for more than 1,5 times.

Table A.5.2: Pavement surface rise

Active layer soil	**Smallest elevation of the pavement surface according to the road-climatic zone [m]**			
	II	*III*	*IV*	*V*
Fine sand, light coarse sandy loam, light sandy loam	1,1/0,9	0,9/0,7	0,75/0,55	0,5/0,3
Silty sand, silty sandy loam	1,5/1,2	1,2/1	1,1/0,8	0,8/1,5
Light loam, heavy loam, clay	2,2/1,6	1,8/1,4	1,5/1,1	1,1/0,8
Heavy silty loam, light silty loam	2,4/1,8	2,1/1,5	1,8/1,3	1,2/0,8

Note: the first number indicates the elevation of the pavement surface above the groundwater level or long-term (more than 30 days) standing water surface, while the second number indicates the elevation above the earth surface in areas with unsecured runoffs or short-term (less than 30 days) standing water surface.

5.2. The moistening scheme on the road sections where water stagnates in the roadside lane is determined taking into account the distance l_y from the edge of the roadbed to the water edge stagnating on the roadside in autumn. The value of the safety distance l_y can be determined using a special method. In the absence of actual data necessary for

the calculation, l_y should be taken for sandy loams equal to 10 m, for light and silty loams equal 3 m and for heavy loams and clays equal to 2 m.

5.3. The pavement drainage system includes planar horizontal drainage supplemented, if required, by edge, as well as shallow transverse drainage.
When installing all layers of road pavement made of monolithic materials, it is allowed to use, instead of a drainage stratum, a geotextile layer with a thickness of at least 4 mm and a filtration coefficient of at least 50 m/day as planar horizontal drainage, with an appropriate feasibility study, with the release of panels on the slopes of the embankment to a height not less than 0,5 m. The choice of geotextiles, in this case, is made according to special instructions.

5.4. The design of measures for the drainage of pavement is carried out in the following sequence:

- the road is divided into typical sections according to the type of longitudinal profile and natural conditions (the nature of the terrain, the presence of watercourses crossing the road, etc.), taking into account the design features of the subgrade (embankment with a height corresponding to SNiP, excavation, embankment below the required SNiP, transitional section from embankment to excavation) and pavement (the presence of monolithic base layers, as well as frost-protective or heat-insulating layers of reinforced materials), provision of materials for the drainage layer, drainage pipes and geotextiles; implementation of measures to limit the flow of water into the road structure;
- for typical sections, the amount of water entering the base per day and for the billing period is determined, taking into account the measures provided to limit the flow of water into the road structure;
- outline options for drainage structures;
- justify the calculation of the thickness of the drainage layer required under these conditions or determine what value of the filtration coefficient the drainage material should have in a given drainage structure.

When designing a drainage layer, in addition to drainage, it is necessary to take into account the need to ensure the shear stability of the granular material itself and the strength of the entire road structure.

5.5. The drainage structure must be designed to take into account the volume of water inflow entering the pavement base during the design period, the filtration capacity of the material of the drainage layer and the structure of the subgrade.

5.6. A feasibility study of the options should accompany the choice of each specific inflow control measure.

Combined flat horizontal drainage is a universal measure for most road sections.

Shallow transverse drainage is arranged for transverse interception of water moving in the drainage layer along the road, in areas with a longitudinal slope of more than 20‰, also with prolonged longitudinal slopes exceeding the transverse ones, in places of concave vertical curves and in places where longitudinal slopes decrease.

5.7. The drainage layer which works on the principle of drainage must be made of sandy soils or a highly permeable skeletal mixture (crushed stone or gravel) of an open type (with unfilled voids) that meet specific requirements for water permeability and lay this layer under the pavement over its entire width. In this case, it is necessary to provide outlets of the drainage layer to the slope. The drainage layer is also arranged with drainage pipes to collect and quickly drain water outside the subgrade. Anti-silt protection of drains and drainage layers, as well as prevention of freezing of water in pipe outlets, should be provided.

When arranging drainage layers operating on the principle of absorption, it is required to arrange more thick layers of sandy soil and take into account its strength characteristics, considering an unfavorable design state.

5.8. For a drainage layer device operating on the dehumidification principle, materials with a filtration coefficient of at least 1 m^3/day should be used. It is advisable to use a

material with a filtration coefficient of 1-2 m/day in areas where it simultaneously performs drainage and frost protection functions.

CONSTRUCTION OF THE DRAINAGE LAYER

5.9. The drainage design aims to determine the drainage layer required thickness from discrete materials.

Two design stages are taken into account when designing the drainage of road pavements in areas of seasonal freezing of soils. The first refers to the period when the pavement base under the middle of the carriageway has already thawed, the drainage layer at its edges is still frozen and drainage devices do not work.

The second calculation stage refers to the time when the drainage layer has completely thawed and the drainage devices begin to work normally.

5.10. Depending on the specific conditions, the drainage structure can be designed for one of three operation options:

- work on drainage;
- work on drainage with a period of delay in water drainage;
- work on absorption;

5.11. The total thickness of the drainage layer is determined by the formula:

$$h_p = h_{nas} + h_{zap}$$

where h_{nas} is the thickness of the layer completely saturated with water and h_{zap} is the additional layer thickness, depending on the capillary properties of the material and equal for sands of large size to 0,1-0,12 m, average size to 0,14-0,15 m and fine size to 0,18-0,2 m. In all cases, the total thickness of the drainage layer should be taken at least 0,2 m.

5.12. For a drainage layer operating on the principle of drainage, the value of h_{nas} is set using the nomograms in **Figure A.5.1** and **Figure A.5.2** depending on the length of the filtration path L and the design value of water inflow into the drainage layer per 1 m² q_r [m³/m²], determined by the formula:

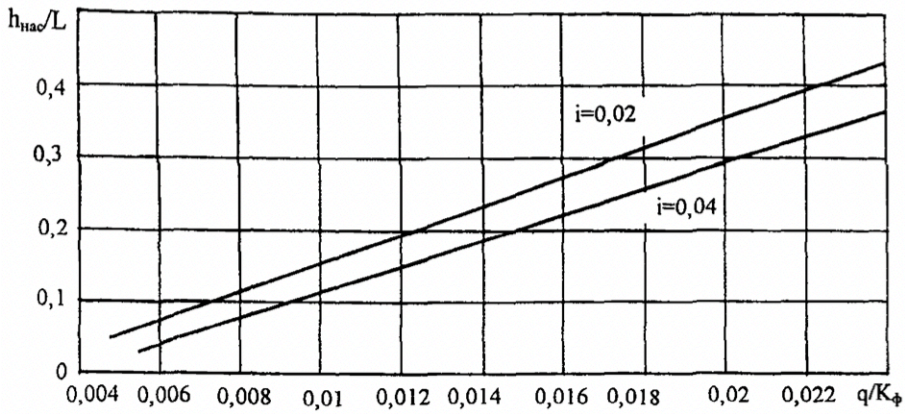

Figure A.5.1: Nomogram for calculating the thickness h_{nas} of the drainage layer for small, medium and coarse-sized sands with a filtration coefficient lower than 10 m/day

Note: with a single slope transverse profile $q' = q_r \cdot B$ [m³/m], with a gable cross-section $q' = 0{,}5 \cdot q_r \cdot B$ [m³/m]; B [m] is the carriageway width and L is the length of the filtration path, equal to B with a single-slope profile and to B/2 for a dual-slope.

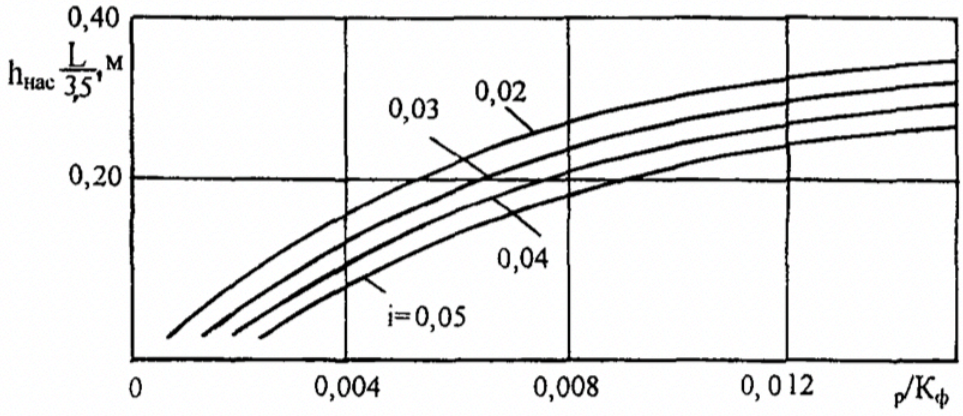

Figure A.5.2: Nomogram for calculating the thickness h_{nas} of the drainage layer for coarse sands with a filtration coefficient greater than 10 m/day

Note: L is the length of the filtration path, equal to B with a single-slope profile and to B/2 for a dual-slope, i is the transverse slope of the bottom of the drainage layer and K_ϕ [m/day] is the filtration coefficient.

$$q_r = \frac{q \cdot K_p \cdot K_g \cdot K_{vog}}{1000}$$

where:

- q [m³/m²] is the averaged (tabular) value of water inflow into the drainage layer with a traditional pavement design, referred to 1 m² of the carriageway (**Table A.5.3**);

Table A.5.3: Suggested values of water inflow

Road-climatic zone	**Subgrade active layer moistening scheme**	**Volume of water entering the base of the pavement**			
		Light sandy loam and silty sand	***Loam and clay***	***Silty loam***	***Sandy loam***
II	*1*	15/2,5	20/2	35/3	80/3,5
	2	25/3	50/3	80/4	130/4,5
	3	60/3,5	90/4	130/4,5	180/5
III	*1*	10/1,5	10/1,5	15/2	30/3
	2	15/2	25/2	30/2,5	40/3
	3	25/2,5	40/2,5	50/3,5	60/4
IV and V	*3*	20/2	20/2	30/2,5	40/3

Note:

1. *The numerator gives the total volume of water Q [L/m²] entering the base for the entire calculation period, per day in the denominator (q). For embankments constructed from non-dusty soils, with a height greater than the one specified in* ***Table A.5.2****, in road-climatic zone II, it is assumed q=1,5 L/(m²·day).*
2. *In the presence of a dividing strip for sections passing at zero marks, embankments with a height higher than the one specified in* ***Table A.5.2****, in road-climatic zone II, the values of q are increased by 20%.*

- K_p is the peak coefficient, taking into account the unsteady regime of water intake due to uneven thawing and precipitation (**Table A.5.4**);

Table A.5.4: Suggested values of K_p

Road climatic zone	**Moistening scheme**	**K_p for non-dusty soils**	**Dusty soils**	
			K_p	**K_g**
II	*1*	1,5	1,5	1/1
	2	1,5	1,6	1,2/1,2
	3	1,6	1,7	1,3/1,2
III	*1*	1,4	1,5	1/1
	2	1,4	1,5	1,1/1
	3	1,5	1,6	1,2/1,1
III and IV	*3*	1,5	1,3	1,1/1

Notes:

1. *For non-dusty soils K_g=1.*
2. *The numerator indicates the value for roads of the I and II category, the denominator for category II and IV.*

- K_g is the coefficient of hydrological reserve, taking into account the decrease in the filtration capacity of the drainage layer during the operation of the road (**Table A.5.4**);
- K_{vog} is a coefficient that takes into account the accumulation of water in places where the longitudinal slope changes, determined with the same direction of the profile sections at the fracture according to the nomogram in **Figure A.5.3;**

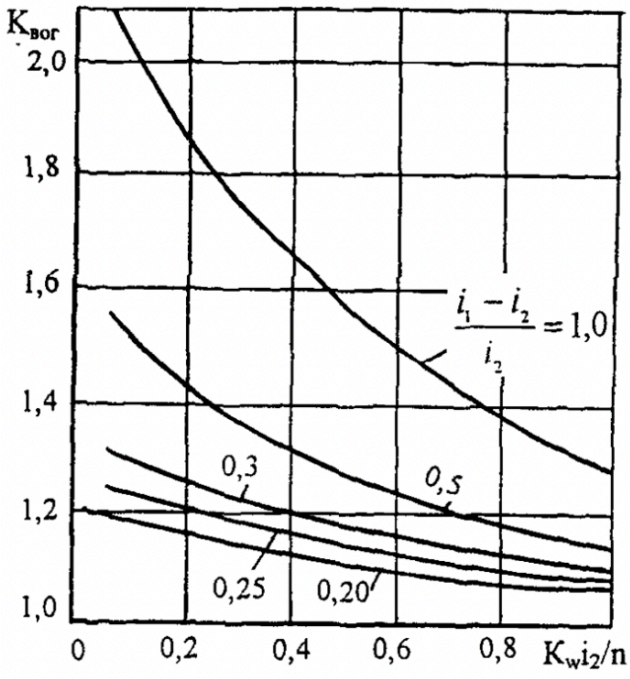

Figure A.5.3: Nomogram for the determination of K_{vog}

Note: i_1 and i_2 are the longitudinal slopes above and below the profile break, K_ϕ [m/day] is the filtration coefficient and n is the porosity coefficient of the drainage layer.

- K_p is a coefficient that takes into account the decrease in water inflow when special measures are taken to regulate the water-thermal regime (**Table A.5.5**);

Table A.5.5: Tabular values of K_p

Event	**Road-climatic zone**	**Soil**		
		Sandy loam	***Light loam***	***Heavy loam, clay***
Strengthening of shoulders in the 1st moistening condition	II	0,45	0,3	0,15
	III	0,4	-	-
	IV	0,35	-	-
Monolithic base layers with material porosity up to 5%	I, II, III	0,1	0,1	0,1

5.13. The total thickness of the drainage layer, operating on the absorption principle, is determined by the formula:

$$h_p = \frac{\frac{Q}{1000 \cdot n} + 0{,}3 \cdot h_{zap}}{1 - \varphi_{zim}}$$

where Q [L/m²] is the estimated amount of water accumulating in the drainage layer for the entire calculation period (**Table A.5.3**), φ_{zim} is the coefficient of filling of pores with moisture in the material of the drainage layer by the beginning of thawing (**Table A.5.6**) and n is the porosity of the material, in fractions of a unit.

Table A.5.6: Suggested values of φ_{zim}

Drainage layer thickness [cm]	**φ_{zim} in II road-climatic zone depending on the porosity**			
	0,4	*0,36*	*0,32*	*0,28*
<20	0,4	0,5	0,6	0,7
Between 20 and 40	0,35	0,4	0,5	0,6
>40	0,3	0,35	0,45	0,55

Note: in road-climatic zone III, φ_{zim} values should be reduced by 20%.

5.14. The drainage layer in a structure with edge drainage, which enhances the process of water movement in fine and medium-sized sand, is calculated using nomograms (**Figure A.5.4**).

According to nomograms in **Figure A.5.1**, **Figure A.5.2** and **Figure A.5.4**, it is also possible to determine the required values of the filtration coefficient of the drainage layer with other known parameters of the drainage structure.

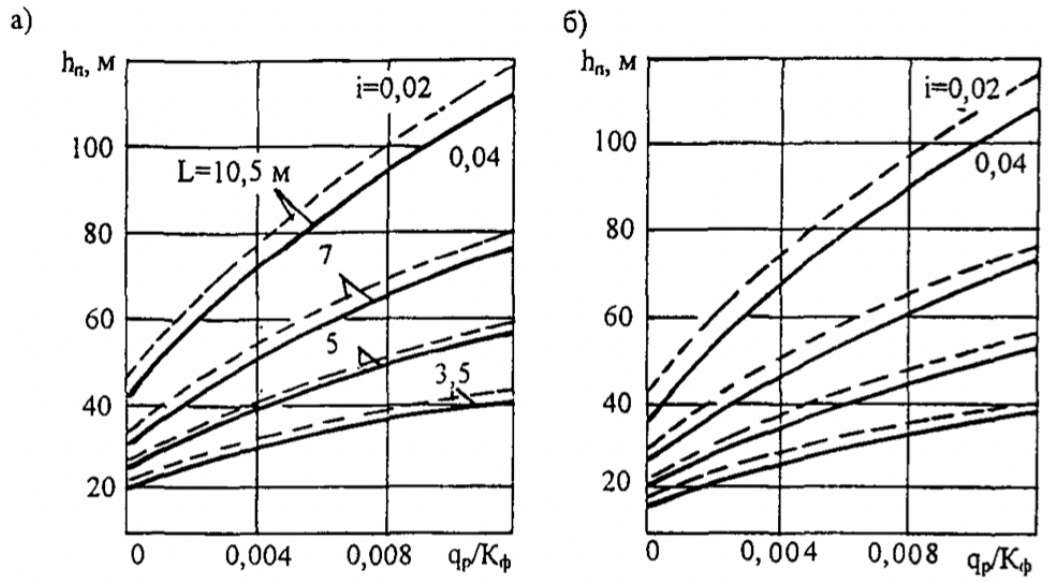

Figure A.5.4: Nomograms for the evaluation of the thickness of the drainage layer working with the edge draining principle

Note: a-fine sands, b-medium sands.

5.15. The total thickness of the drainage layer h_p [m], operating on the principle of drainage with a lag period for water drainage, sufficient for temporary placement in its pores of water entering the structure during the initial period of its thawing, is determined by the formula:

$$h_p = \frac{\frac{q_r \cdot T_{zap}}{n} + 0{,}3 \cdot h_{zap}}{1 - \varphi_{zim}}$$

where T_{zap} is the average duration of the delay in the start of operation of drainage devices, taken for road-climatic zone II equal to 4-6 days and for road-climatic zone III equal to 3-4 days (the greater value is for fine sands), φ_{zim} is the coefficient of filling the pores with moisture in the material of the drainage layer by the beginning of thawing (**Table A.5.6**) and q_r is the design value of water supplied per day.

5.16. In areas where the length of the filtration path is L>10 m, the drainage layer must be designed to absorb the entire amount of water supplied over the entire design period.

The length of the filtration path is taken to be half the width of the drainage layer with a gable transverse profile and the entire width of the drainage layer with a pitched one.

APPENDIX 1: DESIGN LOADS

P.1.1. When designing pavements, loads corresponding to the maximum axle load of the design two-axle vehicle are taken as the reference ones.

If the design load is not specified in the design assignment, values are taken from **Table P.1.1**.

Table P.1.1: Reference values of the design load

Design load group	**Standard static axle load [kN]**	**Standard static load on the pavement surface from the wheel of the design vehicle Q_{rasc} [kN]**	**Design load parameters**	
			p [MPa]	**D [cm]***
A1	100	50	0,6	37/33
A2	110	55	0,6	39/34
A3	130	65	0,6	42/37

**numerator: moving wheel; denominator: stationary wheel.*

P.1.2. Data on the loads transmitted to the road surface by serially produced vehicles should be taken according to special reference books.

P.1.3. The total reduction coefficient $S_{t,sum}$ is given in the following equation:

$$S_{t,sum} = \sum_{1}^{n} S_n$$

where:

- n is the number of axles in a given vehicle;
- S_n is a coefficient to bring the nominal dynamic load from the wheel of each of the n axles of the vehicle to the design dynamic load.

P.1.4. The load reduction factors S_n are determined by the formula:

$$S_n = \left(\frac{Q_{dn}}{Q_{drasc}}\right)^{\beta}$$

where:

- Q_{dn} is the nominal dynamic load from the wheel to the pavement surface;
- Q_{drasc} is the design dynamic load from the wheel to the pavement surface;
- β is a coefficient taken equal to 4,4 for capital, 3 for lightweight and 2 for transitional pavements.

P.1.5. Q_{dn} is determined from the following equation:

$$Q_{dn} = K_{din} \cdot Q_n$$

where K_{din} is the dynamic coefficient, equal to 1,3, and Q_n is the nominal static load on a wheel of the given axle.
When determining the design value of the nominal static load for multi-axle vehicles, the actual nominal wheel load should be multiplied by the coefficient K_s, determined the following equation:

$$K_s = a - v \cdot \sqrt{b_t - c}$$

where b_t is the distance in meters between the extreme axles of the vehicle and a, v and c are determined from **Table P.1.2**.

Table P.1.2: Reference values of the coefficients a, v and c

Trucks	$\boldsymbol{a}$	$\boldsymbol{v}$	$\boldsymbol{c}$
Biaxial	1,7/1,52	0,43/0,36	0,5/0,5
Triaxial	2/1,6	0,46/0,28	1/1

Note: the value in the numerator is for capital and lightweight pavements; the value in the denominator is for transitional pavements.

P.1.6. The total reduction factor is determined in the following sequence:

- designate the design load and determine its parameters Q_{rasc}, p and D;
- for each vehicle type of the prospective traffic, the value of the nominal static load on the wheel for all vehicle axes Q_n is determined;
- by multiplying the obtained values of Q_n and the design load Q_{rasc} by the dynamic coefficient, find the nominal dynamic loads Q_{dn} from the wheel of each axle and the design dynamic load Q_{drasc};
- calculate the S_n factors to bring the nominal load from the wheel of each of the axles to the design one;
- calculate $S_{t,sum}$ to bring the load from the considered type of vehicle to the design value.

P.1.7. It is allowed to approximately take the total reduction coefficient $S_{t,sum}$ according to **Table P.1.3**.

Table P.1.3: Reference values of $S_{t,sum}$ for different types of vehicles

Vehicle type	$\boldsymbol{S_{t,sum}}$
Passenger cars, light trucks (vans) and other vehicles with or without a trailer	0,0015
Two-axle trucks	1,51
Three-axle trucks	2,33
Four-axle trucks	2,56
Four-axle road trains	2,54
Five-axle road trains	2,13
Three-axle truck trains	2,38
Four-axle truck trains	2,96
Five-axle truck trains (two-axle tractors)	2,83
Five-axle truck trains (three-axle tractors)	3,01

Six-axle truck trains	2,12
Vehicles with seven or more axles	1,58
Buses	1,19

APPENDIX 2: DETERMINATION OF THE DESIGN CHARACTERISTICS OF THE SOIL OF THE ACTIVE LAYER OF THE SUBGRADE WHEN DESIGNING PAVEMENTS FOR STRENGTH

A. Determination of the Design Moisture Content of the Soil of the Active Layer

The design moisture content of the dispersed soil W_r (in fractions of moisture at the yield point W_t), with a total thickness of the pavement layers Z_l≥0,75 m, is determined by the formula:

$$W_r = (\overline{W}_{tab} + \Delta_1\overline{W} - \Delta_2\overline{W}) \cdot (1 + 0{,}1 \cdot t) - \Delta_3$$

where:

- $\overline{W}_{tab}$ is the average long-term value of the relative soil moisture, observed in the most unfavorable (spring) period of the year in the active layer of the subgrade that meets the SNiP standards for elevation above moisture sources on roads with improved surface and transitional pavement bases (crushed stone, gravel, etc.) and a total thickness up to 0,75 m, determined from **Table P.2.1** and depending on the road-climatic zone and sub-zone (**Figure P.2.2**), the moistening scheme of the subgrade and the type of soil;

Table P.2.1: Suggested values of $\overline{W}_{tab}$

Road-climatic zone	**Road-climatic sub-zone**	**Moistening scheme of the active layer of the subgrade**	**$\overline{W}_{tab}$ in fractions of W_t**			
			Light sandy loam	*Silty sand*	*Light loam*	*Silty sandy loam and silty loam*
I	*I₁*	*1*	0,53	0,57	0,62	0,65
		2	0,55	0,59	0,65	0,67
		3	0,57	0,62	0,67	0,7
	I₂	*1*	0,57	0,57	0,62	0,65
		2	0,59	0,62	0,67	0,7
		3	0,62	0,65	0,7	0,75
	I₃	*1*	0,6	0,62	0,65	0,7
		2	0,62	0,65	0,7	0,75
		3	0,65	0,7	0,75	0,8
II	*II₁*	*1*	0,6	0,62	0,65	0,7
		2	0,63	0,65	0,68	0,73
		3	0,65	0,67	0,7	0,75
	II₂	*1*	0,57	0,59	0,62	0,67
		2	0,6	0,62	0,65	0,7
		3	0,62	0,64	0,67	0,72
	II₃	*1*	0,63	0,65	0,68	0,73
		2	0,66	0,68	0,71	0,76
		3	0,68	0,7	0,73	0,78
	II₄	*1*	0,6	0,62	0,65	0,7
		2	0,63	0,65	0,68	0,73
		3	0,65	0,67	0,7	0,75
	II₅	*1*	0,65	0,67	0,7	0,75
		2	0,68	0,7	0,73	0,78
		3	0,7	0,72	0,75	0,8
	II₆	*1*	0,62	0,64	0,67	0,72

		2	0,65	0,67	0,7	0,75
		3	0,67	0,69	0,72	0,77
III	*III₁*	*1*	0,55	0,57	0,6	0,63
		2-3	0,59	0,61	0,63	0,67
	III₂	*1*	0,58	0,6	0,63	0,66
		2-3	0,62	0,64	0,66	0,7
	III₃	*1*	0,55	0,57	0,6	0,63
		2-3	0,59	0,61	0,63	0,67
IV	*1*	-	0,53	0,55	0,57	0,6
	2-3		0,57	0,58	0,6	0,64
V	*1*	-	0,52	0,53	0,54	0,57
	2-3		0,55	0,56	0,57	0,6

Note: the table can only be used if the elevation of the subgrade is ensured in accordance with the SNiP regulations. If this is not the case, the $\bar{W}_{tab}$ values are assigned according to forecast, but they must be at least 0,03 times greater than the tabular ones.

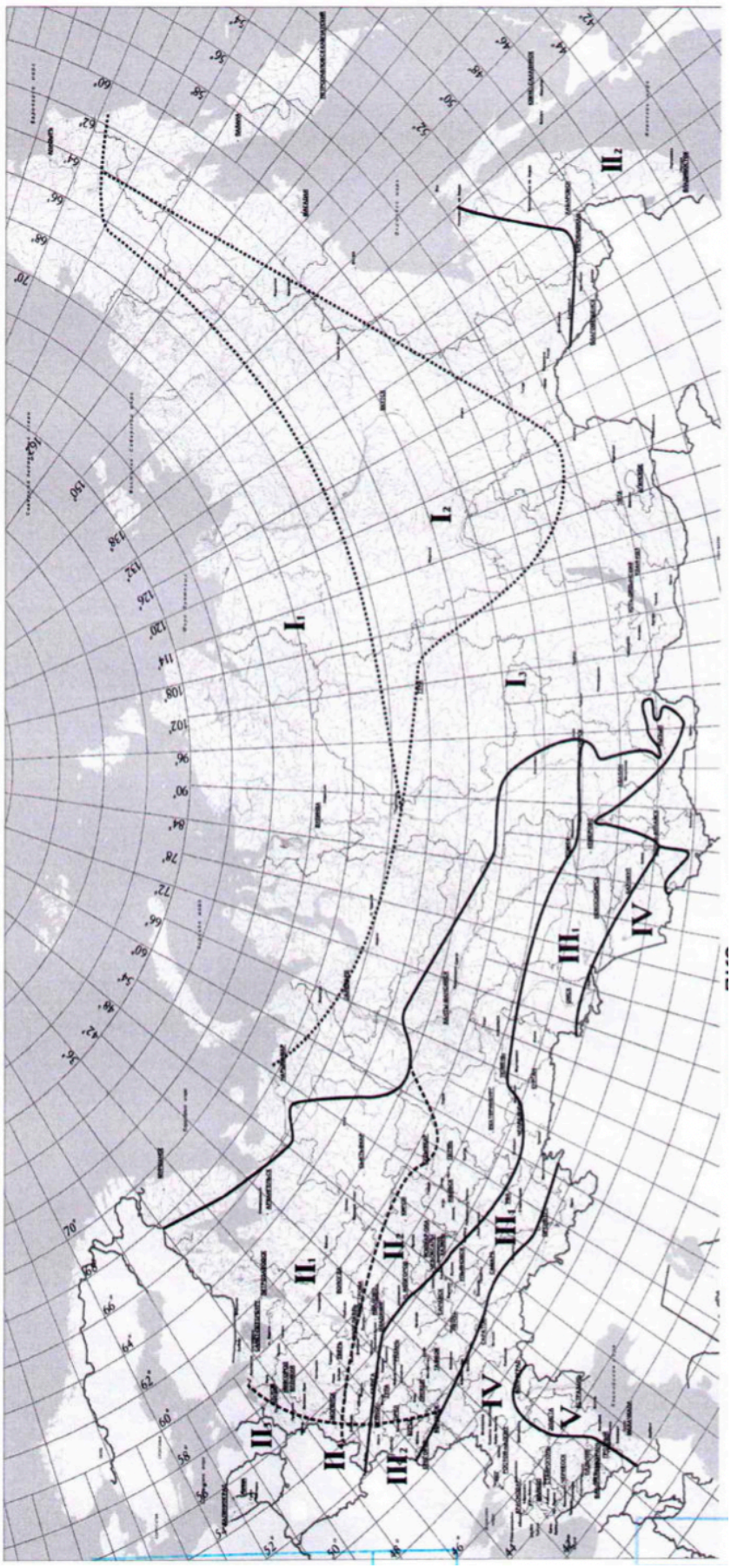

Figure P.2.2: Map of road-climatic zones and sub-zones of the Russian Federation

Note:

1. *When substantiating the general road-climatic zoning of the territory of the Russian Federation, it can be specified within the framework of individual subjects.*
2. *The Kuban and the western part of the North Caucasus should be assigned to RCZ II, Crimea to RCZ IV.*
3. *When designing road sections in border areas and when collecting data on soil hydrological and pedological conditions, it is allowed to make design decisions for the adjacent (northern or southern) zone, also based on the practice of road operations in the area.*
4. *In mountainous areas, the RCZ should be determined considering the natural conditions at a given height.*
5. *The division into sub-zones should be taken into account in the determination of the design moisture content when calculating the strength and frost resistance of pavements.*

- $\Delta_1\overline{W}$ is a correction factor taking into account the territory features, set according to **Table P.2.2;**

Table P.2.2: Suggested values of $\Delta_1\overline{W}$

Category	**Territory type**	$\boldsymbol{\Delta_1\overline{W}}$
1	*Flat areas*	0
2	*Foothill areas (up to 1000 m above sea level)*	0,03
3	*Mountainous areas (more than 1000 m above sea level)*	0,05

- $\Delta_2\overline{W}$ is a correction factor taking into account the design features of the carriageway and shoulders, set according to **Table P.2.3**;

Table P.2.3: Suggested values of $\Delta_2\overline{W}$

Category	Design features	$\Delta_2\overline{W}$ according to the road-climatic zone			
		II	*III*	*IV*	*V*
1	*Presence of the pavement base, including layers at the subgrade interface, realized of reinforced materials and soils:*				
	- coarse soil and sand	0,04	0,04	0,03	0,03
	- sandy loam	0,05	0,05	0,05	0,04
	- silty sands and sandy loams, loam	0,08	0,08	0,06	0,05
2	*Strengthening of the shoulders (at least 2/3 of their width):*				
	- asphalt concrete	0,05	0,04	0,03	0,02
	- crushed stone (gravel)	0,02	0,02	0,02	0,02
3	*Drainage with longitudinal tubular drains*	0,05	0,03	-	-
4	*Installation of waterproofing layers made of polymeric materials*	0,05	0,05	0,03	0,03
5	*Installation of a heat-insulating layer that prevents freezing*	Reduce the design moisture content to the value of full moisture capacity at the required K_{upl}			
6	*Soil in the active zone of the subgrade*	Reduce the design moisture content to optimal			
7	*Soil compacted to K_{upl}=1,03-1,05 in a layer of 0,3-0,5 m from the bottom of the pavement, located below the freezing line*	-	0,03-0,05	0,03-0,05	0,03-0,05

Note: category 1 and 2 specifications should be adopted only with the 1st moistening scheme of the active layer; category 5 specifications should be adopted only with the 2nd and 3rd moistening scheme of the active layer.

- t is a coefficient of normalized deviation, taken depending on the required level of reliability according to *appendix 4*, **Table P.4.2**;
- Δ_3 is a correction factor for the effect of the total thickness of the stable layers of the pavement, set according to **Figure P.2.1**;

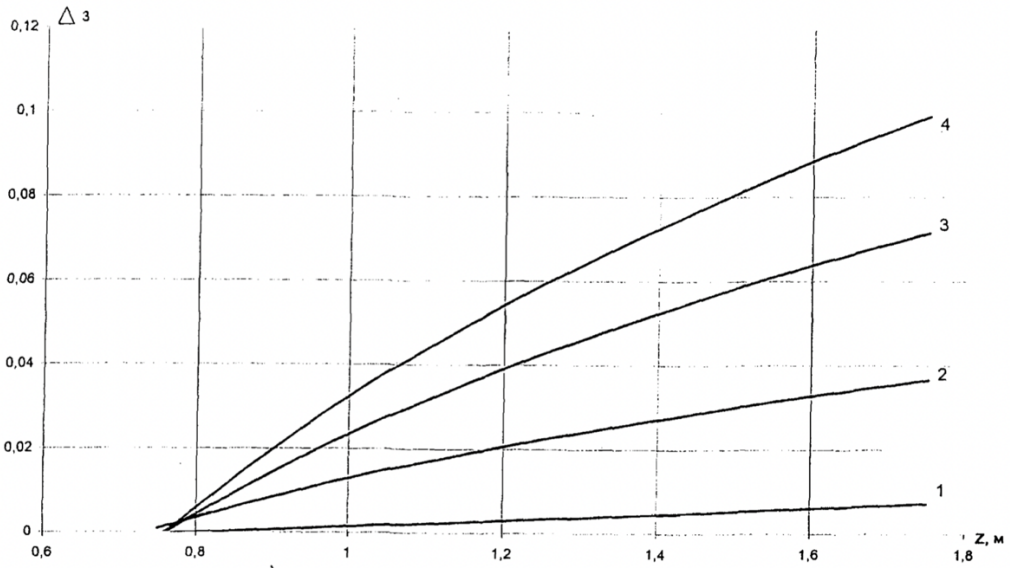

Figure P.2.1: Graphs for determining Δ_3

Note: 1-for initial relative humidity equal to 0,75·W_t; 2-for initial relative humidity equal to 0,8·W_t; 3-for initial relative humidity equal to 0,85·W_t; 4-for initial relative humidity equal to 0,9·W_t. The initial moisture content is determined from the first term in the W_r formula.

B. Recommended Standard Values for the Mechanical Characteristics of Soils and Sandy Structural Layers

Table P.2.4: Normative values of shear characteristics of clayey soils depending on the estimated number of applications of the design load

Design relative humidity	**Adhesion [MPa] according to the total number of load applications ($\sum N_r$)**					**Angle of internal friction [°] according to the total number of load applications ($\sum N_r$)**				
	1	*10^3*	*10^4*	*10^5*	*10^6*	*1*	*10^3*	*10^4*	*10^5*	*10^6*
Loams and clays										
0,6	0,03	0,03	0,016	0,014	0,012	24	20	14,5	11	9
0,65	0,024	0,019	0,013	0,011	0,009	21	15	11	8	7
0,7	0,019	0,013	0,009	0,007	0,006	18	11,5	8,5	6,5	5,5
0,75	0,015	0,009	0,006	0,005	0,004	15	10	7,5	5	4
0,8	0,011	0,007	0,005	0,003	0,002	13	8	5	3	2,5
0,9	0,008	0,004	0,004	0,002	0,001	11,5	6,5	3,5	2,2	2
Sandy loams										
0,6	0,014	0,012	0,008	0,006	0,005	36	24	18	14	12
0,65	0,013	0,01	0,008	0,006	0,004	36	23,5	17	14	12
0,7	0,012	0,009	0,006	0,005	0,004	35	23,5	17	14	12
0,75	0,011	0,008	0,005	0,004	0,003	35	23	17	14	12
0,8	0,01	0,007	0,005	0,004	0,003	34	23	17	14	12
0,85	0,009	0,007	0,004	0,003	0,003	34	22	15	12	10
0,9	0,008	0,004	0,003	0,003	0,003	33	21	12,5	10	8

Note: the values of the shear characteristics at $\sum N_r$=1 are used in the calculation for the static effect of load. When $\sum N_r$>10^6, the design values of c and φ should be taken according to the column "10^6".

Table P.2.5: Normative values of soil elastic moduli

Soil	**Modulus of elasticity [MPa] according to the relative humidity $\frac{W}{W_t}$**									
	0,5	*0,55*	*0,6*	*0,65*	*0,7*	*0,75*	*0,8*	*0,85*	*0,9*	*0,95*
Sands:										
- large	130									
- medium	120									
- small	100									
- homogeneous	75									
- dusty	96	90	84	78	72	60	60	54	48	43
Sandy loams:										
- light	70	60	56	53	49	45	43	42	41	40
- dusty, heavy dusty	108	90	72	54	46	38	32	27	26	25
- light large	65									
Loams:										
- light heavy	108	90	72	50	41	34	29	25	24	23
- light dusty, heavy dusty	108	90	72	54	46	38	32	27	26	25
- clay	108	90	72	50	41	34	29	25	24	23

Note: sand classification is given according to GOST 25 100-95.

Table P.2.6: Design values of the angle of internal friction and adhesion for sandy soils and sands of structural layers depending on the design number of applications of the design load

Soil type		**Adhesion [MPa] and angle of internal friction [°] according to the total number of load applications ($\sum N_r$)**				
		1	*10^3*	*10^4*	*10^5*	*10^6*
Coarse sand with a silt-clay fraction content	0%	35 0,004	33 0,003	32 0,003	31 0,003	29 0,003
	5%	34 0,005	31 0,004	36 0,004	29 0,003	28 0,003
Medium sand with a silt-clay fraction content	0%	32 0,004	30 0,004	30 0,003	28 0,003	22 0,002
	5%	33 0,005	30 0,004	29 0,003	28 0,003	26 0,002
Fine sand with a silt-clay fraction content	0%	11 0,003	28 0,003	22 0,002	26 0,002	25 0,002
	5%	31 0,005	22 0,004	26 0,004	21 0,004	24 0,003
	8%	11 0,006	22 0,005	26 0,004	25 0,003	23 0,002

Note:

1. *Characteristic values are given for the condition of complete filling of pores with water.*
2. *Upper value: angle of internal friction in degrees; lower value: adhesion in MPa.*
3. *When $\sum N_r$>10^6, the design values of c and φ should be taken according to the column "10^6".*

C. Road-Climatic Zones and Sub-Zones

Road-climatic zone and sub-zone	Approximate geographic boundaries
I	***North of the line connecting Nivsky-Sosnovka-Novy Bor-Shchelyabozh-Synyu-Suevatpul-Beloyrasky-Laryak-Ust-Ozernoye-Yartsevo-Kansk-Vyezzhiy Log-Ust-Zolotaya-Sarych-Sep-Novoselovo-Inya-Artybash-state border-Simonovo-Birobidchan-Bolon-Mnogovershiny. Includes geographic zones of the tundra, forest-tundra and the northeastern part of the forest zone with the distribution of permafrost soils.***
I_1	North of the line Naryan-Mar-Salekhard-Kureika-Pipe Udachnaya-Verkhoyansk-Druzhina-Gorny Cape-Markovo.
I_2	East of the line connecting the mouth of the river Lower Tunguska-Erbogachen, Lensk-Bodaibo-Bogdarin and north of the line Mogocha-Skovorodino-Zaya-Okhotsk-Palatka-Slautskoe. It is limited to the north by I_1 sub-zone.
II	***From the border of zone I to the line connecting Lviv-Zhytomyr-Tula-Nizhny Novgorod-Izhevsk-Tomsk-Kansk. From the border of zone I to the state border in the Far East. Includes a geographical area of forests with excessive soil moisture.***
II_1	It is limited to the north and east by zone I, to the west by sub-zone II_3 and to the south by the line Roslavl-Klin-Rybinsk-Berezniki-Ivdel.
II_2	To the north, it is limited by the state border, to the west by the border with sub-zone II_5, to the south by zone III, to the east by the southern border of zone I.
II_3	To the north, it is limited by the state border, to the west by the border with sub-zone II_5, to the south by the line Roslavl-Klin-Rybinsk, to the east by the line Pskov-Smolensk-Orel.

II_4	It is bounded to the north by sub-zone II_3, to the west by sub-zone II_6, to the south by the border with zone III, to the east by the line Baranovichi-Roslavl-Klin-Rybinsk.
II_5	To the north and the west, it is limited by the state border, to the east by the line Minsk-Bobruisk-Gomel, to the south by the line Baranovichi-Roslavl-Klin-Rybinsk.
II_6	To the north, it is limited by sub-zone II_5, to the west by the state border, to the south by the border with zone III, to the east by the line Minsk-Bobruisk-Gomel.
III	***From the southern border of zone II to the line connecting Chisinau-Kirovograd-Belgorod-Samara-Magnitogorsk-Omsk-Bysk-Turan. Includes a forest-steppe geographic zone with significant soil moisture in some years.***
III_1	It is bounded to the north by zone II, to the west by sub-zone III_2, to the south by zone IV, to the east by zone I.
III_2	It is bounded to the north by zone II, to the west by sub-zone III_3, to the south by zone IV, to the east by the line Smolensk-Orel-Voronezh.
III_3	It is limited to the north by zone II, to the west by the state border, to the south by zone IV, to the east by the line Bobruisk-Gomel-Kharkiv.
IV	***It is located from the border of zone III to the line connecting Julfa-Stepanakert-Kizlyar-Volgograd and goes south for 200 km of the line connecting Uralsk-Aktyubinsk-Karaganda. Includes a geographical steppe zone with insufficient soil moisture.***
V	***It is located to the southwest and south of the border of zone IV and includes desert and desert-steppe geographical zones with an arid climate and saline soils.***

APPENDIX 3: TABLES OF NORMATIVE AND DESIGN VALUES OF STRENGTH AND DEFORMATION CHARACTERISTICS OF STRUCTURAL LAYERS FROM VARIOUS ROAD-BUILDING MATERIALS

A. Layers of Asphalt Concrete

Table P.3.1: Characteristics of asphalt concrete to be used in the calculations for tensile bending under short-term loads

Asphalt concrete	**Design values of the modulus of elasticity E [MPa]**	t **[-]**	α **[-]**	**Normative value of the tensile strength in bending R_0 [MPa]**
Highly dense:				
- BND 40/60	8600	6	5/5,6*	10
- BND 60/90	6000	5,5	5,2/5,9	9,8
- BND 90/130	4600	5	5,4/6,3	9,5
- BND 130/200	3500	4,5	5,8/6,8	9,3
- BND 200/300	2500	4,3	5,9/7,1	9
Dense:				
- BND 40/60	6000	6	5/5,6	10
- BND 60/90	4500	5,5	5,2/5,9	9,8
- BND 90/130	3600	5	5,4/6,3	9,5
- BND 130/200	2600	4,5	5,8/6,8	9,3
- BND 200/300	2000	4,3	5,9/7,1	9
Porous:				

- BND 40/60	3600	4,5	5,8/6,8	8,3
- BND 60/90	2800	4,3	5,9/7,1	8
- BND 90/130	2200	4	6,3/7,6	7,8
- BND 130/200	1800	3,75	6,6/8,2	7,6
- BND 200/300	1400	3,7	6,7/8,2	7,1
Highly porous:				
- BND 40/60	3000	4,3	5,9/7,1	5,5/6,5**
- BND 60/90	2100	4	6,3/7,6	5,65/6,2
- BND 90/130	1700	3,8	6,5/7,9	5,5/-
Cold asphalt concrete:				
- Bh	2600	3	8/10,3	4,9
- Vh	2200	2,5	9,8/13,4	4,6
- Gh	1800	2	13,2/19,5	4,2
- Dh	1500	2	13,2/19,5	3,9

**the value in the numerator is for road-climatic zone II, the value in the denominator is for road-climatic zone III, IV and V.*

***for sandy asphalt concrete.*

Table P.3.2: Normative values of the short-term modulus of elasticity of asphalt concrete of various compositions (when designing the structure according to the allowable elastic deflection and shear stability)

Material	**Bitumen type**	**Short-term modulus of elasticity *E* [MPa] depending on the coating temperature [°C]**				
		+10	*+20*	*+30*	*+40*	*+50*
Dense and highly dense asphalt concrete	*Viscous BND and BN:* *40/60, 60/90, 90/130, 130/200, 200/300*	4400, 3200, 2400, 1500, 1200	2600, 1800, 1200, 800, 600	1550, 1100, 550, 670, 500	850, 650, 550, 460, 420	520, 460, 420, 380, 360
	Liquid: *BG-70/130, SG-130/200, SG-70/130, MG-70/130*	1000, 1000, 800, 800	420, 420, 360, 360	400, 400, 350, 350	350, 350, 350, 350	350, 350, 350, 350
Porous and highly porous asphalt concrete	*Viscous BND and BN:* *40/60, 60/90, 90/130, 130/200, 200/300*	2800, 2000, 1400, 1100, 950	1700, 1200, 800, 600, 450	900, 700, 510, 400, 350	540, 460, 380, 340, 330	390, 360, 350, 340, 330
Dense tar concrete *Porous tar concrete*	- -	3800 200	1500 300	800 400	500 350	350 300
Cold asphalt concrete:						

Bh	-	1300	-	-	-	-
Vh	-	1100	-	-	-	-
Gh	-	900	-	-	-	-
Dh	-	750	-	-	-	-

Note:

1. *The modulus of elasticity of porous and highly porous asphalt concrete is given in relation to sand mixtures. At temperatures between 30 °C and 50 °C, the elastic modulus for fine-grained mixtures should be increased by 10% and by 20% for coarse-grained ones.*
2. *When designing for elastic deflection, consider a coating temperature of 10 °C.*

Table P.3.3: Design values of the modulus of elasticity of asphalt concrete when designing for long-term loads

Asphalt concrete type	**Mix type**	**Design modulus of elasticity *E* [MPa] under static load at different design temperatures [°C]**			
		+20	*+30*	*+40*	*+50*
Dense mixtures	*A*	480	420	360	300
	B	400	350	300	250
	V	320	280	240	200
	G	300	270	220	200
	D	200	180	160	150
Porous and highly porous mixtures	*Coarse-grained*	360	320	280	250
	Fine-grained	290	250	220	200
	Sandy	250	225	200	190
Cold asphalt concrete	*Bx*	180	-	-	-
	Vh	170	-	-	-
	Gh	160	-	-	-
	Dh	150	-	-	-

Note: the modulus of elasticity of high-density asphalt concrete is equal to the one of type A dense mixtures.

B. Structural Layers of Organic Mineral Mixtures and Soils Reinforced with an Organic Binder

Table P.3.4: Structural layers of crushed stone-gravel-sand mixtures and soils treated with organic and complex binders, corresponding to GOST 30491-97

Layer material	**Normative values of the modulus of elasticity *E* [MPa]**
Processed crushed stone-gravel-sand mixtures and coarse-grained soils (optimal/non-optimal composition):	
- liquid organic binders or viscous, including emulsified organic binders	450/350
- liquid organic binders together with mineral or emulsified organic binders together with mineral	950/700
Gravelly sands, coarse/medium/fine sands, light and silty sandy loams, lightly processed loams:	
- liquid organic binders or viscous, including emulsified organic binders	430/280
- liquid organic binders together with mineral or emulsified organic binders together with mineral	700/600

Table P.3.5: Structural layers of black crushed stone

Material	**Normative values of the modulus of elasticity *E* [MPa]**
Black crushed stone laid according to the wedge method	600/900
A layer of crushed stone arranged according to the method of impregnation with viscous bitumen and bitumen emulsion	400/600

Note: larger values are for surface courses, smaller values are for base courses.

C. Structural Layers of Organic Mineral Mixtures and Soils Reinforced with an Organic Binder

Table P.3.6: Structural layers of crushed stone-gravel-sand mixtures and soils treated with inorganic binders, corresponding to GOST 223558-94

Material	**Normative values of the modulus of elasticity *E* [MPa]**
Crushed stone-gravel-sand mixtures, coarse-grained soils (optimal/non-optimal composition) treated with cement (depending on the mark):	
- 20	500/400
- 40	600/550
- 60	800/700
- 75	870/830
- 100	1000/950
The same, treated with ash or slag binder (depending on the mark):	
- 20	450/350
- 40	550/500
- 60	750/650
- 75	870/780
- 100	950/910
Gravelly sands, coarse/medium/fine sands, silty, light and heavy sandy loams, light loams treated with cement (depending on the mark):	
- 20	400/250
- 40	550/400

- 60	700/550
- 75	870/750
- 100	950/870
The same, treated with ash or slag binder (depending on the mark):	
- 20	300/200
- 40	450/300
- 60	600/450
- 75	730/600
- 100	870/750

Table P.3.7: Structural layers of active materials (slag, sludge, phosphogypsum, etc.)

Material	**Normative values of the modulus of elasticity *E* [MPa]**
Base made of selected optimal mixtures of highly active materials with a maximum grain size up to 40 mm, compacted at optimal humidity.	650/870
The same, from active materials.	480/700
Base made of ordinary non-optimal mixtures of highly active materials with a maximum grain size up to 70 mm.	450/650
The same, from active materials.	370/480

Note:

1. *Highly active materials include those with a compressive strength between 5 and 10 MPa at the age of 90 days.*
2. *Active materials include those with a compressive strength between 2,5 and 5 MPa and the age of 90 days.*

D. Structural Layers of Crushed Stone-Gravel-Sand Materials Untreated with Binder

Table P.3.8: Structural layers from mixtures of crushed stone-gravel-sand, corresponding to GOST 25607-94 and GOST 3344-83

Layer material	**Normative values of the modulus of elasticity *E* [MPa]**
Crushed stone/gravel mixtures (C) for pavement surfaces with a continuous granulometry (GOST 25607) with a maximum grain size equal to:	
C_1-40 mm	300/280
C_2-20 mm	290/265
The same, for base courses:	
C_3-80 mm	280/240
C_4-80 mm	275/230
C_5-40 mm	260/220
C_6-20 mm	240/200
C_7-20 mm	260/180
Gravel-sand mixtures from inactive and low-active slags (GOST 3344) with a maximum grain size equal to:	
C_1-40 mm	275
C_2-20 mm	260
C_4-80 mm	250
C_6-20 mm	210

Table P.3.9: Crushed stone foundations arranged by the wedge method, corresponding to GOST 25607-94

Layer material	**Normative values of the modulus of elasticity *E* [MPa]**
Fractionated crushed stone 40-80 mm (80-120 mm) with a wedge:	
- fractionated fine gravel	450 350
- limestone fine mixture or active fine slag	400 300
- fine highly active slag	450 400
- asphalt mix	500 450
- cement-sand mixture M75 with an impregnation depth of 0,25-0,75 time the layer height	450-700 350-600

Note: upper value-from easily compacted stone; lower value: from hard-to-compact crushed stone.

E. Mechanical Characteristics of Thermal Insulation Layers

Table P.3.10: Mechanical characteristics of thermal insulation layers

Material	**Normative values of the modulus of elasticity *E* [MPa]**
Styrofoam	13-33,5
Styropor concrete	500-800

Agloporite crushed stone treated with viscous bitumen	400
Expanded clay gravel treated with viscous bitumen	500
Gravel (crushed stone) with light aggregates treated with viscous bitumen	500
Cement soil with perlite *The same, with polystyrene, with the following composition:* *- polystyrene granules 2-3%* *- sand 97-98% (% by weight)* *- cement 6-7%* *The same, with expanded clay, with the following composition:* *- sand 75%* *- expanded clay 25%* *- cement 6%*	130 300 300
Bitumen cement soil with perlite, with the following composition: *- perlite crushed stone 20-25%* *- sand 75-80%* *- cement 4-6%* *- bitumen 10-12% (by weight of sand, perlite and cement)*	250-350
Cement soil with agloporite, with the following composition: *- sandy loam or sand 70-80%* *- agloporite 20-30%*	250-350

- cement 6%	
Ash and slag mixture reinforced with cement	150
Soil reinforced with fly ash *Cement soil treated with bituminous emulsion*	200

APPENDIX 4: ASSIGNMENT OF STATISTICAL PARAMETERS

Table P.4.1: Recommended values for the coefficient of variation

Characteristic	$\boldsymbol{v}$ **[-]**
Relative humidity of the soil of the active layer, cohesion of soil and sand layers, angle of internal friction of soil and sand layers, tensile strength of asphalt concrete layers in bending	0,1

Table P.4.2: Normalized deviation coefficient

$\boldsymbol{K_n}$ **[-]**	*0,85*	*0,9*	*0,95*	*0,98*
$\boldsymbol{t}$ **[-]**	1,06	1,32	1,71	2,19

APPENDIX 5: THERMOPHYSICAL CHARACTERISTICS OF STRUCTURAL LAYERS FROM VARIOUS ROAD-BUILDING MATERIALS

Table P.5.1: Thermophysical characteristics of structural layers from various road-building materials

Material/soil	**Density ρ [kg/m^3]**	**Thermal conductivity coefficient λ [W/(m·K)]**
Hot dense asphalt *The same, porous* *The same, highly porous, including bitumen-sand mixtures (TU 218 RSFSR)*	2400 2300 2200-1900	1,4 1,25 1,1-1
Agloporite crushed stone treated with viscous bitumen	800	0,23
Expanded clay gravel treated with viscous bitumen	1100	0,64
Gravel (crushed stone) with light aggregates treated with viscous bitumen	2000	0,52
Sandy loam reinforced with 10% emulsion	1700-1900	1,456
Cement concrete	2400	1,74
Sand of various sizes reinforced with 10% cement	2100	1,86
Fine sand, one-dimensional, reinforced with 10% cement	2100	1,62
Cement soil with expanded clay, having the following composition: *- sand 75% (mass)* *- expanded clay 25%* *- cement 5%*	1500-1600	-

Cement soil with polystyrene granules, having the following composition: *- sand 97-98%* *- polystyrene granules 2-3%* *- cement 6-7%*	1300-1500	0,41-0,58
Bitumen cement soil with perlite, having the following composition: *- crushed perlite 20-25%* *- sand 75-80%* *- cement 3-4%* *- bitumen 10-12% (by weight of sand, perlite and cement)*	1400	0,52-0,58
Cement soil with agloporite, having the following composition: *- sandy loam or sand 70-80%* *- agloporite 20-30 %* *- cement 6%*	1700-1800	0,64-0,75
Slag concrete	1600	0,58
Expanded clay concrete	1400	0,75
Styropor concrete	1000-1100	0,23
Weak limestone reinforced with lime	2000	1,16
Loam reinforced with 6-12% cement	1750-1900	1,45
Loam reinforced with 2-5% cement and 2-6% lime	1800-1900	1,33
Sandy loam reinforced with 8-10% cement	1700-1900	1,51
Styrofoam	38,5-60	0,03-0,052
Penoplex	38,5-50	0,03-0,032
Coal ash and slag, reinforced with 6-8% cement	1600	0,7
Furnace slag	800	0,46

Crushed stone from granite	1800	1,86
Crushed limestone	1600	1,39
Gravel	1800	1,86
Coarse thawed sand	2000	1,74
Same, frozen	200	2,32
Medium thawed sand	1950	1,91
Same, frozen	1950	2,44
Fine thawed sand	1850	1,91
Same, frozen	1850	2,32
Dusty thawed sand	1750	1,8
Same, frozen	1750	2,2
Thawed sandy loam	2100	1,8
Same, frozen	2100	2,03
Thawed loam and clay	2000	1,62
Same, frozen	2000	1,97
Thawed loess	1500	1,51
Same, frozen	1500	2,09
One-dimensional crushed granite treated with viscous bitumen	1850	1,28
Gravel-sand mixture	2000	2,1
Gravel-sand mixture reinforced with 10% cement	2000	2,02

APPENDIX 6: PARAMETERS FOR DETERMINING THE ESTIMATED TOTAL NUMBER OF LOAD APPLICATIONS DURING THE PAVEMENT SERVICE LIFE

Determination of the Number of Days per Year to Calculate the Total Number of Applications of the Design Load for the Design Life of the Structure

P.6.1. The estimated number of design days per year (T_{rdg}*) for the structure design life (T_{sl}) should be established according to the data of special regional studies and fixed in local norms.

**The design day is considered to be the one during which the combination of the state of the subgrade soil in terms of moisture and the temperature of the asphalt concrete layers of the structure provides the possibility of accumulation of permanent deformations in the subgrade soil or poorly connected layers of the pavement.*

In the absence of regional norms on the territory of Russia, it is allowed to use the following guidelines and the data in **Figure P.6.1** and **Table P.6.1**.

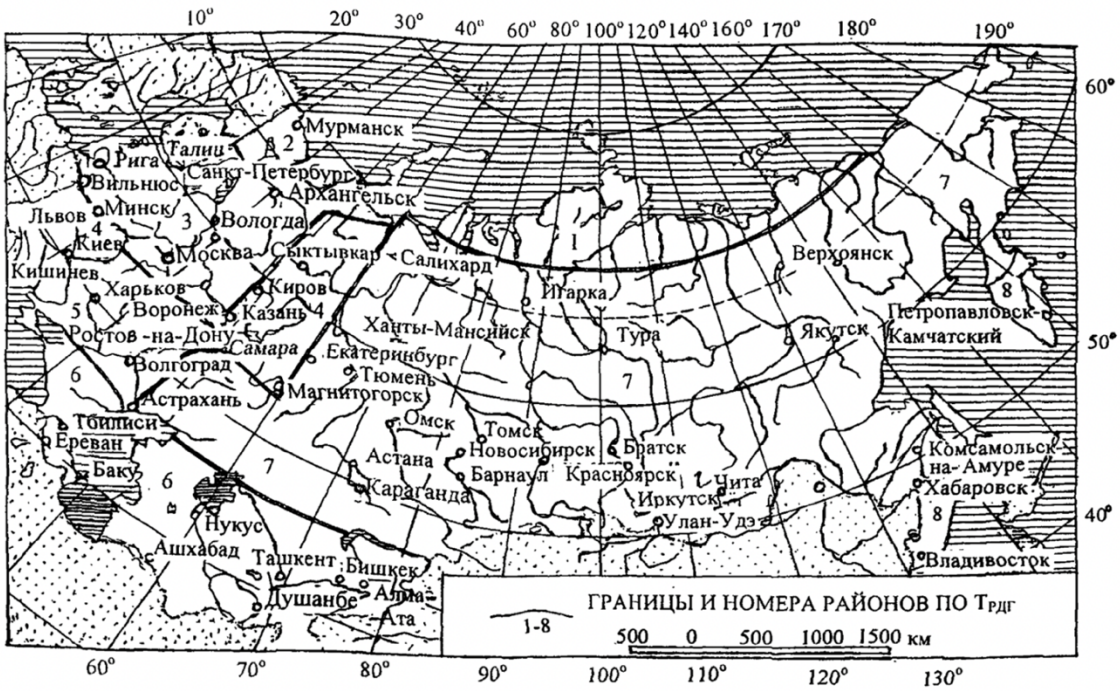

Figure P.6.1: Regional map depending on the T_{rdg} values

Table P.6.1: Recommended T_{rdg} values depending on the location of the road

District number from the map	**Approximate geographical boundaries of the areas**	**T_{rdg} [years]**
1	*The zone of distribution of permafrost soils north of the 70th parallel*	70
2	*North of the line connecting Onega-Arkhangelsk-Mezen-Naryan-Mar-the 60th meridian to the coast of the European part*	145
3	*North of the line connecting Minsk-Smolensk-Kaluga-Ryazan-Saransk-the 48th meridian to the line connecting Onega-Arkhangelsk-Mezen-Naryan-Mar*	125
4	*North of the line connecting Lviv-Kiev-Belgorod-Voronezh-Saratov-Samara-Orenburg-the 60th meridian to the line of regions 2 and 3*	135

5	*North of the line connecting Rostov-on-Don-Elista-Astrakhan to the line Lvov-Kiev-Belgorod-Voronezh-Saratov-Samara*	145
6	*South of the Rostov-on-Don-Elista-Astrakhan line for the European part, south of the 46th parallel for the rest of the territories*	205
7	*Eastern and Western Siberia, the Far East (except for Khabarovsk and Primorsky territories and Kamchatka region), bounded to the north by the 70th parallel and to the south by the 46th parallel*	130-150 (lower values for the central part)
8	*Khabarovsk and Primorsky territories and Kamchatka region*	140

Note: at the boundaries of the districts, the largest of the T_{rdg} values should be taken.

P.6.2. In the absence of regional norms, the estimated service life of the pavement can be assigned in accordance with Table **P.6.2**.

Table P.6.2: Recommended design life of the structure

Road category	**Pavement type**	**T_{sl} [years] depending on the road-climatic zone**		
		I-II	*III*	*IV-V*
I	*Capital*	14-15-18	15-19	16-20
II	*Capital*	11-15	12-16	13-16
III	*Capital*	11-15	12-16	13-16
	Lightweight	10-13	11-14	12-15
IV	*Capital*	11-15	12-16	13-16
	Lightweight	8-10	9-11	10-12
V	*Lightweight*	8-10	9-11	10-12
	Transitional	3-8	3-9	3-9

P.6.3. The value of the summation factor (in the absence of other data) should be taken according to **Table P.6.3**.

Table P.6.3: K_s suggested values

Indicator of change in traffic intensity by years q	**K_s values according to the service life of the pavement T_{sl}**			
	8	*10*	*15*	*20*
0,9	5,7	6,5	7,9	8,8
0,92	6,1	7,1	8,9	10,1
0,94	6,5	7,7	10	11,8
0,96	7	8,4	11,4	13,9
0,98	7,5	9,1	13,1	16,6
1	8	10	15	20
1,02	8,6	10,9	17,2	24,4
1,04	9,2	12	20	29,8
1,06	9,9	13,2	23,2	36
1,08	10,6	14,5	27,2	45,8
1,1	11,4	15,9	31,7	67,3